

NON
CIRCULATING

JOURNAL OF THE
**Electrochemical
Society**

Vol. 108, No. 4

April 1961

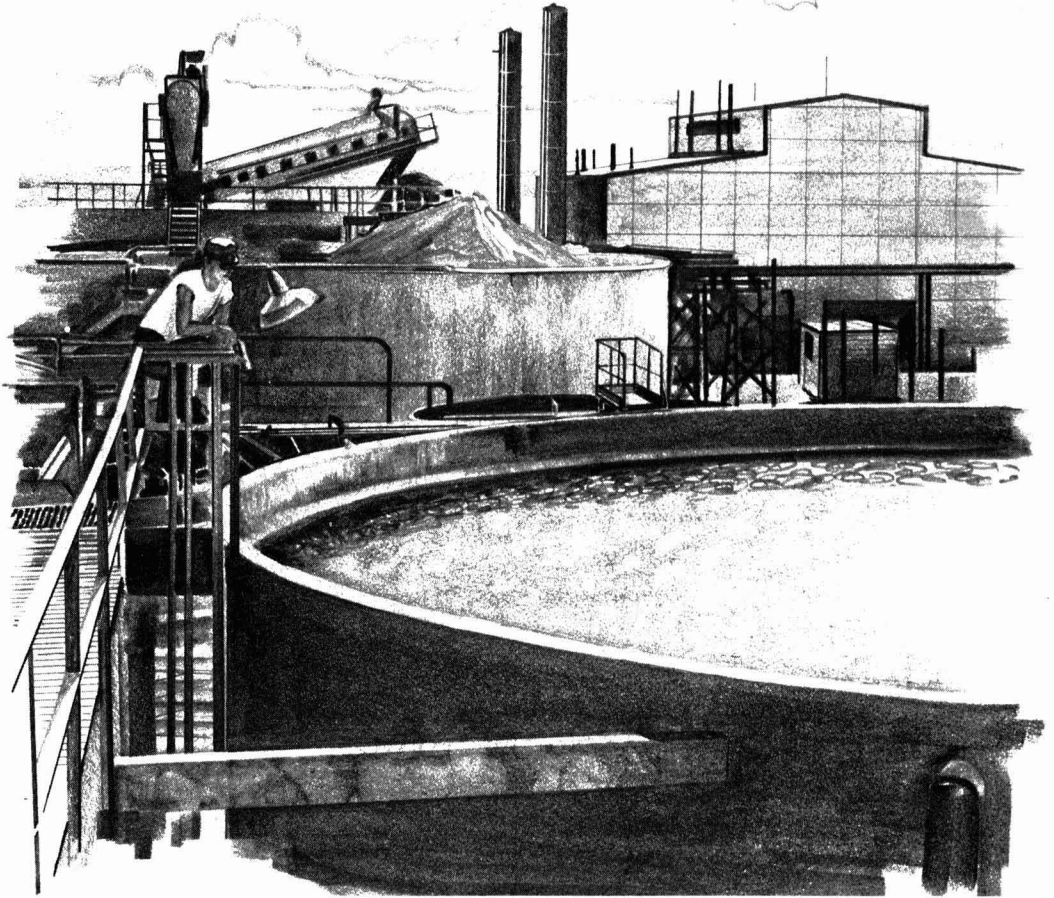
แผนกห้องสมุด กรมวิทยาศาสตร์
กระทรวงอุตสาหกรรม



RECEIVED
APR 7 1961
CENTRAL RESEARCH
LIBRARY



GLC Anodes Are CUSTOM MADE for Stauffer Chemical Company



The Stauffer Chlor-Alkali Plant at Henderson, Nevada

Most chlor-alkali producers have lowered their operating costs by using GLC anodes.

Unless you have some GLC anodes in your cells now, you are missing an opportunity to prove

their outstanding performance to your satisfaction.

The difference lies in custom making GLC anodes to individual cell requirements. May we demonstrate that difference for you?



GREAT LAKES CARBON CORPORATION

18 EAST 48TH STREET, NEW YORK 17, N.Y. OFFICES IN PRINCIPAL CITIES

EDITORIAL STAFF

C. L. Faust, Chairman, Publication Committee
 Cecil V. King, Editor
 Norman Hackerman, Technical Editor
 Ruth G. Sterns, Managing Editor
 U. B. Thomas, News Editor
 H. W. Salzberg, Book Review Editor
 Natalie Michalski, Assistant Editor

DIVISIONAL EDITORS

W. C. Vosburgh, Battery
 Milton Stern, Corrosion, I
 R. T. Foley, Corrosion, II
 T. D. Callinan, Electric Insulation
 Seymour Senderoff, Electrodeposition
 H. C. Froelich, Electronics, I
 Ephraim Banks, Electronics, II
 Ernest Paskell, Electronics—Semiconductors
 Sherlock Swann, Jr., Electro-Organic, I
 Stanley Wawzonek, Electro-Organic, II
 John M. Blocher, Jr., Electrothermics and Metallurgy, I
 J. H. Westbrook, Electrothermics and Metallurgy, II
 N. J. Johnson, Industrial Electrolytic
 C. W. Tobias, Theoretical Electrochemistry, I
 A. J. deBethune, Theoretical Electrochemistry, II
 R. M. Murd, Theoretical Electrochemistry, III

ADVERTISING OFFICE

ECS

1860 Broadway, New York 23, N. Y.

ECS OFFICERS

R. A. Schaefer, President
 Electric Storage Battery Co.,
 Yardley, Pa.
 Henry B. Lintford, Vice-President
 Columbia University, New York, N. Y.
 F. L. LaQue, Vice-President
 International Nickel Co., Inc.,
 New York, N. Y.
 W. J. Hamer, Vice-President
 National Bureau of Standards,
 Washington, D. C.
 Lyle I. Gilbertson, Treasurer
 Air Reduction Co., Murray Hill, N. J.
 I. E. Campbell, Secretary
 National Steel Corp., Weirton, W. Va.
 Robert K. Shannon, Executive Secretary
 National Headquarters, The ECS,
 1860 Broadway, New York 23, N. Y.

Manuscripts submitted to the Journal should be sent, in triplicate, to the Editorial Office at 1860 Broadway, New York 23, N. Y. They should conform to the revised Instructions to Authors, last published on pp. 46C-47C of the March 1961 issue. Manuscripts so submitted become the property of The Electrochemical Society and may not be published elsewhere, in whole or in part, unless permission is requested and granted by the Editor.

Inquiries re positive microfilm copies for volumes should be addressed to University Microfilms, Inc., 313 N. First St., Ann Arbor, Mich.

The Electrochemical Society does not maintain a supply of reprints of papers appearing in its Journal. A photoprint copy of any particular paper, however, may be obtained by corresponding directly with the Engineering Societies Library, 29 W. 39 St., New York 18, N. Y.

Journal of the Electrochemical Society

APRIL 1961

VOL. 108 • NO. 4

CONTENTS

Editorial

Publications of The ECS 82C

Technical Papers

- Investigation of the Electrochemical Characteristics of Organic Compounds, VII. Organic Positive Iodine and Aliphatic Azo Compounds. R. Glucksman and C. K. Morehouse 303
 Oxidation Studies on Ni-Al Alloys. K. Fueki and H. Ishibashi 306
 Oxidation and Equilibrium in Nonstoichiometric Zirconium Dioxide Powder. S. Aronson 312
 The Permeability of Aluminum to Hydrogen. C. N. Cochran 317
 Oxidation of High-Purity Aluminum and 5052 Aluminum-Magnesium Alloy at Elevated Temperatures. C. N. Cochran and W. C. Sleppy 322
 Critical pH and Critical Current Density for Passivity in Metals. H. H. Uhlig 327
 Electrochemical Measurements of Corrosion Rates on Zirconium and Zircaloy-2 at Elevated Temperatures. A. L. Bacarella 331
 Anodic Polarization Behavior of Iron-Nickel Alloys in Sulfuric Acid Solutions. G. Economy, R. Speiser, F. H. Beck, and M. G. Fontana 337
 An Investigation of Columbium as an Electrolytic Capacitor Metal. A. Shtasel and H. T. Knight 343
 Dielectric Characteristics of Tantalum Anodic Films as Related to Film Structure. D. Mohler and G. Hirst 347
 Mechanism of Electrodeposition of Cobalt from Liquid Ammonia Solutions of Spin-Paired Cobalt(III) Complexes; Evidence for a Trans Effect in Octahedral Complexes. G. W. Watt and J. W. Vaughn 351
 Preparation and Properties of Grown P-N Junctions of InSb. H. C. Gorton, A. R. Zaccarioli, F. J. Reid, and C. S. Peet 354
 Preparation of High-Purity Indium Arsenide. D. Effer 357
 Use of Hall Measurements in Evaluating Polycrystalline Silicon. P. J. Olshefski, D. J. Shombert, and I. R. Weingarten 362
 Chemical Etching of Silicon, III. A Temperature Study in the Acid System. B. Schwartz and H. Robbins 365
 Rotating Cathode for the Reduction of Nitrobenzene to Hydrazobenzene. K. S. Udupa, G. S. Subramanian, and H. V. K. Udupa 373
 Adsorption of Hydrogen and Oxygen on Electrode Surfaces. R. F. Amalie, J. B. Ockerman, and P. Rüetschi 377
 Kinetics of Hydrogen Evolution at Zero Hydrogen Partial Pressure. S. Schulzinger 384
 Effect of the Helmholtz-Gouy Double Layer on the A-C Impedance of the Copper/Copper Oxide Electrode in Aqueous Solution. G. R. Hoey 387

Technical Note

The Mechanism of Electrolytic Deposition of Titanium from Fused-Salt Media. W. E. Reid, Jr. 393

Current Affairs 86C-96C

Published monthly by The Electrochemical Society, Inc., from Manchester, N. H., Executive Offices, Editorial Office and Circulation Dept., and Advertising Office at 1860 Broadway, New York 23, N. Y., combining the JOURNAL and TRANSACTIONS OF THE ELECTROCHEMICAL SOCIETY. Statements and opinions given in articles and papers in the JOURNAL OF THE ELECTROCHEMICAL SOCIETY are those of the contributors, and The Electrochemical Society assumes no responsibility for them. Subscription to members as part of membership service: subscription to nonmembers \$24.00, Single copies \$1.70 to members, \$2.25 to nonmembers. Copyright 1961 by The Electrochemical Society, Inc. Entered as second class matter on August 24, 1912. Post Office at Manchester, N. H., and mailing at special rate of postage provided for in Section 1103, Act of October 3, 1917, authorized on August 24, 1961.

81C

מנהל תחנת הכח



Publications of The ECS

THE Technical Section of this JOURNAL is devoted almost entirely to articles describing original research of one kind or another, this policy being approved by the Society's Board of Directors and implemented by the JOURNAL's Editorial Board. A few review articles are published, and may be of two types: comprehensive literature surveys in restricted areas, or wider and less-detailed reviews of informative and instructive nature. In addition, a few Feature articles are published for their general interest.

The object is, of course, to make the Technical Section of high quality and of more than current interest, so that the bound volumes of the JOURNAL will retain their value on library shelves throughout the world for many years, along with the other well-known journals of original research.

Besides the JOURNAL, the Society sponsors the publication of certain Monographs, some of which are planned by the various Divisions to fill definite needs in technical areas, and have no connection with the Society's Meetings. Others are essentially Transactions of Divisional Symposia, which must be planned very carefully so that the resulting volumes will be of wide reader value. The Monographs must, in general, meet the requirements of commercial salability, because publishers must make profits or quit.

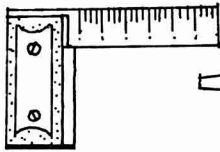
Many but not all of the articles appearing in the JOURNAL are presented at the technical sessions of the National Meetings. Not so many years ago, acceptance for the TRANSACTIONS, predecessor of the JOURNAL, was a requisite for oral presentation at a Meeting. Now, however, in the interest of planning instructive, balanced, well-rounded technical sessions which will attract members and nonmembers alike to the Meetings, there is a great demand for the inclusion of papers for which the Society has no appropriate publishing outlet. Indeed, entire symposia may fall into this category.

Are these papers of current interest only, to be discarded after the oral presentation? The favorable experience of several Divisions with "extended abstract" booklets suggests that inexpensive paperback "Transactions" containing complete manuscripts or long abstracts of all papers presented would be favorably received, especially if initial sales could be made at the Meetings themselves. The continuity of the sessions has an appeal which is lost when the papers are scattered in this and other journals, or are not published at all. However, Transactions of this sort would have to be labeled as *printed but not published* so that regular publication would not be proscribed.

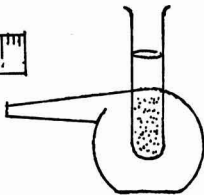
If the Society could undertake the technical part of preparing such Transactions, it would lift a burden from the Divisional officers who have found the extended abstracts of real value. It would extend equal treatment to all sessions in the most economical way. Sales of these booklets would have to be considered a service only, but the undertaking would have to be self-supporting. Dr. C. L. Faust, Chairman of the Publication Committee, has the various possibilities under consideration.

—CVK

any way you measure ANODE PERFORMANCE



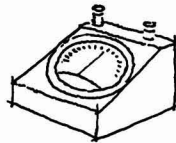
Structural and
Dimensional Uniformity?



Chemical Stability
of Treatments?



Uniform
Texture?

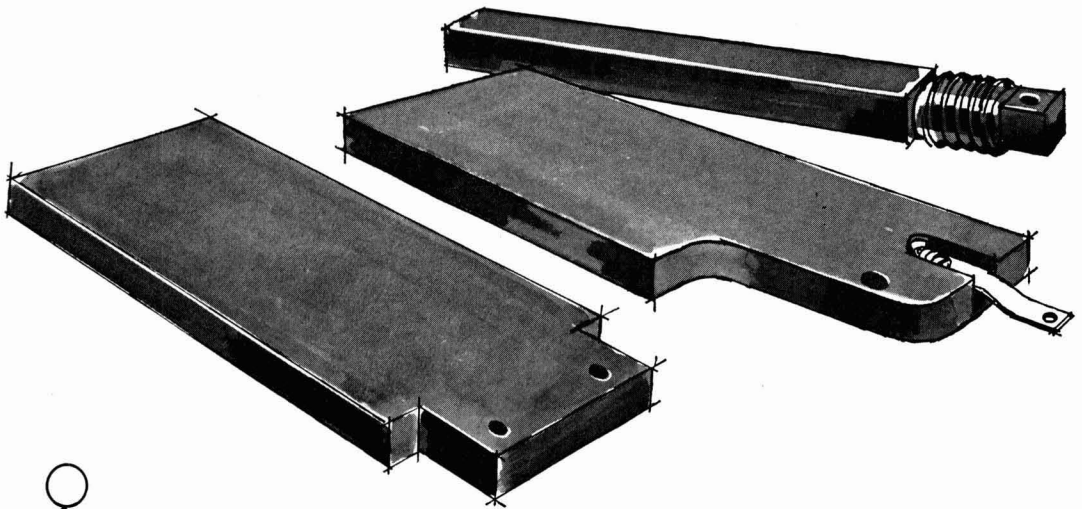


Cell
Voltage?



Pounds Consumed per ton of
Chlorine Produced?

STACKPOLE **GraphAnode® ANODES** prove second to none for **Economical Chlorine Production**



STACKPOLE
CARBON
COMPANY,
St. Marys, Pa.

CATHODIC PROTECTION ANODES • FLUXING & DE-GASSING TUBES • SALT
BATH RECTIFICATION RODS • ROCKET NOZZLES • RISER RODS • GRAPHITE
BEARINGS & SEAL RINGS • ELECTRODES & HEATING ELEMENTS • WELDING
CARBONS • VOLTAGE REGULATOR DISCS • "CERAMAGNET"® CERAMIC MAG-
NETS • ELECTRICAL CONTACTS • BRUSHES FOR ALL ROTATING ELECTRICAL EQUIP-
MENT • AND MANY OTHER CARBON, GRAPHITE AND ELECTRONIC COMPONENTS.

*Now available
for scientific
laboratories...*

THE **NEW** SARGENT CATALOG **109**



An encyclopedia of scientific instruments, apparatus and chemicals—nearly 1500 pages of comprehensive listings—for scientific men working in a professional capacity.

Comprehensive—This new edition lists over 38,000 items of scientific instruments, apparatus and chemicals. Items are compiled in familiar alphabetical order by most commonly used names. Subject finding words are located at the outside top of each page for rapid location of items. Cross references are used throughout.

Up-to-date illustrations—All principle items are illustrated on the same page as the catalog listing. Each illustration is up-to-date and accurate—corresponding with the merchandise supplied under the catalog listing.

Permanent catalog number system—The per-

manent Sargent catalog number system is perpetuated—with numbers in sequence with the alphabetical listing and fully identifying each item to insure ease and accuracy in ordering. Completely descriptive titles in bold-face type distinguish alternatives and similarities between listings.

Current prices—Prices on each item are current at the time of printing.

Detailed index—an elaborate sixty-four page subject index is provided with extensive cross references.

Distribution of Catalog 109 is now being made to scientific and purchasing personnel. Your recommendations for the distribution of this catalog in your laboratory or department will be welcomed.

SARGENT SCIENTIFIC LABORATORY INSTRUMENTS • APPARATUS • SUPPLIES • CHEMICALS

E. H. SARGENT & CO., 4647 W. FOSTER, CHICAGO 30, ILLINOIS
DETROIT 4, MICH. • DALLAS 35, TEXAS • BIRMINGHAM 4, ALA. • SPRINGFIELD, N. J.

Investigation of the Electrochemical Characteristics of Organic Compounds

VII. Organic Positive Iodine and Aliphatic Azo Compounds

R. Glicksman and C. K. Morehouse¹

Semiconductor and Materials Division, Radio Corporation of America, Somerville, New Jersey

ABSTRACT

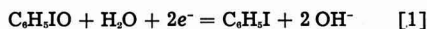
The electrochemical characteristics of organic positive iodine compounds such as iodobenzene and iodoxybenzene, and aliphatic azo compounds such as azodicarbonamide and *N,N'*-dichloroazodicarbonamide in various electrolytes are presented. Performance characteristics of magnesium and aluminum dry cells containing these organic oxidizing agents as cathode materials are also presented.

Organic Positive Iodine Compounds

Electrochemical characteristics.—Organic positive iodine compounds have long been recognized as strong oxidizing agents. For example, both iodoso compounds (RIO) and iodoxy compounds (RIO₂) react quantitatively with iodides in acid solution to yield the parent iodo compound and free iodine (1).

In agreement with the chemical evidence, the half-cell potential discharge data for various iodobenzene compounds and iodoxybenzene shown in Fig. 1 indicate the strong oxidizing character of the organic positive iodine compounds. The half-cell potential data were obtained by discharging these compounds at a rate of 0.005 amp/g in 250 g MgBr₂ · 6H₂O/l electrolyte by a technique previously described (2) and used for the study of other organic oxidizing agents (3-8).

Theoretical capacity and electrode efficiency data for these compounds are presented in Table I. The theoretical capacities were computed according to Faraday's law, assuming a 2 and 4 electron change for the iodoso and iodoxybenzene compounds, respectively, in accordance with the following equations:



The iodobenzene and iodoxybenzene compounds operate initially at potentials comparable to those of organic positive N-halogen compounds and provide considerably higher electrode efficiencies (3). They differ from the latter compounds in that iodine is linked to a carbon atom rather than to a nitrogen

¹ Present address: Globe Battery Company, Division of Globe Union Inc., Milwaukee, Wisconsin.

Table I. Theoretical capacities and electrode efficiencies of various organic positive iodine compounds

Compound	Theoretical capacity, amp-min/g	Experimental capacity,* amp-min/g	Electrode efficiencies, %
iodoxybenzene	27.3	17.0	62.3
iodobenzene	14.6	11.8	80.8
o-iodosobenzoic acid	12.2	10.0	82.0
iodobenzene diacetate	10.0	2.1	21.0

* Capacity calculated on the basis of a -0.40 v end potential.

atom. Further, all of the types of compounds shown in Fig. 1 are peculiar to iodine. Similar compounds of the other halogens either do not exist at all or are so unstable that they may be considered non-existent for all practical purposes (9).

The lower cathode potential of ortho iodosobenzoic acid as compared to the other iodoso compounds is believed due to the heterocyclic iodine-oxygen ring structure of the compound, C₆H₄COOIOH, formed by the interaction of the iodoso and acid groups (9). The poor electrode efficiency of iodobenzene diacetate as compared to the other iodoso compounds is attributed to its instability in aqueous solution.

In addition to iodoso and iodoxy compounds, iodine forms two other types of organic compounds in which it is present in a positive oxidation state, the iodonium salts (R₂IX) and the iodyl compounds (R₂IOX). The iodyl compounds were the last to be discovered and have not yet been studied to any great extent. The more readily available iodonium salts have been investigated both by polarography at the dropping mercury electrode and by coulometry at controlled potential (10, 11). The half-cell potential discharge data shown in Fig. 1 for a compound of this type, diphenyliodonium chloride, show it to be a weaker oxidizing agent than either iodoso or iodoxybenzene.

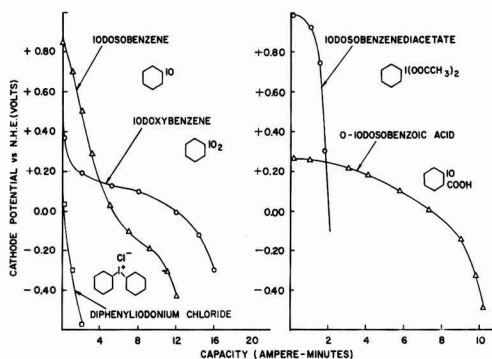


Fig. 1. Half-cell potential discharge curves of various organic positive iodine compounds discharged at a rate of 0.005 amp/g in 250 g MgBr₂ · 6H₂O/l electrolyte.

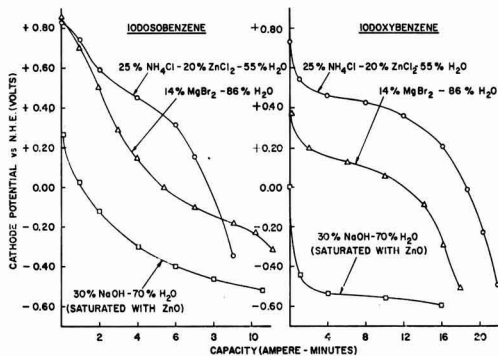


Fig. 2. Half-cell potential discharge curves of iodosobenzene and iodoxybenzene discharged at a rate of 0.005 amp/g in various electrolytes.

Additional half-cell potential discharge data for iodosobenzene and iodoxybenzene in electrolytes of different pH are shown in Fig. 2. In general, the cathode potentials and coulombic capacities of these compounds increase with decreasing electrolyte pH. The low cathode potential of iodoxybenzene in the alkaline electrolyte is attributed to the hydrolysis of iodoxybenzene to iodate and benzene (12) with subsequent reduction of the iodate ion. The similar cathode potentials found for inorganic iodate compounds in alkaline electrolyte (13) are in agreement with this reasoning.

The half-cell potential discharge data shown in Fig. 1 and 2, along with the polarographic data of organic positive iodine compounds in the literature (14), indicate that the reduction of iodoso and iodoxybenzene takes place according to Eq. [1] and [2].

Experimental dry-cell data.—Experimental AA-size magnesium and aluminum dry cells which contained iodoxybenzene, iodosobenzene, and ortho iodosobenzoic acid as cathodes were assembled in the usual manner. Magnesium AZ10A alloy and aluminum Al-M-373 duplex alloy cans were used as the anodes. The aluminum alloy was a duplex product comprised of an inner layer having the composition 95.5% Al, 3% Mg, 1% Zn, and 0.5% Mn, and an external layer of superpurity aluminum which comprised 30% of the total weight of the can. The cathode mix consisted of two parts by weight of the organic positive iodine compound to one part by weight of Cabot experimental battery black. For the magnesium cells, a 371 g MgBr₂ · 6H₂O/1 electrolyte was used. A 2M AlCl₃ electrolyte was used in the aluminum cells.

Performance characteristics of these cells on a 4- and 50-ohm continuous discharge test are shown in Fig. 3 and 4. These data show that, although organic positive iodine cells may be competitive with existing inorganic cells on heavy-drain tests, they do not compare favorably on lighter drain tests. Because these cells have not given adequate shelf life, they appear to be more suitable for use as reserve cells, especially if compounds with two functional groups such as diiodoxybenzene become available.

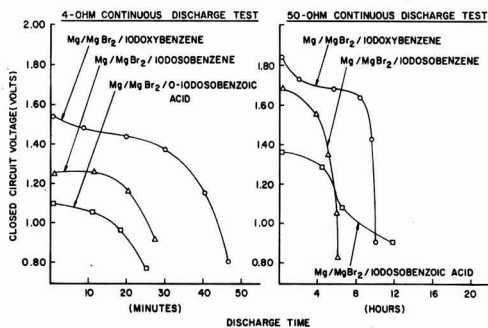


Fig. 3. AA-size magnesium dry cells containing various organic positive iodine compounds as cathodes discharged through 4- and 50-ohm resistances at 70° ± 2°F (50% R.H.).

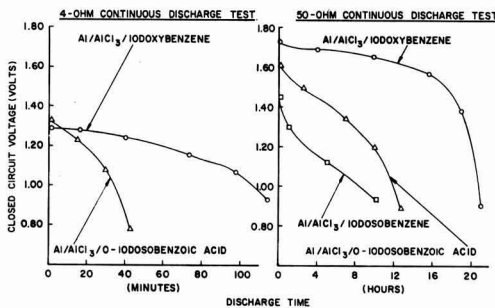
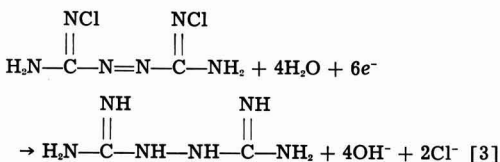


Fig. 4. AA-size aluminum dry cells containing various organic positive iodine compounds as cathodes discharged through 4- and 50-ohm resistances at 70° ± 2°F (50% R.H.).

Organic Azo Compounds

Electrochemical characteristics.—Half-cell potential studies of the reduction products of nitrobenzene in various electrolytes (4) showed azobenzene to operate at too low a cathode potential to be useful as a cathode material in primary batteries. Similarly azo-tert-butane and 2,2'-azodi-iso-butyronitrile also had low cathode potentials when discharged in a magnesium bromide electrolyte.

However, certain aliphatic azo compounds such as azodicarbonamide and azodicarbonamide are strong oxidizing agents able to liberate iodine from iodide solution. The high cathode potential of these compounds in various electrolytes is illustrated by the half-cell potential discharge data shown in Fig. 5 for azodicarbonamide and *N,N'*-dichloroazodicarbonamide. The reduction of this positive N-halogen compound is believed to take place in accordance with the following equation:



In this reaction the azo group is reduced to the hydrazo group with a 2-electron change, while each positive chlorine group is reduced to the chloride ion with a 2-electron change. This type of reaction

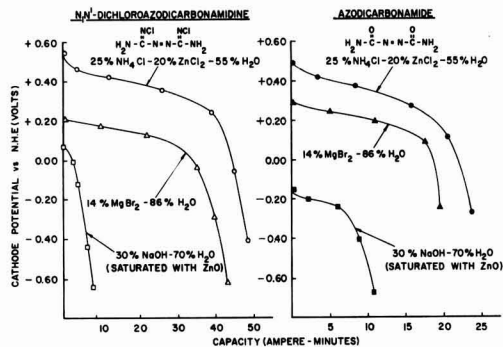
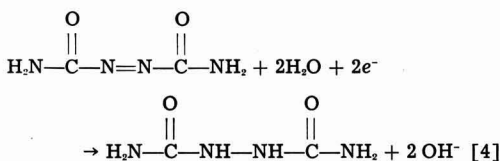


Fig. 5. Half-cell potential discharge curves of N,N' -dichloroazodicarbonamidine and azodicarbonamide discharged at a rate of 0.005 amp/g in various electrolytes.

is in agreement with the analytical data of Schmelkes and Marks (15) which show the compound to liberate 6 equivalents in an iodimetric titration. The high electrode efficiencies for N,N' -dichloroazodicarbonamidine, shown in Table II, further indicate that reduction takes place according to Eq. [3].

Similarly, the reduction of azodicarbonamide is believed to take place according to the following equation:



In agreement with Eq. [4] half-cell potential-discharge data for hydrazodicarbonamide in 25% NH_4Cl -20% ZnCl_2 electrolyte indicate that this compound is difficult to reduce and provides little or no capacity. It should be noted that hydrazodicarbonamide, the reduction product of azodicarbonamide, is a considerably stronger reducing agent and has a higher anode potential than hydrazobenzene and 2,2'-hydrazodi-iso-butyronitrile (16).

Experimental dry-cell data.—Experimental AA-size dry cells which contained N,N' -dichloroazodi-

Table II. Theoretical capacities and electrode efficiencies of N,N' -dichloroazodicarbonamidine and azodicarbonamide in various electrolytes

Compound and electrolyte	Theoretical capacity, amp-min/g	Experimental capacity,* amp-min/g	Electrode efficiencies, %
N,N' -dichloroazodicarbonamidine			
$\text{NH}_4\text{Cl}-\text{ZnCl}_2-\text{H}_2\text{O}$	52.7**	48.2	91.5
$\text{MgBr}_2-\text{H}_2\text{O}$		41.2	78.2
$\text{NaOH}-\text{H}_2\text{O}$		5.9	11.2
Azodicarbonamide			
$\text{NH}_4\text{Cl}-\text{ZnCl}_2-\text{H}_2\text{O}$	27.7	24.2	87.4
$\text{MgBr}_2-\text{H}_2\text{O}$		19.6	70.8
$\text{NaOH}-\text{H}_2\text{O}$		8.8	31.8

* Capacity calculated on basis of a -0.40 v end potential.

** Based on 6-electron change (a 2-electron change for the azo group and a 2-electron change for each positive chlorine group).

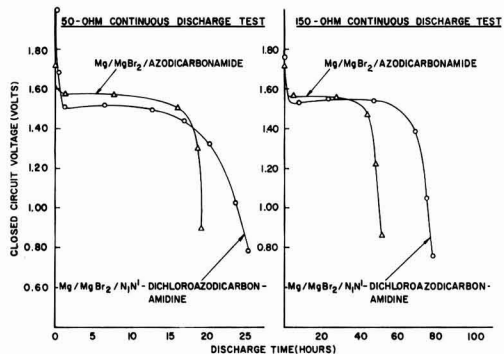


Fig. 6. AA-size $\text{Mg}/\text{MgBr}_2/\text{azodicarbonamide}$ and $\text{Mg}/\text{MgBr}_2/\text{N,N}'\text{-dichloroazodicarbonamidine}$ dry cells discharged through 4- and 50-ohm resistances at $70 \pm 2^\circ\text{F}$ (50% R.H.).

carbonamidine and azodicarbonamide as cathodes were assembled, using a magnesium AZ10A alloy can anode and a 500 g $\text{MgBr}_2 \cdot 6\text{H}_2\text{O}/\text{l}$ electrolyte. The cathode mix consisted of two parts by weight of the azo compound to one part by weight of Shawinigan acetylene black.

Performance characteristics of these cells on 50- and 150-ohm continuous-discharge tests are shown in Fig. 6. These cells have favorably high flat voltage-time discharge curves and provide capacities comparable to those of magnesium- and zinc-African manganese dioxide cells on heavy-drain tests. A preliminary shelf-life study of these dry cell systems indicate that they do not have a favorable shelf life.

Acknowledgment

The authors wish to express their appreciation to Dr. R. Joiner, of the Wallace and Tiernan Company, for supplying some of the azo compounds used in this investigation, and to Dr. F. M. Beringer, of the Brooklyn Polytechnic Institute, for supplying the diphenyl iodonium salt.

Manuscript received Oct. 26, 1960. This paper was prepared for delivery before the Houston Meeting, Oct. 9-13, 1960.

Any discussion of this paper will appear in a Discussion Section to be published in the December 1961 JOURNAL.

REFERENCES

- R. B. Sandin, *Chem. Rev.*, **32**, 249 (1943).
- C. K. Morehouse and R. Glicksman, *This Journal*, **103**, 94 (1956).
- C. K. Morehouse and R. Glicksman, *ibid.*, **104**, 467 (1957).
- R. Glicksman and C. K. Morehouse, *ibid.*, **105**, 299 (1958).
- R. Glicksman and C. K. Morehouse, *ibid.*, **105**, 613 (1958).
- R. Glicksman and C. K. Morehouse, *ibid.*, **106**, 288 (1959).
- R. Glicksman and C. K. Morehouse, *ibid.*, **106**, 741 (1959).
- R. Glicksman and C. K. Morehouse, *ibid.*, **107**, 717 (1960).
- A. C. Loonam, "Encyclopedia of Chemical Technology," Vol. VII, pp. 965-972, Interscience Encyclopedia, Inc., New York (1951).

10. H. E. Bachofner, F. M. Beringer, and L. Meites, *J. Am. Chem. Soc.*, **80**, 4269 (1958).
11. H. E. Bachofner, F. M. Beringer, and L. Meites, *ibid.*, **80**, 4274 (1958).
12. I. Masson, E. Race, and F. E. Pounder, *J. Chem. Soc.*, **1935**, 1669.
13. C. K. Morehouse and R. Glicksman, *This Journal*, **107**, 361 (1960).
14. E. Fornasari, M. Scarpa, and P. Lanza, *Atti. Accad. nazl. Lincei*, **14**, 70, 272 (1953).
15. F. C. Schmelkes and H. C. Marks, *J. Am. Chem. Soc.*, **56**, 1610 (1934).
16. R. Glicksman, "Investigation of the Electrochemical Characteristics of Organic Compounds. VIII. Hydrazine and Hydroxylamine Compounds," paper presented at Electrochemical Society Meeting, October 9-13, 1960, Houston.

Oxidation Studies on Ni-Al Alloys

Kazuo Fueki and Hirotsugu Ishibashi

Department of Applied Chemistry, Faculty of Engineering, University of Tokyo, Tokyo, Japan

ABSTRACT

In order to clarify the oxidation behavior of binary alloys, the oxidation of Ni-Al alloys was studied. Oxidation rates were measured by means of a vacuum microbalance over the temperature range of 700°-900°C. The rate data of all specimens were found to follow the parabolic rate law. Oxide films were examined by means of metallographic, x-ray diffraction, and electron diffraction methods. Quantitative chemical analysis of oxide films stripped from basis alloys was carried out in order to determine oxidized amounts of nickel and aluminum. The change of the composition of alloy surfaces was investigated by measuring lattice parameters of alloy surfaces before and after oxidation. On the basis of these results the oxidation of alloys is discussed.

The oxidation behavior of alloys is considerably complex and not so well understood as that of pure metals. In order to clarify the oxidation behavior of alloys, the authors and their collaborators have carried out a series of studies on the high temperature oxidation of binary alloys. In earlier papers (1, 2) behaviors of Cu-Ni and Ni-Co alloys were described. This paper reports on the similar study of the oxidation of Ni-Al alloys.

Measurement of Oxidation Rate

Specimens and surface preparation.—Five samples (pure Ni, and Ni-Al alloys containing 1.02, 2.95, 7.07, and 12.0 mole % Al, respectively) were prepared from electrolytic Ni of 99.98% purity (impurity: 0.013% Co, 0.001% Cu, 0.002% C, 0.0003% S) and 99.998% Al by induction melting *in vacuo* using alumina crucibles. Ingots were rolled into sheets of 1 and 0.1 mm thickness. From the sheets of 0.1 mm thickness specimens of 4 x 1.5 cm were taken. These were polished with No. 02, 04, and 06 polishing papers, washed with absolute alcohol, dried in a desiccator, and weighed by means of a chemical microbalance.

Apparatus and method.—A vacuum microbalance and accessories were used for all rate measurements. This apparatus was essentially the same as that devised by Gulbransen (3-5). The sensitivity of the microbalance was 8.60 $\mu\text{g}/0.001$ cm deflection. After the temperature of the Nichrome furnace was raised to the desired reaction temperature, a finished and weighed specimen was suspended by a fine platinum wire from the beam of the microbalance placed in the balance tube, which was then closed with a glass cover; then the air in the tube was reduced to the pressure of 150 mm Hg. Weight changes were followed by observing a marked

point on the balance beam by means of a micrometer microscope. The temperature was kept constant within $\pm 3^\circ\text{C}$ deviation during the run. As soon as the run was over, the specimen was removed and weighed by means of a chemical microbalance. The oxidation-time curve was determined from weights of the specimen before and after the oxidation and weight changes during the run.

Results.—Results are shown in Fig. 1 to 5. Reproducible results were obtained on duplicate runs of the alloy specimens. The weight gain of all spec-

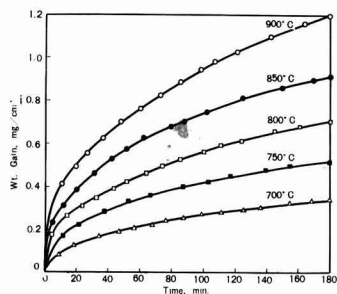


Fig. 1. Oxidation of pure nickel

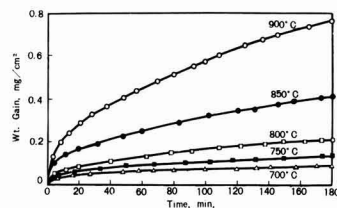


Fig. 2. Oxidation of 1.02% Al alloy

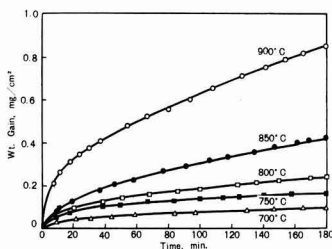


Fig. 3. Oxidation of 2.95% Al alloy

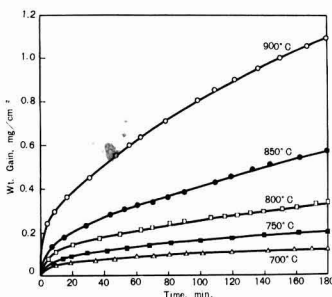


Fig. 4. Oxidation of 7.07% Al alloy

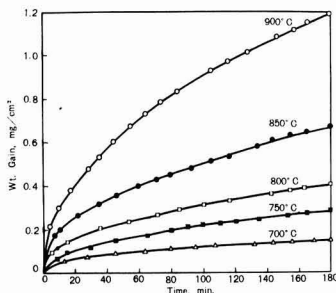


Fig. 5. Oxidation of 12.0% Al alloy

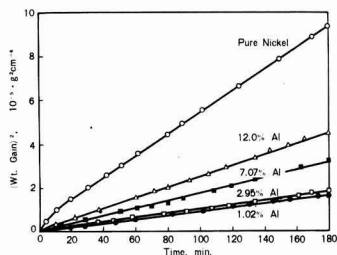


Fig. 6. Parabolic plot of oxidation, 850°C

imens followed the parabolic rate law (Fig. 6). Parabolic rate constants were calculated from parabolic plots in the time interval where the law $W^2 = k_p t + C$ was found to hold. The constants are listed in Table I.

Figure 7 shows the plot of the weight gain after 3 hr of oxidation vs. the alloy composition. The weight gain decreases by the addition of aluminum of 1%. From this percentage onward, it begins to increase with the aluminum content. This depend-

Table I. Parabolic rate constants

Alloy	Temp, °C	Rate constant k_p , $g^2 \text{ cm}^{-4} \text{ sec}^{-1}$
Pure nickel	700	1.02×10^{-11}
	750	2.22×10^{-11}
	800	4.45×10^{-11}
	850	8.15×10^{-11}
	900	1.21×10^{-10}
1.02% Al	700	6.65×10^{-13}
	750	1.94×10^{-12}
	800	4.39×10^{-12}
	850	1.67×10^{-11}
	900	5.65×10^{-11}
2.95% Al	700	7.12×10^{-13}
	750	2.14×10^{-12}
	800	5.76×10^{-12}
	850	1.58×10^{-11}
	900	6.48×10^{-11}
7.07% Al	700	1.16×10^{-12}
	750	3.80×10^{-12}
	800	8.89×10^{-12}
	850	2.97×10^{-11}
	900	1.16×10^{-10}
12.0% Al	700	1.71×10^{-12}
	750	7.96×10^{-12}
	800	1.48×10^{-11}
	850	4.26×10^{-11}
	900	1.35×10^{-10}

ence of weight gain on composition is slightly different from the result of Horn (6).

Figure 8 gives the plot of $\log k_p$ vs. $1/T$. The data of pure nickel can be fitted into a single straight line, and the Arrhenius formula is given in the form

$$k_p = 6.0 \times 10^{-5} \exp(-28,400/RT) \text{ g}^2 \text{ cm}^{-4} \text{ sec}^{-1}$$

On the other hand, the data of alloys cannot be fitted into a straight line. The slope of curves becomes steeper with decreasing $1/T$ value. Preece and Lucas (7) have reported similar results.

Investigations of Oxide Films

Layer structure expected from $T-\Delta G$ diagram.—In general, oxide films formed on metals and alloys consist of several layers. It has been shown in the previous papers (8, 9) that possible layer structures can be predicted by using the $T-\Delta G$ diagram which is a type of thermodynamic diagram.

Free energy equations necessary for the preparation of the diagram of Ni-Al-O system are:

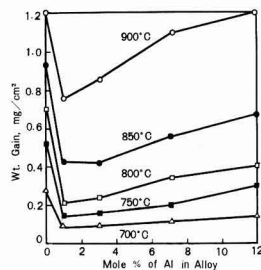


Fig. 7. Plot of weight gain after 3 hr oxidation vs. alloy composition.

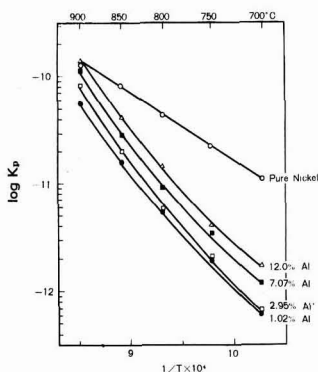
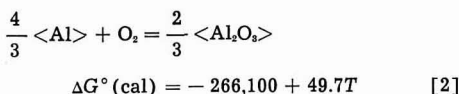
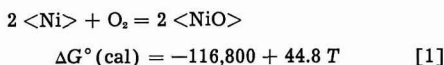


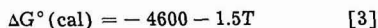
Fig. 8. Temperature dependence of parabolic rate constant



These equations were taken from the paper of Richardson and Jeffes (10). At high temperature NiO and Al₂O₃ may form NiO·Al₂O₃ according to the reaction



However, the free energy change of this reaction is small



Therefore, it is rather insignificant for contribution to the free energy calculation. The change of the chemical potential of metal A or B caused by alloying is several kcal/mole (11), so the contribution to free energy calculation can be neglected as the first approximation. Consequently, the T - ΔG diagram of the Ni-Al-O system can be prepared by using only two equations [1] and [2]. Figure 9 shows the obtained diagram. Since the growth rate of Al₂O₃ is considered to be lower than that of NiO, a layer structure shown in Figure 10 can be expected.

Metallographic studies.—The cross section of alloy specimens oxidized in air at 1000°C for 20 hr

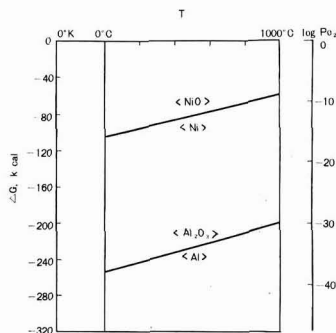


Fig. 9. T - ΔG diagram of Ni-Al-O system

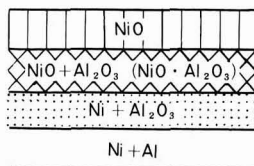


Fig. 10. Expected layer structure of oxide film

was examined by means of a metallographic microscope. A subscale of considerable thickness was found in addition to the outer oxide film consisted of two layers (Fig. 11a and b). Further investigations were carried out to obtain more information on both outer and inner layers. Alloys containing 2.95, 7.07, and 12.0% Al were oxidized in air at 900°C for 3 hr. Then the oxidized specimens were immersed in 10% Br₂-ethanol solution to strip the oxide films. The resulting films were examined by means of a microscope. The outer layer of all oxide films was found to be green and compact. It was also found that the inner layer of oxides of 2.95 and 7.07% Al alloys was porous (Fig. 12a and b), and that the inner layer of the oxide of 12.0% Al alloy was nonporous (Fig. 12c). The stripped film of 12.0% Al alloy was further treated in hot nitric acid solution in order to dissolve nickel oxide. By this treatment only the inner layer was obtained. Microscopic observation revealed the obtained film to be porous (Fig. 13).

X-ray study.—Oxide films on alloys oxidized for 3 hr at temperatures between 700° and 900°C were examined by means of an x-ray diffractometer.

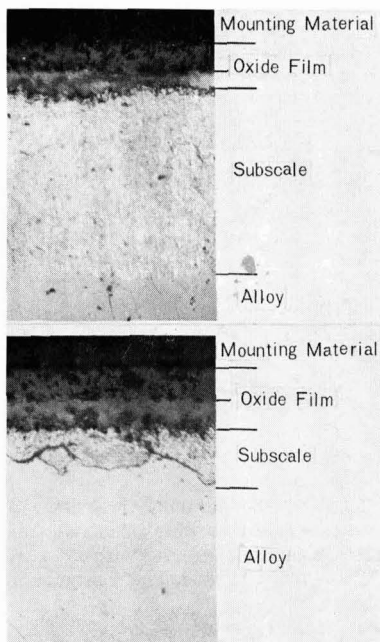


Fig. 11. Cross section of alloys oxidized for 20 hr at 1000°C, under polarized light; (a) (top) 7.07% Al alloy. (b) (bottom) 12.0% Al alloy. Magnification 250X before reduction for publication.

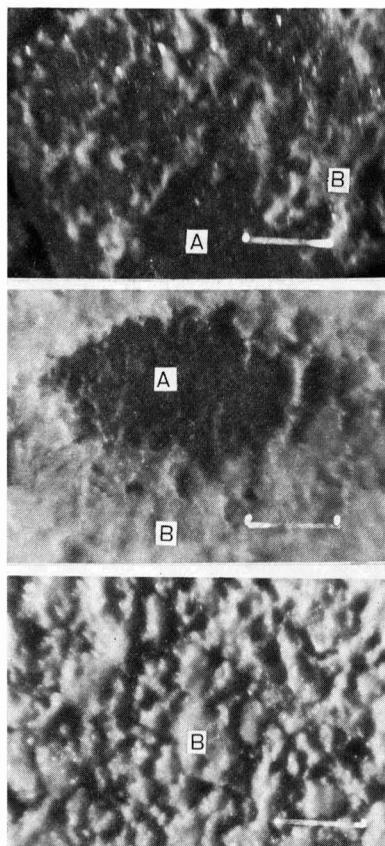


Fig. 12. Lower surface of stripped oxide films. A, outer layer; B, inner layer. (a) (top) 2.95% Al alloy. (b) (center) 7.07% Al alloy. (c) (bottom) 12.0% Al alloy. Magnification 200X before reduction for publication.

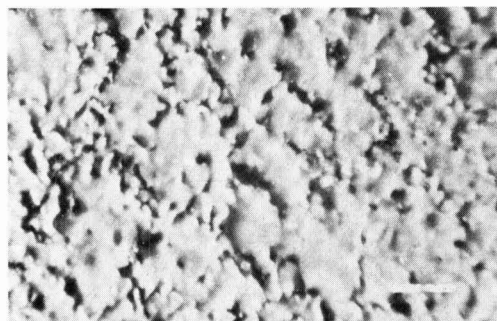


Fig. 13. Lower surface of oxide film treated with nitric acid, 12.0% Al alloy. Magnification 100X.

Strong diffraction lines of NiO and weak diffraction lines of Ni-Al alloy were observed. From these results it is considered that the outer layer consists of only NiO. Neither Al_2O_3 nor $\text{NiO}\cdot\text{Al}_2\text{O}_3$ were detected, although the formation of Al_2O_3 was anticipated.

Electron diffraction study.—Oxide films formed at 700°, 800°, or 900°C were stripped by the al-

Table II. Aluminum compounds identified by the electron transmission method

Temp, °C	Time, hr	2.95% Al	Alloy 7.07% Al	12.0% Al
700	3	$\gamma\text{-Al}_2\text{O}_3$	$\gamma\text{-Al}_2\text{O}_3$	$\gamma\text{-Al}_2\text{O}_3$
800	3	$\gamma\text{-Al}_2\text{O}_3$ $\text{NiO}\cdot\text{Al}_2\text{O}_3$	$\gamma\text{-Al}_2\text{O}_3$ $\text{NiO}\cdot\text{Al}_2\text{O}_3$	$\gamma\text{-Al}_2\text{O}_3$ $\text{NiO}\cdot\text{Al}_2\text{O}_3$
900	3	$\text{NiO}\cdot\text{Al}_2\text{O}_3$	$\text{NiO}\cdot\text{Al}_2\text{O}_3$	$\text{NiO}\cdot\text{Al}_2\text{O}_3$

coholic bromine method and then heated in nitric acid solution. White or bluish white films obtained in this way were investigated by the electron transmission method. The electron beam could penetrate only the thin parts of the film. Aluminum compounds identified by this method are listed in Table II.

From the results of metallographic and electron diffraction studies, it can be concluded that the aluminum compounds in the inner layer are $\gamma\text{-Al}_2\text{O}_3$, $\text{NiO}\cdot\text{Al}_2\text{O}_3$, or both $\gamma\text{-Al}_2\text{O}_3$ and $\text{NiO}\cdot\text{Al}_2\text{O}_3$.

Chemical analysis.—Oxide films formed on alloys oxidized under various conditions were stripped by the alcoholic bromine method. The resulting film was heated in concentrated nitric acid. After filtration, the residue was decomposed by the alkali fusion method and added to the filtrate. The amount of nickel was determined by the polarographic method, while that of aluminum was determined by the colorimetric method. Results are summarized in Table III.

From the comparison of the aluminum content in the alloy with that in the oxide, it can be concluded that aluminum was preferentially oxidized in those cases. Figure 14 shows plots of nickel and aluminum losses of 12% Al alloy at 900°C vs. the square root of the oxidation time. It is apparent from this figure that the conversion of nickel and aluminum into oxides followed the parabolic rate law. Figure 15 gives the relation between nickel and aluminum losses after 3 hr of oxidation at

Table III. Results of chemical analysis

Alloy	Temp, °C	Time, min	Wt. gain, $\mu\text{M}/\text{cm}^2$	Ni loss, $\mu\text{M}/\text{cm}^2$	Al loss, $\mu\text{M}/\text{cm}^2$	Mole % of Al in oxide
Pure Ni	700	180	21.0	21.0*	0	0
	900	180	75.0	75.0*	0	0
1.02% Al	700	180	6.37	5.62	0.375	6.2
	900	180	47.5	43.0	2.14	4.8
2.95% Al	700	180	6.10	5.12	0.695	11.9
	900	180	53.5	44.5	5.00	10.1
7.07% Al	700	180	7.67	5.51	1.28	18.9
	900	180	68.2	45.0	15.3	25.3
12.0% Al	700	180	9.48	6.09	2.17	26.3
	750	180	18.1	10.6	4.97	31.8
	800	180	25.8	13.1	7.74	37.2
	850	180	42.2	21.2	13.6	39.1
	900	30	26.8	14.4	7.72	34.5
	900	65	46.2	23.9	14.4	38.7
	900	120	57.2	27.8	17.5	38.7
	900	180	74.5	38.6	23.9	38.3

* Ni loss calculated from the weight gain.

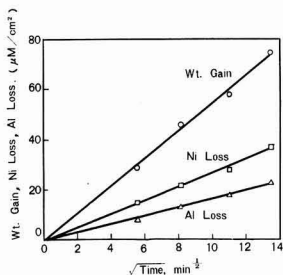


Fig. 14. Plot of nickel and aluminum losses vs. square root of oxidation time.

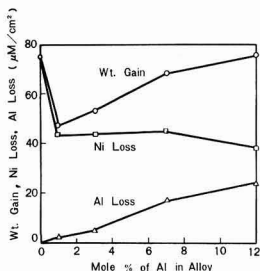


Fig. 15. Plot of nickel and aluminum losses, vs. alloy composition after 3 hr of oxidation at 900°C.

900°C vs. the alloy composition. It is easily seen from this figure that the addition of aluminum of about 1 mole % to nickel decreases the nickel loss but the addition of more aluminum does not cause more decrease of the nickel loss. It is also seen that the aluminum loss increases with the increase in aluminum content of the alloy and that the increased weight gain with increase in aluminum content in the composition range of 1-12 mole % Al is due to the increase of the aluminum loss.

X-ray Study of Alloy Surfaces

In the oxidation of binary alloys the less noble constituent metal is often oxidized preferentially and the constituent is depleted at the alloy surface. Since the lattice parameter varies with the alloy composition, one can estimate the latter by measuring the former. In order to examine the change of the composition of alloy surfaces, lattice parameters were measured before and after oxidation. Specimens used for the determination of lattice parameters of unoxidized alloys were prepared as follows: alloy pieces of 1.5 cm x 2 cm x 1 mm were polished with No. 02, 04, and 06 polishing papers, washed with soap and water, dried in a desiccator, and annealed *in vacuo* at 700°C for 3 hr. Other specimens treated in a similar manner were oxidized in air at 700° or 900°C for 1 or 3 hr and used for the determination of lattice parameters of oxidized alloy surfaces. Lattice parameters were calculated from the diffraction line of (311) plane. The diffraction angle 2θ was about 130°, since the x-ray of $\text{FeK}\alpha_1$ was used. No change was found on alloys oxidized at 700°C, whereas the considerable depletion of aluminum was found on alloys oxidized at 900°C (Fig. 16).

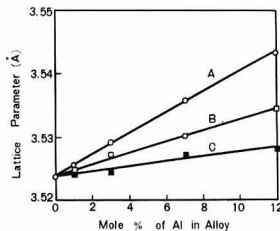


Fig. 16. Lattice parameters of alloy surfaces before and after oxidation at 900°C. A, before oxidation; B, after 1 hr of oxidation; C, after 3 hr of oxidation.

Discussion

Proposed layer structure.—From Fig. 10 and the results of metallographic, x-ray diffraction, and electron diffraction studies, such a layer structure as schematically shown in Fig. 17 is proposed as the structure of the oxide formed at 900°C.

Mechanism of formation of Al_2O_3 and $\text{NiO}\cdot\text{Al}_2\text{O}_3$ Films.—It is well known that the oxidation rate of alloys containing aluminum as an alloying element is often reduced owing to the formation of the protective Al_2O_3 film on these alloys. In order to obtain information on such protective Al_2O_3 film, pure aluminum and Fe-Al alloy containing 15.2 mole % Al were oxidized at 600° and 900°C, respectively. Figure 18 gives oxidation-time curves. It is seen that the weight gain tends to an almost constant value asymptotically with the lapse of time. Oxide films formed on these specimens were stripped by the alcoholic iodine method and examined by the electron diffraction method. It was found that the film on pure aluminum consisted of $\gamma\text{-Al}_2\text{O}_3$ and that the film on Fe-Al alloy consisted of $\alpha\text{-Al}_2\text{O}_3$ and $\alpha\text{-Fe}_2\text{O}_3$. Chemical analysis of the oxide film formed on the Fe-Al alloy after 3 hr oxidation at 900°C showed that the aluminum loss was about 2.3 $\mu\text{M}/\text{cm}^2$ and that the aluminum content in the oxide was 85 mole %.

In case of the oxidation of Ni-Al alloy containing 12 mole % of aluminum at 900°C, the conversion of aluminum into its oxide followed the parabolic rate law and the aluminum loss after 3 hr oxidation was 23.9 $\mu\text{M}/\text{cm}^2$. This aluminum loss is about ten times

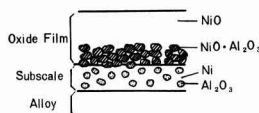


Fig. 17. Schematic drawing of proposed layer structure

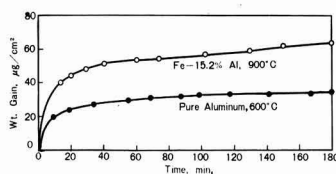


Fig. 18. Oxidation of pure aluminum and oxidation of Fe-Al alloy containing 15.2% Al.

as much as that in case of the formation of the protective film of Al_2O_3 . The electron diffraction study revealed that the oxide of aluminum was $NiO \cdot Al_2O_3$, and microscopic observation of the $NiO \cdot Al_2O_3$ film showed the film to be porous. These facts suggest that the oxidation mechanism of aluminum contained in Ni-Al alloys is different from that of aluminum contained in the Fe-Al alloy.

From the comparison of two oxidation curves in Fig. 18, it is concluded that the protective Al_2O_3 film on the Fe-Al alloy was formed directly on the alloy surface from metallic aluminum. In case of the oxidation of Ni-Al alloys at $900^\circ C$, a subscale of considerable depth was observed. The metallographic observation on the $NiO \cdot Al_2O_3$ film showed that the film was a conglomerate of $NiO \cdot Al_2O_3$ grains. These findings suggest that the $NiO \cdot Al_2O_3$ film is formed according to the following mechanism: Oxygen is dissolved at the oxide-subscale interface, diffuses inward and combines with aluminum to form Al_2O_3 particles, which go into the oxide phase as the oxide-subscale interface advances toward the interior, and reacts with NiO so that $NiO \cdot Al_2O_3$ is produced. The resulting $NiO \cdot Al_2O_3$ grains form a porous film as a result of conglomeration.

In case of the oxidation of Ni-Al alloys at $700^\circ C$, the existence of $\gamma-Al_2O_3$ was shown by the electron diffraction study. X-ray study of alloy surfaces suggested that there was no subscale. Accordingly, a similar mechanism of the formation of Al_2O_3 film can be expected as in case of the oxidation of the Fe-Al alloy containing 15.2 mole % aluminum.

Rate-determining step.—X-ray study of alloy surfaces and metallographic study showed that the surface of alloys oxidized at $900^\circ C$ consisted of nickel containing Al_2O_3 particles in the dispersed form. The oxidation of alloys was found to follow the parabolic rate law which is fitted to the oxidation of pure nickel. In addition, the loss of nickel alloys was found to be as much as that of pure nickel. These facts suggest that the rate-determining step of the oxidation of Ni-Al alloys may be the diffusion of nickel ions through the nickel oxide layer.

Effect of added aluminum.—As may be seen in Fig. 7 and 8, the addition of small amounts of aluminum improves the oxidation resistance of nickel at $700^\circ C$. This is considered to be due to the formation of the adherent and protective $\gamma-Al_2O_3$ film on the alloy. On the other hand, the oxidation rate of Ni-Al alloys at $900^\circ C$ is not so reduced by the addition of aluminum. This is considered to be due to the formation of the porous $NiO \cdot Al_2O_3$ film which cannot suppress the flow of nickel ions effectively. As discussed above, a close relation between the formation of the porous $NiO \cdot Al_2O_3$ film and the subscale formation seems to exist. Accordingly, it is considered that a close relationship exists between the

effect of added aluminum on the oxidation of nickel and the subscale formation.

It is known that the oxidation rate of metals forming oxide layers consisting of metal-deficient semiconductors is often increased by adding metals of higher valence than that of the basis metal. For instance, the addition of small amounts of chromium to nickel increases the oxidation rate of nickel (6, 12). Wagner (13) has explained that this is due to the increase in the concentration of cation vacancies in NiO. It was found that the oxidation rate of Ni-Al alloys at $900^\circ C$ increases with the increase in the aluminum content in the composition range of 1-12 mole % aluminum. If this increase is due to the aforementioned Wagner mechanism, the nickel loss after the same time of exposure would be increased with the aluminum content in the alloy. Chemical analysis of oxide films did not show any increase in the nickel loss. Consequently, it is concluded Wagner's theory is not applicable to this increased rate of oxidation with aluminum additions.

Acknowledgment

The authors wish to express their sincere thanks to Professors Y. Nagai, S. Oka, and T. Mukaibo for their suggestions and discussions. The authors are also indebted to Mr. M. Shibuya and Mr. Y. Oyama for their help in carrying out the experiments.

Manuscript received Oct. 9, 1959.

Any discussion of this paper will appear in a Discussion Section to be published in the December 1961 JOURNAL.

REFERENCES

1. K. Fueki, *Kogyo Kagaku Zasshi* (J. Chem. Soc. Japan, Industrial Chemistry Section), **63**, 717 (1960).
2. K. Fueki, *ibid.*, **63**, 724 (1960).
3. E. A. Gulbransen, *Trans. Electrochem. Soc.*, **81**, 187 (1942).
4. E. A. Gulbransen, *Rev. Sci. Instruments*, **15**, 201 (1944).
5. E. A. Gulbransen, "Advance in Catalysis," Vol. V, p. 119, Academic Press Inc., New York (1953).
6. L. Horn, *Z. Metallk.*, **40**, 73 (1949).
7. A. Preece and G. Lucas, *J. Inst. Metals*, **81**, 219 (1952/53).
8. K. Fueki, *J. Electrochem. Soc. Japan* (Overseas Edition), **26 E**, 99 (1958).
9. K. Fueki, *ibid.*, **26 E**, 120 (1958).
10. F. D. Richardson and J. H. E. Jeffes, *J. Iron & Steel Inst.*, **160**, 261 (1948).
11. O. Kubaschewski and E. L. L. Evans, "Metallurgical Thermochemistry," Butterworth-Springer Ltd., London (1951).
12. G. E. Zima, *Trans. Am. Soc. Metals*, **49**, 924 (1957).
13. O. Kubaschewski and B. E. Hopkins, "Oxidation of Metals and Alloys," p. 126, Academic Press Inc., New York (1953).

SYMBOLS

C	= a constant
ΔG°	= standard free energy change of reaction
k_p	= parabolic rate constant
T	= absolute temperature
t	= time
W	= weight gain per unit area

Oxidation and Equilibrium in Nonstoichiometric Zirconium Dioxide Powder

Seymour Aronson

Bettis Atomic Power Laboratory, Westinghouse Electric Corporation, Pittsburgh, Pennsylvania

ABSTRACT

Two properties of nonstoichiometric zirconium dioxide powder have been studied. Pressures of oxygen in equilibrium with ZrO_{2-x} , with $0.03 > x > 0$, have been determined at temperatures of 900°, 1000°, and 1100°C by passing hydrogen-water vapor mixtures over the oxide. The measured pressures are in the range 10^{-20} to 10^{-12} atm. Rates of oxidation of $ZrO_{1.975}$ to ZrO_2 in oxygen have been measured at 500°-650°C. The activation energy for the oxidation, based on a diffusion mechanism, is 58.0 kcal/mole. A comparison of the rates of oxidation of $ZrO_{1.975}$ with the rates of oxidation of zirconium metal indicates that different mechanisms are operative.

Phase relationships in the zirconium-oxygen system have been studied in detail by Domagala and McPherson (1). Using a technique of examining quenched samples metallographically, they found that a wide range of nonstoichiometry exists in the zirconium dioxide phase. The metal rich boundary of the phase occurs at compositions ranging from $ZrO_{1.75}$ at 1900°C to $ZrO_{1.90}$ at 700°C. Other investigators have observed color and weight changes on reduction of ZrO_2 (2-5), and Kubaschewski and Dench have estimated partial free energies of dissociation in the nonstoichiometric range at 1000°C (5). The oxidation of zirconium and the formation and properties of oxide films on zirconium have been studied extensively (6-9). Despite these efforts, however, little quantitative information is available on the nature and stability of the nonstoichiometric region.

In the present study, two properties of nonstoichiometric oxide, ZrO_{2-x} , have been investigated. Pressures of oxygen in equilibrium with ZrO_{2-x} compositions ranging from $ZrO_{1.970}$ to $ZrO_{1.990}$ have been determined at temperatures of 900°, 1000°, and 1100°C by passing hydrogen-water vapor mixtures over powder samples of the oxide. Rates of oxidation of $ZrO_{1.975}$ in oxygen have been measured at 500°-650°C. The rates of oxidation of $ZrO_{1.975}$ to ZrO_2 are compared to the rates of oxidation of zirconium metal.

Experimental

Materials.—The source material for all the experimental work was Reactor Grade zirconium dioxide powder obtained from the Carborundum Metals Co. The major metallic impurities were 200 ppm Fe, 300 ppm Si, 97 ppm Al, 130 ppm Mg, 100 ppm Ca, and 50 ppm Hf. The concentrations of Cu, Co, Ni, Pb, Mo, Ti, Mn, V, Sn, Cr, and W totalled less than 180 ppm. The accuracies of the spectrochemical analyses are estimated to be $\pm 30\%$. The powder was heated in air at 1000°C to remove excess water and to ensure that the metallic impurities were fully oxidized. Oxalic acid dihydrate and anhydrous oxalic acid were obtained from the Fisher Scientific Company, in the Fisher Certified grades. Compressed oxygen and hydrogen were obtained from

the Matheson Company. The purities of the gases were specified to be 99.6% and 99.9%, respectively. Hydrogen-helium and hydrogen-argon mixtures were also obtained from the Matheson Company. The purities of the helium and argon used for these mixtures were specified to be 99.99% and 99.98%, respectively. An analysis of the hydrogen content of each mixture was supplied by the Matheson Company.

Equilibrium measurements.—The experimental technique for the measurement of oxygen pressures was similar to the method employed by Foster and Welch (10) in studying equilibria in FeO-MnO solid solutions. Known mixtures of hydrogen and water vapor were prepared by passing either hydrogen-helium or hydrogen-argon mixtures through a tube containing a mixture of 90% oxalic acid dihydrate-10% anhydrous oxalic acid in a thermostatted bath according to the method of Baxter and Lansing (11). Their equation for the water vapor pressure, which was checked by Bookey and Tombs (12), is

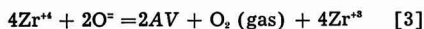
$$\log_{10} P(\text{mm}) = 18.053 - \frac{9661}{T + 250} \quad (T \text{ in } ^\circ\text{K}) \quad [1]$$

The rate of gas flow was controlled by a modified Moore flow controller which has been described elsewhere (13). The gas mixture was passed through the flow controller, through a palladium-asbestos tube heated to 450°C to remove oxygen, and was then dried by passing over magnesium perchlorate. The gas passed through a long tube containing the oxalic acid mixture and then passed over the zirconium oxide sample placed inside a 1 in. diameter clear quartz tube at the center of a tube furnace. The temperature of the sample was determined to about $\pm 3^\circ\text{C}$ with a Pt, Pt-10% Rh thermocouple placed near the sample on the outside of the quartz tube. The water content of the gas was determined by passing the gas through a magnesium perchlorate tube. The tube was removed and weighed after each run to determine the water content. The quantity of gas passed through the system was determined with a wet test meter. The vapor pressure of the water, calculated from the ratio of the quantity of water vapor passed during

+ O₂(g) = 2H₂O(g) · P_{O₂}, P_{H₂}, and P_{H₂O} are the pressures of oxygen, hydrogen, and water vapor, respectively. Results of the measurements are shown in Table I. To ensure that equilibrium conditions were attained during the measurements, the experimental conditions were varied in several ways. Hydrogen-helium and hydrogen-argon mixtures were employed; ZrO₂ and ZrO_{1.976} were used as starting materials; rates of gas flow of 10 and 25 cc/min were employed. Since the results obtained using these variations in the experimental procedure were approximately the same, it seems reasonable to assume that equilibrium was attained and that thermal diffusion effects (10) were minimized. Some experiments were attempted using a pure hydrogen-water vapor environment. Erroneous results were obtained. On the basis of weight pickup on oxidation, the compositions of the samples were closer to stoichiometric ZrO₂ than in the case of samples exposed to the diluted hydrogen gases. The oxidized powders were pink rather than white, probably indicating the presence of an impurity. Attempts to identify the impurity by chemical and spectrographic analyses were unsuccessful. The reason for the erroneous results is, therefore, unknown.

The color of the ZrO₂ powder changed gradually from white to medium-gray as oxygen was removed from the structure. X-ray diffraction spectrometer tracings of nonstoichiometric powder samples, taken at room temperature, showed that the monoclinic structure of the stoichiometric oxide was unchanged. However, no attempt was made to determine if small changes in the lattice parameters occurred.

An attempt was made to interpret the data in a manner similar to recent treatments of nonstoichiometry in such systems as MnO (14), TiO₂ (15), and UO₂ (16). Since the nonstoichiometry in ZrO₂ probably results from the formation of anion vacancies (6,7), mechanisms of the following types were considered.



The symbols have the meanings (AV) anion vacancies, (O²⁻) lattice anions, (Zr⁴⁺, Zr³⁺) lattice cations, (e) electrons in the conduction band of the solid. These equations are representative and are not intended to exclude other possibilities. The data were not found to be amenable to treatments based on such mechanisms. It is felt, however, that the data are not sufficiently extensive or precise to test the available mechanisms adequately. From a qualitative point of view, the data appear unusual in several respects. The pressures of oxygen decrease with increasing temperature which indicates that the partial molar heats of solution of oxygen in the solid,¹ \bar{H}_{O_2} , are positive. Since the partial molar free energies of solution of oxygen, \bar{F}_{O_2} , are large negative terms (see Fig. 1), and are related to the partial molar heats by the standard expression,

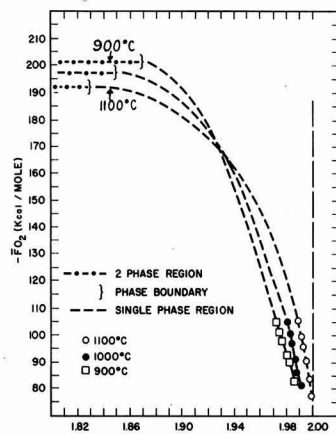


Fig. 1. Partial molar free energies of solution of oxygen in ZrO_{2-x}.

$\bar{F}_{\text{O}_2} = \bar{H}_{\text{O}_2} - T\bar{S}_{\text{O}_2}$, negative values for the partial molar heats would appear more probable.

Partial molar free energies of solution of oxygen in ZrO_{2-x}, calculated from the standard relationship, $\bar{F}_{\text{O}_2} = RT \ln P_{\text{O}_2}$, are plotted in Fig. 1. Each plotted point represents an average of several values in Table I. The compositions at the metal-metal oxide phase boundaries are estimated from the data of Domagala and McPherson (1). The partial molar free energy value for the two-phase region at 1000°C is that estimated by Kubaschewski and Dench (5). The partial molar free energy values at 1100° and 900°C are estimated on the assumption that the partial molar free energy in the two-phase region varies with temperature in approximately the same manner as the free energy of formation of ZrO₂. It is observed that the free energy curves cross in the nonstoichiometric region. The implication of this phenomenon is that the partial molar heat and entropy of solution each change sign in the nonstoichiometric region. Although this is thermodynamically possible, it seems unusual. The thermodynamic properties of the nonstoichiometric region, thus, appear to be complex and require further study. A factor which may effect the zirconia-oxygen equilibria is the monoclinic-tetragonal transformation which occurs in the vicinity of 800°-1200°C (6, 17, 18). The effects of this transformation on the properties of the nonstoichiometric region are not known at present.

Oxidation Kinetics

Some typical rate curves for the oxidation of ZrO_{1.976} powder to ZrO₂ at an oxygen pressure of 100 mm Hg are shown in Fig. 2. The form of the rate curves indicates that a diffusion mechanism may be operative. A standard rate equation for the diffusion of a gas, at constant pressure, into uniform spherical particles (19, 20) is

$$C = 1 - \frac{6}{\pi^2} \sum_{n=1}^{\infty} \left(\frac{1}{n^2} \right) \exp \left(\frac{-\pi^2 n^2 Kt}{a^2} \right) \quad [5]$$

¹ The partial molar properties are defined as the changes in the properties of the system which occur when a mole of oxygen is transferred from the gas phase at 1 atm pressure to a large amount of the solid. The term "partial molar free energy of solution," as used here, is the negative of the term "partial free energy of dissociation" as used by Kubaschewski and Dench (5).

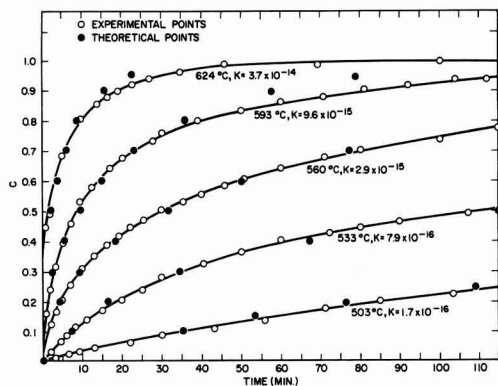


Fig. 2. Rate curves for the oxidation of $ZrO_{1.975}$ to ZrO_2

C is the fractional completion of the reaction and has values from 0 to 1; a is the particle radius; t is the reaction time; K is a rate constant which is ordinarily a simple diffusion coefficient; in the case of the oxidation of $ZrO_{1.975}$, however, K may be a more complex parameter. This is discussed further below.

The rate data obtained on the oxidation of $ZrO_{1.975}$ have been analyzed on the basis of Eq. [5] on the assumption that the powder may be approximated by the uniform sphere model. The experimental rate curves were compared to a theoretical curve of C vs. the parameter $\tau \equiv \pi^2 Kt/a^2$. The forms of the experimental curves were found to be in good agreement with the theoretical curve in all cases. The value of the particle radius, a , calculated from the BET surface area and the density of the powder, was 1.35×10^{-5} cm. Some theoretical points, calculated on the basis of Eq. [5] using the K values shown below the curves in Fig. 2 are superimposed on the experimental data. The agreement is seen to be good except possibly toward the completion of the oxidation. The divergence at high C values may result from the fact that the powder has a distribution of sizes and shapes. As the smaller particles become fully oxidized, the rate of reaction decreases more rapidly than would occur in the case of uniform spheres. K values for the rate curves were calculated by comparison with the theoretical curve. Plots of $\log K$ vs. reciprocal temperature are shown in Fig. 3 for oxygen pressures of 100 and 20 mm Hg. The activation energy calculated from the slope of the $\log K$ vs. $1/T$ plot at an oxygen pressure of 100 mm Hg is 58.0 kcal/mole.

The parameter, K , would correspond to the diffusion coefficient for oxygen ions in nonstoichiometric zirconium dioxide, ZrO_{2-x} , only if the mobility of oxygen ions in ZrO_{2-x} were much smaller than the mobility of electrons. In that case, the diffusion of oxygen ions would be the rate-controlling step in the oxidation. Measurements of the ionic transport numbers in oxide films on zirconium (21) indicate that the mobilities of electrons and ions are comparable. The measured ionic transport number increased from 0.35 to 0.5 in the temperature range 500°-

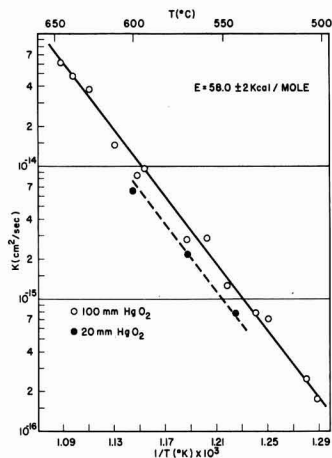


Fig. 3. Variation of the rate constant, K , with temperature

650°C. These results indicate that both electronic and ionic transport processes are important factors in determining the rate of oxidation. The rate constant K , therefore, appears to be a complex parameter containing the diffusion coefficients for the transport of oxygen ions and electrons.

A few experiments were performed at an oxygen pressure of 20 mm Hg to determine if K varies significantly with pressure. On the basis of the simple diffusion mechanism leading to Eq. [5], the pressure dependence of K would be expected to be negligibly small. Equation [5] is based on the assumption that the surface of the powder becomes oxidized to stoichiometric ZrO_2 on exposure to oxygen. The value of K should be independent of moderate variations in pressure. The pressure dependence, noted in Fig. 3, appears to be significant and, hence, not in accord with the simple theory. It may be well to consider other factors than diffusion in explaining the oxidation of ZrO_{2-x} . The effect of space charge boundary layers in the vicinity of the oxide-gas interface may be of importance (22). Space charge effects have been postulated to be of primary importance in the oxidation of nickel and cuprous oxide (22). Experiments to determine the exact pressure dependence of the oxidation of nonstoichiometric ZrO_2 and the effect of the particle size of the powder may be of great help in further elucidating the mechanism of oxidation.

Quantitative comparison between film formation rates on zirconium and rates of oxidation of $ZrO_{1.975}$ is difficult because of the uncertainty concerning the correct mechanism in each case. In the case of the oxidation of zirconium metal (6, 7, 9), there is uncertainty with regard to the nature of the rate law (cubic or parabolic) and the activation energy (18-47 kcal/mole). The oxidation is further complicated by the dissolution of oxygen in the metal (23, 24). It is evident, however, that the activation energy for the oxidation of $ZrO_{1.975}$, 58.0 kcal/mole, is higher than the activation energies found for the oxidation of zirconium. Data obtained on the forma-

tion of oxide films on zirconium and the oxidation of $ZrO_{1.975}$ have been examined in detail to determine if the two oxidation processes can be related. The comparison was made by assuming similar mechanisms for the two processes. The fact that the oxidation of zirconium is a complex process involving film formation, transport of oxygen through the oxide film, and solution of oxygen in zirconium was taken into account. For the sake of brevity, the details of the comparison and the calculations that were made are not presented. The conclusion which was reached concerning the two processes is that the rates of oxide film formation on zirconium are much higher than would be expected from the rates of oxidation of nonstoichiometric zirconium dioxide. If, therefore, the oxidation of $ZrO_{1.975}$ represents, as assumed above, a case of oxygen transport through a bulk oxide phase, then the oxidation of zirconium probably does not proceed primarily through the bulk oxide film. Short circuiting of some sort may occur to obtain the high rates of oxidation observed. Gulbransen and Andrew (9) have suggested that the oxidation of zirconium at temperatures below 525°C proceeds via grain boundaries on other short-circuiting paths. The lack of agreement between the rates of oxidation of zirconium and the rates of oxidation of $ZrO_{1.975}$ at temperatures up to 650°C indicates that short circuiting may also occur in the oxidation of zirconium at temperatures above 525°C.

Acknowledgments

This work was performed under contract AT-11-1-GEN-14. The author is grateful to the U. S. Atomic Energy Commission and the Westinghouse Electric Corporation for permission to publish this paper.

The author wishes to acknowledge the aid of J. E. Rulli in the design and construction of the experimental equipment and in performing the various measurements. The author also wishes to thank Dr. J. Belle and Dr. B. Lustman for their helpful discussion of this work.

Manuscript received Sept. 27, 1960; revised manuscript received Dec. 9, 1960.

Any discussion of this paper will appear in a Discussion Section to be published in the December 1961 JOURNAL.

REFERENCES

1. R. F. Domagala and D. J. McPherson, *Trans. AIME*, **200**, 238 (1954).
2. D. Cubicciotti, *J. Am. Chem. Soc.*, **73**, 2032 (1951).
3. E. Friedrich and L. Sittig, *Z. Anorg. Chem.*, **145**, 129 (1925).
4. H. von Wartenberg, J. Broy, and R. Reinicke, *Z. Elektrochem.*, **29**, 1923 (214).
5. O. Kubaschewski and W. A. Dench, *J. Inst. Metals*, **84**, 440 (1956).
6. B. Lustman and F. Kerze, Jr., "The Metallurgy of Zirconium," National Nuclear Energy Series, Division VII, Volume 4, Chap. 11, McGraw-Hill Book Co., New York (1955).
7. H. A. Porte, J. G. Schnizlein, R. C. Vogel, and D. F. Fischer, *This Journal*, **107**, 506 (1960).
8. R. D. Misch and F. H. Gunzel, Jr., *ibid.*, **106**, 15 (1959).
9. E. A. Gulbransen and K. F. Andrew, *Trans. AIME*, **209**, 394 (1957).
10. P. K. Foster and A. J. E. Welch, *Trans. Faraday Soc.*, **52**, 1636 (1956).
11. G. P. Baxter and J. E. Lansing, *J. Am. Chem. Soc.*, **42**, (419) 1920.
12. J. B. Bookey and N. C. Tombs, *J. Iron Steel Inst.*, **172**, 86 (1952).
13. J. C. Clayton and J. E. Rulli, *Chemist-Analyst*, **47**, 62 (1958).
14. M. W. Davies and F. D. Richardson, *Trans. Faraday Soc.*, **55**, 604 (1959).
15. W. R. Buessem and S. R. Butler, "Defect Reactions in TiO_2 ," in "Kinetics of High Temperature Processes," W. D. Kingery, Editor, Technology Press of M.I.T. (1959).
16. S. Aronson and J. C. Clayton, *J. Chem. Phys.*, **32**, 749 (1960).
17. F. A. Mumpton and R. Roy, *J. Ceram. Soc.*, **43**, 234 (1960).
18. L. Ochs, *Z. Naturforschung*, **12b**, 215 (1957).
19. H. S. Carslaw and J. C. Jaeger, "Conduction of Heat in Solids," p. 200, Oxford University Press, Cambridge (1947).
20. K. B. Alberman and J. S. Anderson, *J. Chem. Soc.*, **1949**, 5303.
21. L. D. Kirkbride and D. E. Thomas, "Ionic Transport in Zirconium Dioxide," Westinghouse Electric Corp. Report WAPD-T-308, 1956.
22. K. Hauffe, "Investigations on the Oxidation of Metals as a Tool for the Exploration of the Movement of Ions in Solid Oxides" in "Kinetics of High Temperature Processes," W. D. Kingery, Editor, Technology Press, M.I.T. (1959).
23. R. D. Misch, *Acta Met.*, **5**, 179 (1957).
24. J. P. Pemsler, *This Journal*, **105**, 315 (1958).

The Permeability of Aluminum to Hydrogen

C. N. Cochran

Alcoa Research Laboratories, Aluminum Company of America, New Kensington, Pennsylvania

ABSTRACT

The permeability constant for hydrogen in aluminum at 500°C was found to be sensitive to surface films. The constant varied over a four hundredfold range in normal hydrogen atmospheres and over a thousandfold range in the presence of a glow discharge. These differences are attributed to the varying ability of the respective surface films to catalyze the $H_2 \rightleftharpoons 2H$ equilibrium and to bar the diffusion of hydrogen. Surface films having high catalytic activity protect aluminum against attack by hydrogen generated in the reaction with water.

Films of tungsten, iron, cobalt, nickel, molybdenum, chromium, and various halides reduced the permeability constants in the presence of the glow discharge. Etching with caustic reduced the permeability constant in normal unexcited hydrogen to as little as one hundredth of the value for untreated aluminum. A nickel-aluminum alloy formed an oxide film in water at 350°C that is very impermeable to hydrogen. The permeability of 99% aluminum was measured at temperatures from 400° to 600°C and compared with other values in the literature.

The dependence of the permeability of aluminum to hydrogen on heating time and surface conditions has been variously attributed to oxide films (1, 2), recrystallization of the metal (2), and rates of the dissociation and adsorption reactions on the surface (3). Surface films and alloy composition seem to be particularly important in controlling permeation by hydrogen generated in the corrosive reaction of water with aluminum at elevated temperatures. This reaction can lead to blistering of the surface and formation of hydrogen-filled voids within the metal (4) or, with liquid water above 200°C, to catastrophic attack of the metal (5).

Stroup (4) found that the attack by water vapor could be reduced if the aluminum were heated in the presence of sodium, potassium, or ammonium fluoborate. Eborall and Ransley (6) noted that gassing of an aluminum-magnesium alloy at 600°C in 16 mm pressure of water vapor was strongly retarded if the alloy was exposed initially to the vapors of concentrated hydrofluoric acid. Recently, Blackburn and Gulbransen (7) found that pre-treatment of high-purity aluminum in 1M HCl at 55°C inhibited blister formation and prevented gassing of the metal upon heating in water vapor at 600°C. Draley and Ruther (5) learned that the catastrophic attack of liquid water on aluminum at temperatures near 350°C could be reduced by addition of 1% nickel to the aluminum. They suggested that the added nickel or any added metal that has a low hydrogen overvoltage may catalyze the formation of hydrogen molecules at the oxide-metal interface.

Equilibria and Reaction Rates

The direct relationship of hydrogen solubility to the square root of the hydrogen pressure, as observed by Ransley and Neufeld (8), establishes that hydrogen dissolves in aluminum in monatomic form in accordance with Sievert's rule. The atoms may ionize to protons on dissolving in the aluminum, but the dissolved hydrogen will be referred to as

atoms in this work. The observed solution and permeation of hydrogen in aluminum from hydrogen at 1 atm pressure at 500°C results from the extremely small equilibrium atomic hydrogen pressure of 10^{-12} atm. Nascent hydrogen from the reaction of aluminum with water can be produced at pressures above this equilibrium value and cause increased diffusion into the metal if the equilibration reaction with molecular hydrogen is slow. In the metal, this high concentration of atomic hydrogen can equilibrate with molecular hydrogen at favorable sites (perhaps inclusions, shrinkage porosity, vacancies, etc.). The blisters and hydrogen-filled voids that can form from this reaction are evidence that the pressure of molecular hydrogen in these voids can reach high enough values to exceed the yield strength of the metal.

The upper limiting equilibrium pressures that can result from reaction of water vapor with aluminum to form alumina and hydrogen can be calculated from the following expressions.

$$P_{H_2} = P_{H_2O} e^{-\frac{(\Delta F^{\circ} f_{Al_2O_3} - 3\Delta F^{\circ} f_{H_2O})}{RT}}$$

$$P_H = (P_{H_2})^{1/2} e^{-\frac{\Delta F^{\circ} f_{H}}{RT}}$$

The equilibrium pressures given in Table I were calculated from these expressions. The last column gives the atomic hydrogen pressure in equilibrium

Table I. Equilibrium in atmospheres hydrogen pressures

°C	$2Al(c) + 3H_2O(1 atm) \rightarrow Al_2O_3(c) + 3H_2(v)$ log P_{H_2}	$H_2(1 atm) \rightarrow 2H$ log P_H	$H_2(1 atm) \rightarrow 2H$ log P_H
25	52.0	-9.6	-35.6
127	38.0	-6.9	-25.9
227	29.8	-5.3	-20.2
327	24.4	-4.2	-16.3
427	20.5	-3.4	-13.6
527	17.6	-2.7	-11.5
627	15.4	-2.3	-9.9

with 1 atm of hydrogen. Free energy data for these calculations were taken from Selected Values of Chemical Thermodynamic Properties, Series III, Tables 8 and 59, National Bureau of Standards. The symbols are the same as those employed in this reference.

The extent to which reaction of aluminum with water can cause gassing and internal destruction of the metal is thus determined by kinetic considerations and can be controlled to a great extent by altering the nature of the surface or surface film. In the presence of a catalytically active surface, the hydrogen atoms can rapidly equilibrate with molecular hydrogen that, under ordinary circumstances, will be evolved at or below 1 atm pressure from the reacting surface.

Experimental Approach

The ability of various surface films on aluminum to catalyze the equilibration of atomic with molecular hydrogen and to bar hydrogen diffusion was determined for two conditions: (a) where an excess of atoms must reassociate on the surface, and (b) where the atoms must be produced by dissociation of molecular hydrogen on the surface.

The most direct means for producing condition (a) would be to generate the atoms by the reaction of water with the aluminum. However, the rate of the oxidation reaction declines rapidly as the oxide generated in the reaction forms a barrier film on the surface. Furthermore, it is very difficult to prevent oxide film formation during the preliminary outgassing operation necessary for such experiments. To circumvent these difficulties, the high concentration of hydrogen atoms required for condition (a) was generated in an electrical glow discharge at reduced pressure.

Condition (b) was realized in an atmosphere of ordinary, unexcited hydrogen.¹

Apparatus

The specimen consisted of a coil of $\frac{1}{4}$ in. OD aluminum alloy tubing (16 to 20 turns, 6 in. long, 2- $\frac{1}{2}$ in. to 2- $\frac{3}{8}$ in. OD), closed at one end. It was placed at the center of a 12-in. long heated zone at 500°C in a vacuum-tight chamber. Both 1100 and 5050 alloys² were used with wall thicknesses ranging from 0.041 to 0.081 cm. An aluminum alloy, X8001, containing 1% nickel and 0.5% iron, that showed exceptional resistance to corrosion by water at high temperatures and high pressures, was employed in a few tests.

The apparatus is shown in Fig. 1. A 200-w glow discharge between the tubing and spark plugs in the two ends of the quartz tube was operated from a 1100 v, 2 kva transformer, fed from a 0-230-v adjustable autotransformer. A 500-w incandescent

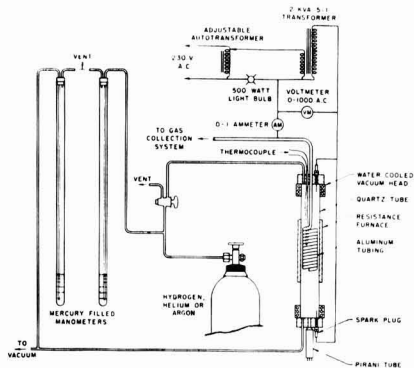


Fig. 1. Apparatus for measuring permeability of aluminum to hydrogen.

light bulb in the low voltage side served as ballast for the discharge. The hydrogen pressure, which was read on both a Pirani gauge and a mercury manometer, was held at 500 μ while the glow discharge was operated. The hydrogen that permeated the tubing was pumped into a gas collection and measurement system. Temperatures were controlled to within $\pm 10^\circ\text{C}$ using a shielded thermocouple located inside the coil of tubing.

Procedure

The tubing was degassed for at least 16 hr at 500°C in the apparatus, or until the pressure in the reaction chamber was in the low micron range, and a pressure less than 5×10^{-5} mm was reached in the gas collection system. The tubing was tested for leaks by admitting either an atmosphere of commercial tank helium or commercial tank argon to the reaction chamber and observing any pressure rise inside the tubing. With a liquid-nitrogen cooled trap in the gas collection system, the rate of background gas evolution was determined. Ordinarily, all of this gas was hydrogen, as determined by a hydrogen-sensitive McLeod gauge (9). Using commercial tank hydrogen, the gas collection rates at 500 μ pressure, at 1 atm pressure hydrogen, and at 500 μ pressure with the glow discharge operating were determined successively for at least 1 hr each. In most cases, the rates increased within the first $\frac{1}{2}$ hr to values constant to within $\pm 10\%$ over a $\frac{1}{2}$ hr period. However, with samples having exceptional ability to catalyze the hydrogen atom-hydrogen molecule conversion, the rates in the glow discharge decreased for about the first $\frac{1}{2}$ hr of measurement and reached values constant to within $\pm 10\%$. Part of the fluctuation after the $\frac{1}{2}$ hr period is explainable by cycling of the temperature about the control temperature.

Permeability Constants and Relative Catalytic Activity

The results are expressed as permeability constants, as listed in Table II. For the samples tested, the permeability constants varied over one hundred thousandfold with the highest values being obtained in the glow discharge and the lowest

¹ From the calculated partial pressure of atomic hydrogen (10^{-12} atm) in equilibrium with 1 atm of hydrogen at 500°C, and from the volume of the system, it was calculated that the number of hydrogen atoms in the gas phase could not sustain the observed permeation rates for more than a few microseconds. Since the atoms could not possibly diffuse to the aluminum surface from every point in the reaction chamber volume in this time, the hydrogen molecules must dissociate at the atoms on the surface of the aluminum during the steady state as fast as they permeate the metal.

² Nominal compositions. 1100 Alloy, 99% minimum Al, maximum limits 1% Si + Fe, 0.2% Cu, 0.05% Mn, 0.10% Zn, 0.15% others; 5050 Alloy limits, 0.4% Si, 0.7% Fe, 0.2% Cu, 0.1% Mn, 1.0-1.8% Mg, 0.1% Cr, 0.25% Zn, 0.15% others.

Table II. Effect of surface films on permeability of aluminum alloys to hydrogen at 500°C

Pretreatment	Permeability constant ml cm		Relative catalytic activity
	sec cm ² (mm) ^{1/2} 740 mm H ₂	$\times 10^{10}$ 0.5 mm H ₂ Glow discharge	
1100 Alloy ¹			
None	4.6	880	0.005
2 Min in 5% HF, 25°-40°C	6.2	440	0.01
2 Min in 2.5N HCl, 70°C	5.5	300	0.02
1 Hr in air with NaBF ₄ , 500°C	10	940	0.01
1 Hr in air with KBF ₄ , 600°C	8.8	230	0.04
1 Hr in air with KBF ₄ , 500°C	8.8	1300	0.007
1 Hr in air with NH ₄ BF ₄ , 500°C	8.5	46	0.2
0.0006 in. Nickel plate, 0.00005 in. copper strike and zinc immersion coating underneath	3.7	7	0.5
0.00005 in. Copper strike and zinc immersion coating underneath	0.81	730	0.001
0.0006 in. Cobalt plate, 0.00005 in. copper strike and zinc immersion coating underneath	2.9	14	0.2
0.0002 in. Iron plate	3.0	14	0.2
0.0002 in. Chromium plate	7.4	2.8	3
Above tubing with plating removed with scratch brush	7.0	1300	0.005
Metallized with molybde- num	10	6.5	1.5
Metallized with tungsten in plasma flame	5.9	15	0.4
10 Min, 20% NaOH, 25°C	0.63	1400	0.0004
Alcoa R-5 bright dip ³ process	0.04	4000	0.00001
X8001 Alloy (1.0% Ni, 0.5% Fe, remainder similar to 1100 alloy)			
None	6.6	1200	0.006
In water 24 hr at 360°C	0.1	16	0.006
5050 Alloy ²			
None	12	1700	0.007
2 Min in 5% HF, 25°-60°C	7.0	61	0.1
2 Min in 2.5N HCl, 70°C	14	61	0.2
120 Min, saturated NaCl, 110°C	2.7	85	0.03
1 Hr in air with NaBF ₄ , 500°C	7.7	240	0.03
1 Hr in air with KBF ₄ , 500°C	0.74	30	0.02
1 Hr in air with NH ₄ BF ₄ , 500°C	0.74	30	0.02
Nickel immersion coating, inside and outside sur- faces (electroless pro- cess, 20 min, 200°F)	15	66	0.2
10 Min in 20% NaOH, 20°C	0.1	1300	0.0001
10 Min, 20% KOH, 29°- 45°C	1.1	1400	0.0008
1 Min, bright dip	2	550	0.004

¹ 1.0% Si + Fe, 0.2% Cu, 0.05% Mn, 0.1% Zn, 0.15% others, nominal composition.

² 0.4% Si, 0.7% Fe, 0.2% Cu, 0.1% Mn, 1.0-1.8% Mg, 0.10% Cr, 0.25% Zn, 0.15% others, nominal composition.

³ Patented process.

values being obtained in the atmosphere of ordinary hydrogen.

Differences in permeability constants from sample to sample can result not only from differences in the ability of the surface films to catalyze the hydrogen atom-molecule reaction but also from differences in diffusion barriers at the surfaces as well. These barriers can result from the surface treatments and from oxidation during outgassing. The ratio of the permeability constant in unexcited hydrogen to the permeability constant in the glow discharge offers a means for separating the barrier and the catalytic effects. If the barrier lowers the permeability constants for both cases by proportionate amounts, this ratio cancels out the barrier effect and expresses in a rough and perhaps non-linear way the catalytic action of the surface film. This ratio is designated the relative catalytic activity.

The values found for this ratio covered a three hundred thousandfold range in this work. Ideally, this ratio should reach a maximum value of unity for a perfect catalyst. Actually, a value of three was found experimentally for a chromium plated 1100 alloy tube. This high value may have resulted from oxidation between the time the permeability was measured in the normal atmosphere and in the glow discharge. This oxidation could have been caused by sorbed oxidizing gases that were released by ion bombardment when the glow discharge was operated. Regardless of the source of the discrepancy, a value of three is considered sufficiently close to unity to justify the concept of catalytic activity, considering the many orders of magnitude that this quantity covers.

It might be expected from this catalytic mechanism that the same surface films which increase the permeability constant in the normal atmosphere should decrease the permeability constant in the glow discharge. This relationship, if it exists, may be masked in most of the results by the effect of the diffusion barriers at the surface. However, one indication of this dependence was obtained with the tube of 1100 alloy which has been chemically brightened by the Alcoa R-5 bright dip process. In this study, it had the highest permeability constant in the glow discharge and the lowest permeability constant in the normal atmosphere of hydrogen. Also, the surfaces which had the very highest permeability constants in the normal atmosphere of hydrogen had low permeability constants in the glow discharge.

Halide Films

All three of the halide surface treatments that were shown by previous workers to reduce permeation of corrosion hydrogen were found to increase the catalytic activity from the values found for untreated surfaces, principally by reducing the permeability in the glow discharge. The most effective of these for 1100 alloy was heating in the presence of ammonium fluoborate in air for 1 hr at 500°C. For testing the fluoborates about 25 g of the appropriate fluoborate in a quartz dish was placed with the sample in a preheated electric muffle furnace ($\frac{1}{4}$ ft³ volume) and the furnace door was closed.

At a given temperature of application, the effectiveness of the fluoroborates with 1100 and 5050 alloys fell off in order of their decreasing decomposition pressures, ammonium fluoroborates being highest, sodium fluoroborate next, and potassium fluoroborate the least. The films formed on 5050 alloy by the action of fluoroborates were also good barriers to the diffusion of hydrogen, as judged by the lowering of the permeability constants in both the normal atmosphere and in the glow discharge.

Etching the surface of the specimens with 5% aqueous HF or 2.5N HCl increased the catalytic activity of 5050 alloy more than that for 1100 alloy.

Treatment of 5050 alloy in a saturated boiling solution of sodium chloride in water for 2 hr resulted in a surface with a low permeability constant in the glow discharge similar to the value obtained in the treatment with hydrochloric acid, but with a permeability constant in the normal atmosphere below that produced by hydrochloric acid.

High-Temperature Water Alloy

Unoxidized X8001 alloy had permeability constants very much like untreated 1100 or 5050 alloys in both the normal atmosphere of hydrogen and the glow discharge. The X8001 alloy was oxidized in water for 24 hr at 360°C, conditions which would have completely consumed 1100 alloy. The permeability constants of the oxidized X8001 alloy in both atmospheres at 500°C were reduced about seventyfold, with a relative catalytic activity of 0.006, the same value as for the unoxidized material. This indicates the presence of a barrier to hydrogen diffusion by the oxidized surface which can contribute to the relatively high resistance to corrosion of X8001 when exposed to water at high temperatures or pressures. However, Tragert (12) did not find appreciable differences in the permeability of alloy 1245 (99.45% Al) and alloy X8001 to hydrogen during oxidation by water for 4½ hr at 300°C. He concluded that the nickel alters the corrosion product film to render it less permeable to the diffusing reactants, aluminum or water, than to the hydrogen.

Metallic Films

Lowering of the permeability constants in the glow discharge by metallic films on 1100 alloy became more pronounced in this approximate order: tungsten, iron, cobalt, nickel, molybdenum, and chromium. The permeability constants in the normal atmosphere were large and varied over a four-fold range for these materials, with little apparent relationship to the values in the glow discharge. The action of these metal films is mainly catalytic in contrast to the action of nickel in X8001 alloy. As evidence of the catalytic action of these metallic films, the nickel-coated sample had the highest permeability in a normal hydrogen atmosphere, and the chromium plated sample had the lowest permeability in the glow discharge of any of the materials tested. In the latter case, removal of the loose chromium plate with a scratch brush at the end of the test returned the permeability constant in the glow discharge to a high value typical for untreated

surfaces. Nickel coatings were as effective on 5050 alloy as on 1100 alloy.

These results bear out the suggestion of Draley and Ruther that metals of relatively low hydrogen overvoltages should catalyze the conversion of hydrogen atoms to molecules on aluminum. Copper, on the other hand, which has a relatively high hydrogen overvoltage did not lower the permeability constant in the glow discharge when plated on the aluminum, and the permeability constant in the normal atmosphere of hydrogen was far below the value for an untreated aluminum surface.

Caustic and Chemical Brightening Solutions

Etching in sodium hydroxide produced surfaces on both alloys with very low permeability constants in the normal hydrogen atmosphere. Potassium hydroxide had less effect than sodium hydroxide on 5050 alloy. Treatment of 1100 alloy with a phosphoric-nitric acid brightening solution reduced the permeability constant in the normal hydrogen atmosphere to one hundredth of the value for an untreated tube; it raised the permeability constant in the glow discharge to almost five times the value for the untreated tube. Similar treatment of 5050 alloy lowered the permeability constants in the glow discharge and in the normal atmosphere by three- and sixfold, respectively, from the values for untreated surfaces.

Change of Permeability Constant with Temperature

The change of the permeability constant with temperatures between 400° and 600°C was measured for 1100 alloy having an untreated surface. The permeability of this material at 500°C in a normal atmosphere of hydrogen was only 37% below the highest value found in this work in the absence of the discharge, indicating that the untreated surface had appreciable catalytic activity. The permeability constants are compared in Fig. 2 with the values from the literature.

Smithells and Ransley (1) found that the per-

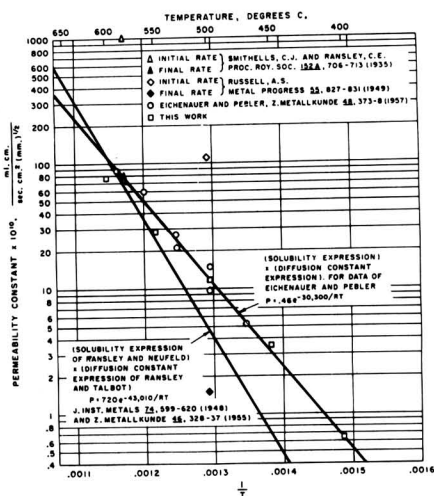


Fig. 2. Permeability constant of hydrogen in solid aluminum

meability of aluminum to hydrogen at 580°C varied strongly with the condition of the surface. Abrading the inside and outside surfaces of their samples in hydrogen increased the diffusion rate manyfold. After abrading, these rates declined to about half of the initial values within ½ hr and to one tenth of the initial value within 5 hr. They attributed this decline to formation of barrier films on the surface. Their highest rates are about twenty times higher than the value interpolated from the measurements of this work.

Russell (2) obtained similar results with a decay in permeability constant from 110×10^{-10} to 2×10^{-10} ml cm/sec cm² (mm)^{3/2} after prolonged heating at 500°C. He indicated both recrystallization and grain growth as well as thermally formed barrier oxide films as possible explanations.

The oxidation of samples observed in both the Smithell-Ransley and the Russell work indicated the presence of water vapor in the hydrogen. Part of the atomic hydrogen formed in the reaction of the water vapor with the aluminum surface could have diffused through the surface and led to erroneously high permeation rates for the hydrogen pressure employed. When the oxide reached its ultimate thickness (1 hr at 580°C; 16 hr at 500°C) (13), the rate of the oxidation reaction may have reached a low enough level that it did not contribute much to the observed hydrogen permeation rate. However, the oxide formed by the water-metal reaction may have limited the permeation rate observed at this time.

The products of the solubilities and the diffusion constants measured by Eichenauer and Pebler (10) and also by Ransley and co-workers (8, 11) indicate that the initial rates obtained by Smithells and

Ransley and by Russell are probably high. The data of Eichenauer and Pebler very closely match the values found in the present work. Most of the possible errors (slow dissociation of hydrogen, slow permeation of an oxide barrier, slow dissolution or ionization steps, etc.) in assuming that the products of solubilities and diffusion constants are equal to permeability constants lead to higher values for the products. Most of the differences are in the other direction.

Manuscript received July 1, 1960; revised manuscript received Nov. 21, 1960.

Any discussion of this paper will appear in a Discussion Section to be published in the December 1961 JOURNAL.

REFERENCES

1. C. J. Smithells and C. E. Ransley, *Proc. Roy. Soc.*, **A152**, 706 (1935).
2. A. S. Russell, *Metal Progr.*, **55**, 827 (1949).
3. H. Kostron, *Z. Metallk.*, **43**, 269 (1952).
4. P. T. Stroup, U.S. Pat. 2,092,034 and 2,092,033 (1937); also "Controlled Atmospheres," American Society for Metals, Cleveland, Ohio (1941).
5. J. E. Draley and W. E. Ruther, *Corrosion*, **12**, 441t, 480t (1956).
6. R. Eborall and C. E. Ransley, *J. Inst. Metals*, **71**, 525 (1945).
7. P. E. Blackburn and E. A. Gulbransen, *This Journal*, **107**, 944, (1960).
8. C. E. Ransley and H. Neufeld, *J. Inst. Metals*, **74**, 599 (1948).
9. C. N. Cochran, *Rev. Sci. Instr.*, **29**, 69 (1958).
10. W. Eichenauer and A. Pebler, *Z. Metallk.*, **48**, 373 (1957).
11. C. E. Ransley and D. E. J. Talbot, *ibid.*, **46**, 328 (1955).
12. W. E. Tragert, *This Journal*, **106**, 903 (1959).
13. C. N. Cochran and W. C. Sleppey, *ibid.*, **107**, 322 (1961).

Brief Communications

The JOURNAL accepts short technical reports having unusual importance or timely interest, where speed of publication is a consideration. The communication may summarize results of important research justifying announcement before such time as a more detailed manuscript can be published. Consideration also will be given to reports of significant unfinished research which the author cannot pursue further, but the results of which are of potential use to others. Comments on papers already published in the JOURNAL should be reserved for the Discussion Section published biannually.

Submit communications in triplicate, typewritten double-spaced, to the Editor, Journal of The Electrochemical Society, 1860 Broadway, New York 23, N. Y.

Oxidation of High-Purity Aluminum and 5052 Aluminum-Magnesium Alloy at Elevated Temperatures

C. N. Cochran and W. C. Sleppy

Alcoa Research Laboratories, Aluminum Company of America, New Kensington, Pennsylvania

ABSTRACT

Oxidation of chemically polished high-purity aluminum in dry oxygen, water vapor, and moist air at temperatures from 450° to 640°C is characterized by a near-linear reaction rate to a weight gain of 3 $\mu\text{g}/\text{cm}^2$, followed by a rate that decreases rapidly with further weight gain. Oxidation beyond the 5-7 $\mu\text{g}/\text{cm}^2$ weight gain range is very slow. Oxidation is slightly faster in the moist atmospheres than in dry oxygen at temperatures above 550°C. Oxidation of a commercial aluminum-magnesium alloy (5052) in dry oxygen and in moist air is much faster than for high-purity aluminum and proceeds to much higher weight gains. The rate does not conform to any recognized oxidation law, but it is more nearly parabolic than linear. The much higher weight gains obtained by other workers who used mechanically polished samples of both high-purity aluminum and aluminum-magnesium alloy are attributed to surface roughness. Electron diffraction examination of oxidized specimens show only eta alumina on the high-purity metal and magnesium oxide on the aluminum-magnesium alloy.

Previous studies of the oxidation of solid aluminum at elevated temperatures showed differences in the amount of oxide formed and in the oxidation law followed. Of the more comprehensive studies, Gulbransen and Wysong (1), Smeltzer (2), and Aylmore, Gregg, and Jepson (3) found that weight gains of metallographically polished high-purity aluminum in oxygen exceeded the 30 $\mu\text{g}/\text{cm}^2$ level before the rate diminished sharply. Gulbransen and Wysong found in 2-hr tests that a parabolic law was obeyed from 350° to 475°C and a linear law from 500° to 550°C. Smeltzer found that oxidation followed a two-step parabolic law during the early stages, then decreased to a lower rate after the weight gain had reached 30-40 $\mu\text{g}/\text{cm}^2$. The time required for completion of the initial rapid rate decreased from 20 hr at 450°C to 1 hr at 600°C. Aylmore, Gregg, and Jepson found that oxidation curves were parabolic after the first 2 hr at 400°C but had three distinct branches at higher temperatures, each with a succeeding lower rate. They explained their results in terms of an amorphous oxide which forms initially and crystallizes to eta alumina.

Using chemically polished samples of high-purity aluminum, Hunter and Fowle (4) learned that, upon oxidation, eta alumina formed to a thickness of 160-210Å (2.7-3.4 $\mu\text{g}/\text{cm}^2$ for an oxide density of 3.4 g/cm^3) at temperatures above 475°C. Below 450°C, the oxide was amorphous and did not grow beyond 50Å. They noticed no difference between oxidation in air and in oxygen, but oxidation in moist air from 125° to 275°C was slower than in dry air, although the same ultimate thickness was reached. Their oxide thickness determination was to measure the voltage required to cause normal current leakage through oxide films in a nondissolving electrolyte, and to convert this to oxide thickness by the relationship that $1 \text{ v} = 14\text{Å}$ for barrier oxides on aluminum.

A possible explanation for the differences in the references just cited was contained in the work of Lewis and Plumb (5, 6) on the effect of surface preparation on the surface roughness of aluminum. Using both radiochemical and electrochemical methods of surface area determination, surface roughnesses as high as twenty-five times the geometric area were found after some special polishing procedures. They showed that "as-rolled" metal had a roughness of 2.5, a carefully dry-machined surface had a roughness near 1.5, and a chemically polished surface had a roughness slightly greater than 2.

Plumb showed that an initially rough surface becomes smoother as oxidation proceeds. Oxidation of a surface roughened by abrasion with No. 320 aloxite cloth smoothed the surface from a roughness of 6 at an oxide thickness of 30Å, to 4 at an oxide thickness of 100Å, with further decrease with continued oxidation. Data for oxidation of such a surface would be misleading, not only with regard to the thickness of oxide that forms, but also to the oxidation law that is followed, since the area of the reacting surface would decrease with oxide thickness.

Gulbransen and Wysong (1) and Aziz and Godard (7) reported that unpolished aluminum surfaces gained much less weight than mechanically polished ones, but did not ascribe the differences to surface roughness.

Blackburn and Gulbransen (8), aware of the effects of surface roughness, investigated the oxidation of chemically polished 99.993% aluminum in water vapor, dry oxygen, moist oxygen, and moist hydrogen at temperatures between 500° and 625°C. The oxidation rate was strongly temperature dependent and decreased markedly at the 5-6 $\mu\text{g}/\text{cm}^2$ level. The data failed to fit any theoretical oxidation law. The oxidation rate in 0.1 atm water vapor was about twice that in 0.1 atm dry oxygen throughout this temperature range. The initial portions of the

curves were linear, except for ones obtained at temperatures below 550°C. The rate for the first 0.5 to 1.0 $\mu\text{g}/\text{cm}^2$ was more rapid than for the subsequent gain. In comparing the results of Blackburn and Gulbransen with those of Smeltzer, it would appear that the latter's high-purity aluminum samples actually had surface roughnesses of 8-10.

Aylmore, Gregg, and Jepson (3) obtained lower amounts of oxide per unit surface area if they interrupted the oxidation with vacuum anneals at 500°C. They explained that crystallization and sintering of the oxide continued during the vacuum anneal and reduced the rate of the subsequent oxidation. Possibly the metal surface may have sintered also during these anneals to give a more planar surface to account for the lower levels of oxidation after annealing.

Using metallographically polished samples, Smeltzer (9) found that oxidation of an aluminum alloy containing 3% magnesium was immeasurably low below 200°C. Above 350°C, oxidation was parabolic, transforming to a linear rate when the weight gain reached 10 $\mu\text{g}/\text{cm}^2$. Weight gains as high as 70 $\mu\text{g}/\text{cm}^2$ were found in 10 min at 550°C. Selective oxidation of magnesium in the alloy at temperatures above 400°C formed a film of MgO and MgAl_2O_4 , that contained aluminum inclusions which imparted a black discoloration to the alloy surface. The oxidation rate was found to be less than the magnesium evaporation rate at all temperatures.

Methods and Materials

Two measuring methods were employed in the present investigation. First, the weight gain during oxidation was determined with an automatic recording vacuum microbalance (10), and second, the decrease in pressure of oxygen was measured as the metal oxidized in a fixed volume (11).

High-purity aluminum and the aluminum-magnesium alloy, 5052, were investigated. The composition of these materials, determined spectroscopically is given in Table I.

Table I

Element	%
High-purity aluminum	
Cu	0.004
Fe	0.001
Si	0.003
Mg	0.004
Zn	0.003
Mn, Ni, Cr, Ti, Pb	<0.001
5052 Alloy	
Cu	0.03
Fe	0.25
Si	0.12
Mn	0.07
Mg	2.35
Zn	0.02
Ni	0.004
Cr	0.22
Ti	0.007
V	0.006
Pb	0.001
B	0.001
Be, Sn, Bi	<0.001

The samples were usually 0.003 in. thick aluminum foil, 4x2 in. for the manometric measurements, and 2x1½ in. for the gravimetric measurements.

Unless otherwise specified, the surfaces of samples for both methods were smoothed and freed of thick oxide by chemical polishing by the Alcoa R5 Bright Dip¹ process. A rinse in 50% nitric acid solution and several rinses in distilled water followed by drying in air completed the sample preparation. The oxide layer on the surface after this treatment is thought to be 20-30Å thick which is equivalent to a weight gain of approximately 1/3 to 1/2 $\mu\text{g}/\text{cm}^2$. This is not included in the weight gains reported here.

Gravimetric Method

A sample was suspended from one arm of the microbalance and evacuated to the 10^{-5} mm Hg pressure range for 6 hr at room temperature. With a preheated furnace pulled over the Vycor tube enclosing the sample, the desired temperature was reached within 20 min. In heating the 5052 alloy samples to temperature, magnesium evaporated rapidly above 500°C. In the higher temperature experiments, this loss may have been great enough to affect the course of the oxidation curve.

The desired atmosphere was introduced to begin the experiment. Regular tank-grade oxygen was purified by passing through a train of ascarite, heated platinum foil, and magnesium perchlorate. Room air was saturated with water vapor at 23°C by bubbling it through a fritted glass disk immersed in water. Vacuum-distilled water in a trap at 0°C was employed for oxidation in water vapor alone.

Temperatures were controlled to within $\pm 0.5^\circ\text{C}$, employing a thermocouple sealed into the refractory coil form of the furnace. The relationship between temperatures at the couple and temperatures at the sample was established in blank experiments with thermocouples sealed inside the vacuum system at the inside fold of the top, middle, and bottom of the sample. The temperature at the top and bottom averaged 1° and 0.5°C higher than the temperature at the middle position. The temperature at the control thermocouple averaged 25°C higher than the average sample temperatures through the whole temperature range.

Manometric Method

The manometric apparatus is illustrated in Fig. 1. Two identical all-quartz cells were mounted side by side inside a 4 in. diameter Kanthal wire-wound

¹ Patented process.

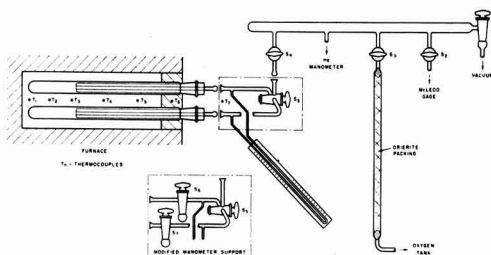


Fig. 1. Manometric apparatus

furnace core. One of the cells contained an aluminum sample and the other cell was used to compensate for pressure changes resulting from changes in the furnace temperature. A differential oil manometer, tilted at an angle of 60° and filled with Octoil-S oil, was connected between the tubes leading to the cells. The cells were evacuated, outgassed, and brought slowly to temperature; then 200 mm of dry oxygen was expanded into both quartz cells simultaneously through the T-bore stopcock S_5 . This stopcock was closed quickly and the differential pressure recorded at suitable time intervals for periods up to 100 min.

The respective temperatures of the sample and of the cooler zones leading to the room temperature portion of the system all were constant to within $\pm 1^\circ\text{C}$ during the course of an experiment. The maximum temperature difference from either end of the sample to the middle of the sample never exceeded 7°C .

The modified mercury manometer support, illustrated in Fig. 1, was used to determine if any significant oxidation was missed in the first second of exposure to oxygen before stopcock S_5 could be closed. Before the start of the measurement, oxygen at a pressure of 350 mm was admitted from the manifold to the volume confined by stopcocks S_4 , S_6 , and S_7 . Stopcock S_5 was then closed. The trapped gas was expanded into the empty cell by opening stopcock S_3 . Stopcock S_6 was then opened, allowing a similar amount of gas to expand into the cell containing the aluminum. The mercury manometer immediately fell to a low reading, and, since S_5 was already closed, any reaction which occurred during the first instant of contact of oxygen with the aluminum was registered on the manometer. This reaction was found to be negligibly low. Blank runs were made at temperature to establish the pressure correction resulting from the small difference in volume between stopcocks S_4 and S_5 and the volume between stopcocks S_5 and S_6 .

Some experiments were conducted in which the reactant gas was introduced into the sample chamber at room temperature after degassing the foil or wire sample for several hours under high vacuum. The sample then was heated to the desired temperature and held for a long enough time for the low rate portion of the oxidation curve to be reached. The amount of oxidation indicated by the pressure difference (corrected by pressure difference developed in a similar experiment with no aluminum present) was the same as when the sample was oxidized to the same low rate portion of the oxidation curve using the normal procedure. This proves that preoxidation of the aluminum before admitting the oxygen was negligible.

Sample calculation of manometric data.—The weight gain of the aluminum is given in terms of the experimentally measured quantities by Eq. [1].

$$\Delta W = K_1 h (1 + K_2) \quad [1]$$

where

$$K_1 = 37.7 \left[\sum_i \frac{V_i}{T_i} \right] \rho \quad [2]$$

$$K_2 = \frac{1.36 P_o \pi R^2}{T_1 \left[\sum_i \frac{V_i}{T_i} \right] \rho} \left[\frac{\sum_i \frac{V_i}{T_i} + \sum_i \frac{V_i'}{T_i}}{2 \sum_i \frac{V_i'}{T_i}} \right] \quad [3]$$

and ρ is the density of the manometer fluid in g/ml; P_o , the gas pressure in mm Hg; R , the radius of the manometer capillary, cm; ΔW , the weight of oxygen consumed in μg ; h , the reading on the differential manometer, mm; T_1 , the temperature of the tubing outside the furnace, $^\circ\text{K}$; V_i/T_i , the volume in ml of sample cell at temperature T_i , divided by the reference temperature T_i in $^\circ\text{K}$; V_i'/T_i' , the volume in ml of reference cell at temperature T_i divided by the temperature T_i in $^\circ\text{K}$.

The first term in Eq. [1] arises from the consumption of oxygen by the metal specimen in the sample chamber. The second term is a correction for changes in the room temperature volume due to the rise and fall of oil in the manometer arms and for differences in the volume-temperature terms of the reaction and reference cells.

In a typical experiment at 600°C , $K_1 = 2.03$, and $K_2 = 0.746$.

Surface Roughness

The effect of surface roughness on oxidation was demonstrated in a number of tests (Fig. 2) in which the surfaces of high-purity aluminum samples were given various treatments before they were oxidized on a manually operated version of the microbalance used in this work. One treatment consisted of polishing the sample with 000 metallographic paper under a solution of paraffin in kerosene, as done in a number of the published works on the oxidation of aluminum (1-3). This resulted in weight gains which were about five times higher than for as-rolled material and about ten times higher than for the chemically polished samples.

It might be thought that polishing removed a film from the as-rolled material which prevented oxidation, and that the R-5 treatment caused a film which further limited oxidation. These possibilities are disproved by the finding that continued polishing to

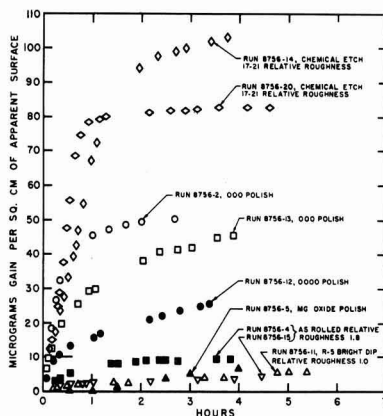


Fig. 2. Effect of surface roughness on oxidation of high-purity aluminum foil at 525°C in 25 cm of moist air.

progressively finer finishes, i.e., 0000 metallographic paper and a magnesium oxide polish, lowered the weight gain on oxidation to the value obtained with the R-5 treated sample.

Oxidation of samples that had been etched with a solution of hydrochloric acid and copper nitrate at 80°C (Alcoa U.S. Patents 2,796,334 and 2,796,335) gave weight gains about twenty times higher than for the R-5 treated samples. Additional evidence that these differences are produced by surface roughness is provided by measurement of the surface roughness of several of these samples by the radioactive phosphoric-chromic acid method of Lewis and Plumb (5). Relative roughnesses of 17-21, 1.8, and 1.0 were measured, respectively, for etched, as-rolled, and R-5 Bright Dip samples.

The different shapes for the oxidation curves shown in Fig. 2 may result from the spacing of the individual asperities relative to the thickness of oxide that forms. The linearity of the initial portions of the curves for the chemically etched surface implies that the high roughness factor of these samples (17-21) results from asperities separated by at least the thickness of the barrier film that forms during oxidation. The rounding of the oxidation curves for the samples polished with 000 paper and 0000 paper indicates that the asperities that cause the roughness in these cases are more closely spaced such that the oxide films forming on adjacent asperities meet before the barrier thickness is reached. This would cause a reduction in oxidizing area as oxidation proceeds.

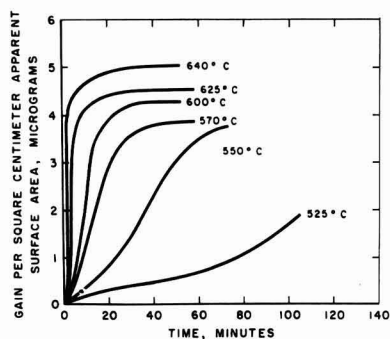


Fig. 3. Oxidation of high-purity aluminum in 150 mm of dry oxygen, manometric data.

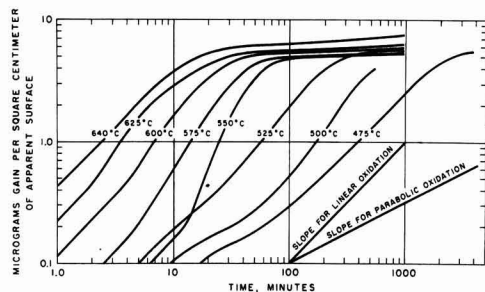


Fig. 4. Oxidation of chemically polished high-purity aluminum in 50 mm of dry oxygen.

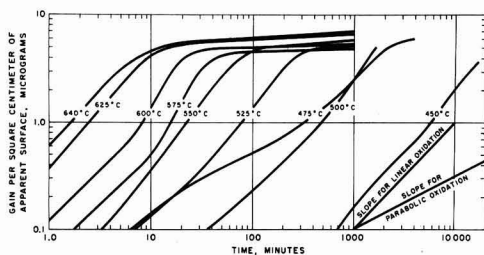


Fig. 5. Oxidation of chemically polished high-purity aluminum in 50 mm of air containing 1.4 mm of water vapor.

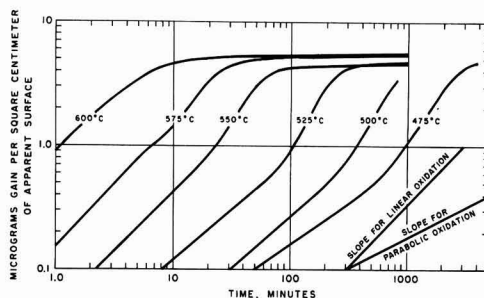


Fig. 6. Oxidation of chemically polished high-purity aluminum in 4.6 mm of water vapor.

Oxidation Rates

The results from the oxidation of high-purity aluminum in 150 mm of dry oxygen, as measured by the manometric method, are shown in Fig. 3. The results by the gravimetric method are shown for oxidation in 50 mm of dry oxygen in Fig. 4; for 50 mm of air containing 1.4 mm of water vapor in Fig. 5; and for 4.6 mm of water vapor alone in Fig. 6. Data were taken over a temperature range of 475°-640°C in all cases.

Oxidation of 5052 alloy in dry oxygen and moist air was measured by the gravimetric method over a temperature range of 350°-550°C. The results are shown in Fig. 7 and 8, respectively.

High-Purity Aluminum

The agreement between data obtained by the manometric and the gravimetric methods is good. Differences between the two were of the same order of magnitude as deviations between identical experiments on the same system. The only appreciable

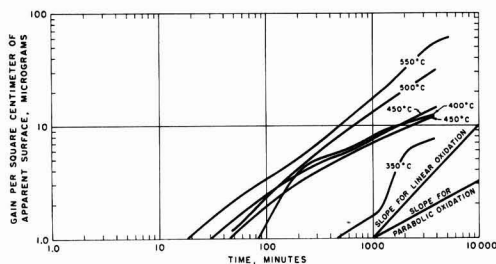


Fig. 7. Oxidation of chemically polished 5052 aluminum alloy in 50 mm of dry oxygen.

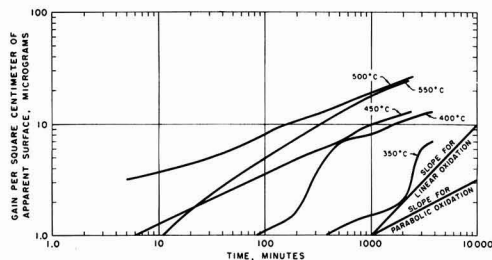


Fig. 8. Oxidation of chemically polished 5052 aluminum alloy in 50 mm of air containing 4.6 mm of water vapor.

differences approached $\pm 0.15 \mu\text{g}/\text{cm}^2$ and occurred in the first 5-10 min of oxidation. The oxidation data do not follow any of the known rate formulas in any of the atmospheres tried. Except for a few cases at the lower temperatures, the initial stages of oxidation appear to be linear. Below the $1 \mu\text{g}/\text{cm}^2$ weight gain level, the reaction accelerates and reaches a maximum between 1 and $2 \mu\text{g}/\text{cm}^2$. The rate begins to decline between 3 and $4 \mu\text{g}/\text{cm}^2$. Beyond this it decreases rapidly to a much lower rate in the 5-7 $\mu\text{g}/\text{cm}^2$ range. The oxidation rates in all three atmospheres were surprisingly similar, even though the pressure employed in the oxidations with water vapor was less than one-tenth of that employed in the oxidations with dry oxygen. Gulbransen and Wyszog (1) have shown that the amount of oxidation after 2 hr in dry oxygen at 500°C was only 20% greater at 7.6 cm pressure than at 0.076 cm pressure. However, Wilkins and Wanklyn (12) have shown that the corrosion rate of an aluminum-nickel alloy at 325°C increased as the fourth power of the steam pressure in the pressure range from 550 to 1520 psi. In this work, the rates in the moist atmospheres were slightly faster than in dry oxygen at each temperature above 550°C . Below 550°C , the opposite was true. The rates in moist air were about the same as in water vapor, indicating that the basic kinetic reactions are not altered by the presence of oxygen and nitrogen. This is similar to the findings of Blackburn and Gulbransen (8), in which the rates in moisture alone and in combination with oxygen or hydrogen, were essentially the same. The time required for the oxidation to reach the low rate represented by the nearly horizontal straight line in the figures decreased from 4000 min at 475°C to around 20 min at 640°C .

5052 Alloy

Oxidation of 5052 alloy is much faster and proceeds to much higher weight gains than in the case of high-purity aluminum at any of the temperatures tried. The oxidation curves showed no sign of leveling off in a fixed weight gain range. The slopes of the curves are generally less than that corresponding to linear oxidation and approach those for parabolic oxidation, particularly in moist air. The curves are quite irregular in shape, and data obtained at different temperatures overlap in many cases. Samples which had considerable magnesium losses during the 20 min period that the samples were heated to temperature showed less oxidation than ones in

which there was no magnesium loss. Magnesium evaporation was prevented if a trace of water vapor at the 10^{-6} mm Hg pressure level was present in the balance envelope.

The rate of magnesium evaporation from unoxidized surfaces in vacuum was much greater than the oxidation rate of the same metal exposed to an oxidizing atmosphere. The weight losses of magnesium in the 20 min heating period for the experiments at 550°C in dry oxygen were, respectively, 75 and $145 \mu\text{g}/\text{cm}^2$, compared to subsequent oxidation weight gains of 32 and $55 \mu\text{g}/\text{cm}^2$, respectively, in 4000 min. This bears out Smeltzer's (9) findings that diffusion of magnesium to the metal surface is not normally a rate-determining step in this oxidation.

The temperature dependence of the oxidation rate of 5052 alloy found in this work is much less than found by Smeltzer for an aluminum-3% magnesium alloy. The rate of weight gain in his work is roughly ten times greater than in this work at 550°C . This factor decreases to 6 at 500°C , 3 at 450°C , 1 at 400°C , and $\frac{1}{2}$ at 350°C . The large difference at higher temperatures could be explained by the same surface roughnesses of 8 to 10 found for Smeltzer's work with high-purity aluminum. The reason for the smaller differences at lower temperatures is not apparent unless it is associated with the additional components in 5052 alloy compared to the binary alloy used by Smeltzer.

Nearly all of the samples oxidized in water vapor and moist air developed small blisters on the surface, but none were formed in dry oxygen. Blackburn and Gulbransen (8) found that all of their samples that were oxidized in water vapor blistered either on grain boundaries or along lines parallel to the rolling direction except ones partially oxidized in dry oxygen or pretreated in 1M HCl solution. They found that the rate of oxidation of the HCl treated sample in water vapor at 600°C was the same as for untreated aluminum. By vacuum fusion they found only 0.8 ml/100 g of hydrogen in the oxidized HCl treated sample compared to 2.8 ml/100 g for an oxidized specimen which had not received the HCl treatment. In the present work, this effect of HCl has been verified. In addition, treatment of 5052 alloy with the decomposition vapors of ammonium chloride or ammonium fluoborate prevented blistering. Treatment with aqueous solutions of lithium or potassium fluoride did not prevent blistering. Free energy relationships show that neither lithium nor potassium fluoride can react with any of the components in this metal. The mechanism by which these surface treatments prevent blister formation was shown to be catalysis of the $2\text{H} = \text{H}_2$ equilibrium at the reaction surface and formation of barrier films (13).

The cause for faster oxidation in the presence of water vapor is not established. A possible explanation is that blistering may disrupt the oxide film and expose fresh metal surface to the oxidizing atmosphere. The surface roughness would be greater after oxidation than before in this case. An attempt to measure surface roughness after oxidation by the method of Lewis and Plumb (5) failed when the

thick oxide could not be removed to provide the necessary bare metal surfaces.

Electron diffraction examination of the surface oxidation products showed only eta alumina on the high-purity aluminum and only magnesium oxide on the 5052 alloy, regardless of the atmosphere.

Manuscript received July 1, 1960; revised manuscript received Nov. 21, 1960.

Any discussion of this paper will appear in a Discussion Section to be published in the December 1961 JOURNAL.

REFERENCES

1. E. A. Gulbransen and W. S. Wysong, *J. Phys. Chem.*, **51**, 1087 (1947).
2. W. W. Smeltzer, *This Journal*, **103**, 209 (1956).
3. D. W. Aylmore, S. J. Gregg, and W. B. Jepson, *J. Inst. Metals*, **88**, 205 (1960).
4. M. S. Hunter and P. Fowle, *This Journal*, **103**, 482 (1956).
5. J. E. Lewis and R. C. Plumb, *Internat. J. Appl. Radiation and Isotopes*, **1**, 33 (1956).
6. R. C. Plumb, *This Journal*, **105**, 502 (1958).
7. P. M. Aziz and H. P. Godard, *ibid.*, **104**, 738 (1957).
8. P. E. Blackburn and E. A. Gulbransen, *ibid.*, **107**, 944 (1960).
9. W. W. Smeltzer, *ibid.*, **105**, 67 (1958).
10. C. N. Cochran, *Rev. Sci. Instr.*, **29**, 1135 (1958).
11. W. E. Campbell and U. B. Thomas, *This Journal*, **91**, 623 (1947).
12. N. J. M. Wilkins and J. N. Wanklyn, *J. Inst. Metals*, **88**, 134 (1959).
13. C. N. Cochran, *This Journal*, **108**, 317 (1961).

Critical pH and Critical Current Density for Passivity in Metals

Herbert H. Uhlig

Corrosion Laboratory, Department of Metallurgy, Massachusetts Institute of Technology, Cambridge, Massachusetts

ABSTRACT

Based on electrochemical mechanisms, an equation is derived for the relation of pH to the critical current density necessary to passivate metals: $i(\text{crit.}) = K(H^+)^\lambda$ where K and λ are constants. Accordingly, a linear relation between $\log i(\text{crit.})$ and pH is observed for Cr, Ni and 14% Cr-Fe alloys. When passivity occurs by reason of dissolved oxygen, it is shown that $i(\text{crit.})$ usually equals the limiting diffusion current density for O_2 . A critical pH exists above which passivity is stable, but not below. This critical pH decreases linearly with the logarithm of dissolved O_2 concentration. Calculated and observed values for the critical pH of 14% Cr-Fe alloy are in reasonable agreement.

In absence of O_2 , passivity is achieved when the rate of reduction of H^+ exceeds $i(\text{crit.})$. Metals in this category must have Flade potentials more active than the hydrogen electrode in the same solution. More active Flade potentials accompany greater thermodynamic stability of the passive film, accounting in part for greater resistance to breakdown of passivity by specific anions. Among the metals in this category achieving high corrosion resistance in deaerated acids are Ti, Ta, Zr, and Mo.

Some metals with a pronounced tendency to corrode nevertheless react with their environment at a very low rate and are said to be passive. For certain metals, passivity results from exposure to air or to an oxidizing medium; for others passivity occurs in almost any aqueous solution. It is characteristic of passive metals, as presently considered, that their corrosion potentials in the passive state are more noble than their activation or Flade potentials, the latter marking the potential which divides the active from the passive region. The Flade potential of iron, for example, is determined empirically as the least noble value of the potential arrest just before spontaneous decay of passivity to the active state.

In general, hydrogen ion activity is one of the variables in a given aqueous environment determining passivity, and a critical pH exists which marks the boundary between stable and unstable passivity. This concept was first discussed by Rocha and Lenartz (1) in connection with passivity in the Cr-Fe alloy system. The present paper deals with the relation of critical pH to Flade potential and the evaluation of critical pH from a knowledge of polarization and potential behavior.

Anodic Polarization Curve

The shape of the anodic polarization curve determined potentiostatically for a metal like iron in a dilute electrolyte, e.g., H_2SO_4 , (neglecting local action current) is given schematically by curve E_a BFG in Fig. 1. On flow of current, the potential moves in the noble direction from the equilibrium potential at E_a for $Fe \rightleftharpoons Fe^{2+} + 2e$ to the critical potential for passivity B corresponding to the critical current density, $i(\text{crit.})$. The critical potential at B for iron approximates the Flade potential E_f , but in 1N H_2SO_4 tends to be somewhat more active probably because the surface pH is slightly higher than in the bulk of solution. Further change of potential results in reduction of the steady-state current density to a very small value i_p corresponding to the passive state and a low corrosion rate. The current again increases at a potential corresponding to evolution of oxygen, with some increase in corrosion of the electrode. This is called the transpassive region. For passive Cr, corrosion occurs with formation of $Cr_2O_7^{2-}$ equivalent to Faraday's law before the O_2 potential is reached, and hence increased corrosion may take place in the transpassive region without O_2 evolu-

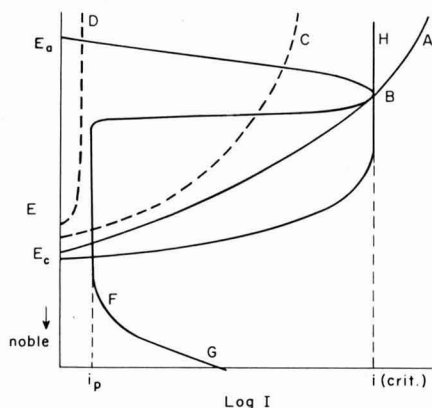


Fig. 1. Cathodic and anodic polarization curves showing effect on passivity of dissolved oxygen.

tion. Nickel behaves similarly forming Ni^{++} in both the passive and transpassive regions.

The Flade potential E_f is related to pH of the solution in which passivity decays by

$$E_f = E_f^\circ - \frac{RT}{nF} \ln (H^+) \quad [1]$$

where n for iron is unity (2), but which is reported to be as low as 0.5 for Fe-Cr alloys or Cr cathodically activated (1). The term n , however, is also approximately unity for the latter metals when they are self-activated by immersing in acids of specific pH (3). Knowing the equation, therefore, expressing anodic polarization of the metal, and the initial equilibrium potential for the anodic reaction, one can evaluate the relation between $i(\text{crit.})$ and pH at the intersection of the polarization curve with the critical potential for passivity, or the approximate Flade potential. The equation for anodic polarization is given by the sum of terms representing activation polarization, concentration polarization, and IR drop through films at the surface of the electrode. The actual potential at the metal surface determining whether or not the passive film can form is independent of potential drop through surface films (e.g., FeSO_4), hence the IR term should be omitted for present considerations. Assuming that the critical potential at B is approximated by the Flade potential

$E_a - E_f = \text{Activation polarization}$

+ Concentration polarization [2]

Activation polarization is given by the usual Tafel relation $RT/\alpha zF \ln i_a/i_a^\circ$ where i_a° is the exchange current density, α is the transfer coefficient, i_a is the current density required to polarize to potential E_f , and z is the valence of metal ion. The term i_a° may depend on H^+ activity, which can be expressed by

$$i_a^\circ = k(H^+)^{-\gamma} \quad [3]$$

where k and γ are constants. Heusler (4) observed an hydroxyl ion dependence of i_a° for iron in H_2SO_4 , consistent with Eq. [3].

On the other hand, the concentration polarization term (5) is given by $\frac{RT}{zF} \ln \left(1 + \frac{i_a}{k'A}\right)$ where A is the activity of metal ion in solution away from the metal surface. It is equivalent to the activity of metal ion at the electrode surface when the metal is first immersed in an electrolyte initially free of metal ions, hence A is almost always small. The term $k' = DnF/\delta(1-t_+)$ where D is the diffusion constant for metal ions, δ is the thickness of the stagnant diffusion layer adjacent the metal surface, and t_+ is the transference number for the metal ion. At the high values of i_a presently considered, $i_a/k'A$ is large compared to unity, and the concentration polarization term becomes $\frac{RT}{zF} \ln \frac{i_a}{k'A}$.

Substituting into Eq. [2] on the condition that $i_a = i(\text{crit.})$ when the polarized potential equals E_f , it follows that

$$i(\text{crit.}) = K(H^+)^\lambda \quad [4]$$

where

$$\lambda = \left(\frac{1}{\alpha + 1}\right) \left(\frac{z\alpha}{n} - \gamma\right)$$

and

$$K = k \left(\frac{1}{\alpha + 1}\right) (k'A) \left(\frac{\alpha}{\alpha + 1}\right) \exp \frac{zF}{RT} \left(\frac{\alpha}{\alpha + 1}\right) (E_a - E_f^\circ)$$

Equation [4] illustrates that the critical current density for any metal is greater the larger the difference between the equilibrium potential E_a and the standard Flade potential E_f° , and, depending on the value of λ , usually increases with hydrogen ion activity. Stirring the solution increases $i(\text{crit.})$ because δ is made smaller which increases in turn the value of k' . The value of λ , on the other hand, is unaffected by stirring.

In accord with Eq. [4], the logarithm of critical current density should be approximately linear with pH. This relation is observed for Cr (6), Ni (7) and for 14% Cr-Fe alloy (3, 8) as plotted in Fig. 2. In absence of reliable data for anodic polarization of iron and other transition metals, a more detailed numerical evaluation of Eq. [4] is not yet possible.

Passivity in Presence of O_2

If on exposing a metal to an aqueous environment in which reduction of dissolved O_2 is the cathodic reaction accompanying passivation, two general cases must be considered. The first concerns the situation for which $i(\text{crit.})$ is less than the limiting diffusion current i_L for oxygen (curve A, Fig. 1), and the second concerns the situation $i(\text{crit.}) = i_L$ (curve H, Fig. 1). When i_L is less than $i(\text{crit.})$, stable passivity is no longer attained; instead only either unstable passivity (curve C) or activity (curve D) is possible. It is assumed that the shape of the cathodic polarization curve for reduction of O_2 is determined largely by the concentration polarization term $\frac{RT}{4F} \ln \frac{i_L}{i_L - i_c}$ where i_c is the cathodic current

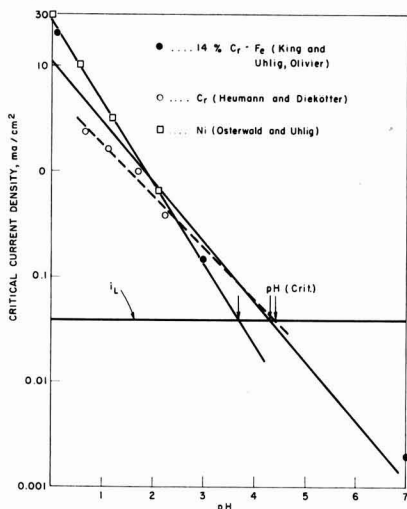
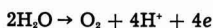


Fig. 2. Relation of critical current density for passivity to pH and to limiting diffusion current for reduction of oxygen.

density. For the first case, therefore, under conditions resulting in passivity, the polarized potential $E' = E_p$ at $i_o = i(\text{crit.})$. Assuming for Eq. [1] that $n = 1$,

$$E_p = E_o + \frac{0.059}{4} \log \frac{i_L}{i_L - i(\text{crit.})} = E_p^o + 0.059 \text{ pH} \quad [5]$$

where E_o is the equilibrium potential of the oxygen electrode. Because the O_2 potential is not truly reversible, E_o is only approximated by the potential for the following reaction:



$$E_o \text{ (volts)} = -1.23 + 0.059 \text{ pH} - \frac{0.059}{4} \log p_{O_2} \quad [6]$$

Substituting Eq. [6] in Eq. [5]

$$\log \left(1 - \frac{i(\text{crit.})}{i_L} \right) = -\frac{4}{0.059} \left(1.23 + \frac{0.059}{4} \log p_{O_2} + E_p^o \right) \quad [7]$$

The right-hand term for $p_{O_2} = 0.2$ atm is equal to $-82.5 - 68 E_p^o$. Considering the fact that E_p^o for Fe, the Fe-Cr alloys and Cr range from -0.6 to $+0.2$ v, it is obvious that the logarithm term has so large a negative value that for all practical purposes whenever passivity is achieved, $i(\text{crit.}) = i_L$. This is true even if the actual O_2 potential at E_o is several tenths volt more active than the assumed reversible value.

We shall consider, therefore, the next case for which the limiting diffusion current equals the critical current.

Since $i_L = \frac{DnF}{\delta} c$ it follows that

$$i(\text{crit.}) = \frac{DnF}{\delta} c \quad [8]$$

where D is the diffusion constant for O_2 (2×10^{-8} cm²/sec), $n = 4$, $F = 96,500$ coulombs/equivalent, δ as before is the thickness of the stagnant diffusion layer (about 0.05 cm) and c is the concentration of dissolved oxygen (2.5×10^{-7} mole/cm³ for air-saturated water). At room temperature i_L is calculated equal to 0.039 ma/cm². Since $i(\text{crit.}) = i_L = K(H^+)^n$, we can substitute this relation into Eq. [8]. Taking logarithms of both sides:

$$\text{pH}(\text{crit.}) = -\frac{1}{\lambda} \log \frac{DnF}{K\delta} c \quad [9]$$

Data of King (3) provide values for the critical current density at pH 3 and 7 for 14% Cr-Fe alloy giving approximate value of λ and K equal to 0.5 and 5.5×10^{-3} , respectively. Substituting these values into Eq. [9], the calculated value for $\text{pH}(\text{crit.}) = 4.3$. Alternatively, the critical pH can be evaluated graphically by plotting $i(\text{crit.})$ vs. pH and determining the intersection with i_L as is done in Fig. 2. For 14% Cr-Fe the critical pH, is found to be 4.3, for Cr it is 4.4, and for Ni it is 3.7. This means that in aerated acids of lower pH, passivity of these metals may break down, whereas at higher pH values passivity is self-repairing. The observed critical pH for 14% Cr-Fe of about 3.3, measured by Rocha and Lennartz (1), is consistent with the calculated value.

Although Eq. [9] may not hold quantitatively in the alkaline region for iron, it permits nevertheless certain reasonable predictions. The observed value of K is larger than for Cr-Fe alloys [$i(\text{crit.}) = K(H^+)^n = 0.2$ amp/cm² in 1N H₂SO₄ taking into account concentration polarization, or about 17 amp/cm² in its absence (9)], hence assuming, a positive λ as measurements indicate, $\text{pH}(\text{crit.})$ is moved to more positive values. In accord, the observed critical pH for iron is about 10 compared to 3.3 for 14% Cr-Fe. Furthermore, if i_L is increased by increasing the partial pressure of O_2 , Eq. [9] indicates that the critical pH moves to lower values since $\text{pH}(\text{crit.})$ is proportional to $\log 1/O_2$ conc. In accord with this prediction, iron can be passivated in distilled water if saturated with pure O_2 (10), but only in water of pH 10 or higher when air-saturated (11). Equation [9] also predicts in accord with observation that passivity is achieved at a lower pH if the solution is stirred (δ is made smaller).

Passivity in Absence of O_2

In absence of O_2 or other cathodic depolarizers, H^+ is reduced at cathodic areas of a corroding metal. If we consider only the case for which concentration polarization is negligible, the polarized cathodic potential E' becomes the sum of the equilibrium potential for the hydrogen electrode and a term describing hydrogen overvoltage.

$$E' = -\frac{RT}{F} \ln (H^+) + \frac{RT}{\alpha_c F} \ln \frac{i_o}{i_c} \quad [10]$$

In line with Eq. [3], it can be assumed that $i_o^o = k''(H^+)^n$. This assumption is reasonable even though for small intervals of pH the exchange current den-

sity for the hydrogen evolution reaction is normally assumed to be independent of pH. As before, passivity is achieved when E' reaches E_f at $i_c = i(\text{crit.})$. By making use of Eq. [1], it follows that

$$i(\text{crit.}) = K'(H^+)^{\lambda'} \quad [11]$$

$$\text{where } K' = k' \exp \frac{\alpha_e F E_f^{\circ}}{RT} \text{ and } \lambda' = \left(\frac{n-1}{n} \right) + \epsilon.$$

Equation [11] is of the same form as Eq. [4]. Within the limitations of simplifying assumptions made in the derivations, comparison of the two equations leads to $\lambda = \lambda'$ and $K = K'$.

Equation [11] can be rearranged in terms of a critical pH, above which for a given $i(\text{crit.})$, passivity may break down because local action current falls below $i(\text{crit.})$, and below which passivity is stable.

$$\text{pH}(\text{crit.}) = \frac{1}{\lambda'} \log \frac{k'}{i(\text{crit.})} + \frac{\alpha_e F E_f^{\circ}}{2.3 \lambda' RT} \quad [12]$$

The above equation does not hold for metals like Fe for which E_f is more noble than the H_2 electrode. On the other hand, it holds for metals like Ti, for which E_f according to potentiostatic data falls between approximately +0.01 and +0.25 v, H_2 scale, in 20% H_2SO_4 (12). Passivity in this case can in principle break down not only on raising the pH, but also and more often, on lowering of pH through another mechanism accounted for by high anion concentrations in concentrated acids. For example, in HCl or H_2SO_4 , loss of passivity of Ti may result from destruction of the passive film by Cl^- or SO_4^{2-} . These anions, according to the oxide film theory of passivity, easily penetrate the oxide destroying its protective qualities. According to the adsorbed film theory, Cl^- or SO_4^{2-} in competition with OH^- adsorb on the metal surface, simultaneously increasing the value of the exchange current density i_0 for dissolution of metal to its ions, compared to a characteristic low i_0 when oxygen is adsorbed [$2 OH^- (\text{adsorbed}) \rightarrow O (\text{adsorbed}) + H_2O$]. In either case $i(\text{crit.})$ increases. However, by increasing the anodic current density in such environments, for example through coupling or alloying with a lower H_2 -overvoltage metal like Pd, passivity is again restored, as discussed by Stern and Wissenberg (13) for Ti, and by Tomashov (14) for stainless steels.

Other examples of metals which become passive in absence of dissolved O_2 are tantalum, zirconium, and molybdenum which retain passivity in many air-free acids even at the boiling point. Local action

currents in acids with accompanying hydrogen evolution are sufficient to reach or exceed the critical current density necessary to form the passive film. In accord with the preceding discussion, critical potentials for passivation, or Flade potentials, of these metals must be active compared to the H_2 electrode in the same media. More active Flade potentials parallel increased thermodynamic stability of the passive film as discussed by King and Uhlig (3) and demonstrated by Feller and Uhlig (15) making it more difficult for anions to displace adsorbed species responsible for passivity. It is also possible that for metals in this category anions such as Cl^- have less effect on the exchange current density for metal dissolution than in the case of Fe or Cr. Such properties provide a basis for understanding the stable passivity of these metals under extremely corrosive conditions.

Acknowledgment

This investigation was supported by the International Nickel Company, Inc., to whom the author expresses his appreciation. He is also pleased to acknowledge helpful discussions with Jörg Osterwald.

Manuscript received Aug. 30, 1960; revised manuscript received Dec. 5, 1960. This paper was prepared for delivery before the Houston Meeting, Oct. 9-13, 1960.

Any discussion of this paper will appear in a Discussion Section to be published in the December 1961 JOURNAL.

REFERENCES

1. H. Rocha and G. Lennartz, *Archiv. Eisenhüttenw.*, **26**, 117 (1955).
2. U. F. Franck, *Z. Naturforschung*, **4A**, 378 (1949).
3. P. F. King and H. H. Uhlig, *J. Phys. Chem.*, **63**, 2026 (1959).
4. K. Heusler, *Z. Elektrochem.*, **62**, 582 (1958).
5. S. Glasstone, "Introduction to Electrochemistry," pp. 445-9, 457-9, D. Van Nostrand Co., New York (1942).
6. Th. Heumann and F. Dieckötter, *Z. Elektrochem.*, **62**, 745 (1958).
7. J. Osterwald and H. Uhlig, submitted to *This Journal*.
8. R. Olivier, Proc. Int. Com. Elect. Therm. and Kinetics, 6th Meeting, Poitiers p. 314, Butterworths, London (1954).
9. K. Bonhoeffer, *Z. Metallkunde*, **44**, 77 (1953).
10. E. Groesbeck and L. Waldron, *Proc. Am. Soc. Test. Mat.*, **31**, Part II, 279-291 (1931).
11. H. H. Uhlig, Editor, "Corrosion Handbook," p. 130, John Wiley & Sons Inc., New York (1948).
12. M. Stern and H. Wissenberg, *This Journal*, **106**, 755 (1959).
13. M. Stern and H. Wissenberg, *ibid.*, **106**, 759 (1959).
14. N. Tomashov, *Corrosion*, **14**, 229t (1958).
15. H. Feller and H. Uhlig, *This Journal*, **107**, 864 (1960).

Electrochemical Measurements of Corrosion Rates on Zirconium and Zircaloy-2 at Elevated Temperatures

A. L. Bacarella

Chemistry Division, Oak Ridge National Laboratory, operated by
Union Carbide Corporation for the U. S. Atomic Energy Commission, Oak Ridge, Tennessee

ABSTRACT

Electrochemical measurements of corrosion rates have been performed on crystal bar zirconium and Zircaloy-2 in highly oxygenated, dilute sulfuric acid at 167° and 208°C. The calculated rates of corrosion obtained from the small current polarizability measurements are roughly hyperbolic in rate-time. Some reproducible but unexplained observations concerning the potentials and polarizabilities of the Zircaloy-2 during the first several minutes of reaction are also discussed.

Corrosion measurements by weight loss methods, particularly when the rate is changing rapidly with time, are tedious and time consuming. The measurements involve the frequent removal of the sample for weight change measurements, which often affect the subsequent corrosion rate upon re-exposure to the environment. The measurements at best yield only average rates over significantly extended time intervals. Furthermore, when applied to metals such as zirconium and titanium, which passivate rapidly to very low rates, the measurements become inadequate. Methods based on manometric techniques and chemical analysis also do not produce satisfactory results for many of the same reasons. Recently however, several investigators (1-5) have shown that the slope of the linear portion of the polarization curve can be related to the corrosion rate. Stern and Geary (6) and Posey (7) have further demonstrated that this relationship has some foundation in theory. The method shows great promise for the investigation of many corrosion systems previously incapable of study. It is a rapid method which yields instantaneous rates,¹ and very importantly, the measurements are made with a minimum disturbance to the system. It is a method capable of measuring rapid changes in rates and of determining rates too low for measurement by other techniques. It is the purpose of this report to demonstrate that this technique can be employed to study the corrosion of zirconium and Zircaloy-2 in oxygenated aqueous acid at temperatures in excess of 100°C.

Experimental

The measurements were carried out in a titanium reaction cell designed to contain approximately 50 cc of aqueous acid at 300°C and 2000 psi. The reaction cell was mounted in a vertical position and contained five convenience ports, four at the top

¹The statement "instantaneous rates" has meaning only from an experimental basis, i.e., the rates are calculable from a "single" linear-polarization measurement rather than from a difference between two measurements, such as weight-changes, pressure-drops, etc. The time duration for the establishment of the overvoltage is, however, a function of the rate of corrosion of the zirconium and varies from about 1-10 sec for rates of 10^{-4} - 10^{-6} amp/cm² to about 10-100 sec for rates of 10^{-8} - 10^{-9} amp/cm². The corrosion rate of the metal is high and is decreasing most rapidly during the initial period of exposure to the high-temperature aqueous environment. It is also during this period that the measurements can be made most rapidly.

and one at the bottom. Solution entered the cell through the bottom and exited from one of the top ports. The three other ports provided for the electrodes: a Zircaloy-2 test electrode, a platinum "reference" electrode, and a titanium polarizing electrode (which also contained a thermocouple well for temperature measurements). A Teflon cone was used to insulate these electrodes from the reaction cell. A drawing of the reaction cell and the insulated fittings is shown in Fig. 1. A schematic diagram of the high-pressure components is shown in Fig. 2. All the room temperature components were constructed of stainless steel and the high-temperature components of titanium. It has been demonstrated by numerous analyses of the solutions that with these materials of construction negligible amounts of corrosion products entered the solution.

The Zr-2 electrodes were used in the as-received state. They were rod type specimens, 0.093 in. diameter and 4 in. long, only 2 in. of its length ex-

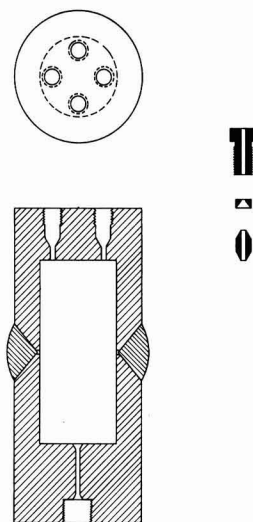


Fig. 1. Reaction cell

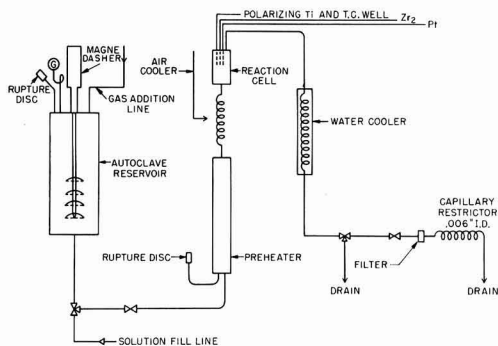


Fig. 2. Equipment for electrochemical measurements at high temperature and pressure.

tending beyond the Teflon mount. A more accurate estimate of the length was made at the termination of the experiment from a measurement of the corroded portion.

Before immersion into the cell the electrodes were scrubbed with soap and water, rinsed thoroughly with distilled water and then with acetone.

The solutions were made from triply distilled water, and concentrated C.P. H_2SO_4 . Twelve liters of solution were prepared for each experimental run.

The entire assembly was rinsed with 48-60 l of distilled water prior to loading with the test solution. The solution was aspirated into the 20-l stainless autoclave and saturated with 250 psi O_2 gas with a Magne-Dasher.² A super-pressure of helium, 1300 psi total pressure, was used to maintain the O_2 and steam in solution at 250°C and provided the pressure differential for solution flow through the reaction cell. Partial opening of an Autoclave Engineers' valve provided the adjustment for a solution flow rate of about 1 cc/min through the reaction cell.

The solution was preheated to 250°C in a 3-ft section of 2 in. Schedule 40 titanium pipe prior to its entry into the reaction cell. The volume of solution contained at this temperature is approximately 1200 cc. Another furnace was designed in two half sections to fit around the titanium reaction cell and was mounted on tracks in the open position. This furnace was maintained at 210°C. With a flow rate of 1 cc/min and a vigorous stream of air directed past the reaction cell, the temperature in the reaction cell rose to a maximum of 38°C at the test electrode position. Conditions were deemed ready to commence the experiment at operating temperature, 208°C, after approximately 1 liter of solution flowed through the system. Both furnace temperatures were controlled to $\pm 2^\circ C$ with commercially available temperature controllers.

To realize rapid attainment of temperature, the following sequence of operations were performed: the air-flow was turned off, the split furnace was clamped into position around the reaction cell, and the exit valve was fully opened. These operations permitted the 1200 cc of 250°C solution to flow

through the system at a rate of about 300 cc/min, and attain operating temperature, 208°C, in 1-2 min. The solution flowed from the cell into water-cooled titanium tubing. After operating temperature was attained, the solution flow rate was decreased to 1 cc/min by closing the exit valve partially. At this time polarization measurements were performed.

Suitable safety facilities were installed to protect the operating personnel. These included safety shields, special cast-iron blast shields, rupture disks, and automatic relays to turn off the power to the system.

The potentials were measured with a modified L&N Model 7664 pH meter used as a potentiometer. The signal from the L&N meter was fed into a 10 mv Brown recorder. The very high input impedance of the pH meter precluded any polarization of the electrodes by the measuring circuit, even at the highest measured polarizability of the Zr-2.

Polarizing currents from 2×10^{-2} to 2×10^{-8} amp were obtained by imposing a selected voltage, from a bank of 22½-45 v Burgess "B" batteries connected in series, across a chosen resistance from $10 \cdot 10^6$ ohms provided by a series of decade switches. The currents were measured with time by recording the voltage drop across precision resistors connected in series with the decade switches in the polarizing circuit.

A typical rate-time experiment at 208°C would require polarizing currents of about 75 μa at the beginning, decreasing to 0.5 μa at the end. The currents for the linear polarization data were adjusted to obtain less than 20 mv overvoltage. The amount an electrode may be polarized and still exhibit linear behavior has been determined by Stern (8) for various values of the Tafel constants. It is estimated, from the values of the Tafel constants obtained, that a 20 mv polarization results in less than a 1 mv deviation from linearity in the current-potential plot.

Prior to terminating two of the experiments, the Tafel slope for O_2 reduction on Pt was determined. These measurements were performed to test the reliability of Pt as a reference electrode. The Zr-2 was made the reference electrode and the Pt the test electrode. The potential of Zr-2 vs. Pt had already attained a steady-state value to allow these measurements to be performed.

Calculations and Results

The expression which forms the basis for the calculations is reproduced in Eq. [1]:

$$(d\eta/dI)_{\eta \rightarrow 0} = \frac{b_a \times b_c}{2.3 I_{corr} (b_a + b_c)} \quad [1]$$

Here, I_{corr} is the corrosion rate of the electrode in amp/cm², $\eta = E - E_0$ in volts, and b_a and b_c are the Tafel slopes ($d\eta/d \log I$) for the oxidation and reduction reactions. The experimentally determined polarization resistance is defined as $(d\eta/dI)_{\eta \rightarrow 0}$,

where I is the net current in amp/cm² flowing through the electrode at the measured potential E ,

² Commercial agitator obtained from Autoclave Engineers.

and E_o is the potential at open circuit, or zero net current. Equation [1] is the form of the expression as obtained by Stern and Geary (6) and Posey (7).

In order to use this method,³ it must be demonstrated that the open-circuit potential results from the intersection of two logarithmic polarization curves, one anodic and one cathodic. There must be no significant oxidation reaction other than the oxidation of metal, and the sum of the Tafel slopes should remain constant or nearly so during the course of an entire reaction, or obtained as a function of time by additional experiments. The formation of a film should not preclude its applicability. Meyer (9) and Stern (10) recently applied these techniques to systems forming a passive oxide layer and demonstrated that logarithmic current-potential behavior is obtained on film-covered electrodes.

In the experiments reported, the rate-time behavior for oxide film growth on two Zr-2 alloys in 0.05F H₂SO₄, containing 600 ppm O₂, at 208°C has been determined. One alloy was obtained from Firth-Sterling, FS-Zr-2 and the other from Westinghouse, W-Zr-2. An experiment performed at 167°C on crystal bar zirconium, in 0.05F H₂SO₄, containing about 300 ppm O₂ is also reported. The over-all reaction is presumed to be the oxidation of zirconium to zirconium dioxide, ZrO₂, the anodic process being the oxidation of zirconium, and the cathodic process the reduction of O₂. A zirconium

alloy was chosen because it does not produce any soluble corrosion products which could possibly interfere with the principal reactions. The presence of impurities such as Fe¹³, Cu¹², etc., cannot be well controlled in the present experimental system. Numerous analyses however, put an upper limit of 10⁻⁶M, ranging mostly around 10⁻⁸ to 10⁻⁷M for the concentration of these constituents. With an oxygen concentration of 10⁻⁶M, it is expected that the rate of reduction of these species is negligible compared to the oxygen reduction rate. The concentration of any impurities which could lead to interfering anodic currents is most certainly insignificant in this highly oxygenated high-temperature environment.

In Fig. 3-7 the current-potential behavior for the reduction reaction is interpreted according to an equation of the form

$$I_c = I_{o,c} \exp \frac{\alpha_c Z_c F}{RT} \quad [2]$$

where α_c is the transfer coefficient⁴ of the cathodic process, Z_c is the charge number, and $I_{o,c}$ is a constant. This equation is the Tafel equation written in exponential form, with the Tafel constant $b_c = 2.3 RT/\alpha_c Z_c F$. If a similar expression for the anodic current, I_a , at constant film thickness, is assumed⁵

⁴ Other nomenclature in use has α as a symmetry factor, Z as a charge number, and the product of the two, αZ , as a transfer coefficient.

⁵ An expression of the form of Eq. [3] has been reported valid for the anodizing of zirconium at constant film thickness by Adams and Van Ryselberghe (11).

³ For a more complete description of the method than presented in this report see Stern and Weisert (4).

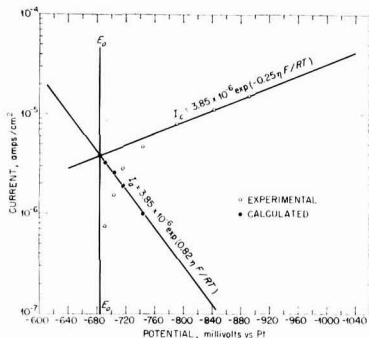


Fig. 3. Experimental current-potential plot (in 0.05F H₂SO₄, 600 ppm O₂, at 165°C, time 18 min) Run No. 1.

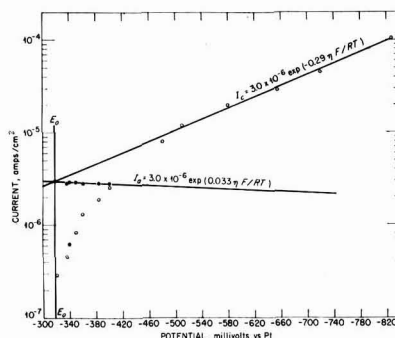


Fig. 5. Experimental current-potential plot (in 0.05F H₂SO₄, 600 ppm O₂, 208°C, time 6.2 hr) Run No. 10.

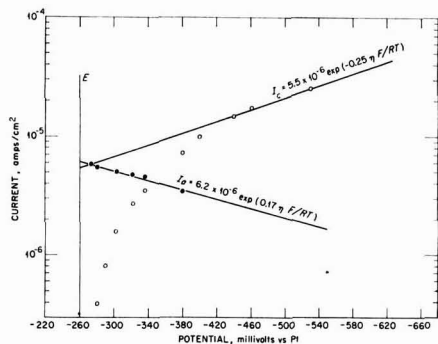


Fig. 4. Experimental current-potential plot (in 0.05F H₂SO₄, 600 ppm O₂, 208°C, time 96 min) Run No. 9.

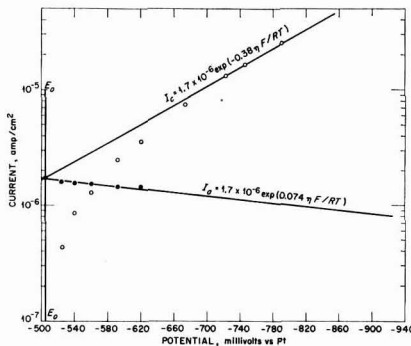


Fig. 6. Experimental current-potential plot (Zr-2 in 0.05F H₂SO₄, 600 ppm O₂, 208°C, time 11 hr) Run No. 8.

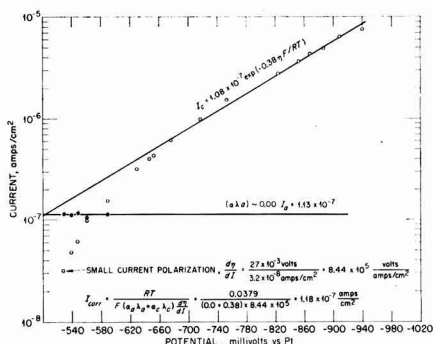


Fig. 7. Experimental current-potential plot (Zr-2 in 0.05F H₂SO₄, 600 ppm O₂, 165°C, time 27.9 hr) Run No. 1.

$$I_a = I_{o,a} \exp \frac{\alpha_a Z_a F}{RT} \quad [3]$$

where α_a and Z_a are the transfer coefficient and charge number for the anodic reaction, then Eq. [3] can be expressed in terms of these variables as

$$I_{corr} = \frac{RT/F}{(\alpha_c Z_c + \alpha_a Z_a) (d\eta/dI)_{\eta \rightarrow 0}} \quad [4]$$

The quantity $d\eta/dI$ is determined from a plot of I vs. E on a linear scale, and the slope determined at $E = E_o$. For larger applied currents, Eq. [2] and [3] determine the αZ values. However, the application of large anodic currents can affect the surface of a corroding electrode materially by forming significant quantities of film. Consequently, the data reported here have been determined for the most part by the method demonstrated in Fig. 3-7. Here the points for the anodic curve (9) are obtained as a difference between the net current and the extrapolated cathodic current.⁶ However, it has been consistently observed, even from the very earliest measurements, (after several minutes of reaction at temperature) that the anodic reaction is much more polarizable than the cathodic reaction. Consequently, an estimate of 0.1 ± 0.05 for the anodic $\alpha_a Z_a$ cannot be in great error. Numerous estimates obtained by extrapolating a single measurement of applied anodic current (of sufficient magnitude to be in the Tafel region) to the intersection of the extrapolated cathodic curve with E_o , also yielded values of $\alpha_a Z_a = 0.1 \pm 0.05$.

It has been found that the values obtained for $\alpha_a Z_a$ [with the exception of the very earliest measurement at 167°C (Fig. 3) where $\alpha_a Z_a = 0.82$] ranged from 0.17 to 0.00, averaging about 0.1 ± 0.05 , and showed no correlation with time. The cathodic αZ values however increased with time from 0.25 to 0.41.

In order to calculate the corrosion current from the small current polarizabilities, a constant average value, 0.45 ± 0.1 , has been assumed for the sum $(\alpha_a Z_a + \alpha_c Z_c)$. With the possible exception of the first several minutes, the rates are then deter-

⁶ Another method of obtaining the anodic Tafel slope from the complete cathodic polarization curve has been described by Stern and Roth (5).

mined to $\pm 20\%$ by a series of small current polarizations which determine $(d\eta/dI)_{\eta \rightarrow 0}$.

The potentials of the corroding Zr-2 electrodes were measured with respect to platinum as a "reference" electrode.⁷ Several observations demonstrate that platinum is a satisfactory reference electrode for the purpose of these measurements. The potential-time measurements for Zr-2 from the same alloy stock are reproducible. The potential difference between the Pt electrode and the passivated Ti polarizing electrode is constant for all experiments. The small current polarizability of the Pt is independent of time, and also the Tafel slope for O₂ reduction on Pt and the calculated exchange current are constant and independent of time.

A typical potential-time plot is presented in Fig. 8 for the FS-Zr-2 alloy. It was observed that a sudden increase in potential to more positive values occurred after the reaction had proceeded for several minutes. The time it took to undergo this transition varied and was a function of the temperature of the reaction. The higher the temperature the sooner the transition occurred. The transition began at about -580 mv vs. Pt and rose about 320 mv to the potential about -260 mv vs. Pt. It was observed, however, that the small current polarizability suddenly decreased by a factor of two. This latter observation implied either that the corrosion current increased or for constant corrosion current the sum of the αZ values increased (see Eq. [4]). Insufficient experimental data are available to decide on either of these suppositions. It was demonstrated that Pt was not responsible for this sudden potential rise. Two experiments were performed without Pt in the system, using a Ti electrode as reference in place of the Pt electrode. (This Ti electrode was used in all the experiments performed as a combination polarizing electrode and thermocouple well.) The potential excursion was reproduced, and occurred at -450 mv vs. Ti. The difference of 130 mv is precisely the measured difference in potential between the Ti and Pt electrodes.

Furthermore, if during the very first minutes of the experiment, when the potential is at least 100 mv below the critical potential (-580 mv vs. Pt), sufficient anodic current is applied to polarize the electrode to this "critical potential" the spontaneous rise in potential to about -260 mv vs. Pt is again observed. However, when the polarizing cur-

⁷ A true reference electrode for high-temperature emf measurements is difficult to obtain. These several observations are made to demonstrate that Pt in this environment serves as a satisfactory fixed potential if not as a true reference.

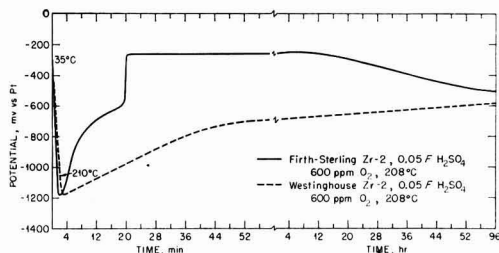


Fig. 8. Potential-time plot

rent is removed, the potential returns to the more negative potential compatible with the condition of the electrode at that time. If the polarizing current is maintained for a sufficient period of time, then the potential will remain "positive." The potential then steadily decreased with time to about -550 mv vs. Pt.

A potential-time plot for the W-Zr-2 alloy is also presented in Fig. 8. This behavior is typical for metals on which an oxide film is formed, i.e., the potential rising to more positive values as the film grows in thickness.

However, if anodic polarizations are performed during the first minutes of the corrosion reaction, as described above for the FS-Zr-2 stock, the potential excursion at the same "critical potential" (-580 mv vs. Pt) is again observed. The amplitude however is only 160 ± 5 mv as compared to 320 ± 20 mv. When the polarizing current is removed, the potential again returns to the more negative potential compatible with the electrode. For this W-Zr-2 alloy however, the positive potential cannot be maintained. The potential always returns to the original open-circuit potential.

At the present time no explanation for these observations is proposed.⁸ Several Tafel-like polarizations have been performed on the FS-Zr-2 alloy during this initial period and yielded ambiguous results. The temperature, open-circuit potential, and the small current polarizabilities are all changing rapidly with time.

The data presented in Fig. 9 as log rate-log time plots have been calculated from Eq. [4] and were based on the assumption that the sum of the αZ values was constant at 0.45 ± 0.10 . To obtain the rate in amp/cm² the total current, I , was divided by the area of the specimen (3.75 - 5.00) cm² ± 0.05 cm². Assuming the film to be ZrO₂ of density of 5.5 g/cm³, and the reaction $Zr + O_2 \rightarrow ZrO_2$, then the relation 10^{-3} amp/cm² = 400 mpy was obtained. The rate data which are presented for the Firth-Sterling alloy do not include the measurements prior to the sudden potential increase.

⁸ A later publication, which includes measurements at temperatures above 250°C , will discuss these observations more fully.

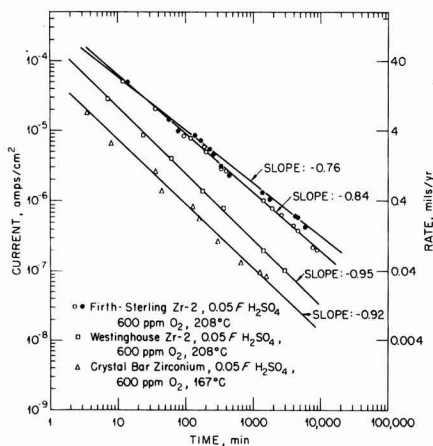


Fig. 9. Rate-time plot

Figures 10 and 11 present the results obtained for the cathodic reduction of O₂ on Pt in 0.05F H₂SO₄, 600 ppm O₂, at 208°C. The value of the constant $\alpha_c Z_c$ is 2.1 ± 0.1 . This is greatly different from that which is observed (13) at 25°C for the electro-reduction of O₂ on Pt in 0.05F H₂SO₄, where $\alpha_c Z_c = 0.5$.

Summary and Discussion

The corrosion rate of a metal which forms a passive oxide decreases as the film thickness increases. The measured polarization resistances were observed to increase with time, indicating an inverse correlation with the corrosion rate. To obtain quantitative estimates of the corrosion rates a knowledge of the Tafel slopes for the anodic and cathodic reactions were needed. To a first approximation the current-potential behavior for the cathodic reaction was interpreted according to the Tafel kinetics. The

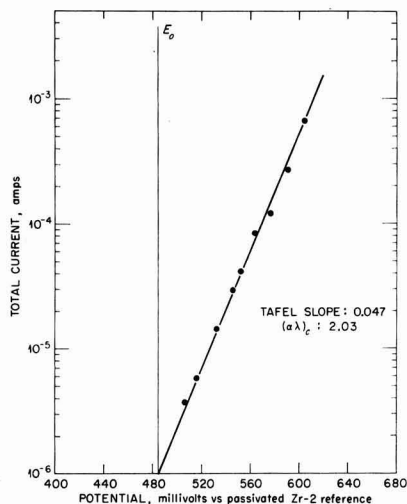


Fig. 10. O₂ overvoltage on Pt (in 0.05F H₂SO₄, 600 ppm O₂, 208°C) Run No. 10.

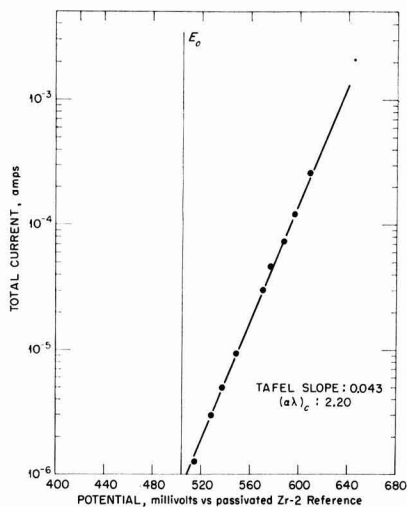


Fig. 11. O₂ overvoltage on Pt (in 0.05F H₂SO₄, 600 ppm O₂, 208°C) Run No. 11.

Tafel slopes or the derived $\alpha_c Z_c$ values were then determined as a function of time and were found not to change greatly, increasing with time from 0.25 to 0.41. The anodic current-potential results were then obtained indirectly from the complete cathodic polarization curves. These calculated results also demonstrated exponential current-potential behavior for the anodic reaction in the region close to the corrosion potential. The calculated anodic $\alpha_a Z_a$ values were observed to be small, $\alpha_a Z_a = 0.1$, in agreement with measured estimates, and were independent of time. On the basis of these measurements, the range of values for the sum was estimated to be $0.35 < (\alpha_a Z_a + \alpha_c Z_c) < 0.51$. Consequently a constant value of 0.45 was used to determine the corrosion rates from the measured polarization resistances, and the rate-time data were interpreted accordingly.

The internal self-consistency of the data was further demonstrated by the results shown in Fig. 7. Here the corrosion current obtained from the extrapolation of the cathodic Tafel line to the corrosion potential (open-circuit potential) was in very satisfactory agreement with the value obtained using Eq. [4]. Furthermore a study of the available data in the literature (12) shows that the range of experimental αZ values is limited, and that for a large majority of corrosion systems a simple measurement of the polarization resistance yields an estimate of the corrosion rate within a factor of two.⁹ Consequently a measurement of the Tafel slopes as a function of time (and the values obtained are reasonable) provides more reliable estimates of the rate-time behavior.

On this basis then it is demonstrated that when the data are formulated on a log (rate)-log (time) basis, as shown in Fig. 9, satisfactory straight lines are obtained. The points for the W-Zr-2 alloy fall on a good straight line, and the slope -0.95 is close to -1 . One other experiment for the same alloy stock, but of shorter time duration (250 min), gave identical rate-time behavior and a slope of -1 in log (rate)-log (time). Such behavior implies a hyperbolic relationship between the rate and time, and since the corrosion current is proportional to the rate of growth of oxide (9, 10), it further implies a logarithmic relation between thickness of film (x) and time.

The behavior for the FS-Zr-2 stock deviates somewhat from the hyperbolic rate-time relationship, but again the rate-time correlation is more like to hyperbolic than other formulations of the data, i.e., parabolic or cubic. The slopes for many other experiments performed on this alloy, but of shorter time durations, ranged between -0.82 to -0.91 . Stern (10), by a different electrochemical technique, also demonstrated such logarithmic oxidation kinetics for stainless steel in $\text{Fe}^{2+}/\text{Fe}^{3+}$ (Cl^- or SO_4^{2-}) environments at 25°C . Meyer (9) has demonstrated that the rate-time behavior for crystal bar zirconium in oxygenated Na_2SO_4 solutions, pH 3.5, and temperatures from 25° to 88°C is also approximately represented by the logarithmic oxidation equation.

⁹ Again, Stern and Weisert (4) demonstrate in further detail the general applicability of the method.

Jenks (14) obtained a correlation of the data obtained by Gulbransen and Andrews and others for zirconium and Zircaloy-2 in steam and O_2 at temperatures from 275° - 600°C on the basis of a modified logarithmic equation expressed as

$$\frac{dx'}{dt} = (A-J) e^{-Bx'} + J \quad [5]$$

where x' is the total oxide formed at time t in $\mu\text{g O}_2/\text{cm}^2$, A is the initial rate, at $x' = 0$, in $\mu\text{g O}_2/\text{cm}^2 \text{ min}$, B is a constant, and J is a constant steady-state rate.

It is not the purpose of this report to justify the logarithmic oxidation kinetics, but to demonstrate that the results obtained are reasonable, and that the electrochemical method can be employed successfully under these more severe experimental conditions.

Furthermore, the values obtained for the anodic and cathodic αZ constants are in good agreement with those obtained by Meyer (9). In the present study on the FS-Zr-2 alloy, however, the cathodic αZ was not observed to decrease but rather to increase with time. It is not unreasonable, however, to expect that the first several minutes of reaction at these elevated temperatures is equivalent to a period of several days reaction at the lower temperatures (25° - 88°C). This would suggest from Meyer's observations that both the anodic and cathodic αZ 's decrease during this initial period and are then followed by the observed subsequent slow increase in the cathodic αZ at nearly constant anodic αZ . These observations are also consistent with the observed decrease of E_0 with time.

Acknowledgment

The author wishes to express his great appreciation to Dr. G. H. Jenks, Dr. F. A. Posey, and Dr. R. E. Meyer, all of this Laboratory, for their kind encouragement and many helpful discussions.

Manuscript received Aug. 29, 1960; revised manuscript received Dec. 12, 1960.

Any discussion of this paper will appear in a Discussion Section to be published in the December 1961 JOURNAL.

REFERENCES

1. R. V. Skold and T. E. Larson, *Corrosion*, **13**, 139 (1957).
2. E. J. Simmons, *ibid.*, **11**, 255 (1953).
3. K. F. Bonhoeffer and W. Jena, *Z. Elektrochem.*, **55**, 151 (1951).
4. M. Stern and E. D. Weisert, *A.S.T.M. Proceedings*, **59**, 1280 (1959).
5. M. Stern and R. M. Roth, *This Journal*, **104**, 390 (1957).
6. M. Stern and A. L. Geary, *ibid.*, **104**, 56 (1957).
7. F. A. Posey, *ibid.*, **106**, 571 (1959).
8. M. Stern, *Corrosion*, **14**, 440t (1958).
9. R. E. Meyer, *This Journal*, **106**, 930 (1959).
10. M. Stern, *ibid.*, **106**, 376 (1959).
11. G. B. Adams, Jr. and P. Van Rysselberghe, *ibid.*, **102**, 502 (1955).
12. J. O'M. Bockris and B. E. Conway, "Modern Aspects of Electrochemistry," pp. 220-221, Butterworths Scientific Publications, London, (1954).
13. J. O'M. Bockris, *National Bureau of Standards, Circular 524*, 243 (1953).
14. G. H. Jenks, ORNL Report to be published.

Anodic Polarization Behavior of Iron-Nickel Alloys in Sulfuric Acid Solutions

George Economy

Finishes Division, Alcoa Research Laboratories, Aluminum Company of America, New Kensington, Pennsylvania

and Rudolph Speiser, F. H. Beck, and M. G. Fontana

Department of Metallurgical Engineering, The Ohio State University, Columbus, Ohio

ABSTRACT

The anodic behavior of twelve annealed iron-nickel alloys in hydrogen saturated H_2SO_4 solutions at $25^\circ \pm 1^\circ C$ was investigated by galvanostatic and potentiostatic techniques. The anodic behavior was correlated with the metallurgical structure and electrochemical environment. Particular emphasis was placed on the interpretation of corrosion potential, passivation current, passive current, and the passive-active transition. All the alloys became passive at noble potentials. In general, the behavior of the alloys was intermediate to the behavior of iron and nickel.

The anodic behavior of pure iron and nickel has been a subject of scientific observation for many years. The passivity of iron was recognized over 150 years ago. The numerous recent investigations show substantial agreement as to how these two metals behave anodically, but there remains considerable controversy concerning the mechanism of many of the anodic phenomena. It was not the intention of this investigation to resolve any of these controversies. The purpose was to investigate the iron-nickel alloys by the same methods used for the pure metals and examine the transition in behavior with changing alloy compositions and solution pH.

Investigations of the electrochemical behavior of iron-nickel alloys have been confined principally to studies on hydrogen and oxygen overvoltage and evaluations of corrosion resistance. A study of the anodic behavior of iron-nickel alloys in sulfuric acid at $25^\circ C$ was conducted by Morioka and Sakiyama (1). They investigated 16 alloys ranging in composition from 0 to 100% Ni, in 1.0 and 5.0% deaerated H_2SO_4 . The potential-current curves were obtained by increasing and decreasing the electrolysis voltage at a rate of 0.3 v/min. However, their results showed substantial variation from the steady-state values obtained in this investigation.

Apparatus and Procedure

Anodes were prepared from pure iron and nickel. The nickel was reagent grade shot (J. T. Baker Chemical Company) assaying 99.99%, and the iron was Ferrovac E (Crucible Steel Company) at 99.97%. Twelve alloys covered the composition range 0-100% Ni. The pure metal specimens were arc-melted three times and the alloy specimens were arc-melted six times for homogenization. The arc-melted buttons were milled into square rods about 0.2 by 0.2 in., and 1 in. long. One end was tapped for connection to the cell, and the other end was polished through 000 paper. The specimens were vacuum annealed at $1000^\circ C$ for 1 hr and furnace cooled to room temperature in 3 hr. The sides of the

specimens were coated with Varno cement so that only the polished end (about 0.25 cm^2) was exposed to the solution.

The solution used was H_2SO_4 with 0.5N K_2SO_4 as supporting electrolyte. The pH was adjusted by varying the concentration of the acid, and the solutions with their experimental pH were as follows.

$N H_2SO_4$	pH
10.0	-0.47
1.0	0.56
0.1	1.67
0.01	2.73
0.001	3.73

The polarization cell consisted of two $3\frac{1}{2}$ in. diameter Teflon disks clamped to the top and bottom of a 70 mm diameter Pyrex cylinder ($3\frac{3}{4}$ in. high). The Teflon disks were perforated to accommodate electrodes, reference probes and other auxiliary connections. Installation of "O" ring seals at all joints insured an air-tight cell and allowed vertical adjustment of the cathode and reference probe. A large area platinized platinum cylindrical cathode provided a low polarization resistance, and the proximity of the anode and cathode offered a low solution resistance. The Luggin tubulus used as a probe for the saturated calomel reference electrode was filled with a 4% agar-saturated KNO_3 gel. Convection in the vicinity of the anode was decreased by having the anode surface face upwards. This decreased the current requirements and consequently aided the potentiostatic control. The stopcocks on the gas inlets were made of Teflon to avoid contamination of the solution.

The anode-reference cell potential was measured by a Curtiss Wright electrometer, in which the 0-1 v range was extended to 2 v by using a Weston standard cell as a bias cell. A recorder was connected to the recorder jack in the electrometer. Another recorder was connected across a small series resistor (0.1, 1.0, or 10.0 ohms) to measure cell current.

A selector switch was used to choose either constant current or constant potential. The constant current source consisted of a regulated d-c power supply (Heathkit PS-3, 0-500 v, 0-200 ma), 12 resistors, and a 12 position rotary shorting switch, to provide 12 current ranges from 0-200 ma down to 0-1 μ a. The constant potential supply was a standard battery-potentiometer arrangement, except that the external resistance was minimized for better potentiostatic control. A 0.5-ohm, 100-w potentiometer was used for potential control in the active region, and a 10-turn, 3-ohm, 2-w precision potentiometer was used in the passive region. The power was supplied by a 6 v, 216 amp-hr Ni-Cd battery.

All measurements were conducted in a room maintained at $25^\circ \pm 1^\circ\text{C}$. After assembly of the cell, hydrogen gas was bubbled through it vigorously for 15 min to deaerate and saturate the solution with hydrogen. The hydrogen was passed through a Deoxo Purifier to decrease the oxygen content to 1 ppm. The anode was electropolished for 20 min at a current density of about 40 ma/cm². It was necessary that the anode be active during the electropolishing treatment for, if a film were initially present, this current density could lead to oxygen evolution. Film reduction was accomplished by (a) cathodic polarization of the specimen, or (b) constant potential electrolysis at an active potential, or (c) the first treatment quickly followed by the second. Since the anodic reaction was in some cases disturbed with the reference probe touching the anode, a cathetometer was used to set the probe at a distance of 2.0 mm from the anode. This introduced an ohmic overpotential, and to correct for this, the ohmic overpotential was determined at various current densities and a correction plot made.

The general procedure was to use galvanostatic measurements when the polarization resistance was low, i.e., E relatively insensitive to changes in I/A , and potentiostatic measurements where the polarization resistance was high. The rate of hydrogen bubbling was reduced so as not to stir the solution, and the corrosion potential noted after it had reached a steady value. Starting at a current density of 1 μ a/cm², the current was increased by factors of ten, noting the steady-state potential at each current density value. As the current density required for oxygen evolution was neared, current increments were decreased to obtain a value for the passivation current density. On passivation, the anode potential took a characteristic jump in the noble direction. Current density was decreased in tenfold increments starting with 100 ma/cm², and the steady-state value of the potential was recorded. When the potential started to drift in the active direction, the high-speed recorder was plugged into the electrometer to obtain a high-speed trace of the potential as the anode activated.

The anode was activated and measurements were made at constant potential, reading the steady-state current at each potential. When the anode became passive, as indicated by a sudden decrease in current, the potential was set at + 1.200 v. At

this potential, the time required to reach a steady-state current, or optimum passivity, varied with the acidity. Approximately 15 min were required for the 0.001N H₂SO₄ solution, but this increased to approximately 2 hr for the 10.0N solution. The potential was decreased in steps of 0.2 v and the steady-state passive current noted at each potential. Potential-current data for the activation (negative resistance) curve required a pseudogalvanostatic technique. The low polarization resistance of the active-passive transition curve indicated the use of a constant current method, but the regular galvanostatic source was not usable since the stable potential value lies on a positive resistance curve (either active or O₂ evolution). The procedure was to choose an approximate current value at which the potential was to be determined and set the potential at some active value until the current increased to the desired magnitude. The potential was then made more noble until the current started to slowly decrease. By manipulating the 10-turn precision potentiometer, the current was made to increase and decrease at a slower and slower rate, until a steady current value was attained. To avoid a significant rise in pH of the 0.001N solution, the preceding procedure was abbreviated to the determination of the corrosion potential, passive current density, activation potential, and passivation current density.

Results and Discussion

In the presentation and discussion of the results, it will be understood that (a) potentials are referred to the standard hydrogen electrode (SHE), (b) current density is calculated on the basis of geometric area, and (c) the composition of an alloy is given in the order atomic % Fe-at. % Ni, i.e., 80-20 alloy will signify 80 at.% Fe-20 at.% Ni alloy.

Metallurgical structure.—Structures of iron-nickel alloys are a function of both heat treatment and composition. An x-ray analysis to determine the structures of the annealed specimens showed (a) α (ferrite) up to 5 at.% Ni, (b) $\alpha + \gamma$ from 10 to 40 at.% Ni, and (c) γ (austenite) from 50 to 100 at.% Ni. These correspond to structures expected for annealed alloys (2).

No significant information was obtained in a microscopic examination of the alloy specimens after electrolysis. As might be expected, there was a marked attack of the grain boundary for all alloys, and in the two-phase alloys, there was additional selective attack of some of the grains. The attack of the selected grains initiated at the grain boundary and proceeded inwards. Indirect evidence that the selective attack occurred in the ferrite grains of the two-phase alloys was determined from galvanic couples of the wholly ferritic (95-5) alloy and the wholly austenitic (40-60) alloy in the test solutions. An anodic current passed from the ferritic to the austenitic electrode. The current magnitude depended on the acidity, being about 200 μ a/cm² in the 10.0N H₂SO₄ solution, and about 20 μ a/cm² in the 0.001N solution.

Anodic polarization curves.—The anodic polarization curves of the twelve Fe-Ni alloys were de-

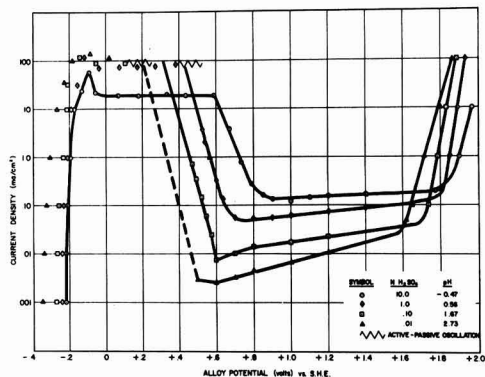


Fig. 1. Anodic polarization of 95 at.% Fe-5 at.% Ni alloy at various pH.

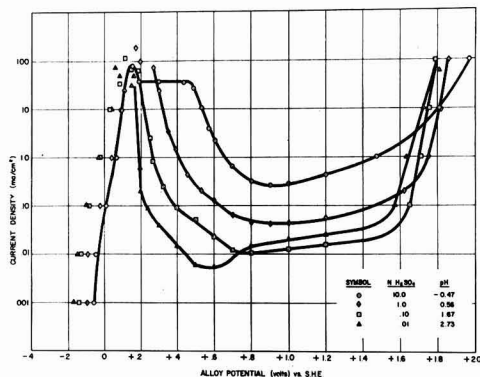


Fig. 3. Anodic polarization of 40 at.% Fe-60 at.% Ni alloy at various pH.

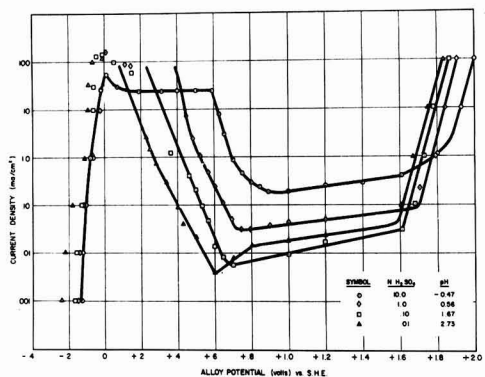


Fig. 2. Anodic polarization of 70 at.% Fe-30 at.% Ni alloy at various pH.

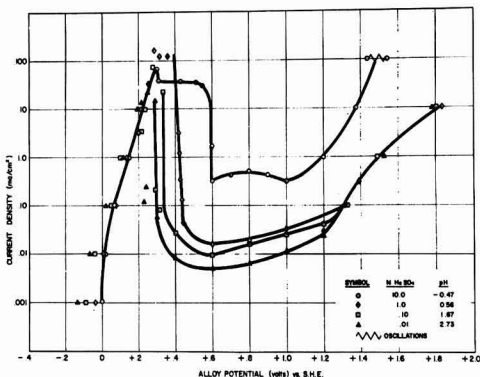


Fig. 4. Anodic polarization of 0 at.% Fe-100 at.% Ni alloy at various pH.

terminated by galvanostatic and potentiostatic techniques. The curves for the 95-5, 70-30, 40-60, and 0-100 alloys are shown in Fig. 1 to 4. These four compositions were chosen as representative of the twelve Fe-Ni alloys and adequately show the transition behavior with changing composition. With respect to the general shape of the curves, there was no sharp effect found with either changing composition or changing structure. Since the passivation reaction occurred for every alloy composition and at every pH, all the polarization curves were of a general S-shape. The porous film formed at the limiting current density (I_L) was stable over a wide potential range (0.5-0.6 v) for pure iron. With increasing nickel, the Tafel curve for anodic dissolution shifted to a more noble potential, and the active-passive transition curve shifted to a more active potential, so that with pure nickel the I_L plateau had a potential range of only 0.1-0.2 v. The effect of increasing pH was to shift the entire polarization curve to more active potentials. The irregular potential shift at noble potentials for nickel (Fig. 4) in 10.0N H_2SO_4 is probably caused by a transpassivity phenomenon similar to that of iron and stainless steel. If the passive nickel layer were oxidized to NiO_2 , which is unstable in acid solution, the current could be attributed to anodic

dissolution instead of oxygen evolution. Latimer (3) gives



with $E^\circ = +1.32$, which is in the correct potential range.

Corrosion potential.—The corrosion, or open-circuit (o.c.) potential, displayed a regular dependence on both composition and pH. The variation in o.c. potential with composition is shown in Fig. 5. The γ -phase alloys were about 0.20 v noble with respect to the α -phase alloys. For the two-phase alloys, there was a regular increase in corrosion potential from the α -potential (minimum γ area) to the γ -potential (minimum α area), indicating control of the potential by the major constituent and polarization of the minor constituent. This is in fair agreement with the results of Morioka and Sakiyama (1), except that they did not indicate the existence of a two-phase field in the range 10-40 at.% Ni, but showed the α -phase up to 30 at.% Ni and the γ -phase at higher Ni content.

Since iron in HCl acts in the same manner as a reversible hydrogen electrode ($dE/dpH = -0.059$) in the pH range 1-4 (4-7), a similar relationship might be expected for the iron-nickel alloys in H_2SO_4 . Data from Fig. 5 were replotted in the form

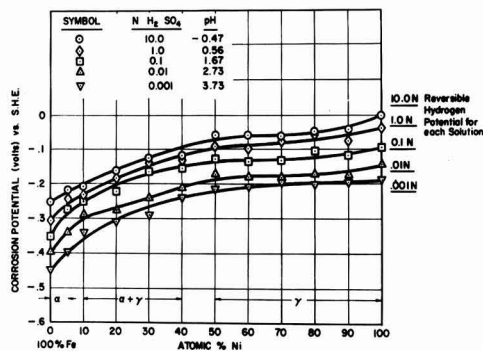


Fig. 5. Corrosion potential vs. composition at different pH

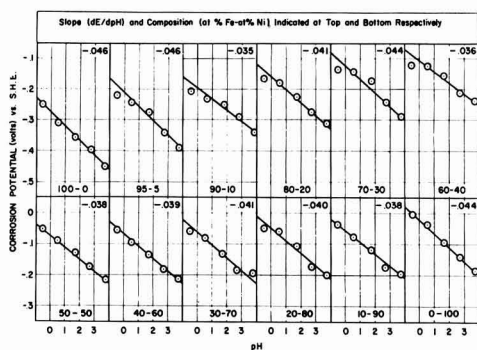


Fig. 6. Corrosion potential vs. pH for each alloy

shown in Fig. 6 to verify the anticipated o.c.-pH relationship. Values for dE/dpH varied from -0.035 to -0.046 , less than the value for a reversible hydrogen electrode, or Stern's (4) value of -0.056 . The slopes of Fig. 6 are somewhat closer to the value of -0.047 found by Makrides, Komodromos, and Hackerman (7); however, the other two investigations were in HCl so that substantial agreement is not necessarily expected. Approximately half of the Fe-Ni alloys deviated from the linear relationship at very high acidities. The literature did not indicate whether the linear relationship should exist at negative or very low pH values.

Passivation current.—No special trend in passivation current density (I_p) was noted with changing composition. However, as shown in Fig. 7, the I_p value of each alloy went through a maximum with changing pH, the maximum occurring in the pH range 0-2. Since the highest corrosion rates reported (8-9) were the current equivalent of only 1 ma/cm^2 , the variation in local cell current is a negligible factor in explaining the maximum in I_p . The explanation for the variation in I_p with pH must therefore lie in the nature of the porous non-protective films formed at high current densities. These films ranged in color from gray-black for high iron alloys, to a greenish black for the 50-50 alloy, to a light green for the high nickel alloys. The colored films disappeared when the alloy became passive. The following reactions are of possible interest here:

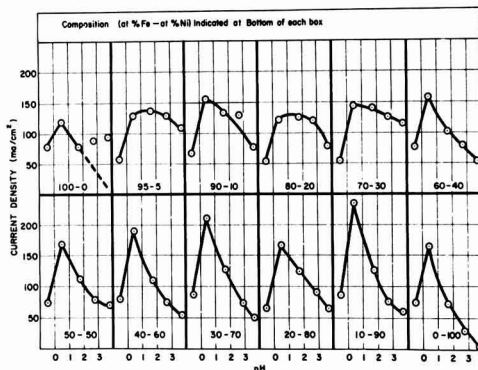
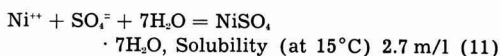
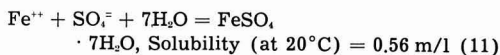
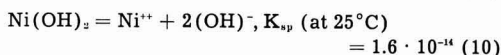
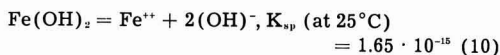


Fig. 7. Passivation current density vs. pH for each alloy



If the basis for I_p is an adequate ionic concentration to precipitate the hydroxide, the controlling factor should be

$$K_{sp} = [\text{M}^{++}] [\text{OH}^-]^2$$

so that a decrease of one unit of pH would require a hundredfold increase in metal ion concentration for precipitation. Starting with the highest pH, a marked increase in I_p was noted as pH decreased, the higher current value being required to achieve a greater metal ion concentration at the surface of the electrode. As the pH was reduced further, the metal ion concentration required was increased still more, but now the possibility of the precipitation of the metal sulfate must be considered. Since low acid concentrations favor the precipitation of metal hydroxide and high acid concentrations favor the precipitation of metal sulfate, intermediate acid concentrations require a higher metal ion concentration for precipitation, and consequently the I_p value is higher.

Passive current.—The passive current density is defined as the minimum current density required to maintain passivity. The minimum current was evaluated from anodic polarization curves such as in Fig. 1-4. The passive current density did not vary significantly with changing composition. However, a plot of passive current density vs. pH for each alloy indicated a rapid increase in passive current density with increasing acidity as shown in Fig. 8. The passive film is free of pores under these conditions so that the passive current represents dissolution of the passive film instead of dissolution of the metal. However, the dissolution of the film is counterbalanced by film formation by the process which determines the Flade potential, and

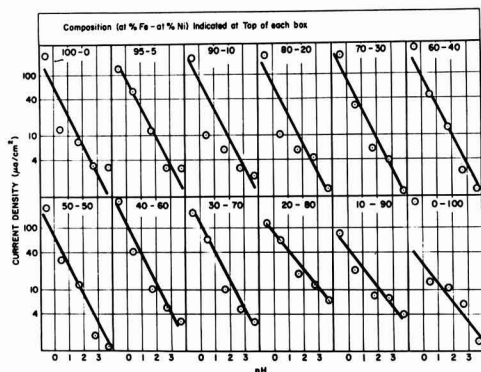


Fig. 8. Passive current density vs. pH for each alloy

at the steady state, the rates of dissolution and formation are equal. Weil (12) has reported that the dissolution rate of the passive layer of iron follows the relation

$$\log J_k = \log J_k^0 - a \text{ pH}$$

up to a pH value of 6.0, where J_k is the passive current density. The current-pH data in Fig. 8 show that this equation is more or less followed by each alloy.

Flade potential.—Flade potentials were determined from high-speed recorder traces of the potential decay of the passive alloys. In the decay trace, there is a halt in the potential corresponding to dissolution of the passive film. Uhlig (13), following the method of Flade, obtained the decay trace on open circuit and recorded the Flade potential as the potential value just before the abrupt drop. This method was adequate for evaluation of Flade potentials in this study for moderate acidities. However, at the highest acidity, the potential decay was so rapid that the halt disappeared completely, and at the lowest acidity, the decay was so slow that the halt was indistinct. The rate of decay also depended on the composition, the decay time increasing with increasing nickel content. To compensate for the different decay rates, small cathodic currents were impressed to speed up sluggish reactions, and small anodic currents (but less than the passive current) were impressed to slow down the fast reactions. Prominent halts were obtained for the α - and two-phase alloys. The γ -alloys had less definite halts because of the slower transition between the active and passive states. The decay traces for the γ -alloys were examined visually from all angles to deduce "breaks" in the curve. In extreme cases, it was necessary to assume that an inflection point in the decay trace was the Flade potential. Such tenuous criteria gave considerable scatter in the data as shown in Fig. 9.

The Flade potential as a function of pH is shown for each alloy in Fig. 9. The range of the data is shown by the vertical dotted lines. Since the Flade potentials of both iron and nickel are known to have a 0.0591 pH dependence, the assumption was made that all the Fe-Ni alloys would have the

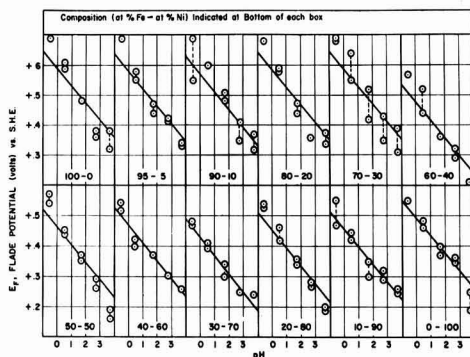


Fig. 9. Flade potential vs. pH for each alloy

0.0591 pH dependence. The E_f -pH data were accumulated according to the equation

$$\Sigma E_f = n E_f^0 - 0.0591 \Sigma \text{pH}$$

to evaluate E_f^0 , the standard Flade potential ($E_f = E_f^0$ at pH = 0), for each alloy. The curves of Fig. 9 were drawn through the E_f^0 value at pH = 0 and at a slope of -0.0591. The relatively good fit with the data justifies the value assumed for the slope, and indicates that the Flade relation ($E_f = E_f^0 - 0.0591 \text{ pH}$) is substantially followed at every composition.

The experimental standard Flade potentials (E_f^0) are plotted vs. composition in Fig. 10. The E_f^0 value of +0.59 for iron is slightly higher than the accepted value of +0.58. An E_f^0 value of +0.45 for nickel was computed from the E_f value of +0.43 for nickel in 1.0N H₂SO₄ reported by Okamoto, Takaishi, and Sato (14). The experimental E_f^0 for nickel was +0.49, but this value is not as reliable as the experimental E_f^0 of iron because of the difficulty in evaluating the decay traces for high nickel alloys. This difficulty in the high nickel range manifests itself in Fig. 10, where the E_f^0 values for the γ -alloys show an erratic trend with changing composition. However, the median E_f^0 value of +0.47 for the γ -alloys is only 0.02 v higher than the value for nickel reported in the other investigation.

One would predict that a two-phase alloy should be as noble as its most active constituent, i.e., the E_f^0 of the two-phase alloy should be controlled by the E_f^0 of the α constituent. This behavior was fol-

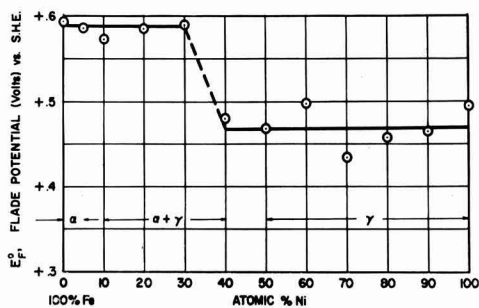


Fig. 10. Standard Flade potential vs. composition

lowed by the 90-10, 80-20, and 70-30 alloys. However, the E_i° value of the 60-40 alloy did not follow the predicted behavior, but was apparently controlled by the E_i° of the γ -phase. This effect at 40 at.% nickel could be attributed to a small α -phase area, the active current of the α -phase being insufficient to activate the γ -phase through galvanic contact. The explanation of this effect could also lie in the change of the occupancy of the d band energy levels with changing composition, the passive state corresponding to unfilled d bands, according to the electron configuration theory (15, 16). In this theory, nickel is an electron acceptor, and at a certain critical composition of nickel, the alloy becomes passive because the d levels of iron are no longer full. The critical composition has been calculated to be 33.3 at.% Ni. (16).

Transition from passive to active state.—The steady-state potential-current values for the passive-active transition are shown in Fig. 1-4. In some cases, the potential became completely unstable as the current increased from the passive value. This situation arose for the 95-5 alloy (Fig. 1) in 0.01N H_2SO_4 . The instability of the other alloys ensued at current values much higher than the passive current, compared to the 95-5 alloy. The current at which instability set in tended to be lower with increasing pH. The criterion for stability during the passive-active transition was discussed by Franck (17). Since all the stationary states of the electrode are given by the polarization curve, and all the stationary states of the external circuit by a "resistance line" representing the total external resistance, the intersection of both curves represents the stationary state in which the entire circuit (electrode and external circuit) can exist. Two general cases were considered by Franck, E-I diagrams resulting in N-shaped curves and E-I diagrams resulting in S-shaped curves. An analysis of each type of curve leads to the conclusion that mixed electrode states (the electrode surface has both active areas and passive areas in the transition state) on S-form curves are stable, but on N-form curves unstable. Since the polarization curves (Fig. 1-4) are of a general S-form, the stability of points on the passive-active transition are explained by Franck's theory. The decreasing stability with increasing pH would be concerned with a changed "resistance line" because of the lowered conductivity.

The passive-active transitions (Fig. 1-4) give rise to negative slopes which are in some cases quite linear. In a recent paper by Mueller (18), an equation was derived which covered the curve of the density of anodic dissolution current as a function of the potential including the active and passive states. In the active-passive transition zone, the differential form of Mueller's equation reduces to $d \ln I/dE = -k$. Since Fig. 1-4 are also on a semi-logarithmic basis, this equation adequately describes the experimental active-passive transition curve.

Similar to the effect of pH on the Flade potential, the active-passive transition curve shifted to the left with increasing pH. It should be noted that the

Flade potential obtained from a decay trace is active with respect to the potential at which the transition to the active state starts. This may be seen from a comparison of Fig. 1-4 with Fig. 9. The Flade potential is seen to fall between the potential limits of the active-passive transition curve, and it is not possible to differentiate the Flade potential from any of the other mixed electrode states.

Since the Flade potential is incorporated into the transition curve, it would be expected that the transition curve should shift with composition in much the same manner as the Flade potential. An examination of all the polarization curves (including those not presented in Fig. 1-4) indicates that the transitions are alike for all alloys up to 30 at.% Ni. Alloys with 70 at.% Ni and higher also behave alike, but the transition occurs at a potential 0.2 or 0.3 v more active with respect to the lower nickel (up to 30 at.%) alloys. The transition for nickel contents between 40 and 60 at.% Ni is interesting. The slopes are less steep than those of alloys with either higher or lower nickel content, as shown in Fig. 3 for the 40-60 alloy. The alloys with nickel content between 40-60 at.% thus represent a bridge between iron-like and nickel-like behavior, since the transition from the passive to the active state starts at potentials characteristic of the high iron alloys, but ends at potentials characteristic of the high nickel alloys. Thus the change from ferritic to austenitic-type behavior between 40 and 60 at.% Ni does not correlate exactly with the metallurgical structures of the alloys.

Acknowledgment

The interest and support of this investigation by the Office of Naval Research is gratefully acknowledged. This paper is based on a dissertation presented in partial fulfillment of the degree, Doctor of Philosophy, at The Ohio State University. Mr. Economy held the International Nickel Company Fellowship for two years of the above investigation.

Manuscript received Sept. 19, 1960; revised manuscript received Dec. 12, 1960. This paper was prepared for delivery before the Houston Meeting, Oct. 9-13, 1960.

Any discussion of this paper will appear in a Discussion Section to be published in the December 1961 JOURNAL.

REFERENCES

1. S. Morioka and K. Sakiyama, *Nippon Kinzoku Gakkaishi*, **19**, 31 (1955).
2. "Metals Handbook," (George Sachs) p. 1211, A.S.M., Cleveland (1948).
3. W. M. Latimer, "The Oxidation States of the Elements and Their Potentials in Aqueous Solutions," p. 202, Prentice-Hall, Inc., New York, (1952).
4. M. Stern, *This Journal*, **102**, 609 (1955).
5. M. Stern and R. M. Roth, *ibid.*, **104**, 390 (1957).
6. M. Pourbaix, *Corrosion*, **5**, 121 (1949).
7. A. C. Makrides, N. M. Komodromos, and N. Hackerman, *This Journal*, **102**, 363 (1955).
8. H. H. Uhlig, Editor, "The Corrosion Handbook," p. 194, John Wiley & Sons Inc., New York (1948).
9. J. S. Marsh, "The Alloys of Iron and Nickel," Vol. I, p. 497, McGraw-Hill Book Company, Inc., New York (1938).

10. "Corrosion Handbook," *op. cit.*, pp. 1138-39.
11. C. D. Hodgeman, Editor, "Handbook of Chemistry and Physics," pp. 532, 556, Chemical Rubber Publishing Company, Cleveland (1958).
12. K. G. Weil, *Z. Elektrochem.*, **62**, 638 (1958).
13. H. H. Uhlig and P. F. King, *This Journal*, **106**, 1 (1959).
14. G. Ohamoto, T. Takaishi, and N. Sato, *J. Electrochem. Soc., Japan (Overseas ed.)*, **20**, E-183 (1958).
15. H. H. Uhlig, *Z. Elektrochem.*, **62**, 700 (1958).
16. "Corrosion Handbook," *op. cit.*, p. 24.
17. U. F. Franck, *Z. Elektrochem.*, **62**, 649 (1958).
18. W. A. Mueller, *This Journal*, **107**, 157 (1960).

An Investigation of Columbium as an Electrolytic Capacitor Metal

A. Shtasel and H. T. Knight

Research Department, Fansteel Metallurgical Corporation, North Chicago, Illinois

ABSTRACT

The anodic oxidation characteristics of columbium metal were studied in relation to the manufacture of both wet and solid electrolytic capacitors. Capacitors prepared from columbium were very similar to those prepared from tantalum except that the working voltages of the columbium capacitors were about one third and the d-c leakages about double that of similar tantalum capacitors. Solid columbium capacitors were demonstrated to have an advantage over solid tantalum capacitors in a severe nuclear environment.

The anodic oxidation properties of columbium have been known since 1908 (1). However, attempts to utilize these properties in commercial capacitors never have been successful. This has been attributed to the fact that the early technology of columbium and its sister metal, tantalum, was such that the production of high-purity tantalum was favored and the production of an equivalent grade of columbium was rather difficult. In about 1955, considerable interest in columbium was aroused due to its nuclear and high-temperature properties and the fact that it was found to be in relatively abundant supply. This interest prompted the development of new methods of refining and reduction which facilitated the production of high-purity columbium. In order to determine if the improved purity would be reflected in the electrical properties of columbium capacitors, samples from two sources and of various purities were investigated in this work.

Anodic Oxidation Studies

A comparison of the anodic oxidation properties of columbium and tantalum was made by two methods. First, the capacitance of these metals was measured as a function of the formation voltage, and then the rate of the formation voltage was measured at a constant current density. From the former experiment, the capacitance values and the maximum working voltages were obtained. Differential field strengths were obtained from the latter experiment and were used in calculating the theoretical capacitance values which then were compared with the experimental values. Also, a comparison of the voltages of incipient graying for the various samples was made from these rate curves.

Sample preparation.—The anodes used in this investigation were prepared from a lot of commercial columbium powder which was made by the carbon reduction of columbium oxide obtained by liquid-liquid extraction from columbite ore. The powder

was arbitrarily sieved to the same mesh fraction as the tantalum powder used to prepare the tantalum controls. No attempt was made to determine if this was the optimum blend to give the maximum capacitance per unit weight for columbium. The sintering temperature, however, was varied from 1750° to 2100°C. A temperature of 2000°C for 1 hr was selected as the optimum sintering schedule for this powder. Three sources of columbium sheet were used. Sample No. 1 was prepared from the same powder used for the sintered anodes. It was rolled to 0.010 in. with a mill finish. Sample No. 2 was obtained as an example of columbium foil of exceptional purity produced by the same process as Sample No. 1. It was reduced on a Sendzimir mill to 0.0005 in. with a mirror finish. Sample No. 3 was prepared from a rod of columbium which had been made by the thermal decomposition of columbium bromide on a hot columbium wire. It was cold rolled without annealing to 0.005 in. and was the most ductile of the three samples. The tantalum foil used as a control was selected from a production lot of capacitor grade foil as a typical example. It also was reduced on the Sendzimir mill to 0.0005 in. with a mirror finish. The samples were cut into tabs 1 in.² in total area and were degreased with carbon tetrachloride and acetone before use, but they were neither etched nor polished. The chemical analyses of these samples are given in Table I. It is seen that Samples No. 2 and 3 are of the same order of purity as the capacitor grade tantalum foil, but that Sample No. 1 is high in the nonmetallic elements C, O, and N.

Experimental.—Some of the forming and measuring electrolytes ordinarily used with tantalum were found to be unsatisfactory for columbium due, no doubt, to the greater chemical reactivity of columbium. An aqueous solution of oxalic acid actually dissolves the anodic film on columbium, and concentrated sulfuric acid slowly attacks the film

Table I. Analysis of columbium and tantalum sheet
(Atomic per cent)

	Columbium Sample No. 1	Columbium Sample No. 2	Columbium Sample No. 3	Capacitor grade tantalum	Method
C	0.39	0.08—	0.14	0.15	A
O	0.46	0.06	0.12	0.17	B
N	0.99	0.07	0.07	0.07	C
Si	0.07	0.03	0.03	0.06—	D
Fe	0.02	0.02	0.01	0.02	D, E
Ni	0.02—	0.02—	0.02—	0.02—	D, E
Ti	0.02	0.01—	0.01—	0.04—	D, E
Zr	0.05—	0.05—	0.05—	0.02—	D, E
Mo	0.01—	0.01—	0.01—	0.02—	D
W	0.005—	0.005—	0.005—	0.01—	D
Ta	0.025—	0.025—	0.025—	—	E
Cb	—	—	—	0.02—	D

Methods: A, Leco volumetric or Leco conductometric; B, Leco argon gas fusion in Pt bath with conductometric finish; C, Micro-Kjeldahl with conductometric finish; D, emission spectroscopy; E, x-ray fluorescence spectroscopy (columbium samples only).

at elevated temperatures. However, several electrolytes, both aqueous and nonaqueous, were found to be satisfactory.

A plot of the reciprocal capacitance *vs.* the formation voltage for samples of columbium and tantalum foil is shown in Fig. 1. These data were obtained by forming (anodizing) specimens at a constant potential at 100°C in a mixture of 100 g of ammonium borate, 200 ml of water, and 300 ml of ethylene glycol until an arbitrary low value of current was obtained. After washing, the capacitance was measured at room temperature in 21% sulfuric acid at 120 cps using a General Radio capacitance bridge. The specimens then were rewashed and reformed to a higher potential. This process was repeated until the current would not drop back to the same low value, which point usually was marked by a visible scintillation and a graying of the film.

By this procedure, it was possible to form the tantalum foil to 320 v, whereas the columbium foil (Sample No. 2) could only be formed to 50 v. Both of these samples had been rolled to a mirror finish and it was assumed that they had the same surface area although no independent measurements of surface area were made. It is seen from Fig. 1 that within experimental error the capacitance per unit area for these two samples is identical.

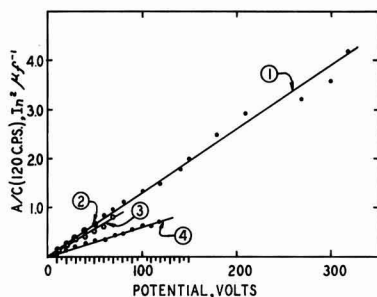


Fig. 1. Anodization curves of tantalum and columbium tabs: 1, Ta foil; 2, Cb sample No. 2; 3, Cb sample No. 1; and 4, Cb sample No. 1 after vacuum clean-up.

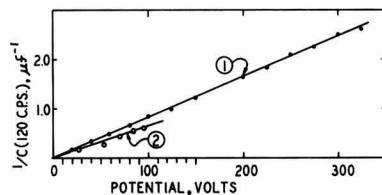


Fig. 2. Anodization curves of tantalum and columbium sintered anodes: 1, 0.1 g Ta anode; and 2, 0.07 g Cb anode.

Columbium Sample No. 1 was formed to a maximum of 70 v. A somewhat higher capacitance per unit area was observed, which was in agreement with the dull finish. After this sample was formed, it was cleaned and heated in a vacuum at 1800°C for 1 hr. This treatment removed the oxide film. It was then reformed, this time to a maximum of 120 v with a marked increase in capacitance. It should be pointed out, however, that the d-c leakage was higher for all the columbium samples, including the thermally etched sample, than for the tantalum sample. Attempts to increase the voltage or to decrease the d-c leakage of the columbium samples by known chemical etching or polishing techniques were not successful.

This experiment was repeated using sintered anodes instead of sheet. The results in Fig. 2 show that the columbium anodes began to gray at 95 v which is much less than the 325 v attained by the tantalum anode but higher than the value achieved by the untreated sheet (Sample No. 1) made from the same powder. The curves for the two sintered anodes cannot be compared directly since the area was not measured independently. However, the apparent area can be deduced from the data of Fig. 1. A value of 2.15 in.² is obtained for the area of the columbium anode and 1.66 in.² for the tantalum anode. This simply reflects that the sintering condition selected for the columbium anode did not produce the same surface area as was obtained when the tantalum anode was sintered. The figure of merit, CE/g, for the tantalum anode is 1168 which is normal for electrolytic tantalum powder, but it is 2260 for the columbium anode. The higher figure of merit is favorable for columbium and is a reflection of the favorable density ratio (16.6/8.55 = 1.99). However, no significant conclusion can be reached because other types of tantalum powder give figures of merit as high or higher than the value obtained for columbium.

Another method for comparing the working voltages of valve metals is to examine the rate-of-formation curve. At a constant current density the rate of film formation for valve metals is usually linear. At some potential which seems to be a function of the surface purity of the metal, the rate changes, indicating a new mechanism which is usually a crystallization or graying of the film. In the following experiments illustrated in Fig. 3, the rate of formation of the columbium foil (Sample No. 2) was compared with that of the tantalum foil at a current density of 10 ma/in.². The potentials were measured

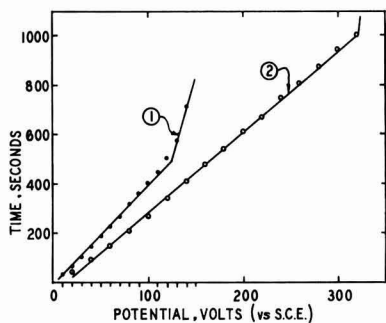


Fig. 3. Rate curves of the anodization of tantalum and columbium tabs: 1, Cb sample No. 2; and 2, Ta foil.

against a saturated calomel electrode (S.C.E.) and all formations were in an ethylene glycol-ammonium borate electrolyte at 100°C. The rate for the tantalum foil changed at 320 v whereas the rate for the columbium foil changed at about 125 v. The rate of formation also was investigated at 5 and at 20 ma/in.². At all three current densities, the voltage at which the slope changes for tantalum is approximately three times the value for columbium although the absolute values vary, of course, with the current density. Using the ratio of the differential field strengths from Fig. 3 as a measure of thickness and the reported ratio of the dielectric constants of Cb_2O_5 : $Ta_2O_5 = 1.52$ (2-4), the ratio of the capacitances per unit area $C_{Cb_2O_5}/C_{Ta_2O_5}$ was found to be 1.07 which agrees well with the ratio of unity observed in Fig. 1.

The rates of formation of the three columbium samples, with the potentials measured vs. a tantalum cathode, are illustrated in Fig. 4. The sample with the highest impurity content (Sample No. 1) changes slope at a significantly lower voltage than the other two samples. This is further substantiated by earlier observations of the authors that less pure samples of columbium changed slope at potentials as low as 50 v by this technique. These results indicate that the point of incipient graying as detected by the change of slope is a function of the purity of the columbium and that even with columbium which is of the same order of purity as capacitor

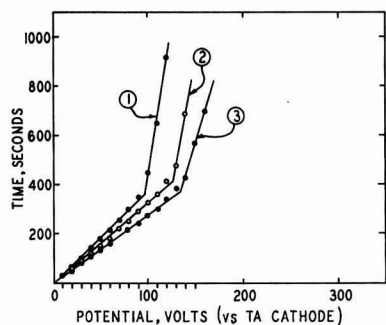


Fig. 4. Rate curves of the anodization of various columbium tabs: 1, Cb sample No. 1; 2, Cb sample No. 2; and 3, Cb sample No. 3.

Table II. Electrical characteristics of wet 2.5 g-10 V columbium capacitors

Anode	Cathode	$C_{130}, \mu f$	D.F., %	E.S.R., ohms	I_L (room temp), μa	I_L 85°C, μa
Before life test						
Cb	Ag (no Pt)	219	42	2.40	1.0	5
Cb	Ag (Pt)	252	31	1.30	0.9	4.5
Ta	Ag (no Pt)	261	32	1.30	0.2	2
Ta	Ag (Pt)	285	25	0.92	0.5	1
After life test (250 hr at 85°C)						
Cb	Ag (no Pt)	133	29		2.4	
Cb	Ag (Pt)	253	29	1.30	2.4	
Ta	Ag (no Pt)	230	43	1.30	1.0	
Ta	Ag (Pt)	286	25	0.92	1.0	

grade tantalum, the graying occurs at a potential which is one third of the tantalum value.

Wet Electrolytic Capacitors

Low voltage-high capacitance wet electrolytic columbium capacitors (10 v-250 μ fd) were prepared and their electrical characteristics compared to similar tantalum units. This particular size was chosen since any instability in capacitance and dissipation factor is more likely to show up in this type of capacitor. Columbium anodes weighing 2.5 g, which had been sintered at 2000°C for 1 hr, were formed in concentrated ammonium chloride (26%) at 100°C to 13 v and canned in a silver case with concentrated lithium chloride (25%) solution as the fill electrolyte. The construction used was exactly the same as is used for Fansteel tantalum wet capacitors. However, severe capacitance losses were observed on life tests due probably to polarization effects at the silver cathode induced by the higher leakage current of the columbium capacitors. By plating the cathode with platinum black, the problem was overcome and the subsequent platinized units did not suffer any capacitance loss after life testing. The summary of 250-hr life tests at 85°C and 10 v is shown in Table II where each value is the average for 23 capacitors. In general, the 2.5-g columbium capacitors had electrical characteristics very similar to the 3.7-g tantalum capacitors which were used as controls. The dissipation factor values were slightly higher for columbium than for tantalum, but they can be considered to be satisfactory. Smaller capacitors also were made, but higher voltage capacitors were not attempted due to the higher d-c leakages of the columbium. It should be noted that with these larger anodes the ratio of the figure of merit, $(CE/g) Cb/Ta = 1310/1000 = 1.31$ is less favorable for columbium than was found for the smaller anodes previously described.

Solid Electrolytic Columbium Capacitors

Anodes weighing 0.07 g were used for the investigation of solid electrolytic columbium capacitors. These units described in Table III were constructed with only minor modifications in the procedure employed for the production of comparable tantalum solid capacitors. They were formed at 27, 54, 85, and 95 v with the intention of operating them at 10, 20, 30, and 35 v. The room-temperature

Table III. Cb solid electrolytic capacitor characteristics

For- mation voltage, v	Rated voltage, v	C, μf	D.F., %	I_L , 25°C, μa	I_L , 85°C, μa	I_L , 85°C, μa		
A. Life test (0.07 g Sintered powder anode)								
27	10	5.0	3	0.4	1	1.8 (after 340 hr)		
54	20	3.0	2	0.4	1	50 (after 190 hr)		
85	30	2.2	1.5	0.7	1.5	(short) (after 24 hr)		
95	35	1.6	1.5	1.2	(short)			
B. Thermal cycling (0.32 g Sintered powder anode)								
25°C		85°C			-55°C		25°C	
C, μf	D.F., %	I_L , μa	C, μf	D.F., %	I_L , μa	C, μf	D.F., %	I_L , μa
10.5	6.9	0.40	11.3	6.3	1.9	9.2	10	0.18
						10.4	7.2	0.34

properties of these capacitors were very similar to comparable tantalum capacitors although the dissipation factors and leakage currents were slightly higher.

These anodes were life-tested by maintaining them at the test voltage at 85°C. As is seen in Table III, only the 10-v units were satisfactory. After 340 hr, their leakage was still below 2 μa and the test was discontinued. The higher voltage solid electrolytic columbium capacitors developed high leakage and rapid failures on life test.

So far, it has been shown that it is possible to make low voltage columbium capacitors which are similar to tantalum capacitors, but which have no advantage except for a slight saving in weight.

One possible area where columbium capacitors might have an advantage over tantalum capacitors is in a severe nuclear radiation environment. The activation cross section for columbium is 1.1 barns compared to 21.3 barns for tantalum. Also, the possible isotopes for columbium all have a very short half life, a few hours, whereas for tantalum the half-life for the isotope formed is about 113 days. In other words, a tantalum capacitor subjected to neutron irradiation would remain very active for an extended period of time, while the activity from a

columbium capacitor would be relatively low; most of the radiation would be due to the electrolyte and can.

In order to determine the influence of radiation on columbium capacitors, 10-v solid electrolytic columbium capacitors (0.3 g by weight) and similar tantalum capacitors were irradiated in a nuclear pile and tested by Bendix Aviation Corporation (5). Eight capacitors were subjected to a fast neutron flux of approximately 6×10^{19} neutrons/cm² sec for a total integrated fast neutron flux of about 4×10^{20} neutrons/cm², while at rated voltage. An additional eight capacitors were irradiated at the same time without any applied potential. The results summarized in Table IV indicate that neither group of columbium solid electrolytic capacitors suffered any degradation from the intense radiation. At the conclusion of the test, the columbium capacitors were relatively inactive in comparison with the tantalum capacitors of comparable size and electrical characteristics which had undergone the same test (6). It is therefore concluded that for certain nuclear applications columbium solid capacitors may have some advantage over tantalum capacitors.

Summary

The properties of columbium as a capacitor metal were investigated and compared with those of tantalum. The following conclusions were reached:

1. The capacitance per unit area of anodized foil was found to be approximately the same for columbium as for tantalum, but the capacitance per unit weight for columbium sintered anodes is double that of tantalum sintered anodes prepared from electrolytic powder.
2. The working voltage of sintered columbium electrolytic capacitors is only about one third that of tantalum electrolytic capacitors for presently available materials and processing technology.
3. The d-c leakage of the best columbium capacitors investigated was approximately twice the leakage obtained with tantalum capacitors of similar ratings.
4. The dissipation factor of columbium capacitors is similar to that of tantalum capacitors.
5. With the presently available columbium, it is possible to make low voltage columbium electrolytic capacitors of both the wet and solid types which are

Table IV. Electrical characteristics of Cb solid electrolytic capacitors before and after irradiation with fast neutrons

	Pre-test			Post-test		
	Capacitance, μf	Dissipation factor, %	Leakage, μa	Capacitance, μf	Dissipation factor, %	Leakage, μa
With applied potential						
1.	9.5	8.8	0.027	9.3	6.1	0.059
2.	9.0	8.0	12.0	8.8	5.2	5.0
3.	9.8	6.2	3.3	9.6	4.2	30.0
4.	9.8	5.8	0.052	9.6	2.9	0.16
5.	13.3	3.0	0.047	13.0	1.6	0.026
6.	12.8	3.0	0.54	12.4	1.7	0.19
7.	12.8	2.9	0.071	12.4	1.2	0.16
8.	14.7	2.8	0.69	15.3	0.7	0.88
Without applied potential						
9.	9.6	8.2	0.135	9.2	6.8	0.33
10.	9.9	6.4	0.67	9.8	5.6	0.36
11.	12.1	5.0	0.048	11.8	3.8	0.17
12.	9.9	5.4	0.022	9.8	5.0	0.37
13.	13.2	2.4	4.6	13.2	1.3	2.8
14.	13.2	3.5	0.44	13.1	1.4	0.22
15.	13.5	3.5	0.027	13.4	1.4	0.13
16.	13.2	3.4	6.3	13.0	1.3	5.0

similar to tantalum capacitors of the same ratings.

6. Solid columbium electrolytic capacitors may offer some advantage over solid tantalum electrolytic capacitors in a nuclear environment.

Acknowledgment

The hot wire columbium was prepared by Battelle Memorial Institute. The nuclear tests conducted by Bendix Aviation Corporation were supported by Air Force Contract AF 33(600)-35026. The authors wish to thank Bendix for permission to publish the results of this test but no endorsement of columbium capacitors by Bendix or the Air Force is implied.

Manuscript received July 5, 1960; revised manuscript received Nov. 30, 1960. This paper was prepared for delivery before the Chicago Meeting, May 1-5, 1960.

Any discussion of this paper will appear in a Discussion Section to be published in the December 1961 JOURNAL.

REFERENCES

1. A. Güntersulze, *Ann. Physik*, **25**, 775 (1908).
2. L. Young, *Trans. Faraday Soc.*, **52**, 513 (1956).
3. L. Young, *Proc. Roy. Soc.*, **244**, 50 (1958).
4. L. Young, Private communication (1960).
5. R. Magee, K. More, and P. Sandeen, *Bendix Test Report BSR-95* (April 1959).
6. R. Magee, Paper presented before the American Nuclear Society (July 1959).

Dielectric Characteristics of Tantalum Anodic Films as Related to Film Structure

Donald Mohler and Robert G. Hirst

Transformer Division, General Electric Company, Pittsfield, Massachusetts

ABSTRACT

The variation of the dielectric characteristics of tantalum anodic films cannot be explained on the basis of bulk metal impurities alone. Very thin films on the metal surface influence the structural properties and leakage current characteristics of anodic films formed thereon. Sufficiently long exposure to hydrofluoric acid removes these films leaving clean metallic tantalum exposed and when this is anodized excellent anodic oxide films result. These anodic films are crystalline in structure (distorted Ta_2O_5) as opposed to amorphous films previously associated with good dielectric tantalum anodic films. Electron diffraction and spectrographic data support the above views by quantitatively identifying the metallic impurities in electrolytic grade tantalum and tentatively identifying the structures of the various films on tantalum foil.

It has long been recognized that tantalum metal showing essentially similar chemical and physical properties as measured by conventional means does not necessarily form anodic oxide films having the same dielectric properties. The leakage current characteristics of tantalum anodic films are highly variable. Previous interpretation has been that metallic bulk and surface impurities of tantalum contribute to these variations. This present work indicates that additional factors such as very thin surface films on the tantalum metal substrate substantially influence the structure and electrical properties of the anodic films.

In general "low leakage" currents are associated with tantalum foil which anodizes with a high degree of electrochemical efficiency. Typical current, measurements are $0.3-0.5 \mu\text{a}/\text{cm}^2$ at 150 v d.c. for foils anodized to 200 v d.c. for 1 hr. Theoretical weight increases based on Faraday's law are approached on tantalum of this quality when it is assumed that the anodic film is Ta_2O_5 . During the anodic formation of the film, little gassing is observed on the surface of the tantalum. The resulting anodic films are highly reflective, mirror-like surfaces when examined microscopically and show bright, sharp interference colors.

In contrast, gassing occurs on the surface of tantalum when anodizing if the quality of the metal is

sufficiently poor to produce anodic films characterized by "high leakage" currents. High leakage currents in this work are considered to be greater than $3 \mu\text{a}/\text{cm}^2$ or at least 10 times higher than the low leakage currents referred to just previously when measured under the same conditions. It has been the opinion that dull or gray anodic oxide films sometimes arise from tantalum containing metallic impurities. Since most metals do not form insulating anodic films, it seems reasonable to expect films formed on impure tantalum to be non-homogeneous, porous or lacking in continuity, and passing current easily.

Spectrographic Analysis

A spectrographic study of 12μ (0.0005 in.) tantalum foil formed to 200 v d.c. and subsequently degraded to a powder oxide in a 500°C muffle for ease of sample preparation failed to distinguish between tantalum characterized by high or low leakage current anodic films. A Baird grating-type emission spectrograph was used for this quantitative work, and the oxide powders were "arced" between essentially pure carbon electrodes. A spectrographic analysis of the various tantalum samples inspected is shown in the Appendix.

The elements Cr, Co, Pb, Mn, Ti, and W were not present in any of the tantalum samples while all

showed trace amounts of Cu and Zr. The content of Al, Ca, Mg, Mo, Ni, Pb, Si, and V varied from sample to sample. A close examination of the spectrographic data showing the common tantalum metal contaminates does not disclose correlation between the amount and kind of metallic impurities present and the leakage current characteristics of tantalum foil anodic films. In short, the electrical characteristics of the anodic films formed on the tantalum samples seem to be independent of the small amounts of impurities associated with commercial electrolytic grade tantalum foil. These results certainly do not imply that sufficient amounts of impurities in tantalum do not affect the anodic film properties; however they do suggest that for such electrolytic grade tantalum further study of the surface of this metal both anodized and unanodized is in order.

Experimental Electron Diffraction Examination of Tantalum Surfaces

During the course of work on a recent government contract (Project 2006A) for the Signal Corps it was learned that high leakage quality foil could be upgraded to low leakage quality by cleaning the tantalum surfaces with concentrated hydrofluoric acid for short time intervals. Capacitors made from such foils were electrically stable for over 2000 hr. This seems to confirm the idea that the properties of anodic films are related to the surface condition of the metal prior to anodizing. One might expect that HF cleansing removes the thin oxide film on tantalum [estimated by Torrisi (1) to be 300Å or less] since it is known that tantalum oxides dissolve with ease in concentrated HF solutions. It is reasonable to think that this oxide film is highly variable with respect to structure or thickness on tantalum due to the drastic rolling conditions in processing. Unless some treatment such as vacuum annealing is provided after final rolling it seems only logical to conclude that the oxide film is variable when sheet stock is reduced by Sendzimir mill to 12 μ foil. It is improbable that the surface temperature of the stock being rolled is maintained constant and this would certainly contribute to the formation of a nonuniform thin oxide film.

It was decided to study by means of electron diffraction techniques the very thin oxide film on tantalum as received, the effect of treating tantalum with HF, and the structures of the anodic films formed subsequently. It was hoped that such a study might uncover differences between high and low leakage quality foils and might explain the up-grading of poor quality tantalum by hydrofluoric acid treatment.

A number of 2.54 cm x 2.54 cm x 12 μ foil samples were cut from known high and low leakage quality foil stock. All foils were given a preliminary cleaning in a boiling 1% Alkanox solution for 15 min to remove surface dirt and oils. This was followed by rinsing in distilled water, acetone, and ether. Various foil samples were further cleaned by immersing in 40% HF for varying time intervals of up to 300 sec and rinsed immediately after with copious quan-

ties of distilled water. Upon drying, one-half of the samples were anodized in a glycol-ammonium pentaborate-water electrolyte to a potential of 200 v d.c. at 95°C and held for 1 hr. All foil samples, both unanodized and anodized, were next examined using a standard General Electric electron diffraction unit operated at 40 kv and 15 μ a. The electron beam was reflected from the surface of the foils, and photographs were taken of the diffraction patterns. Several areas of each sample were inspected and the electron diffraction patterns with photographs are reported in the Appendix.

The thin oxide film on all the unformed or unanodized samples both high and low leakage quality tantalum, prior to HF treatment showed amorphous patterns even though the maximum thickness is estimated at less than 300Å. No pattern for metallic tantalum was observed which is in agreement with the results previously reported by Spauschus (2). Thus it appears that a very thin oxide protective film, similar to that found on aluminum, is also present on tantalum foil. Microscopic examination of the surface of unformed foils further substantiated this view by revealing weak interference colors characteristic of thin oxide coatings.

Two crystalline diffraction patterns were associated with unformed samples cleaned by HF regardless of the film quality. The predominant pattern depends on the length of time of acid contact. With short cleaning times (10-120 sec) only pattern C was observed. From 120 to 300 sec both patterns C and D were observed. Pattern C became weaker and D stronger as the cleaning times increased. At 300 sec, pattern D alone was observed in some cases. The "d" spacings of pattern C were found to match quite closely the ASTM values for tantalum fluoride (TaF₃) and tantalum oxyfluoride (TaO₂F). Since TaF₃ and TaO₂F are isomorphous, positive identification based on our data could not be made. These samples exhibited areas of white crystalline material when examined microscopically. Pattern D was identified as the pattern arising from tantalum metal. This pattern was always highly oriented which is characteristic of a rolled metal. Microscopic examination of these samples showed only the parallel rolling marks and the surfaces were highly reflective.

Apparently the hydrofluoric acid attacks the thin tantalum oxide film and forms either TaF₃ or TaO₂F or both on the surface. Further acid attack dissolves the tantalum compound and produces a clean tantalum surface.

From the results of the diffraction patterns of the anodized samples shown in the Appendix it can be seen that none of the "electrically good" foils show crystalline compounds on the surface when anodized without previous hydrofluoric acid cleaning. On the other hand, "electrically poor" foils show both an amorphous pattern and a pattern due to some crystalline component (Pattern A). Spauschus and Vermilyea (3) have reported previously that the tantalum anodic film was amorphous. This is in agreement with our observations when the tantalum was of "low" leakage quality and not treated with HF prior to anodizing. However, all HF treated tanta-

lum foil in this work produced strongly crystalline anodic films. There was no difference in the physical appearance of the amorphous and crystalline films, both characterized by highly reflective interference colors without gray or dull areas. The diffraction pattern (Pattern A) for the crystalline material on the anodized samples was thought to arise from Ta_2O_5 . Precise matching against established ASTM values for Ta_2O_5 was not possible. However, the similarity of the pattern to Ta_2O_5 suggests a distorted Ta_2O_5 structure. Perhaps only the surface of the crystalline material is distorted. The structure of the underlying film is indeterminable since penetration of the electron beam by reflection is something less than 500Å while the 200 v film is approximately 4000Å thick.

All HF cleaned high and low leakage quality tantalum samples show the same general diffraction patterns. Two crystalline species appear simultaneously, one distorted Ta_2O_5 , the other an unidentified compound (Pattern B). The distorted Ta_2O_5 pattern appeared strongest and the unknown pattern weakest for those samples cleaned with HF for 300 sec before anodizing. This suggests that the Ta_2O_5 results from a clean tantalum surface while the unidentified compound arises from a reaction product of HF and tantalum which had been left on the surface. It will be recalled that short time cleaning leaves TaF_5 and/or Ta_2O_5F on the tantalum surface.

The previously discussed electron diffraction patterns are summarized in the following chart.

Electron Diffraction Patterns

Unanodized tantalum samples		200 v d.c. Anodic films formed on tantalum samples
Amorphous	— low leakage quality foil	→ AMORPHOUS
	— high leakage quality foil	→ AMORPHOUS + Distorted Ta_2O_5
↓ HF		
Tantalum Fluoride	— high & low leakage quality foil	→ Distorted Ta_2O_5 + UNIDENTIFIED CRYSTALLINE MATERIAL
↓ HF		
Tantalum	— high & low leakage quality foil	→ DISTORTED Ta_2O_5 + Unidentified Crystalline Material

Electrical Characteristics of Anodic Films Formed for 1 Hr

The electrical characteristics of the anodic films were determined for the samples used to obtain the electron diffraction data. Capacity per unit area and power factor values for all samples were found to be relatively independent of the tantalum quality of the samples and the HF cleaning. Since there was no increase in capacity as a result of the HF treatment it can be presumed that the dissolving action of the reagent was uniformly attacking all points of the tantalum surface, thus not changing the original surface area. In short, no etch gain was observed. The leakage currents show a definite trend toward lower values as a function of contact time with the acid. Unfortunately there is no clear relation between the diffraction patterns and leakage

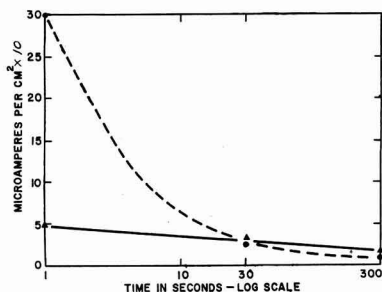


Fig. 1. Leakage current characteristics of 200 v d.c. tantalum anodic films as a function of immersion time in 40% HF prior to anodizing. ●, high leakage quality tantalum foil; ▲, low leakage quality tantalum foil.

currents except with the most drastic cleaning treatment. Here it would appear that when clean metallic tantalum is present, anodic films are formed which show superior leakage current characteristics. These anodic films have excellent insulating properties when measured in electrolytes. We postulate that a bare tantalum surface produced by HF cleaning gives rise to anodic films, crystalline in nature, uniform in composition, and relatively defect free. These films produce a crystalline structure that will not easily permit the passage of ions and current. The leakage current characteristics of 200 v anodic films vs. HF cleaning time are shown in Fig. 1. Note that there was no significant difference in leakage between high and low leakage quality foil after im-

mersing for 300 sec in concentrated HF followed by anodizing.

Conclusions

1. Bulk metallic impurities in electrolytic grade tantalum foil do not account for the differences between high and low leakage quality tantalum.
2. Thin oxide films on tantalum foil in the as-received condition are amorphous regardless of metal quality and electron diffraction examination is unable to distinguish between high and low leakage quality tantalum.
3. When anodized, low leakage quality tantalum foil, not HF treated, produces an amorphous film while high leakage quality foil shows both an amorphous film and crystalline Ta_2O_5 . On the other hand, after anodizing all foils cleaned with HF show crystalline Ta_2O_5 , plus an unidentified crystalline ma-

terial. Ta_2O_5 predominates for long cleaning times and gives good electrical characteristics. The above facts appear to be anomalous and from the results of foils not HF cleaned one might expect cleansing to give rise to an amorphous oxide on anodizing. Perhaps the thin oxide film on high leakage quality foil is discontinuous and porous and on anodizing produces a porous film partly crystalline and partly amorphous. The thin amorphous oxide on low leakage quality foil on the other hand may be a tightly adherent, continuous film which on anodizing allows a buildup of the same amorphous type of film. HF cleaning of both types of foil produces a clean tantalum surface which allows a buildup of a continuous crystalline film which is excellent electrically.

4. Treating tantalum foil with HF prior to anodizing improves the formation properties and the electrical characteristics of the anodic films.

5. The oxide film on tantalum foil is replaced by a thin tantalum fluoride or oxyfluoride film after short interval HF cleaning. Further cleaning, 180 sec or longer, exposed metallic tantalum.

6. The best anodic films were found on tantalum when HF was used to remove all surface films. The surface condition of high and low leakage quality tantalum was reduced to a common denominator by this acid treatment. Subsequent anodization produces superior crystalline anodic films on both high and low leakage quality tantalum.

Manuscript received Sept. 29, 1960. This paper was prepared for delivery before the Chicago Meeting, May 1-5, 1960.

Any discussion of this paper will appear in a Discussion Section to be published in the December 1961 JOURNAL.

REFERENCES

1. A. F. Torrisi, *This Journal*, **102**, 176 (1955).
2. H. O. Spauschus, Private communication, February 1952.
3. D. A. Vermilyea, *Acta Met.*, **1**, 282 (1953).
4. R. G. Hirst, Private communication, January 1954.

APPENDIX

Spectrographic Analysis

Sample No. Impurity	Low leakage quality tantalum, 0.3-0.5 $\mu\text{a}/\text{cm}^2$			High leakage quality tantalum, >3 $\mu\text{a}/\text{cm}^2$	
	14	17	19	13	18
Aluminum	H	T	L	T	L
Calcium	L	L	T	T	L
Chromium	NDA	NDA	NDA	NDA	NDA
Cobalt	NDA	NDA	NDA	NDA	NDA
Copper	T	T	T	T	T
Iron	L	L	L	L	H
Lead	NDA	NDA	NDA	NDA	NDA
Magnesium	H	H	L	L	H
Manganese	NDA	NDA	NDA	NDA	NDA
Molybdenum	NDA	NDA	NDA	NDA	H
Nickel	T	L	T	NDA	H
Niobium	NDA	H	NDA	NDA	NDA
Silicon	H	T	L	L	L
Titanium	NDA	NDA	NDA	NDA	NDA
Tungsten	NDA	NDA	NDA	NDA	NDA
Vanadium	T	T	NDA	T	L
Zirconium	T	T	T	T	T

High—H = 0.003-0.1% impurity.
Low—L = 0.0005-0.02% impurity.
Trace—T = below 0.003% impurity.
NDA—nondetectable, less than trace.

Diffraction pattern photographs



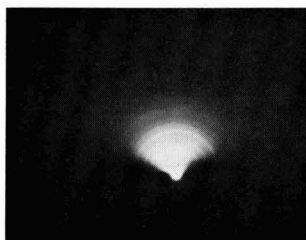
Amorphous



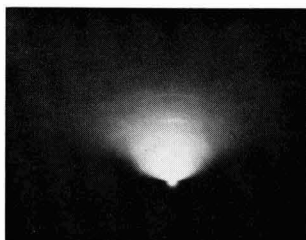
Pattern A



Patterns A & B



Pattern C



Patterns C & D



Pattern D

Electron diffraction patterns, unanodized tantalum foil

Foil coil No.	Sam- ple	Tantalum quality	HF treat, sec	Diffraction pattern	Remarks
1	A	High leakage	0	Amorphous	
1	B	High leakage	10	Pattern C*	
1	C	High leakage	30	Pattern C	
1	D	High leakage	300	Pattern D	
2	A	Low leakage	0	Amorphous	
2	B	Low leakage	10	Pattern C	
2	C	Low leakage	30	Pattern C	
2	D	Low leakage	300	Pattern D	
3	A	Low leakage	0	Amorphous	
3	B	Low leakage	10	Pattern C	
3	C	Low leakage	30	Pattern C	
3	D	Low leakage	300	Pattern D	
3A	E	Low leakage	0	Amorphous	
3A	F	Low leakage	60	Pattern C	
3A	G	Low leakage	120	Pattern C	
3A	H	Low leakage	180	C & D	Stronger C
3A	I	Low leakage	240	C & D	Stronger D
3A	J	Low leakage	300	C & D	Stronger D
4	E	High leakage	0	Amorphous	
4	F	High leakage	60	Pattern C	
4	G	High leakage	120	Pattern C	
4	H	High leakage	180	C & D	Stronger C
4	I	High leakage	240	C & D	Stronger D
4	J	High leakage	300	C & D	Stronger D

Electron diffraction patterns, tantalum foil anodized to 200 v. d.c.

Foil coil No.	Sam- ple	Tantalum quality	HF treat, sec	Diffraction pattern	Remarks
1	A _r	High leakage	0	Pattern A	
1	B _r	High leakage	10	A & B	
1	C _r	High leakage	30	A & B	
1	D _r	High leakage	300	A & B	
2	A _r	Low leakage	0	Amorphous	
2	B _r	Low leakage	10	A & B	
2	C _r	Low leakage	30	A & B	
2	D _r	Low leakage	300	A & B	
3	A _r	Low leakage	0	Amorphous	
3	B _r	Low leakage	10	A & B	
3	C _r	Low leakage	30	A & B	
3	D _r	Low leakage	300	A & B	
3A	E _r	Low leakage	0	Amorphous	
3A	F _r	Low leakage	60	A & B	
3A	G _r	Low leakage	120	A & B	
3A	H _r	Low leakage	180	A & B	
3A	I _r	Low leakage	240	A & B	
3A	J _r	Low leakage	300	A & B	
4	E _r	High leakage	0	Amorphous + A	
4	F _r	High leakage	60	A & B	
4	G _r	High leakage	120	A & B	
4	H _r	High leakage	180	A & B	
4	I _r	High leakage	240	A & B	
4	J _r	High leakage	300	A & B	Strong A

Pattern A—Not positively identified but appears to be that of Ta₂O₅ with some distortion.

Pattern B—Pattern B not positively identified.

Pattern C—Pattern found on unformed-etched foils. Could be either Ta₂O₅ or TaF₅. (These compounds are nearly isomorphous.)

Pattern D—Highly oriented, pattern of metallic tantalum.

Mechanism of Electrodeposition of Cobalt from Liquid Ammonia Solutions of Spin-Paired Cobalt(III) Complexes

Evidence for a Trans Effect in Octahedral Complexes

George W. Watt and Joe W. Vaughn

Department of Chemistry, The University of Texas, Austin, Texas

ABSTRACT

Cathode current efficiency data for the electrolysis of liquid ammonia solutions of certain spin-paired cobalt(III) complexes are interpreted as supporting a previously proposed mechanism of generation of the electrochemically active species. The possibility of a trans effect in octahedral complexes is discussed as such and in relation to the trans effect in square planar complexes.

Earlier work in this laboratory (1) has shown that the electrodeposition of nickel from ammonia solutions of spin-free nickel (II) complexes is profoundly influenced by specific properties of added competitive ligands. Cathode current efficiency data were interpreted on the basis that the initial process involved a bimolecular ligand substitution,



followed by a trans labilization-induced dissociative process of the type proposed by Lyons (2).



and that gives rise to the electrochemically active species. Although Lyons concluded that deposition is not to be expected from aqueous solutions of spin-paired ("inner-orbital") complexes of the type $[CoL_6]^{3+}$, the results reported here demonstrate

that deposition does occur from liquid ammonia solutions.¹

Although there is an abundance of evidence relating to the trans labilizing influence of a wide variety of ligands in square planar complexes of (particularly) platinum (3, 4), there are only limited indications that a similar effect may be operative in complexes that exhibit octahedral symmetry. Yatsimerskii and Pankova (5) have used thermochemical data as a basis for the establishment of a partial "trans effect series" for octahedral complexes of cobalt (III), and it is noteworthy that their conclusions differ significantly from those that apparently apply to square planar complexes of platinum (4). More recently, Palmer and Basolo (6) have reported that the lability of

¹Other experiments in this laboratory (G. W. Watt and J. A. Cunningham, Unpublished work) show that deposition occurs readily from aqueous solutions of spin-paired complexes of Pt, Pd, and Au.

hydrogen toward hydrogen exchange in substituted amines of cobalt (III) depends on both the charge on the central metal ion and the identity and position of the substituent ligand(s). Vlcek and Kuta (7) have applied the bimolecular ligand substitution mechanism to the explanation of the influence of a variety of anions upon the reduction of complexes of the type $[\text{Co}(\text{NH}_3)_5\text{X}]^{2+}$ at the dropping mercury electrode. Closely analogous studies by Maki, *et al.* (8) have been concerned with the "polarographic stability" of cobalt (III) complexes; these workers list the relative effects of a considerable number of ligands in an order that differs in major respects from orders based on other criteria.

There were several reasons for undertaking the work described in the present paper. First, it seemed worthwhile to test the previously postulated S_82 mechanism (1) in application to a case other than nickel (II). Second, only a narrow range of competitive ligand properties in the case of nickel (II) complexes resulted in cathode current efficiencies that ranged from 0 to 100%; hence, this case is not suitable as a basis for the investigation of a wider variety of potentially transbilizing ligands. Third, if the postulated mechanism has merit, there seems to be no *a priori* reason why deposition should not occur from solutions of spin-paired as well as spin-free complexes.

Experimental

Materials.—The following cobalt (III) complexes were prepared and purified by procedures to which reference is made; the calculated and experimentally determined cobalt content, respectively, are given in parentheses in each case: Hexamminecobalt (III) nitrate, (9), (17.0, 16.7); iodopentamminecobalt (III) nitrate, (10), (14.9, 14.4); isothiocyanatopentamminecobalt (III) nitrate, (11), (18.1, 18.0); nitrosopentamminecobalt (III) nitrate, (12), (19.4, 19.0); aquopentamminecobalt (III) nitrate, (13), (17.0, 17.3); nitritopentamminecobalt (III) nitrate, (14), (18.8, 18.4). X-ray diffraction data are given in Table I.

Table I. X-ray diffraction data^a

$[\text{Co}(\text{NH}_3)_6](\text{NO}_3)_3$		$[\text{Co}(\text{NH}_3)_5\text{I}](\text{NO}_3)_2$		$[\text{Co}(\text{NH}_3)_5(\text{H}_2\text{O})](\text{NO}_3)_3$	
d, Å	I/I ₀	d, Å	I/I ₀	d, Å	I/I ₀
6.3	1.0	6.1	1.0	6.2	1.0
5.2	0.7	5.4	0.5	5.3	0.8
3.9	0.8	5.1	0.5	4.0	0.1 ^b
2.8	0.1	3.8	0.8	3.8	1.0
2.7	0.1 ^b	3.0	0.5		
		2.7	0.5		
		2.4	0.5 ^b		
$[\text{Co}(\text{NH}_3)_5\text{NCS}](\text{NO}_3)_2$		$[\text{Co}(\text{NH}_3)_5\text{NO}_2](\text{NO}_3)_2$		$[\text{Co}(\text{NH}_3)_5\text{NO}](\text{NO}_3)_2$	
d, Å	I/I ₀	d, Å	I/I ₀	d, Å	I/I ₀
6.2	0.8	6.2	1.0	6.2	0.7
5.2	0.7	5.2	0.5	5.7	0.7
3.8	1.0	3.8	0.4	5.3	1.0
3.2	0.3	2.7	0.1 ^b	4.4	0.5
2.7	0.2 ^b	2.1	0.1	3.6	0.1 ^b

^a $\text{CuK}\alpha$ radiation, Ni filter, 40 kv and 15 ma; exposure time, 7-8 hr; relative intensities estimated visually.

^b Less intense lines not included here.

Table II. Electrolysis of liquid ammonia solutions of cobalt(III) complexes at -34°

Complex	Current density, ma/cm ²	Time, hr	Added salt	Cathode current efficiency, %
$[\text{Co}(\text{NH}_3)_6](\text{NO}_3)_3$	0.48	3.25	—	21
	0.64	3.0	—	25
	0.89	1.8	—	29
$[\text{Co}(\text{NH}_3)_5\text{I}](\text{NO}_3)_2$	1.30	2.0	—	43
	0.48	3.0	—	28
	0.65	3.25	—	32
$[\text{Co}(\text{NH}_3)_5(\text{NCS})](\text{NO}_3)_2$	0.84	3.0	—	35
	1.3	2.5	—	44
	0.71	3.0	—	45
$[\text{Co}(\text{NH}_3)_5(\text{NO})](\text{NO}_3)_2$	0.93	3.3	—	49
	1.3	4.0	—	51
	0.68	3.0	—	68
$[\text{Co}(\text{NH}_3)_5(\text{H}_2\text{O})](\text{NO}_3)_3$	0.75	3.5	—	73
	0.68	3.0	—	34
	0.98	3.0	—	36
$[\text{Co}(\text{NH}_3)_5(\text{NO}_2)](\text{NO}_3)_2$	1.3	3.0	—	43
	0.68	3.0	—	5.8
	0.71	4.2	—	5.9
$[\text{Co}(\text{NH}_3)_5](\text{NO}_3)_3$	1.3	2.8	KI	42
	1.3	2.5	KSCN	49
	1.3	3.0	KNO ₂	15

Reagent grade potassium iodide was dried at 150° and used without further purification. Reagent grade potassium thiocyanate was dried over magnesium perchlorate and used without further purification. Potassium nitrite was recrystallized from hot water and dried at 120° .

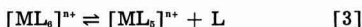
Equipment and procedures.—The electrolysis cell and the electrode holders, as well as most of the experimental procedures, were essentially the same as those described previously (1). Bright platinum electrodes, 5.0 x 0.90 cm, were used in all experiments; the circuit included a silver coulometer. Concentration polarization was minimized by stirring the solutions with a magnetic stirrer.

Experimental data.—In experiments that employed the cobalt(III) salts listed above, the total solution volume was 100 ml, the concentration of the cobalt(III) salt was $3.5\text{--}3.7 \times 10^{-4}\text{M}$, and the concentration of the added potassium salt (where used) was $7.0\text{--}7.4 \times 10^{-4}\text{M}$. The resulting data are given in Table II. The physical character of the metal deposited on the cathode varied, but in a manner that could not be correlated with the conditions that prevailed. Thus in a series of repetitive runs involving the same solution composition and all other conditions held constant, both very bright and black finely divided deposits were observed. In all cases, however, the deposits were sufficiently adherent to permit direct weighing of the deposited metal.

Several measurements (not included in Table II) showed that cathode current efficiency does not vary significantly as a function of the duration of electrolysis, *i.e.*, over periods of the order of 1.5-4.0 hr at constant current density. Similarly it was demonstrated that the use of cathodes cleaned by immersion in concentrated hydrochloric acid followed by washing with distilled water and heating to redness led to reproducible results.

Discussion

Although the magnitude of the effects produced by competitive ligands in the case of cobalt(III) is somewhat less than that for nickel(II), the results given in Table II are clearly compatible with and in support of the mechanism (1) represented by the general Eq. [1] and [2]. Thus, the enhancement of cathode current efficiency for $[\text{Co}(\text{NH}_3)_6\text{I}]^{3+}$ as compared with $[\text{Co}(\text{NH}_3)_6]^{3+}$ is attributed to the transblabilizing effect of the I^- ligand. It must be recognized however that, in contrast to the nickel(II) case, the fact that deposition occurs at all from solutions of $[\text{Co}(\text{NH}_3)_6]^{3+}$ alone must be attributed to a simple dissociative ($\text{S}_{\text{N}}1$) process of the type proposed by Lyons (2). Accordingly, reaction [1] would be preceded by



The data of Table II show that cathode current efficiency is dependent on current density, but that the effects of specific competitive ligands is clearly evident at current densities in the range of $0.67 \pm 0.05 \text{ ma/cm}^2$. Plots of cathode current efficiency vs. current density for $[\text{Co}(\text{NH}_3)_6]^{3+}$ and $[\text{Co}(\text{NH}_3)_6\text{I}]^{3+}$ are linear and converge at a current density of 1.3 ma/cm^2 . The corresponding curve for $[\text{Co}(\text{NH}_3)_6(\text{NCS})]^{3+}$ lies above that for $[\text{Co}(\text{NH}_3)_6\text{I}]^{3+}$ and does not converge with the hexammine curve at 1.3 ma/cm^2 . An analysis of the data for $[\text{Co}(\text{NH}_3)_6]^{3+} + \text{KSCN}$ would seem to indicate that the electrochemically active species is the same as that which is operative when $[\text{Co}(\text{NH}_3)_6(\text{NCS})]^{3+}$ alone is used since the efficiencies are identical within experimental error. The low cathode current efficiency found for $[\text{Co}(\text{NH}_3)_6(\text{NO}_2)]^{3+}$ is surprising in that this suggests that the transblabilizing influence of the NO_2^- ligand is less than is usually attributed to this ligand (see below). Nevertheless, the data for the three cases $[\text{Co}(\text{NH}_3)_6]^{3+}$, $[\text{Co}(\text{NH}_3)_6(\text{NO}_2)]^{3+}$, and $[\text{Co}(\text{NH}_3)_6]^{3+}$ plus KNO_3 are both internally consistent and compatible with the earlier interpretation (1). It is indicated however that in the latter instance the *in situ* conversion of $[\text{Co}(\text{NH}_3)_6]^{3+}$ to $[\text{Co}(\text{NH}_3)_6(\text{NO}_2)]^{3+}$ must be incomplete; the same is apparently true for $[\text{Co}(\text{NH}_3)_6]^{3+}$ plus KSCN .

For the case of $[\text{Co}(\text{NH}_3)_6]^{3+}$ plus I^- , it is not possible to conclude that ligand substitution occurs since the efficiencies found for $[\text{Co}(\text{NH}_3)_6]^{3+}$ and $[\text{Co}(\text{NH}_3)_6\text{I}]^{3+}$ are essentially the same, particularly at high current densities. The curves for cathode current efficiency vs. current density for these two species show a maximum difference of about 8% at a current density of 0.5 ma/cm^2 . Allowing for the possibility of incomplete conversion of the hexammine to the iodopentammine and the somewhat greater experimental error at lower current densities, the available evidence is inconclusive. This particular aspect of the problem is currently being investigated by another method.

The data listed in Table II are also of interest in connection with the relative transblabilizing effects of ligands in octahedral complexes. Thus from the present data, and in the light of the interpretation

given above, the increasing order of transblabilizing effect of the ligands studied is,

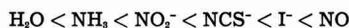


The most nearly comparable results, also for octahedral complexes of cobalt(III), are those of Yatsimskii (15) who has reported that $\text{NO}_2^- > \text{NH}_3$ and $\text{H}_2\text{O} > \text{Cl}^-$. The obvious discrepancy is concerned with the status of the nitrito ligand; the present results suggest that this ligand is slightly transblabilized by the NH_3 ligand. There is however an alternative and more attractive explanation of the relative effects of these two ligands. Vlcek (16, 7) has interpreted certain polarographic data as indicating that complexes of the type $[\text{Co}(\text{NH}_3)_5\text{X}]^{3+}$ orient in a manner such that the hetero atom or group X is always as far as possible from the electrode surface. The complex $[\text{Co}(\text{NH}_3)_5\text{NO}_2]^{3+}$ however is reported to be an exception in that it orients with the NO_2^- ligand somewhat closer to the electrode. We may now consider the consequences of such preferential orientation in relation to the relative transblabilizing effects of the NO_2^- and NH_3 ligands. If the trans effect of the NO_2^- is greater than that of NH_3 , the former would transblabilize the latter, thus providing an available bonding orbital for the establishment of a partially metallic bond with the cathode metal lattice (2). But owing to the above mode of orientation, the bonding orbital thus made available would project away from the electrode and the trans effect of the NO_2^- would be cancelled effectively. Under these circumstances reduction to metal would require rupture of the Co- NO_2 bond; hence the cathode current efficiency would be low even if the NO_2^- ligand had a large trans effect. If, on the other hand, the trans effect of NH_3 exceeds that of NO_2^- , the foregoing argument would still apply and the net result would be the conversion of $[\text{Co}(\text{NH}_3)_5\text{NO}_2]^{3+}$ to $[\text{Co}(\text{NH}_3)_6]^{3+}$. Should this occur, orientation at the electrode surface would no longer be of importance, and the measured cathode current efficiency should be the same as for the case in which $[\text{Co}(\text{NH}_3)_6]^{3+}$ is introduced initially. It is clear from Table II that such is not the case, and therefore it must be concluded that the NO_2^- ligand probably has a greater trans effect than NH_3 but that the effect is masked by preferential orientation at the electrode surface.²

It is also of interest to compare the trans effect sequence deduced from the present studies with the positions of these same ligands in series that relate to square planar complexes. The interrelationship given by Chatt and co-workers (4) is



while that resulting from the work of Hel'man and Karandashova (17) is



In this connection it should be recalled that these two series are based not on any measurable parameter but rather result from qualitative observa-

²For other recent data on the unusual transblabilizing effect of NO_2^- and numerous references to earlier related work, see: A. A. Grinberg, Russ. J. Inorg. Chem., 4, 683 (1959).

tions made during the course of synthesis. Even though the positions of some of the above ligands may be in doubt, the results reported in this paper indicate that, if a trans effect is indeed operative in octahedral complexes, the relative positions of ligands may be considerably different than for square planar complexes. It is also reasonable to suggest that the relative trans-labilizing effects of ligands may differ as a function of the charge on the central metal ion as well as on the symmetry of the complex. The water molecule is a case in point; it appears that this ligand has a greater trans effect in octahedral cobalt(III) complexes than in square planar platinum(II) complexes. It is also of interest to note that the NO ligand exhibits a very great effect in both of these types.

Other experiments that bear on the views expressed above are in progress and the results will be presented in forthcoming papers from this laboratory.

Acknowledgment

This work was supported, in part, by the Robert A. Welch Foundation and by the U.S. Atomic Energy Commission, Contract AT-(40-1)-1639.

Manuscript received Aug. 3, 1960; revised manuscript received Nov. 9, 1960.

Any discussion of this paper will appear in a Discussion Section to be published in the December 1961 JOURNAL.

REFERENCES

1. G. W. Watt and D. A. Hazlehurst, *This Journal*, **106**, 117 (1959).
2. E. H. Lyons, Jr., *ibid.*, **101**, 363, 376 (1954).
3. I. I. Chernyaev, *Ann. inst. platine U.S.S.R.*, **4**, 261 (1926).
4. J. Chatt, L. A. Duncanson, and L. M. Venanzi, *J. Chem. Soc.*, **1955**, 4456.
5. K. B. Yatsimerskii and L. L. Pankova, *J. Gen. Chem. U.S.S.R.*, **18**, 2051 (1948); **19**, 617, 623 (1949).
6. J. W. Palmer and F. Basolo, *J. Phys. Chem.*, **64**, 778 (1960).
7. A. A. Vlcek and J. Kuta, *Nature*, **185**, 95 (1960); cf. G. W. Watt and J. W. Vaughn, *ibid.*, **186**, 309 (1960).
8. N. Maki, Y. Shimuri, and R. Tsuchida, *Bull. Chem. Soc. Japan*, **32**, 23 (1959).
9. J. Bjerrum and J. P. McReynolds, *Inorg. Syntheses*, **2**, 218 (1946).
10. R. G. Yalman, *J. Am. Chem. Soc.*, **77**, 3219 (1955).
11. A. Werner, *Z. anorg. Chem.*, **22**, 110 (1900).
12. E. P. Bertin, S. Mizushima, T. J. Lane, and J. V. Quagliano, *J. Am. Chem. Soc.*, **81**, 3821 (1959).
13. A. Werner, *Ber.*, **40**, 4104 (1907).
14. S. M. Jorgensen, *Z. anorg. Chem.*, **5**, 170 (1894).
15. K. B. Yatsimerskii, *Doklady Akad. Nauk. S.S.S.R.*, **72**, 307 (1950).
16. A. A. Vlcek, *Discussions Faraday Soc.*, **26**, 164 (1958).
17. A. D. Hel'man and E. F. Karandashova, *Doklady Akad. Nauk. S.S.S.R.*, **87**, 597 (1952).

Preparation and Properties of Grown P-N Junctions of InSb

H. C. Gorton, A. R. Zaccaroli, F. J. Reid, and C. S. Peet

Battelle Memorial Institute, Columbus, Ohio

ABSTRACT

Grown p-n junctions of InSb were produced by doping high-purity n-type melts with zinc. The crystals were oriented such that the growth axes of the crystals were perpendicular to a (111) plane. The effects of anisotropic distribution of impurities within the crystals were observed in the electrical properties of the diodes. The lifetime of minority carriers at high injection levels (forward bias) was observed. Anomalous values are attributed to changes in properties of the bulk material rather than the surface. The curves of current density as a function of temperature showed leakage currents to predominate at lower temperatures and saturation currents to predominate at higher temperatures. This observation was verified by current-voltage profiles at appropriate temperatures.

Crystal Growth and Junction Formation

Single crystals of InSb were grown by the Czochralski technique from zone-refined material. The material was heat treated in a vacuum for 2 hr at about 530°C to remove highly volatile impurities, such as zinc. The crystals were pulled in an atmosphere of hydrogen which had been purified by diffusion through palladium.

To produce a junction, an n-type crystal was grown to a diameter of about 0.75 in. The crystal was then raised from the melt to which zinc was added in the form of ZnSb for the higher acceptor concentrations, and in the form of InSb containing about 10^{18} zinc atoms cm^{-3} for the lower acceptor con-

centrations. About 10 min was allowed for the zinc to become evenly distributed throughout the melt before pulling was resumed.

The seed crystals used to pull these crystals were oriented such that the growth axis of the crystal was perpendicular to a (111) plane. This produces the coring effect resulting from the anisotropic distribution of impurities within the crystal, as reported by Allred and Willardson (1), and by Hulme and Mullin (2). In some high-purity crystals, where the impurity concentrations on either side of the junction were nearly equal, junctions were achieved only around the edge of the ingot because of the buildup of donor impurities near the center.

Table I. Carrier concentrations and mobilities near the p-n junctions in InSb crystals 17 and 37

Diode No.	Majority carrier concentrations, at 77°K, cm ⁻³		Charge carrier mobility at 77°K, cm ² V ⁻¹ sec ⁻¹	
	n-side	p-side	n-side	p-side
17-D16	5.2×10^{14}	4.8×10^{14}	3.5×10^6	6.2×10^6
37-D11	1.5×10^{16}	1.6×10^{17}	3.5×10^6	1.4×10^6

Bridge-type Hall samples for determining the electrical characteristics of the bulk p- and n-type material were cut from the crystals about 2 mm from either side of the junction.

In this paper, we will report on the electrical characteristics of one diode taken from each of two crystals. The electrical characteristics of the bulk material on either side of the junctions are shown in Table I. Majority carrier concentrations on the n- and p-sides of the junction of the diode cut from crystal 17 were nearly identical, while majority carrier concentrations on the two sides of the diode taken from crystal 37 differed by two orders of magnitude. The lower hole mobility on the p-type side of the junction on diode 37-D11 would be expected from the higher acceptor concentration.

Diode Preparation

A 4-mm thick slice of the ingot containing the p-n junction was diced into diodes of about 0.05 cm² cross-sectional area. The junctions were located by thermally probing the diodes while immersed in liquid nitrogen. Electrical contact to both the p- and n-sides was made by alloying an electrodeposited film of gold with the material. Specific contact resistances on the order of 0.035 ohm cm² at 77°K were achieved. The diodes were etched in a solution of 10:10:7 HCl:HNO₃:HAc at 95°F. Pressure contacts were made to the diodes, and they were sealed off under fore-pump vacuum.

Results and Conclusions

The lifetime of minority carriers in the diodes at high injection levels was obtained at 77°K by the open-circuit voltage decay method (3,4). In this method, the diode is biased in the forward direction, the current is interrupted suddenly, and the time rate of decay of injected charge-carriers is observed.

The high level lifetime at 77°K was measured on the diode from crystal 17 immediately after etching and was observed to be 25 mμ sec. After storage for about a month at room temperature, a much larger value of 150 mμ sec was observed. Since the conductance through a diode in the low-dynamic-impedance portion of the forward characteristic, in which region the high level lifetime is observed, is a bulk phenomenon, surface recombination velocities would be relatively unimportant in controlling high level lifetime so long as the diffusion length were short with respect to the cross-sectional dimension of the diode. The diffusion lengths of the charge carriers on both the n- and p-sides of the junction of crystal 17, as determined from the relationship $L = (\mu\tau kT/q)^{1/2}$, are less than 10⁻² cm, whereas the diameter of the diode is 0.2 cm. Therefore, it is as-

sumed that the observed change in lifetime was the result of some change in the bulk material, rather than in the surface. That the high level lifetime at 77°K is independent of surface conditions is further indicated by similar lifetime measurements made on the diode from crystal 37. Here the lifetime was obtained after markedly different surface treatments and was found to be relatively constant. The lifetime was first measured after lapping and polishing the diode. It was again observed after etching the diode in the same manner as the one from crystal 17. In both cases, a value of about 0.5 μ sec was obtained, which is near that reported by Wertheim for n-type InSb below 150°K (5).

An expression for the temperature dependence of the current density through the junction, developed from basic considerations (6), is

$$j = j_0 e^{-E_g/kT} (e^{qV/kT} - 1) \quad [1]$$

where j_0 may be considered a constant. V is the voltage across the junction, E_g is the energy gap of the material, and q/kT has the usual connotation. At a reverse bias of 0.1 v in the temperature region of interest, $e^{qV/kT}$ is small with respect to 1, and may be neglected, so that Eq. [1] becomes $j_r = j_0 e^{-E_g/kT}$ for the reverse current through the junction. The slope of the log j_r vs. T^{-1} plot of the ideal diode equation at low reverse bias then is related to the band gap, E_g .

Figure 1 is a plot of the reverse current density with a constant impressed voltage of 0.1 v as a function of reciprocal temperature for a representative diode from each of the two ingots. One run is shown for the diode cut from crystal 17, and three runs are shown for the diode cut from crystal 37 after different treatments of the surface.

In Fig. 1 two curves are superimposed on the experimental points with slopes corresponding to the band gap of InSb at the indicated temperatures (0.23 - 2.9 × 10⁻⁴ T ev). A very close fit of the experimental data to the slopes of these curves is ob-

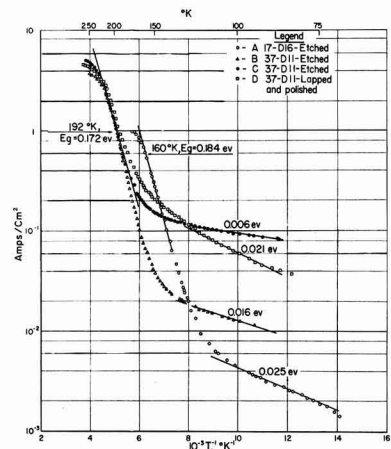


Fig. 1. Reverse current density at 0.1 v applied potential vs. reciprocal temperature for InSb grown junction diodes 37-D11 and 17-D16.

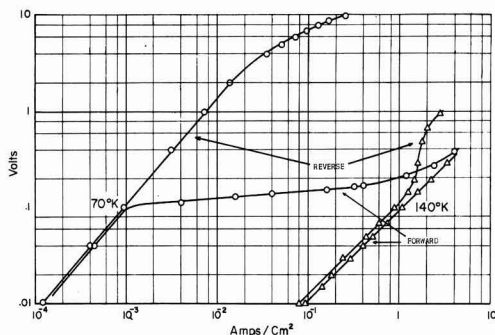


Fig. 2. Current-voltage profiles of diode 17-D16 at 70° and 140°K.

served, which agrees with the mechanism invoked by the ideal diode equation and indicates the predominance of minority carrier diffusion under reverse bias at the indicated temperatures. At lower temperatures, the slopes of the curves again have constant values which represent relatively low activation energies. It is suggested that these values correspond to the activation energies of the carriers contributing to leakage current, and are presumably associated with surface states in the material. If such were the case, it should be possible to change both the magnitude and the slope of that portion of the curve by selected surface treatment of the material. Such a procedure was carried out with the diode from crystal 37. Curves B and C were obtained after etching the diode, and the curve D was obtained after lapping and polishing. As was expected, both the magnitude and the slope of the curves were affected by the surface treatments. However, very little difference was observed in the slopes or the magnitudes of the curves in the saturation region. The greater magnitude of the saturation current in diode 17-D16 is explained, at least qualitatively, by the fact that it has the lower majority carrier concentration and, consequently, the higher minority carrier concentration of the two diodes.

If it is indeed true that the predominant contribution to the reverse current in the lower temperature region results from surface leakage, and at higher temperatures from the thermal generation of minority carriers, the different reverse current mechanisms should be manifest in the current-voltage profiles of the junctions in the two temperature regions. Figure 2 shows a log-log plot of the current-voltage characteristics of diode 17-D16 at 70° and at 140°K. The reverse characteristic of the plot at 70°K is seen to be ohmic, indicative of the predominance of surface leakage currents, whereas a degree of saturation is observed in the reverse characteristic at 140°K, which indicates the predominance of the thermal generation of minority carriers in the bulk material. The same effect was observed with diode 37-D11.

This research indicates that below a certain temperature ($\sim 110^\circ\text{K}$ for diode 17-D16, and $\sim 130^\circ\text{K}$ for diode 37-D11) surface leakage predominates the reverse current. At higher temperatures, saturation current is predominant. Furthermore, the temperature at which surface leakage predominates over saturation current and the magnitude of the surface current vary with surface treatment.

Manuscript received June 2, 1960; revised manuscript received Nov. 22, 1960. This paper was prepared for delivery before the Chicago Meeting, May 1-5, 1960. Research on this paper was supported jointly by the Electronics Components Lab., Wright Air Development Division and Battelle Memorial Institute.

Any discussion of this paper will appear in a Discussion Section to be published in the December 1961 JOURNAL.

REFERENCES

1. W. P. Allred and R. K. Willardson, *This Journal*, **107**, 52C (1960).
2. K. F. Hulme and J. B. Mullin, *Phil. Mag.*, **4**, 47 (1959).
3. B. R. Gossick, *Phys. Rev.*, **91**, 1012 (1953).
4. S. A. Lederhandler and L. J. Giacoletto, *Proc. IRE*, **43**, 477 (1955).
5. G. K. Wertheim, *Phys. Rev.*, **104**, 622 (1956).
6. I. M. Shive, "Semiconductor Devices," D. Van Nostrand Co., Princeton (1959).

Preparation of High-Purity Indium Arsenide

D. Effer

Research Department, Associated Electrical Industries (Manchester) Limited, Manchester, England

ABSTRACT

The purest indium arsenide so far reported has a carrier concentration of about $1.3 \cdot 10^{18}$ electrons/cm³ at room temperature. This is several times the intrinsic value and it has been suggested that the limiting impurity may be sulfur originating in the arsenic component. Arsenic has been prepared by the thermal decomposition of highly purified arsine gas and has been combined with samples of indium purified by a variety of processes. Mass spectrographic analysis of the resultant ingots showed in all cases a sulfur content less than 0.05 ppm. The purest sample had a Hall coefficient of 795 cm²/coulomb at 77°K, corresponding to an electron concentration of 8.10^{18} /cm³ while the Hall mobility was 75,700 cm²/v/sec. Analytical techniques failed to detect the prime source of the free electron concentration, but it is concluded that sulfur is not the dominant impurity in these samples.

Indium arsenide has been prepared by various workers (1, 2) from highly purified indium and arsenic. Methods of purification of these elements have varied considerably, but an apparent limit has been reached in the purity of the indium arsenide produced. Uncompensated material containing less than 10^{18} carriers cm⁻³ has not been reported, whereas the room temperature intrinsic concentration is probably 1.25×10^{18} (3). Extensive zone refining of very pure samples in this laboratory has produced, at the most, a 3 to 1 variation from front to back of the ingot. Due to its segregation coefficient of unity in indium arsenide (4), sulfur has been regarded as the probable limiting impurity. This element is found in combination with arsenic naturally in many of its ores, and it is due to the difficulty of removing its last traces that sulfur has been regarded as primarily associated with the arsenic component in indium arsenide.

This investigation is concerned with the preparation of sulfur-free arsenic and the properties and analysis of indium arsenide prepared from it. The indium samples used were purified by three methods: (a) zone refining, (b) vacuum baking at 800°C, and (c) electrolysis of indium amalgam.

Preparation of Pure Arsenic

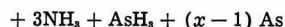
Two methods were investigated: (a) preparation and purification of arsine gas followed by thermal decomposition to give arsenic; (b) reduction of 99.999% As₂O₃ with pure hydrogen.

Preparation of arsenic from pure arsine.—Arsine gas offered a convenient method for the purification of arsenic, as possible gaseous impurity hydrides formed during the preparation may be removed selectively by treatment with liquid and solid reagents. Liquefaction and fractionation of arsine may also be carried out as a final purification step prior to thermal decomposition.

Of the possible gaseous hydrides that may be produced with arsine, H₂S, H₂Se, H₂Te, SiH₄, and the halogen hydrides may be absorbed rapidly in a solution of caustic alkali while SnH₄ may be decomposed by solid CaCl₂ and P₂O₅. SbH₃ and GeH₄, if

present, may be fractionated from liquid arsine (bp -62°C), their respective boiling points being -17° and -90°C.

Of the methods investigated for the preparation of arsine in reasonably large quantities, the liquid ammonia reaction of ammonium bromide on sodium arsenides (5) was found to yield the highest efficiencies, values in excess of 60% being obtained with reference to the weight of sodium charged. The reaction is illustrated as follows



where x is equal to 3, 5, or 7 representing polyarsenides that may be present if excess arsenic is used in the reaction.

The apparatus used for the preparation of the pure arsenic and final encapsulation with indium is shown in Fig. 1.

Commercial, anhydrous ammonia was condensed into vessel A over a few grams of sodium to dry the gas completely. The required amount of sodium and a slight excess of pure resublimed arsenic powder were placed in vessel B which was fitted with a mechanical stirrer working through a gas-tight stirring gland. The dry ammonia was condensed into B and maintained at -40° to -45°C by means of solid CO₂ additions to alcohol contained in a Dewar vessel. The sodium and arsenic reacted to form a brick-red colored arsenide which was constantly stirred while powdered NH₄Br was added from vessel D. This was connected to B by means of a short length of polythene tubing fitted with two

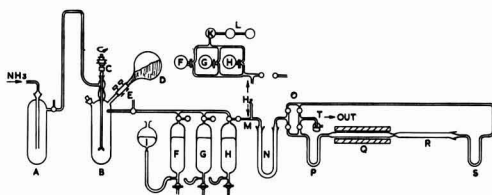


Fig. 1. Preparation of pure arsenic from arsine

screw clips an inch apart such that small amounts of NH_4Br could be added carefully. The evolved gases were collected over mercury in vessels F, G, and H in which pressures could be adjusted to atmospheric by means of levelling bulbs such as I. Each volume of gas collected was washed with water to remove NH_3 , and then washed with 33% caustic alkali at least three times in vessels K and L. These were fitted with sintered glass distribution filters in order to disperse and wash the gas thoroughly. The batch washing system was designed such that each volume of gas produced could be washed as many times as necessary to remove impurity hydrides, particularly H_2S . Due to the increasing acidic properties of the group H_2S , H_2Se , and H_2Te the removal of H_2S insures the absence of the other two. As each volume was washed, a further volume of fresh gas could be collected and another purified volume passed to the drying tube N containing fused CaCl_2 , gamma Al_2O_3 , and resublimed P_2O_5 . A carrier gas of electrolytic hydrogen which had been passed through a Deoxo catalytic purifier was led in at M prior to the drying tube.

The pure arsine was decomposed into arsenic and hydrogen by passing through a quartz tube heated to 600°C in furnace Q. Provision was made for the reversal of the gas flow through this tube by means of the system of taps O, and the tube was closed by U tubes P and S which could be cooled in liquid nitrogen to trap any undecomposed AsH_3 . On completion of the reaction the arsenic was sublimed completely into reaction tube R. A quartz boat coated with carbon obtained from the pyrolytic decomposition of pure acetone and containing the calculated (see Preparation of InAs Samples) amount of indium was inserted into reaction tube R and encapsulated together with the arsenic under vacuum.

This method of preparing arsine by means of liquid ammonia at -40° to -50°C reduces the concentration of SbH_3 (bp -17°C) in the purified gas. GeH_4 is thus the only impurity hydride that would be unaffected by the various reagents. Fractional distillation of liquid arsine should remove this impurity, but as Ge has the low segregation coefficient of 0.07 (2) in indium arsenide it is easily zoned out, and its presence was disregarded.

Preparation of arsenic by oxide reduction.—Pure arsenic was also prepared by a method initiated in this laboratory in which pure arsenic oxide is reduced with hydrogen (6, 7). The oxide used was a sample of 99.999% spectrographically standardized

material obtained from Johnson Matthey and Company Ltd. A current analysis report from the suppliers indicated the presence of 2 ppm Na, 1 ppm Ca, and less than 1 ppm each of Cu and Mg. Neutron activation analysis of the oxide showed that it contained 23.8 ppm sulfur (Table I).

A known weight of the oxide was charged into a quartz tube over which a furnace set at approximately 800°C could travel. The tube was provided with ground joints at each end and a reversing system for the hydrogen flow so that during the reduction process the furnace and hydrogen moved in opposite directions. The hydrogen, of electrolytic purity, was further purified by passing through a Deoxo catalytic purifier to remove oxygen, solid potash pellets to remove carbon dioxide, and γ alumina and P_2O_5 to remove water. A liquid air trap was provided as an additional precaution in the final stages of the process. The furnace was set to advance slowly over the oxide which readily vaporized in front of it, the arsenic formed by the reduction being evenly deposited behind. With careful adjustment of the furnace speed and hydrogen flow, water condensation could be kept to a minimum and the apparatus required little attention. The bulk of the oxide was normally reduced during the first pass after which the direction of the furnace and hydrogen flow were reversed to deposit the arsenic at the other end of the tube again. After six passes the furnace was cooled and the arsenic encapsulated under vacuum with a calculated quantity of indium as described above.

Sulfur estimation in arsenic.—Samples of arsenic produced by the two methods, along with a sample of arsenic oxide starting material, were analyzed for sulfur by the method of neutron activation at the Atomic Energy Research Establishment, Harwell. Identical samples and standards were irradiated at two positions in BEPO with a flux of approximately 10^{22} neutrons/cm²/sec and approximately 10^{21} neutrons/cm²/sec, respectively. In this way phosphorus activity produced from any phosphorus present in the arsenic by the slow neutron (n, γ) reaction and that produced from sulfur by the fast reaction (n, p) were obtained in different proportions in the two positions.

The results obtained are given in Table I.

As all the samples were irradiated and analyzed at the same time the results are strictly comparable and show that, for these samples, the arsine method is capable of producing arsenic with a sulfur con-

Table I. Results of analyses for sulfur

Sample	Sulfur ppm by wt	Sulfur ppm atomic	Remarks
Arsenic used in preparation of arsine	40	94	Sulfide estimation by chemical analysis
Pure arsenic prepared by arsine method	0.1 or less	0.2 or less	Neutron activation analysis
As_2O_3 used in preparation of arsenic by hydrogen reduction	23.8	56	Neutron activation analysis
Arsenic obtained by H_2 reduction of As_2O_3	1.2	2.8	Neutron activation analysis

centration at least a factor 10 times lower than the oxide reduction method. It must be borne in mind that the over-all purity of the arsenic obtained from the latter method is also dependent on the purity of the oxide starting material.

Preparation of Pure Indium

Three methods were investigated.

Zone refining.—A clean quartz boat 15 in. long was coated with pure carbon obtained from the flame of pure burning acetone and filled with 99.999% indium (Johnson Matthey and Company Ltd.). The indium was baked under vacuum at 800°C in a quartz tube for a few minutes to remove indium oxide and finally encapsulated under a pressure of a few centimeters of hydrogen. The ingot was zone refined for 30 passes using the reciprocating method. Zones were produced by strip heaters situated below the ingot so as to keep the top of the capsule relatively cool. The zone width was controlled by means of an arrangement of water-cooled phosphor-bronze fingers which gripped the tube round its circumference on either side of each zone.

Vacuum baking.—99.999% indium obtained from the Mining and Chemical Products Ltd., Alperion, Essex, was vacuum baked at 800°C for 48 hr in a quartz boat coated with pure carbon. The vacuum obtained was of the order of 10^{-3} mm Hg, and under these conditions very little indium vaporized out of the furnace.

Electrolysis of indium amalgam.—Indium may be obtained in a high state of purity by using the principle of the electrolysis of indium amalgam (8). In this process indium is deposited on a mercury cathode from an indium anode in an electrolyte of pure indium trichloride solution. The indium amalgam is electrolyzed as the anode in a similar solution, pure indium being deposited on a tantalum cathode.

The two operations were carried out in a single polythene rectangular cell fitted with a vertical partition extending downward to within $\frac{1}{2}$ in. of the bottom. Mercury, purified by Hulett's technique (9) and containing approximately 1% by weight of 99.999% In, was poured into the cell to a level of about 1 in. thus forming two separate half-cells. A pure solution of InCl_3 , slightly acidified with pure HCl was poured into each compartment. The InCl_3 had been prepared by the action of chlorine on pure indium and slowly sublimed several times before being dissolved in deionized water. Arrangements were made for the solution and amalgam in each cell to be mechanically stirred through dust-proof seals. An ingot of 99.999% indium was made the anode in the "impure" half-cell and a spiral of tantalum wire the cathode in the "pure" compartment. Passage of a controlled current dissolved the indium anode and its impurities in the electrolyte of the impure cell, but only indium and more "noble" metals were deposited at the mercury cathode (8). The amalgam formed was stirred into the pure cell compartment where theoretically only indium as the basest element goes into solution and is plated out. The cell was run for several hours initially to reach the stage of equilibrium where remaining impurities

Table II. Elements detected in indium (in ppm atomic) by mass spectrographic analysis

Element	Pure end zone refined ingot	Electrolyzed indium
Bi	0.3	<0.01
Pb	2	0.06
Tl	0.6	0.02
Hg	0.1	2
Pt	1	<0.03
Zn	2	0.3
Cu	10	1
Ni	2	0.5
Fe	1	0.05
Mn	0.1	<0.03
Cr	1	0.3
Ti	3	0.3
Ca	3	1
K	0.3	0.03
Cl	(4)	1
S	(5)	(5)
Si	10	2
Al	10	0.1
F	0.3	0.3
B	0.3	0.1

Figures given in parenthesis are taken from variable results indicating surface or segregated impurities.

in the electrolyte and mercury had plated out on to the cathode.

The indium deposited in "tree" form and was easily detached from the electrode and washed with deionized water. After drying under vacuum the samples were melted in a quartz boat coated with pure carbon. It was found advisable to bake the indium at 800°C under vacuum for a short time in order to remove traces of mercury present.

Mass spectrographic analysis of indium samples.—Mass spectrographic analysis of mercury cell indium was carried out in an A.E.I. M.S. 7 mass spectrometer for the analysis of solids, the results being shown in Table II together with those obtained on a sample of Johnson Matthey 99.999% In which had been zone refined as detailed above.

Detection limits for impurities not found are in the range 0.01–0.06 ppm atomic with the exception of the elements shown in Table III.

Preparation of InAs Samples

All indium samples were thoroughly degreased with acetone before being etched electrolytically as the anode in a very dilute solution of pure hydrochloric acid obtained by the isopiestic distillation of concentrated hydrochloric acid. After thorough washing in deionized water the indium was melted in a boat and baked at 800°C under vacuum for several minutes to remove indium oxide and leave a mirror surface melt. On cooling, the boat and contents were immediately inserted into the reaction tube containing arsenic as described above. Sufficient excess arsenic was used to produce an equilibrium vapor pres-

Table III. Detection limits for impurities not detected (ppm atomic)

Au	0.1	Cd	0.2	Sr	0.1	All other elements
Ta	1	Pd	0.1	Ge	0.1	0.01–0.06
I	0.1	Ru	0.2	Mg	2	
Te	0.3	Mo	0.3	Be	0.2	

Table IV. Electrical properties of indium arsenide prepared from variously purified materials

Sample	77°K			300°K				Details of sample
	R _H	σ	Rσ	R _H	σ	Rσ		
D20	795	95.5	75,700	604	37.5	22,600	AsH ₃ arsenic	Hg cell In
D21	465	133	61,900	426	54	23,000	AsH ₃ arsenic	Tadanac Research grade In
D22	441	124.4	54,900	357	61.1	21,800	AsH ₃ arsenic	Pure end zone refined In ingot
D23	484	130.1	63,000	399	62.9	25,100	AsH ₃ arsenic	M.C.P. In Vac. baked 800°C for 24 hr
D24	242	200	48,400	226	111	25,100	AsH ₃ arsenic	M.C.P. In as received
G2	341	134	45,600	287	79.3	22,800	As ₂ O ₃ arsenic	J.M. In Vac. baked 750°C for 60 hr
G3	514	96.8	49,800	412	56	23,000	As ₂ O ₃ arsenic	M.C.P. In Vac. baked 750°C for 48 hr
G4	440	110	48,400	347	69	23,900	As ₂ O ₃ arsenic	M.C.P. In Vac. baked 800°C for 24 hr

R_H = cm²/coulomb.
 σ = (ohm cm)⁻¹.
 J.M. = Johnson Matthey and Co. Ltd.
 M.C.P. = Mining and Chemical Products Ltd.

sure of 1/3 of an atmosphere over the molten indium arsenide. Reaction and zone refining was effected in an R.F. coil with two side furnaces set at 580°C. After reaction each ingot was zone refined three times at a speed of 4 cm/hr.

Polycrystalline ingots were formed using arsenic obtained via arsine and indium purified by each of the methods outlined above. To compare with the sample containing vacuum baked indium (D23) a further ingot was made from the same sample of indium before baking. Included also is an ingot containing a Special Research grade indium from The Consolidated Mining and Smelting Company of Canada (Tadanac).

Samples made with arsenic obtained by oxide reduction were all prepared with indium of 99.999% purity which had been baked out at approximately 800°C under vacuum before being introduced into the reaction tube.

Electrical Measurements.—Measurements of Hall coefficient and electrical conductivity were carried

out on all samples at room temperature and at 77°K. Results including values of the Hall mobility are given in Table IV.

Mass spectrographic analysis of InAs samples.—The analyses were carried out in an A.E.I. M.S. 7 mass spectrometer for the analysis of solids. Results are shown in Table V.

The detection limits for elements not detected are in the range 0.001 to 0.06 ppm with the exception of the following: Ta 1; Pr 0.1; Ba 0.1; Te 0.3; Sn 0.3; Cd 0.3; Ge 0.1. The elements carbon and oxygen are not normally reported, the former because of hydrocarbons present from the oil diffusion pumps. However, the total mass 32 line which includes oxygen and sulfur gave a total of less than 0.1 ppm for all samples.

Discussion and Conclusion

From the electrical properties at low temperatures given in Table IV it can be seen that for a given Hall coefficient samples made from arsenic prepared by the arsine method show a higher mobility than samples made by reducing arsenic oxide. This would imply a greater degree of purity in the arsenic prepared by the former method, and so far as sulfur is concerned this is consistent with the results of neutron activation analysis.

Comparison of ingots D24, D23, and D20 shows a marked improvement in the electrical properties with improvement in the indium. Mass spectrometric analysis of indium shows that the electrolysis method is capable of producing much purer material than zone refining, but even so significant amounts of impurities remain. These appear to have been reduced by zone refining during the preparation of the final ingot of indium arsenide, but an improvement in indium purity is nevertheless required before intrinsic material can be obtained.

The purity of the arsenic is, as yet, unknown, except for sulfur. It is reasonable to expect, however, that both selenium and tellurium are at a concentra-

Table V. Mass spectrographic analysis of InAs samples
(Elements detected ppm atomic)

Element	D20	D21	D22	D23	D24	G3
Fe	0.1	0.1	0.03	0.1	0.1	0.1
Mn	0.01	0.01	0.03	0.01	0.01	0.01
Cu	<0.005	<0.005	<0.005	<0.005	<0.005	<0.005
Ti	0.01	0.01	0.005	<0.01	<0.01	0.01
Ca	0.03	<0.01	0.1	<0.01	0.03	<0.01
K	0.003	<0.003	<0.005	<0.003	<0.003	<0.003
Cl	0.2	0.2	1	0.2	0.2	0.2
S	<0.05	<0.05	<0.05	<0.05	<0.05	<0.05
P	<0.003	<0.003	<0.003	<0.003	<0.003	0.01
Se	<0.06	<0.06	<0.06	<0.06	<0.06	<0.06
Si	0.06	<0.01	0.6	0.06	0.06	0.06
Al	<0.003	0.01	0.01	<0.003	<0.003	0.01
B	<0.002	<0.002	0.002	<0.002	<0.002	<0.002
F	0.003	0.003	0.01	0.003	0.003	0.003
Zn	<0.005	<0.005	0.01	<0.005	<0.005	<0.005
Cr	<0.01	<0.01	0.01	<0.01	<0.01	<0.01

tion of less than 0.1 ppm since they are more easily removed than sulfur in the purification procedure.

The results of the mass spectrometer analysis disclose the surprising fact that the minimum donor impurity content, as estimated from the room temperature values of the Hall coefficient, is greater than the sum total of the donor impurities found, excluding tellurium. This is most marked in the case of D24 where the Hall coefficient indicates a minimum donor impurity content of 0.7 ppm. Tellurium, having the high mass spectrometer detection limit of 0.3 ppm is unlikely to be a major impurity as it has a segregation coefficient of 0.44 (4) in indium arsenide. Selenium is difficult to remove by zone refining owing to its segregation coefficient of 0.93 and yet is detected at a level of less than 0.06 ppm in the final ingot. These factors suggest that the tellurium level in the zoned ingot is probably less than 0.1 ppm.

Iron (0.1 ppm) and chlorine (0.2 ppm) are the most noticeable impurities detected by the mass spectrometer. The effect of both these elements is uncertain although it has been shown in this laboratory that very high concentrations of chlorine can be tolerated in indium arsenide with little or no change in the measured electrical properties (10, 11, 12).

The analysis of all samples of indium arsenide prepared indicates a sulfur concentration of less than 0.05 ppm sulfur. The accuracy of this value has been verified by means of standard samples of indium arsenide containing known amounts of sulfur. The evidence thus suggests that sulfur is not the dominant impurity in indium arsenide since even the purest sample contains 0.3 ppm of n-type impurities as determined by electrical measurement.

The electron concentration in the purest ingot (D20) as calculated from the value of the Hall coefficient at 300°K is approximately $10^{16}/\text{cm}^3$, and this exceeds the calculated intrinsic electron concentration by about $8.10^{16}/\text{cm}^3$. A donor concentration of this order must therefore exist in this ingot, but analytical methods have so far been unable to identify the nature of this donor.

A general analysis of this kind using the mass spectrometer will involve appreciable tolerances in the detection limits quoted, and these can only be

made more specific by preparing standard comparison samples for each element of major interest. Nevertheless it appears that all ingots are substantially uncompensated, and there is no evidence for a large reservoir of segregated donor impurities as suggested by Dixon, *et al.* (13). Further progress will depend on improving the sensitivity of the mass spectrometer and standardizing the instrument for the important donor elements. Consideration should also be given to the influence of stoichiometric unbalance on the properties of indium arsenide.

Acknowledgments

The author wishes to thank Mr. R. P. Chasmar for helpful discussion, Mr. R. Brown for the mass spectrographic analysis, and Messrs. G. R. Antell, W. R. McEwan and E. Durham for their friendly cooperation in making available many of the experimental results. He also wishes to thank Dr. R. Gibbons of the A.E.R.E., Harwell, for his activation analysis results.

Thanks are due to Sir Willis Jackson, F.R.S., Director of Research and Education, Associated Electrical Industries (Manchester) Ltd., for permission to publish.

Manuscript received Oct. 28, 1960; revised manuscript received Nov. 25, 1960.

Any discussion of this paper will appear in a Discussion Section to be published in the December 1961 JOURNAL.

REFERENCES

1. T. C. Harman, H. L. Goering, and A. C. Beer, *Phys. Rev.*, **104**, 1562 (1956).
2. R. H. Harada and A. J. Strauss, *J. Appl. Phys.*, **30**, 121 (1959).
3. O. G. Folberth, O. Madelung, and H. Weiss, *Z. Naturf.*, **9a**, 11, 954 (1954).
4. E. Schillman, *Z. Naturforsch.*, **11a**, 6, 463 (1956).
5. W. C. Johnson and A. Pechukas, *J. Am. Chem. Soc.*, **59**, 2065 (1937).
6. G. R. Antell, Unpublished report.
7. G. R. Antell, R. P. Chasmar, C. H. Champness, and E. Cohen, Paper presented at British Phys. Soc. Meeting on Semiconductors, April 1956.
8. A. Gaumann, *Schweiz. Arch. angew. Wiss.*, **21**, 10, 337 (1955).
9. G. A. Hulett, *Phys. Rev.*, **33**, 307 (1911).
10. D. Effer and G. R. Antell, *This Journal*, **107**, 252 (1960).
11. G. R. Antell and D. Effer, *ibid.*, **106**, 509 (1959).
12. G. R. Antell, *J. Appl. Phys.*, **31**, 1686 (1960).
13. J. R. Dixon and D. P. Enright, *ibid.*, **30**, 753 (1959).

December 1961 Discussion Section

A Discussion Section, covering papers published in the January-June 1961 JOURNALS, is scheduled for publication in the December 1961 issue. Any discussion which did not reach the Editor in time for the June 1961 Discussion Section will be included in the December 1961 issue.

Those who plan to contribute remarks for this Discussion Section should submit their comments or questions in triplicate to the Managing Editor of the JOURNAL, 1860 Broadway, New York 23, N. Y., *not later than September 1, 1961*. All discussion will be forwarded to the author(s) for reply before being printed in the JOURNAL.

Use of Hall Measurements in Evaluating Polycrystalline Silicon

P. J. Olshefski,¹ D. J. Shombert, and I. R. Weingarten²

Research Laboratories, Merck Sharp & Dohme, Division of Merck & Company, Inc., Rahway, New Jersey

ABSTRACT

Hall measurements at room temperature have been used to determine the average net carrier density in polycrystalline silicon. The method does not require cutting of samples and destruction of the rods. Current contacts are made to the ends of a rod with strips of metal foil; Hall contacts are made with two titanium blades which close on the rod. Hall measurements made this way on single-crystal zone-refined rods agree with measurements on samples cut from the rods in the conventional manner. The average carrier densities measured in the polycrystalline rods have been correlated with the resistivities of these same rods after one, two, three floating zone passes.

Measurement of Whole Ingots

The conventional bridge-shaped samples used for Hall measurements require that an ingot be sawed up and thus partially destroyed. It would obviously be advantageous to make Hall measurements on an ingot of semiconductor material without cutting it up (1). This was done with the apparatus³ shown in Fig. 1. The holder was made of Lucite and was clamped between the poles of a Varian 4-in. electromagnet. The sample (which was a round ingot) was placed in the V-shaped blocks of Lucite and rested on a knife-edge titanium blade which formed one Hall contact. A pivoted Lucite arm carrying the other titanium blade Hall contact was placed on top of the sample and was held down with a nonmagnetic (lead) weight. The pivoted arm could be moved laterally by an adjusting screw to align the top blade accurately above the lower blade; this adjustment eliminated the IR voltage between the Hall contacts, so that the measured Hall voltage was zero when the magnetic field was zero. Current contacts to the sample were made on the ends of the ingot either by ultrasonic soldering with indium, by

copper plating, or (most conveniently) by clamping strips of metal foil around the circumference. Measurements were always made several inches or more from the current contacts so that the effective ratio of length to width was greater than three (2). The Hall voltage was measured either with an electrometer or, preferably, with the circuit described by Dauphinee (3). The latter is an a-c method. Magnetic fields up to 10,000 gauss and currents up to several milliamperes were used.

To compute the Hall coefficient with this geometry, imagine that the sample consists of a thin slice instead of a round rod. This slice is shown as the shaded portion in Fig. 2. If the thickness of this slice and the current flowing through it were known, the Hall coefficient could be computed. The current in the shaded slice, however, is simply the total current multiplied by the ratio of the cross-sectional areas of the slice to that of the whole rod:

$$\begin{aligned} \text{area of slice} &= b d \\ \text{area of rod} &= \frac{1}{4} \pi d^2 \end{aligned}$$

$$\text{Current through slice} = (4b/\pi d) I$$

where b is the thickness of the shaded slice, d the diameter of rod, and I the total sample current. We may now disregard the unshaded portions of the rod and think of the sample as a long, thin slice of thickness b , carrying current $(4b/\pi d) I$. The Hall coefficient is then:

$$R = \frac{10^8 b V_H}{\left(\frac{4b}{\pi d}\right) I H} = \frac{10^8 \pi d V_H}{4 I H}$$

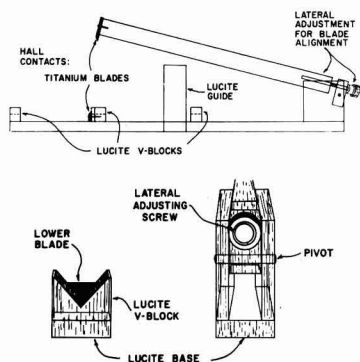
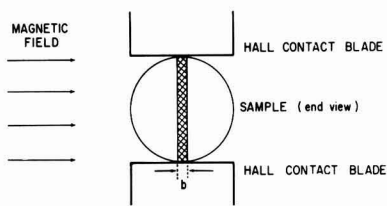


Fig. 1. Two views of the apparatus: top, side view; bottom, end views.



(Current flow is perpendicular to the plane of the page.)

Fig. 2. Sample consisting of a thin slice instead of a round rod.

Table I. Agreement of Hall and resistivity measurements on bridge-shaped samples cut from the same ingots

Sample No.	Type	Average net impurity concentration determined by Hall measurement on whole rod	Net impurity concentration determined by Hall measurement on a bridge-shaped sample from rod
1	N	1.4×10^{18}	1.6×10^{18}
2	N	1.9×10^{18}	2.0×10^{18}
3	N	2.8×10^{18}	5.0×10^{18}
4	N	3.7×10^{18}	4.2×10^{18}
5	N	3.2×10^{18}	3.1×10^{18}
6	N	4.1×10^{18}	4.3×10^{18}
7	P	3×10^{18}	4.0×10^{18}
8	P	3×10^{18}	4.3×10^{18}
9	N	6.1×10^{14}	6.7×10^{14}

where V_H is the Hall voltage in volts, I the total sample current in amperes, H the magnetic field in gauss, and d the diameter of the sample in centimeters. Hall coefficients measured in this way on round multicrystal, zone-refined ingots agreed with Hall and resistivity measurements on bridge-shaped samples cut from the same ingots. This agreement is shown in Table I; the values for the whole ingots are average values, so that the cut samples could have been taken from regions locally different from the average. The agreement is good when this is considered.

Ingots with other cross sections, (e.g., square, hexagonal), can be measured if a suitable geometrical correction is made.

Application to Polycrystalline Materials

Polycrystalline materials present problems in resistivity measurement because the resistance across grain boundaries may be much larger than the resistance of the grains themselves. Resistivity measurements with d.c. or low-frequency a.c. usually are not meaningful. Resistivity can be measured, however, by high-frequency techniques (4, 5).

The Hall measurement can be shown to be valid for polycrystalline materials because the total voltage between the Hall probes is the algebraic sum of the Hall voltages across the individual grains. Consider a sample composed of two grains α and β , of resistance ρ_A and ρ_B , as in Fig. 3. Let each grain be 1 cm thick for convenience, and let their widths be A cm and B cm. If the applied electric field is E v/cm length of material, then the current in each grain is:

$$I_A = \frac{EA}{\rho_A} = EA n_A e \mu$$

$$I_B = \frac{EB}{\rho_B} = EB n_B e \mu$$

It is assumed here that the mobility does not vary

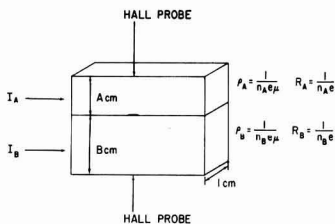


Fig. 3. Sample composed of two grains

substantially with impurity concentration; this is certainly true for n-type silicon below about $10^{18}/\text{cm}^3$.

The Hall voltage across each grain is:

$$V_{HA} = \frac{R_A I_A H}{10^8} = \frac{A H \mu E}{10^8}$$

$$V_{HB} = \frac{R_B I_B H}{10^8} = \frac{B H \mu E}{10^8}$$

and the observed voltage between the Hall probes is:

$$V_H = V_{HA} + V_{HB} = \frac{H \mu E}{10^8} (A + B)$$

The observed sample current is: $I = I_A + I_B = \mu e E (A n_A + B n_B)$ From the observed current and Hall voltage, we would compute a Hall coefficient for the sample of:

$$R = \frac{10^8 E_H}{HI} = \frac{(A + B)}{e(A n_A + B n_B)}$$

and the average net free carrier density computed from these observations would be:

$$n = \frac{1}{R e} = \frac{A n_A + B n_B}{A + B}$$

It can be seen that this is in fact the true average carrier density in the sample.

Thus the Hall measurement has given us a value for the carrier density in a polycrystalline sample which is exactly equal to the carrier density that would result if the sample were completely homogenized. The argument can be extended to include many grains, in both series and parallel combinations. The Hall measurement is valid for d.c. and for low-frequency a.c. (3), and this is sometimes more convenient than the R-F methods. It is also convenient because it is applicable to ingots of any cross-sectional shape.

Resistivity measurements were made on four polycrystalline silicon rods by the contactless R-F method (4). The carrier densities computed from these were then compared with carrier densities obtained from d-c Hall measurements on the same rods. The agreement was well within the uniformity of the rods.

Hall measurements on whole polycrystalline rods were usually taken at four or five places along the length of a rod, and a slight rotation of the rod about the long axis was made between measurements. In this way a good average carrier density was obtained for a rod. The observed Hall coefficient was unaffected by: (a) sample current, from 5 μA to 5 ma; (b) magnetic field strength, up to at least 5000 gauss; (c) nature of the current (end) contacts, metal foil, copper plated, or soldered; (d) rotation of the rod about the long axis; (e) small longitudinal movements of the Hall electrodes at a given spot on the rod; and (f) surface treatment, sandblasted, etched, or natural.

Evaluation of Polycrystalline Rods for Zone Refining

Hall measurements were then made on several hundred standard production rods prior to zone re-

fining. The purpose of this was (a) to predict the resistivity of a rod after a given number of floating zone passes, and (b) to predict how many passes would be required to produce a single-crystal rod with resistivity in a specified range. The advantage of being able to make these predictions is obvious: material can be programmed before zone refining to obtain maximum yield of single-crystal ingots in a desired resistivity range.

Some results are shown in Fig. 4. The resistivity of the ingot after three floating zone passes is plotted against the average net free carrier density before zone refining. The length of each line corresponds to the resistivity variations in an ingot from seed end to cross end. A good correlation was expected because low-temperature measurements on our silicon by Bate (6) at Battelle had shown that the background boron concentration was always negligible, even in rods which contained a high concentration of donors.

Discussion of Results

From the graph of Fig. 4 it can be seen that the scatter of points is much greater at low concentrations of donors than at high concentrations. This is to be expected, because the impurities introduced by handling do not show up in Hall measurements, but do show up in the silicon after zone refining. These impurities are relatively unimportant when the natural donor level is 10^{15} cm⁻³, but they become significant when the natural donor level is 10^{14} or less. Rods were handled carefully with polyethylene foil during measurements, and the ends were broken off before zone refining to reduce the handling impurities to a minimum.

The scatter at low concentrations is large enough to make accurate prediction difficult on zone-refining any single rod. If a large group of rods were taken, however, the scatter would average out. The Hall measurement therefore represents a means of grading polycrystalline silicon for melting and crystal-pulling to an accurately predicted resistivity.

Some correlation was obtained between the resistivity after zone refining and the particular zone refiner which was used. Rods from the same zone refiner showed much less scatter in final resistivity for a given initial carrier concentration. This is not sur-

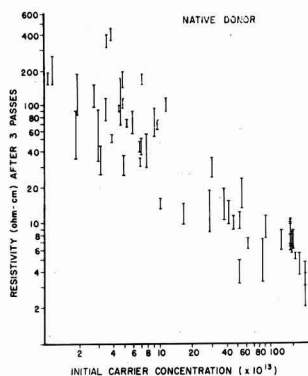


Fig. 4. Some results of Hall measurements

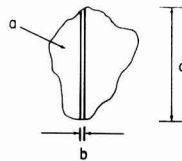


Fig. 5. Geometry correction in cross-sectional shape

prising, since the pressure in different refiners could be different, or the impurities contributed by the refiners themselves could vary from one to another.

In fact, if all the points in Figure 4 fell on a straight line, it would mean that the impurities in all of the rods zone refined out in exactly the same manner. In other words, the same donors would have to be present in the same proportions; in addition, all zone refiners would have to be identical in pressure, cleanliness, etc. Both of these hypotheses are clearly highly improbable. For large numbers of samples, all of these variables are averaged out, and the Hall measurement is useful as a guide to zone refining for maximum yield in a given resistivity range or to melting and pulling single crystals of a given resistivity.

Extension of the Method to Rods of Any Shape

The method has been extended to irregularly shaped ingots of polycrystalline materials, such as gallium arsenide, on which resistivity measurements are meaningless. The geometry correction can be made for any cross-sectional shape, as in Fig. 5. Let the distance between the Hall contacts be d , and let the cross-sectional area be a . Imagine a slice of thickness b ; it has area $b d$. The current in this imaginary slice is then $(b d/a) I$ where I is the total current. The Hall voltage observed is

$$V_H = \frac{R \left(\frac{b d}{a} \right) I H}{10^8 b} = \frac{R I H}{10^8} \left(\frac{d}{a} \right)$$

The thickness of the imaginary slice cancels out, as it does in the case of round rods. For the geometry correction we need only the cross-sectional area and the distance between the Hall contacts. The latter can be measured with calipers for any ingot. The area can be obtained from the weight, density, and length; by measuring the volume (by displacement of water in a graduated cylinder) and dividing by the length; by estimation from caliper measurements, etc.

Carrier concentrations in boat-zoned polycrystalline material can be obtained to one significant figure in this manner without destruction of the ingots.

Manuscript received April 26, 1960; revised manuscript received Dec. 2, 1960. This paper was prepared for delivery before the Columbus Meeting, Oct. 18-22, 1959.

Any discussion of this paper will appear in a Discussion Section to be published in the December 1961 JOURNAL.

REFERENCES

1. Duga, Willardson, and Beer, *Bull. Phys. Soc.*, Ser. II, 1, 332 (1956).
2. I. Isenberg, B. R. Russell, and R. F. Greene, *Rev. Sci. Instruments*, 19, 685 (Oct. 1948).
3. T. M. Dauphinee and E. Mooser, *ibid.*, 26, 660 (July

- 1955); T. M. Dauphinee and H. Preston-Thomas, *J. Sci. Instruments*, **35**, 21 (Jan. 1958).
4. I. R. Weingarten and M. Rothberg, "R-F Carrier and Capacitive Coupling Procedure for Resistivity and Lifetime Measurements on Silicon," paper presented at the Columbus Meeting of the Electrochemical Society, Oct. 21, 1959.
5. "Semiconducting Materials," H. K. Henisch-Butter-

- worth, Editor, 1951, see: E. J. Verwey, pp. 157-160; J. Volger, pp. 166-168; P. H. Miller, pp. 172-175; G. Busch, J. Wieland, and H. Zoller, pp. 190-195.
6. R. T. Bate, I. R. Weingarten, and D. J. Shombert, "Determination and Identification of Impurities in Silicon from Low-Temperature Hall Data," paper presented at the Columbus Meeting of the Electrochemical Society, Oct. 21, 1959.

Chemical Etching of Silicon

III. A Temperature Study in the Acid System

B. Schwartz¹ and H. Robbins

Semiconductor Division, Hughes Aircraft Company, Newport Beach, California

ABSTRACT

The etch rate of silicon in solutions of various compositions selected from the system HF, HNO₃, H₂O, and HC₂H₃O₂ has been investigated over the temperature range 0° to 50°C. The activation energy of the etching process has been found to be different in the different composition regions. In the high HNO₃ region values of about 4 kcal/mole have been observed and interpreted as characteristic of a diffusion governed reaction. In compositions containing H₂O or HC₂H₃O₂ diluents the activation energy increases, and two values are found. In the high HF region two values are also observed, one in the range of 10-14 kcal/mole, and the other in the range of about 20 kcal/mole. The significance of the various values of the activation energy is discussed.

The dissolution of silicon in solutions of nitric acid and hydrofluoric acid is a complicated reaction. The authors have studied the kinetics of this reaction at constant temperature (1, 2), and by plotting the etch rates as a function of the composition of the etchant, it was possible to propose qualitative explanations of the etching behavior of the system. However, it was not possible to fit the rate data into mathematical relationships that were valid over even limited ranges of composition of etchant. In part this was the result of the heterogeneous nature of the reaction, which precluded knowledge of the actual concentrations of reactants and the temperature that prevailed at the reacting surface. The kinetics are further obscured by the complicated chemistry of nitrogen which, on the one hand, provides several parallel paths for the oxidation reaction to proceed and, on the other hand, is subject to autocatalysis. In view of these complications, it was deemed desirable to subject the reaction to further study and, for this purpose, the authors have elected to investigate the rate-temperature dependence of the reaction. The compositions of the etching solutions selected for study are shown in Fig. 1. Four compositions were selected from the high nitric acid region where HF is known to be the kinetically important reagent. Three compositions were selected in the high HF region where nitric acid concentration is known to be rate determining. Etchants were also selected in the areas rich in diluent where the curvature of the constant etch rate contours was indicative of a change in the rate-determining process. No etch-

ants were selected from the region of the maximum etch rate because the rates there were much too rapid to permit the accuracy required for the determination of an "activation energy."

Experimental Procedure

The specimens to be etched were (100), (111), and (110) oriented n-type silicon dice of approximately 3 ohm-cm resistivity, and 1/8 x 1/8 x 0.025 in. in size.

The etching was performed in a cylindrical platinum beaker, 1 1/8 in. in diameter and 2 1/4 in. deep.

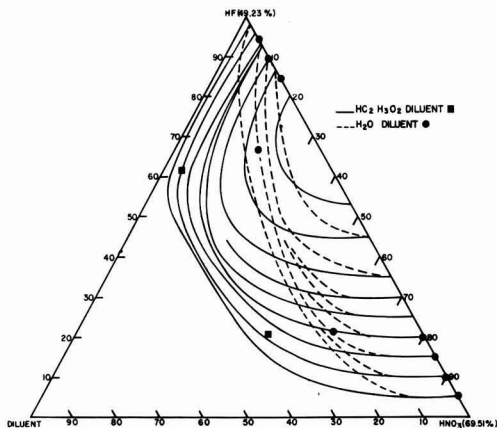


Fig. 1. Constant etch rate contours in the systems HF-HNO₃-H₂O and HF-HNO₃-H₂O-HC₂H₃O₂ obtained at 25°C. The indicated compositions were selected for this temperature study.

¹ Present address: Bell Telephone Laboratories, Inc., Murray Hill, New Jersey.

Twenty cubic centimeters of etchant were placed in the beaker, which was then stoppered and placed in a constant temperature bath at the desired temperature. The solution temperature was controlled to within $\pm 0.02^\circ\text{C}$. Three dice, one from each of the crystal orientations mentioned above, were marked, measured with a micrometer, placed in a small basket made from open mesh platinum, and etched together. Agitation was provided by swirling the basket through the solution with a combined rotational and vertical motion. At the termination of etching the basket was rapidly transferred to a beaker of clean water, washed, rinsed in acetone, and dried. The etch rate was calculated from the observed loss in thickness, expressed in mils, divided by the etching time in minutes. It had been previously established that the etch rates so calculated are independent of the etching time, *i.e.*, that the decrement in thickness is directly proportional to the etching time.

The etching solutions were put together by weighing out, to ± 0.01 g, the calculated amounts of HF, HNO_3 , H_2O , and $\text{HC}_2\text{H}_3\text{O}_2$. A sufficient amount of solution was made up at one time to complete the full range of temperature experiments for any one given composition. Each test solution was discarded immediately after use, so that every experiment was run with a fresh solution. Two sets of experiments were performed with each etchant. In the first set the etch rates were determined for temperatures taken at 5° intervals between 0° and 50°C . The second set was run in the same manner except that to each solution was added 0.1 g of sodium nitrite immediately before starting to etch. In the ensuing discussion we shall refer to these latter etches as "externally catalyzed."

Experimental Results

The data obtained by the above discussed procedure are plotted in Fig. 2 to 7.

In the high nitric acid region (Fig. 2 and 3) the plots are straight lines. The curves corresponding to the externally catalyzed and nonexternally catalyzed etch rates coincide. We use the term externally catalyzed to emphasize that all etch rates are catalyzed, since the reaction is autocatalytic. The curves corresponding to the etch rates of the dif-

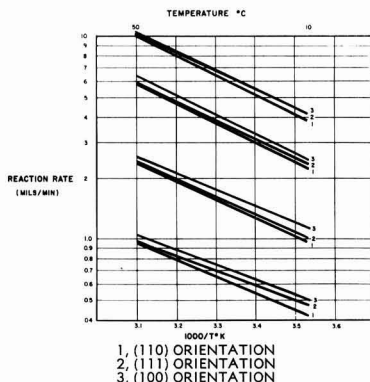


Fig. 3. Influence of surface orientation on the etch rate of silicon in the high HNO_3 region with no added diluent.

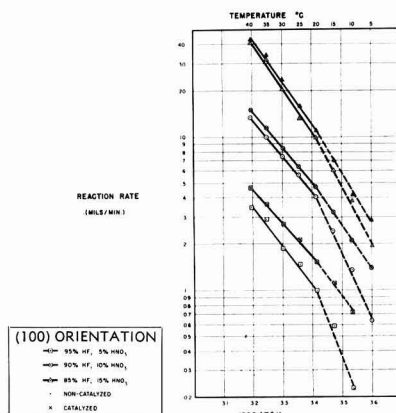


Fig. 4. Plot of the log etch rate vs. $1/T$ in the high HF region with no added diluent.

ferently oriented specimens also practically coincide, although there is an indication, as shown by the consistency in the ordering of the curves of Fig. 3, that the orientation might have a slight effect on the etch rates.

In the high HF region (Fig. 4) the situation is considerably more complex. Within the experimental error the various crystal orientations all etched at the same rate under the same conditions so that only one set of curves will suffice to represent the data. It is seen that the rate data corresponding to the externally catalyzed etches lie on an approximately straight line of steeper slope than the curves corresponding to the high nitric acid etches. The nonexternally catalyzed etches yield data that seem to lie on two intersecting straight lines, although it is not certain that there actually exists a sharp point of intersection as drawn, rather than a curved transition region. The high-temperature portions of the curves run parallel with those of the externally catalyzed etches, whereas the low-temperature branches are considerably steeper.

Two sets of data were taken in the water diluted region (Fig. 5). One is in the high nitric acid region, and the other is in the high HF region. Only

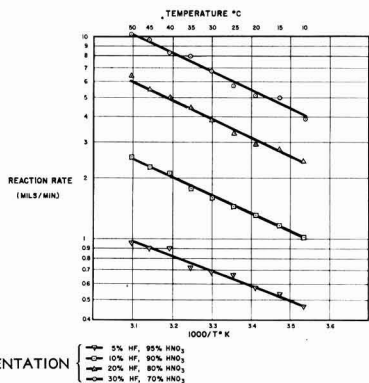


Fig. 2. Plot of log etch rate vs. $1/T$ in the high HNO_3 region with no added diluent.

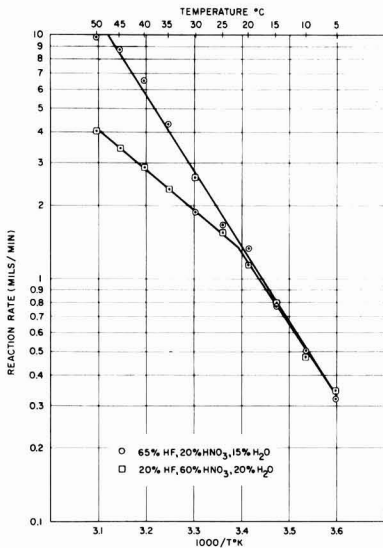


Fig. 5. Plot of the log etch rate vs. $1/T$ in the two water diluted etches.

the externally catalyzed system could be plotted. Without adding catalyst, the data were much too erratic to be meaningful. The curve in the high nitric acid region consists of two branches, a steep low-temperature branch, and a less steep high-temperature branch. The plot in the high HF region consists of a single straight line of slope comparable with that obtained in the low diluent high HF region.

The plots for the systems containing large amounts of acetic acid as diluent are shown in Fig. 6 and 7. The results are comparable with those obtained in the water diluted systems, with the exception that the nonexternally catalyzed etch rates can be plotted in the nitric acid rich compositions. The non-externally catalyzed data are also shown in the HF rich region, but because of the large amount of scatter, a curve is not drawn.

Activation Energy of a Heterogeneous Reaction

In a chemical reaction



the rate of the reaction may be formulated in terms of the mass action law as follows:

$$\text{Rate} = k(A)^a(B)^b(C)^c \dots \quad [2]$$

The specific rate constant k is a function of temperature, and from the variation of k with temperature, the activation energy for the process can be determined. Thus, the activation energy is related to the specific rate constant by the Arrhenius expression

$$d \ln k/dT = E_a/RT^2 \quad [3]$$

It often happens that the reaction is too complex to be formulated in terms of the mass action law, and a value of k cannot be extracted conveniently from the kinetic data. In such circumstances an "activa-

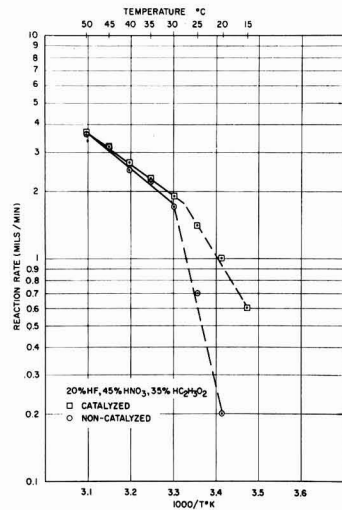


Fig. 6. Plot of the log etch rate vs. $1/T$ in the high HNO_3 region with acetic acid diluent.

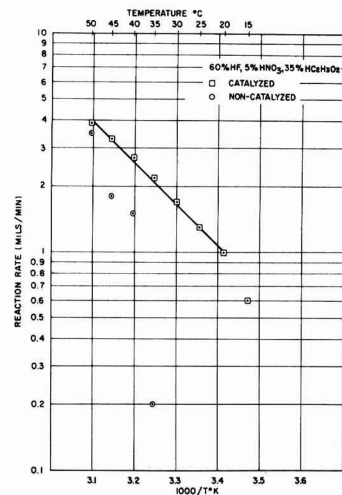


Fig. 7. Plot of the log etch rate vs. $1/T$ in the high HF region with acetic acid diluent.

tion energy" can still be obtained from a plot of the log of the reaction rate itself in place of the specific rate constant, vs. $1/T$. This practice may be justified by rewriting Eq. [2] as follows:

$$\text{Rate} = k f(A, B, C, \dots) \quad [4]$$

The rate is thus seen to be proportional to the specific rate constant if the unknown function of the concentration of the reactants is kept constant, i.e., if the composition of the solution is kept constant. However, such a procedure must be applied with extreme caution, for one can never be quite sure that the unknown function of concentration is truly constant. This is especially true in the case of heterogeneous reactions such as the one under consideration here, because the concentrations of reactants determining the kinetics are those exist-

ing at the solution-solid interface, and not the concentrations existing in the bulk solution. This restriction has been generally ignored in the study of the kinetics of the dissolution of semiconductors. Such a practice can be justified in the case of a very slow reaction where the surface concentration will be essentially equal to the bulk solution concentration, and in the case of a very fast reaction where the surface concentration is reduced practically to zero. However, where these conditions are not met, consideration must be given to the actual surface concentrations rather than to the bulk concentrations. In the ensuing discussion, we shall attempt to interpret our results in the light of the above restrictions.

Activation energy in the high HNO₃ region.—Let us now consider the results in the high HNO₃ region (see Fig. 2). The plots are parallel straight lines whose slopes correspond to an activation energy of about 4 kcal/mole. The temperature dependence is weak, and typical of a diffusion governed reaction (3). Since it is known from previous studies of the system (1, 2) that only HF plays a kinetically important role in this composition region, one may conclude that it is the diffusion of this reagent to the silicon surface that is rate determining. The authors have been led previously to the same conclusion by other considerations, namely, that the etch rates in this region of compositions are practically independent of the resistivity, type, crystal orientation (see Fig. 3), and the addition or accumulation of catalyst in the reacting solution. The work of Klein and D'Stefan also confirms this conclusion (4).

The model for the reaction mechanism may be represented as in Fig. 8. The concentration of HF at the silicon surface, C_s , is assumed to be vanishingly small, and the concentration in the bulk solution, C_b , remains constant as the temperature is varied. We are here neglecting the change in the density of the solution with temperature, the temperature gradient across the boundary layer resulting from the dissipation of the heat of the reaction, and possible changes in the thickness of the boundary layer resulting from such factors as a change in the temperature. This is done so that an initial model can be drawn that enables one to attempt an analysis of the mechanism. The concentration

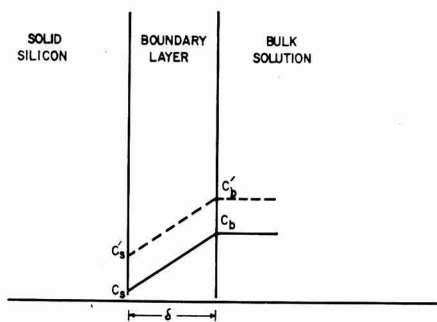


Fig. 8. Simplified diffusion model for the rate-limiting process in the high HNO₃ region.

gradient of HF across the boundary layer is therefore constant, since C_b and C_s are fixed. Thus, changes in the flow rate of HF can be produced only by changes in the value of the diffusion coefficient of HF with temperature, and the activation energy we have measured is that of the diffusion process as it is reflected in the value of D_{HF} at different temperatures.

Effect of diluent on the activation energy.—Let us now examine the results in the adjacent area of compositions that contain sufficient diluent to cause the constant etch rate contours to turn upward slightly, i.e., the compositions 20% HF, 60% HNO₃, 20% H₂O and 20% HF, 45% HNO₃, 35% HC₂H₃O₂. Here the etching process is somewhat more complicated (see Fig. 5 and 6). The $\log R$ vs. $1/T$ plot seems to consist of two intersecting straight lines. The lower temperature region is represented by a straight line corresponding to an activation energy of approximately 14 kcal/mole, whereas the higher temperature region yields a line of lower slope, corresponding to an activation energy of 6.5 kcal/mole in the acetic acid diluent, and to 7.6 kcal/mole in the water diluent.

This behavior is in accord with a two process reaction, the first phase being oxidation, followed by the second, dissolution of the oxide. To understand this behavior, consider Fig. 9.

Since the two steps are in series, the slower one will always limit the over-all rate. At low temperatures, i.e., to the right of the point of intersection of A-B with C-D, the higher activation process will limit the over-all rate. At higher temperatures, i.e., to the left of the point of intersection, the lower activation energy process will limit the over-all rate. Thus the full experimentally observed curve will be B-O-C. We shall identify one of the activation processes with the oxidation step and the other with the dissolution step. Since we are operating in a region adjacent to the one in which the low activation energy process of the diffusion of HF was rate determining, and since the diffusion of HF is still very probably important in the composition region under consideration, we shall assign to the dissolution step the lower acti-

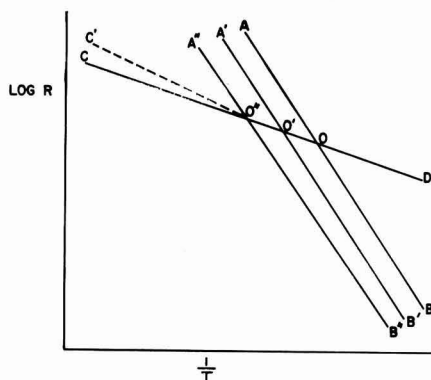


Fig. 9. Model relating the multiplicity of activation energies to a transition from one rate-determining process to another.

vation energy and to the oxidation step the higher activation energy. This is also justifiable on the basis that in the high HF region of compositions, where the oxidation step is known to be rate determining, the value of the activation energy agrees quite well with the value of 14 kcal/mole that we have assigned to the oxidation process.

We shall defer the consideration of the higher activation energy value until we discuss the high HF region. However, some insight into the significance of the lower value can be obtained from the consideration of Fig. 8. Consider first a composition in the high HNO_3 region, say at 20% HF, containing no added diluent. Here we know that the reaction is diffusion governed with respect to HF, and that the concentration gradient from C_1 to C_2 controls the etch rate. If the composition is allowed to vary along a constant etch rate contour by the substitution of diluent for HNO_3 (see Fig. 1), the etch rate and the HF concentration in the solution initially remain constant. However, on the continued addition of diluent, a point is reached at which the contour begins to turn upward. This is the region now under consideration. At this point the etch rate can remain constant only if the HF concentration is increased. This condition may be represented by the line $C_1'-C_2'$ of Fig. 8, which is parallel with C_1-C_2 because the flow rate of HF and thus the concentration gradient is the same for both compositions. Thus, there is a finite surface concentration of HF. This surface concentration of HF is the result of the lagging of the oxidation step, which causes the HF to begin to experience difficulty in locating oxidized silicon with which to react.

The lagging of the oxidation step can also be demonstrated by use of Fig. 9. Let line A-B correspond to the oxidation step for the etching composition containing no diluent. As diluent is added, the curve shifts progressively to A'-B', A''-B'', etc., and the point of intersection with the curve C-D shifts toward higher temperatures. Thus, on A-B the point of intersection with C-D is well below room temperature, and it has not been observed. If the composition corresponding to A''-B'' lies in the region where the constant rate contours are beginning to turn upward, the reaction has become oxidation dependent, and the point of intersection of A''-B'' with C-D will lie at room temperature. Thus, we will observe both branches of the activation energy curve. The fact that the reaction below room temperature is oxidation limited must imply that there is some unoxidized silicon exposed in the surface. An increase in the temperature tends to enhance the oxidation step more than the dissolution step because of the higher activation energy of the oxidation reaction. Therefore a higher concentration of oxidized silicon tends to be built up in the surface. An increase in the rate of the dissolution step is now possible, since C_1' can decrease, causing the slope of $C_1'-C_2'$ (see Fig. 8) to increase. Thus, the effect of increasing the temperature is to increase not only the diffusion coefficient of HF, but also the concentration gradient, and a higher activation energy is ob-

served (C'-O' of Fig. 9) than one corresponding only to the variation of the diffusion coefficient with temperature (C-O'). This can explain the increased values of the observed activation energy in the region under consideration and also cautions that what we are now calling the activation energy has a somewhat different significance from what it had in the absence of added diluent.

Activation energy in the high HF region.—Let us now turn our attention to the high HF region. Here, for each composition we have plotted two curves (see Fig. 4). The upper curve corresponds to the externally catalyzed system. The displacement of the two curves is not primarily the result of the catalytic activity of the added catalyst (NaNO_2), but it is rather caused by the increase in the total amount of oxidizing substances present in the solution as the result of the addition of the nitrite. The amount of material added was 0.1 g in 20 cc, which amount is not negligible in the region of compositions where the nitric acid is low.

There is a sharp break in the activation energy curves of the nonexternally catalyzed systems, and a weaker break in the curves corresponding to the externally catalyzed systems. Although this break indicates a transition from one reaction mechanism at lower temperatures to another at higher temperatures, the change in the reaction mechanism is probably not one from oxidation dependence to oxide removal dependence. The fact that considerably reduced HF concentrations are capable of sustaining reaction rates ten times those under consideration and the fact that the etch rates are susceptible to enhancement by the addition of catalyst indicate that the etch rates on both branches of the activation energy curves are nitric acid dependent. It is also interesting to note that the weight ratio of HF: HNO_3 ,² necessary to sustain a given reaction rate at a given temperature, where the HF concentration is taken at one end of a constant rate contour where the rates are HF dependent, and the HNO_3 concentration is taken at the other end of the same contour where the rates are HNO_3 dependent, is approximately 3.5:1. On a molar basis this gives a molar ratio of HF: HNO_3 of 7. Considering that the stoichiometric ratio of HF: HNO_3 is at most 4.5,³ and bearing in mind that the HF dependent rates are the maximum possible for one of the pair of compositions under consideration because of the diffusion limitation, the diffusion coefficient of HNO_3 would have to be at least 1.6 times that of HF at room temperature, and five times higher at 45°C. This consideration forces us to look for a reaction mechanism that could yield reaction rates somewhat higher than would be expected from a simple diffusion mechanism.

Oxidation Mechanisms

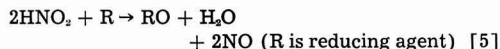
It is the authors' belief that the change in the mechanism indicated by the break in the rate-temperature curves is tied in with a change in the mode of attack on the silicon by the nitric acid. It is therefore necessary to consider the chemistry of HNO_3 .

² The weight ratio given here is 49% aqueous HF : 70% aqueous HNO_3 .

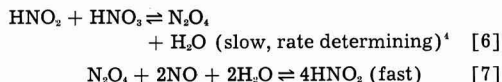
³ This is based on the formation of SiF_6^{2-} as the reaction product, rather than SiF_4 , which requires a lower ratio.

nitric acid before taking up the question of the reaction mechanism.

It has been proposed (5) that oxidation by nitric acid actually proceeds through the intermediate formation of HNO_2 , which is considered to be a more active oxidizing agent than HNO_3 .



The HNO_2 required for the oxidation is formed in a two-step reaction that involves the HNO_2 concentration autocatalytically as follows (5-7)



These reactions are reversible. The formation of HNO_2 from Eq. [6] and [7] proceeds from left to right. The kinetics of this reaction are first order in HNO_2 and HNO_3 , thus

$$d[\text{HNO}_2]/dt = k[\text{HNO}_2][\text{HNO}_3] \quad [8]$$

The decomposition of HNO_2 proceeds by the reversal of Eq. [7], followed by the hydrolysis of N_2O_4 . The kinetics of this reaction are first order in N_2O_4 . However, by the equilibrium of Eq. [7], the concentration of N_2O_4 may be written as follows:

$$[\text{N}_2\text{O}_4] = K [\text{HNO}_2]^2 / P_{\text{NO}}^2 \quad [9]$$

Here the term K is the equilibrium constant for the reaction of Eq. [7], and P_{NO} is the partial pressure of nitric oxide. The kinetics of the reverse process accordingly obey the expression

$$-d[\text{HNO}_2]/dt = k' [\text{HNO}_2]^2 / P_{\text{NO}}^2 \quad [10]$$

It is thus seen that the formation of HNO_2 by this mechanism requires the presence of itself, and that the decomposition of HNO_2 is strongly inhibited by the presence of NO .

An alternative method of formation of HNO_2 has been proposed by Briner (8) that involves a bimolecular reaction between HNO_3 and NO .



This reaction may be followed by reaction [7] above to give additional HNO_2 . The primary reaction [11] probably does not proceed as readily as the alternative Abel and Schmid mechanism, but it probably plays an important role in the induction phase of the oxidation of silicon.

In addition to the mode of oxidation by HNO_3 proposed by Abel and Schmid, one must also consider the possibility of the direct attack of that species on silicon, for we have experienced no difficulty in getting reactions of silicon with nitric acid in etches containing an excess of H_2O_2 , KMnO_4 , or Ce^{4+} ions, all of which quantitatively remove nitrogen compounds of lower valence state by oxidation to HNO_3 .

Mechanism of the induction reaction.—It is possible to set up two different conditions. At low reac-

tion rates and in the absence of HNO_3 , the mechanism probably involves the direct diffusion of HNO_3 to the silicon surface. The primary mode of attack is then via undissociated HNO_3 . Since this process may lead to reduction products of HNO_3 which are themselves also potentially excellent oxidants, e.g., NO_2 , HNO_2 , there is a probability that these may become involved in further reaction with the silicon before they can become dissipated into the bulk solution. There is also a possibility for the formation of HNO_2 and NO_2 on the silicon surface from the interaction of HNO_3 with NO according to Eq. [11]. This latter possibility provides an alternative course for the reduction of HNO_3 that involves chemical species that are supposedly more reactive toward silicon than is HNO_3 itself. The various alternatives probably all make contributions to the over-all reaction, the rate of which becomes limited by the rate at which HNO_3 can diffuse to the silicon surface.

Mechanism of the steady state.—In silicon etching the steady-state condition can be achieved only after a concentration of HNO_3 in excess of a threshold value has been built up in the vicinity of the silicon surface, either through the addition of a small amount of NaNO_2 or as a consequence of the attainment by the etching reaction of a sufficient rate to accomplish this purpose. In this steady-state condition the mode of attack on the silicon is probably almost exclusively via HNO_2 , and the site where the rate-determining processes play their roles has probably shifted from the silicon surface to the boundary layer surrounding the silicon specimen, in a mechanism similar to that suggested by Spahn and Schmid (9). It must be remembered that the formation of HNO_2 by the Abel and Schmid mechanism is autocatalytic, and that it requires the presence of HNO_2 in order for the processes of Eq. [6] and [7] to proceed. As long as the reaction is in the first state described above, the HNO_2 that is formed either by the reduction of HNO_3 or NO_2 , or by the Briner mechanism, is confined to the silicon surface, and it probably reacts with the silicon substrate on which it is adsorbed, rather than with the HNO_2 in the surrounding medium. However, when the reaction attains a sufficiently high rate, the NO , which is the final reduction product of HNO_3 , and which is now being generated in large quantities, diffuses away from the silicon in high concentration, and as a consequence, a high concentration of NO is built up within the boundary layer. The NO can now intercept HNO_3 that is diffusing in from the bulk solution and, by the mechanism of Briner, produce a concentration of HNO_2 within the boundary layer. Once a sufficient concentration of HNO_2 is built up, this HNO_2 can further react with HNO_3 by the Abel and Schmid mechanism, and there then results the autocatalytic buildup to the steady state as depicted in Fig. 10.

Nitric acid diffuses from the bulk solution into the boundary layer. On its way to the silicon surface it is intercepted by the HNO_2 , and it thus becomes depleted within the boundary layer rather

⁴We shall neglect the dissociation of N_2O_4 to NO_2 in this discussion.

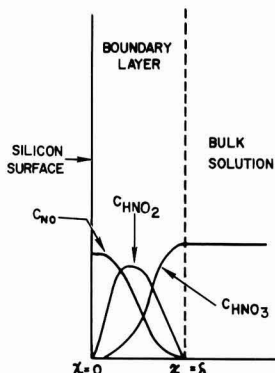


Fig. 10. Model of the reaction mechanism in the high HF region.

than at the silicon surface. This causes an increase in the concentration gradient of HNO_3 , and may result in the enhancement of the etch rates to values in excess of those compatible with simple diffusion according to Fick's law.

The concentration of HNO_2 builds up to a maximum within the boundary layer. In part diffuses toward the silicon surface, where its decomposition is inhibited by the strong concentration of NO , and it reacts with the silicon. In part, it diffuses toward the bulk solution and becomes dissipated there. The stoichiometry of reaction [5] requires that, as a boundary condition, two molecules of NO diffuse away from the silicon surface for every two molecules of HNO_2 that diffuse toward the silicon. The stoichiometry of reactions [6] and [7] indicates that the two molecules of NO can lead to the formation of 3 molecules of HNO_2 . Therefore, one molecule of HNO_2 must diffuse away toward the bulk solution. The net result as seen from the bulk solution is the diffusion of one molecule of HNO_2 into the boundary layer, and one molecule of HNO_2 into the bulk solution. The ultimate form of the reduction product of nitric acid that is produced will depend only on the composition of the bulk solutions, as shown by Spahn and Schmid (9). In dilute HNO_3 solution the HNO_2 that enters the bulk solution will decompose rapidly to NO and HNO_3 by the reversal of Eq. [7] and [6], so that the principal reaction product found analytically will be NO . On the other hand, if the solution is concentrated in HNO_3 and poor in water, the reaction of Eq. [6] will proceed from left to right, and the N_2O will be evolved from the solution in the form of NO_2 . The nature of the reaction product is thus not determined by the actual surface reaction, but by secondary reactions within the boundary layer and in the bulk solution.

The establishment of the steady-state condition shown in Fig. 10 is contingent on several conditions, two of which are the presence of a small amount of HNO_2 and the presence of NO . However, the mere presence of these substances does not guarantee that the steady state will be attained. The rates of formation of HNO_2 and NO must be sufficiently large to overcome the losses resulting

from dissipation of these products. Thus, the reaction must proceed through an induction phase in which the principal mechanism of attack on the silicon is via molecular HNO_2 . The product of this reaction may be NO_2 , NO , or HNO_3 , and probably all three of these are present to some extent. If HNO_2 is not formed as a reduction product of HNO_3 , it can still be formed by the mechanism of Briner. If the rate of the induction reaction is sufficiently great, a threshold concentration of HNO_2 can be built up in the vicinity of the silicon surface, and since the rate of formation of HNO_2 depends autocatalytically on the presence of itself, the rapid buildup of the HNO_2 concentration to the steady-state value by the mechanism of Abel and Schmid becomes assured.

One might also consider the mechanism of Vetter (10), discussed by Cretella and Gatos (11), as an alternative route for the oxidation process. This mechanism involves the oxidation of silicon by NO_2 which is formed in the process of Eq. [6]. However, the equilibrium of that reaction lies far to the left, and no substantial concentration of NO_2 can exist in the boundary layer. Therefore no concentration gradients of NO_2 can be set up over any reasonable distances, and one must consider the Vetter mechanism as a surface reaction and subject to the limitations of diffusion control, where the principal diffusing species is HNO_2 . We therefore consider the Vetter mechanism as potentially making a contribution to the over-all process in the induction phase, but we find it difficult to explain the apparent high diffusion coefficient of HNO_3 , especially at the higher temperatures, as compared with the diffusion coefficient of HF , on this basis.

Let us now return to a consideration of the curves of Fig. 4. At low temperatures the etch rates are low, and the principal mode of attack is by molecular HNO_2 . The high value of the activation energy may result from the possibility that an increment in the etch rates resulting from an increase in the temperature is accompanied by an additional increase in the etch rates resulting from the increased involvement of the reduction products, so that the over-all sensitivity of the etch rates to a temperature change is increased. It may also be possible that the activation energy observed is characteristic of the formation of HNO_2 by the Briner mechanism, which should have a higher activation energy than the formation of HNO_2 by the Abel and Schmid mechanism. As the temperature is increased, a point is reached where the rate of production of NO and HNO_2 becomes sufficient to sustain the steady-state condition of Fig. 10, and the activation energy drops to the lower value. In view of the extreme complexity of the situation, involving the diffusion of three different species and the heat of the reaction, as well as a complex series of chemical interactions and medium changes within the boundary layer, it is difficult to ascribe much significance to the value for the activation energy of approximately 14 kcal/mole. Cretella and Gatos (11) have found similar values for the activation energy of the oxidation of germanium by HNO_2 . We are inclined to consider this as coin-

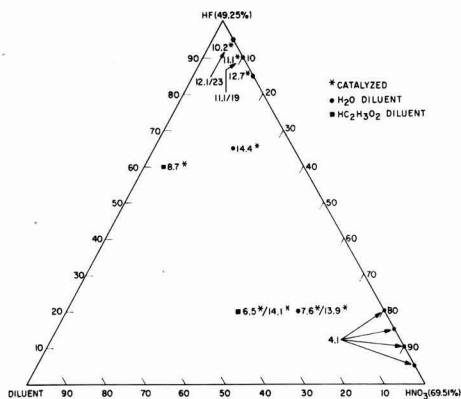


Fig. 11. Summary of the activation energies as a function of composition of the etchant.

cidental, since their reported reaction rates were so low as to preclude the probability of a diffusion influence, whereas the reaction rates under consideration in this research are of a different order of magnitude, and are definitely affected by transport phenomena.

Summary

The activation energies obtained in the different solutions studied are summarized in Fig. 11.

In the high HNO₃ region when small amounts of diluent are present, the reaction is a straightforward diffusion process. The measured activation energy is a true activation energy, and it is associated with the temperature dependence of the diffusion coefficient of HF. The temperature sensitivity of the etch rates is low, and it is not necessary to provide accurate temperature control in order to obtain reproducible etching.

As diluent is added to etchants rich in HNO₃, a point is reached where the observed activation energy begins to increase, and two values, one corresponding to the oxidation process and one to the oxide removal process, will be observed. The value of the activation energy will not have the same significance as in the previous case. The high-temperature value will be affected by the changing surface concentration of HF. The low-temperature value will be typical of an HNO₃ dependent reaction.

In the high HF region the reaction becomes very complex. At low temperatures, especially in the absence of added catalyst, the reaction mechanism probably involves the direct attack of undissociated HNO₃ on silicon, perhaps assisted by the bimolecular reaction of HNO₃ and NO to form HNO₂. At higher temperatures, or in the presence of added catalyst, the reaction probably takes an alternative course in which the attack on the silicon is by means of HNO₂. The HNO₂ is formed in a complex series of reactions within the boundary layer surrounding the silicon surface. The reaction of HNO₂ within the boundary layer instead of at the silicon surface can cause the rate of diffusion of HNO₃ to be increased so that the reaction rate can attain values in excess of those expected from the application of Fick's law to a simple diffusion process.

Acknowledgments

The authors wish to express their indebtedness to Dr. J. J. Grossman for many helpful suggestions and stimulating discussions. We also wish to acknowledge the assistance of Mrs. E. P. Arey in the experimental work.

Manuscript received Aug. 8, 1960; revised manuscript received Dec. 28, 1960. This paper was prepared for delivery before the Columbus Meeting, Oct. 18-22, 1959.

Any discussion of this paper will appear in a Discussion Section to be published in the December 1961 JOURNAL.

REFERENCES

1. H. Robbins and B. Schwartz, *This Journal*, **106**, 505 (1959).
2. H. Robbins and B. Schwartz, *ibid.*, **107**, 108 (1960).
3. E. A. Moelwyn-Hughes, "The Kinetics of Reactions in Solution," p. 370, Clarendon Press, Oxford (1947).
4. D. L. Klein and D. J. D'Stefan, Private communication.
5. E. Abel and H. Schmid, *Z. Physik. Chem.*, **132**, 55 (1928).
6. *Ibid.*, **134**, 279 (1928).
7. E. Abel, H. Schmid, and S. Babad, *ibid.*, **136**, 135 (1928).
8. E. Briner and P. Bolle, *Helv. Chim. Acta*, **18**, 368 (1935).
9. G. Schmid and H. Spahn, *Z. Metallkunde*, **45**, 128 (1955).
10. K. Vetter, *Z. Physik. Chem.*, **194**, 199 (1950).
11. M. C. Cretella and H. C. Gatos, *This Journal*, **105**, 487 (1958).

Rotating Cathode for the Reduction of Nitrobenzene to Hydrazobenzene

K. S. Udupa, G. S. Subramanian, and H. V. K. Udupa

Central Electrochemical Research Institute, Karaikudi, South India

ABSTRACT

The use of a rotating cathode in the reduction of nitrobenzene suspended in alkaline medium is described. Conditions of electrolysis were similar to those established by Dey and co-workers except that, using a rotating cathode, the reduction could be carried out at current densities of 15-30 amp/dm² instead of 2 amp/dm². Reduction proceeded quite smoothly and an almost quantitative yield of hydrazobenzene was obtained. A rotating mild steel disk cathode with a coating of lead was used along with a cylindrical diaphragm of asbestos cloth supported on a mild steel nickel plated cage as the anode chamber. The best conditions are (i) 10-20% alkali (NaOH) as catholyte and anolyte, (ii) a depolarizer ratio of (w/v) 1:4, (iii) current density of the order of 15-30 amp/dm², (iv) temperature between 80°-85°C, (v) addition of 1% (w/v) of PbO to the catholyte. Iron substrate is superior to copper or brass as cathode, when deposited with lead. Addition of ZnO instead of PbO in the proportions suggested by Sugino and Sekine gave very low yields using rotating cathode. The paper also describes the isolation and recovery of the product and subsequent conversion to benzidine. Cathode potential measurements were also carried out and used to explain some of the results.

The reduction of aromatic nitrocompounds in alkaline medium to give the corresponding hydrazo compounds is technically important because of the conversion to benzidines required for the production of direct cotton colors.

The large demand for benzidine in India, which is met at present by import, prompted a re-investigation of the process.

A systematic study of the use of a rotating cathode in the reduction of emulsion of nitrocompound in acid medium to aminophenols has been reported (1). Later (2, 3) very high current densities were employed without adversely affecting the current efficiency. It was shown (1) that beyond a certain rate of rotation of the cathode there was no appreciable improvement in the yield of product.

The use of rotating cathode has now been extended to the reduction of nitrobenzene in alkaline emulsion to hydrazobenzene. The optimum conditions worked out by Dey and co-workers (4) formed the basis of the present study.

Experimental

In the laboratory scale experiments, 10% sodium hydroxide solution was used as catholyte and 20-25% solution of sodium hydroxide as anolyte. Asbestos cloth wound on a mild steel nickel plated cage (5 cm diameter and 20 cm height) was used as a diaphragm. A rotating disk-type iron cathode (total area 0.8 dm²) made by assembling 2.5 cm diameter iron disks (0.158 cm thick) on a 0.67 cm rod with cylindrical spacers of iron of 1.25 cm diameter and 1.25 cm height was used in most of the experiments unless otherwise specified. Either nickel-plated mild steel or nickel-plated copper was used as anode. Distilled C.P. grade nitrobenzene was employed in the reduction studies and C.P. hydrochloric acid (sp gr 1.16) was employed for the

conversion of hydrazobenzene to benzidine hydrochloride.

The cell arrangement consisted of a 1-liter Pyrex beaker without a spout, provided with an asbestos cement sheet lid, 0.3 cm thick. The cover had the necessary openings for the cathode shaft, diaphragm, condenser, and thermometer. A slight suction was maintained through the condenser to prevent loss of nitrobenzene through the opening provided for the rotating cathode. The cathode was attached to the lower end of the shaft of a 1/16 H.P. motor whose speed could be controlled. The speed of rotation of the cathode was kept at 2000 rpm (angular velocity being nearly 200 radians/sec). Contact with the rotating shaft was made by a carbon brush. A depolarizer ratio of 1:4 (1 g of nitrobenzene to 4 ml of catholyte) was chosen.

The iron cathode was coated with lead by electrolyzing sodium plumbite solution. It was found necessary to rotate the electrode during electrodeposition in order to be able to get an adherent deposit. By employing about 5 g of lead monoxide in 400 ml of 10% sodium hydroxide, it is possible to obtain nearly 0.028 mole of lead/dm² of the cathode, when deposition is complete.

After the lead had been deposited on the rotating cathode, 100 g of nitrobenzene was added to the hot electrolyte (85°C) and the theoretical current provided by a selenium rectifier passed. After 90% of the current was passed, xylene (100 ml) was added before completion of the reduction.

The xylene layer from the electrolyte was separated and poured into a mixture of ice and 80 ml of HCl (sp gr 1.16) and stirred for 5 hr in the cold after which the temperature was raised to gentle boiling. Solid benzidine hydrochloride which separated on cooling was isolated and weighed. Total benzidine formed in the solid as well as in the clear

Table I. Comparison of results obtained with stationary and rotating cathodes

Current density, amp/dm ²	Chemical yield of benzidine, † % of theory	
	Rotating	Stationary
10	87.1	13.5
20	88.0	10.7
10*	—	44.3
20*	—	37.6

† Yield is calculated on nitrobenzene taken.

* An iron vessel containing 400 ml of electrolyte was used, spongy lead deposited being greater in these cases.

solution was estimated by precipitation as benzidine sulfate. The yield of benzidine reported in the tables is a percentage of the theoretical chemical yield. The aniline formed was liberated by neutralizing the aqueous portion left after filtering off the benzidine sulfate and steam distilling. The aniline in the distillate was estimated by the bromate-bromide procedure. The xylene layer which contained the azobenzene and any unreduced nitrobenzene was steam distilled. The azobenzene remaining in the still was cooled, filtered, dried, and weighed. Nitrobenzene from the xylene layer was reduced with zinc and hydrochloric acid to aniline and estimated using bromate-bromide mixture.

A current density of 30 amp/dm² was employed in the experiments given in Tables III and IV and in the study of the influence of alkali strength.

Discussion of Results

Effect of rotating cathode.—To compare the effect of high current densities on yields of benzidine using a stationary and a rotating cathode, a few experiments were carried out with the disk-type cathode under otherwise identical conditions (Table I). In the experiments employing a stationary cathode, an auxiliary stirrer was employed. Lead was deposited on both a rotating cathode and a stationary cathode. The advantage of rotation is clearly evident at high current densities. In the case of stationary cathode, it may be seen that the yield is better if an iron vessel is used as a container and cathode. The higher yields of benzidine in this case is probably due to greater surface of spongy lead exposed.

Influence of current density.—A series of experiments were conducted to ascertain the influence of current density on the yield of benzidine using rotating cathode. Current densities of the order of 5–30 amp/dm² were used; results obtained are given in Table II. The advantageous effect of rotation is probably due to acceleration of the dis-

Table II. Effect of current density on the yield of benzidine

Current density, amp/dm ²	Yield of benzidine, %
5	86.5
10	87.1
15	87.5
20	88.0
25	88.5
30	88.2

solution of nitrobenzene and the movement of the organic molecules to and from the cathode so that their reduction becomes preferred to hydrogen evolution. The hydrazobenzene at the cathode is removed as fast as it is formed, and rotation raises the ratio of nitrobenzene to hydrazobenzene on the cathode surface. This increase in surface concentration of nitrobenzene increases the range of current density that can be employed for reduction.

With the cathode stationary, the hydrazobenzene formed is not removed rapidly; this gives a greater chance for its further reaction with partially reduced intermediates. Thus, large quantities of azobenzene were formed with the stationary cathode, presumably due to this. Furthermore, aniline formation was higher at the stationary than with the rotating cathode, and considerable quantities of unreduced nitrobenzene were recovered under stationary conditions.

Influence of different metal oxides.—The effect of various metal oxides for different cathode materials and their influence on the reduction of nitrobenzene to hydrazobenzene has been studied in detail by Sugino and Sekine (6). They carried out electrolytic reduction of nitrobenzene in alkaline emulsion and observed that cathodes of zinc, tin, cadmium, and lead with more than 0.07 moles of spongy metal per dm² of the surface were the most suitable for reduction (7). As base materials for spongy layers, common metals such as lead, iron, and others were found suitable. At these cathodes almost quantitative yields of hydrazobenzene were obtained at relatively high current densities with suitable agitation. They concluded that use of zinc in the form of a smooth deposit gives material yield and current efficiency of a higher order than iron and nickel. The optimum amount of added metals is given as at least 0.05 mole/dm² (zinc or lead) on the cathode (6).

The influence of agents like lead monoxide and zinc oxide using different cathodes like iron, brass, and copper was tried under rotating cathode conditions. With 0.028 mole of lead/dm² very good yields (88%) of benzidine were obtained even though the proportion of lead employed is much less than that employed by Sugino and co-worker. When zinc oxide was used, the yield of benzidine was as low as 14.3%, using iron cathode base, in spite of using proportions of zinc higher than the minimum suggested by the Japanese workers (6). Table III is a summary of the proportions of lead and zinc used by Dey, *et al.* (4), by the Japanese workers (6), and by the present authors.

It was found that the yield of benzidine was reduced from 83.5% to 48% if the quantity of lead was reduced from 0.028 to 0.014 mole/dm². Increasing it above 0.028 mole/dm² was of no added advantage since the spongy lead did not adhere.

Table III. Spongy metal deposited by different investigators

Addition agents	Dey, <i>et al.</i>	In the present investigation	Sugino and Sekine
Moles of lead/dm ² of cathode	0.005	0.028	0.07
Moles of zinc/dm ² of cathode	0.025	0.184	0.07

Table IV. Effect of cathode material on the yield of benzidine

Cathode base material	Yield of benzidine, %
Iron	88
Brass	10
Copper	8.8
Amalgamated copper*	Nil
Nickel-plated copper	58.5

* PbO equivalent to 0.028 mole/dm² added in all experiments except this.

It is concluded that 0.028 mole of lead/dm² is sufficient for obtaining good reduction of nitrobenzene using a rotating iron cathode.

Effect of cathode material.—The next series of experiments was concerned with the influence of cathode material on the yield of benzidine. Different cathode base materials have been tried; results are shown in Table IV.

In the case of nickel-plated copper, it was observed that if 10% excess current was passed, the yield of benzidine increased from 58.5% to 82.0%. But in the case of iron cathode, theoretical current gave a yield of 88%. Although the nickel cathode can give yields approaching that obtained with an iron cathode by passing more current, the current efficiency for hydrazobenzene formation is much better at the latter. As such, iron appears to be the best cathode base material for reduction.

It is interesting to note how the substrate metal influences the yield although in all cases the surface was covered with the deposited lead. This is perhaps connected with the differences in the nature of lead deposits obtained with different base metals. A complete analysis of the products formed at amalgamated copper and nickel plated copper (Pb coated) cathodes by passing theoretical current is given in Table V.

As mentioned earlier, rotating cathode enables the use of much higher current densities and permits reduction to proceed more rapidly to completion, using about the theoretical quantity of current. In the case of a stationary electrode, Dey and co-workers (4, 5) employed 10% excess current, and in their reciprocating type of cathode, Sugino and Sekine (6) employed 25% excess current (using high current densities). In his earlier study on electrolytic reduction, Sekine (8) advocated the use of 3 amp/dm² at the beginning and then reducing this to 2 amp/dm² to obtain a yield of 81.6% of hydrazobenzene with a current efficiency of 73.84%. Experiments now carried out show that when an iron cathode is used, only 5% more than the theoretical current need be passed.

Table V. Products formed at nickel-plated copper and amalgamated copper cathodes

Cathode material	Yield of benzidine, %	Yield of azobenzene, %	Yield of aniline, %	Unreduced nitrobenzene, %
Amalgamated copper	Nil	60	16	20
Nickel-plated copper (Pb coated)	58.5	32.5	4	2.2

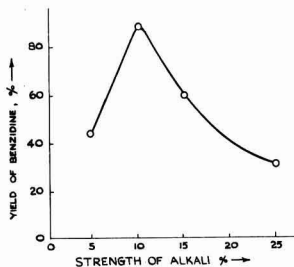


Fig. 1. Influence of alkali strength on the yield of hydrazobenzene.

Atanasiu and Dumitru (9) have studied the preparation of benzidine using a two-stage process in a cell consisting of an iron container as anode and a rotating iron cathode inside a porous porcelain diaphragm. They reported a current efficiency of 93% at 200 rpm, and the over-all yield of benzidine was 88%. In the present investigation, nitrobenzene was reduced in a single step in yields quite comparable to those of Atanasiu and Dumitru.

Influence of alkali strength.—Experiments were carried out to study the influence of alkali strength on the reduction. Sodium hydroxide of various concentrations ranging from 5% to 25% were tried and the results obtained are represented graphically in Fig. 1. The graph clearly indicates that 10% sodium hydroxide gives the maximum yield and a narrow range of approximately 8 to 12% alkali could be employed without seriously affecting the final yield. This is a very important observation because the strength of alkali in the catholyte changes during electrolysis.

Miscellaneous observations.—A cylindrical cathode gave results as efficient as the disk type, but the latter is preferred in view of the very efficient agitation that was produced.

Re-use of the alkali from the catholyte in a subsequent reduction decreased the yield of benzidine from 88 to 74.3% and increased yields of azobenzene and aniline from 6 to 15% and 2 to 6%, respectively. This was due to the increased strength of alkali in the catholyte since, on adjusting the strength of alkali to 10% before re-use, the yield of benzidine could be produced without having to add any fresh lead monoxide. In one experiment using nearly 10% excess current, the yield of benzidine increased from 88 to only 89.5%. The results of the large-scale experiments, re-using the same alkali in 8 runs with the same lead deposited cathode are given in Table VI.

Cathode Potential Studies

Cathode potentials were measured using a 1 cm diameter iron cylindrical cathode with a Hg/HgO/N NaOH reference electrode and a calibrated Heath-kit vacuum tube voltmeter. Potential was measured during deposition of lead on both stationary and rotating cathodes using a current of 1 amp (current density being 2.6 amp/dm²). Potential vs. time during deposition is plotted in Fig. 2. It may be seen that the stationary cathode is polarized to a greater extent than the rotating cathode. Replen-

Table VI. Results of large-scale preparation of benzidine

Catholyte:	4 l 10% NaOH
PbO:	40 g (for the first run only)
Anolyte:	1 l of 30% NaOH
Weight of nitrobenzene taken	1000 g
Cathode:	Disk-type iron having 6 disks of 7.5 cm diameter with a spacing of 3.8 cm
Cathode current density (apparent)	30 amp/dm ²
Duration of electrolysis	Theoretical time for hydrazobenzene formation
Xylene added:	1000 ml
Temperature:	80°-85°C

No. of run	Yield of benzidine, % of theory	Yield of azobenzene, % of theory	Yield of aniline, % of theory
1st	80.0	7.3	6.1
2nd	82.4	12.7	2.1
3rd	81.3	12.3	3.1
4th	80.8	11.7	3.4
5th	} avg 81.0	} 10.4	} 4.5
6th			
7th			
8th			

The cell voltage fluctuated between 4.5-6.0 v and the energy consumption was found to be 4.1 kw-hr/lb of benzidine hydrochloride.

ishment of lead ions in the cathode film is faster with rotation, thereby leading to less polarization and a more compact deposit than on stationary cathode.

The influence of current density on cathode potential was studied for the cathode that was plated rotating as well as that plated stationary. Curves 1 and 2 in Fig. 3 show the polarization under stationary conditions of the cathode plated under stationary and rotating conditions. The rotating cathode is polarized to a greater extent because the deposit is less spongy. The cathode potential was also measured at different current densities after adding nitrobenzene. The potential was noted for each current density as the latter was increased stepwise at 2-min intervals. Curves 3 and 4 of Fig. 3 show considerable lowering of the cathodic polarization on addition of nitrobenzene. This effect

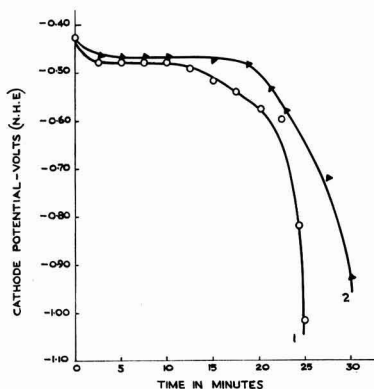


Fig. 2. Cathode potential vs. time of deposition of lead on: curve 1, stationary cathode; curve 2, rotating cathode.

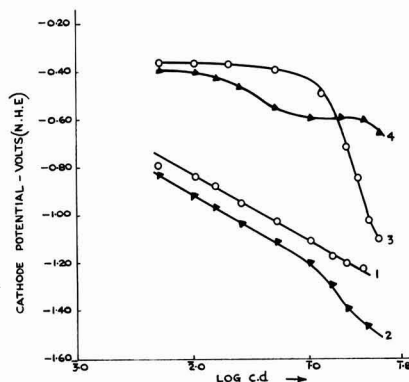


Fig. 3. Cathode potential vs. log C.D.: curve 1, stationary cathode; and curve 2, rotating cathode without addition of nitrobenzene; curve 3, stationary cathode; and curve 4, rotating cathode with addition of nitrobenzene.

has also been reported by Leslie and Butler (10) who attributed it to the reduction taking place by direct electron transfer. It may be seen from the curves that, with a stationary cathode, in presence of nitrobenzene, increase of current density quickly raises the potential of the cathode to a high negative value corresponding to hydrogen discharge. This explains the low current efficiency met with in the case of stationary electrodes. The rotating cathode, however, is depolarized effectively even at very high current densities.

The cathode potential was also measured throughout a typical experiment using a cylindrical rotating cathode in a bath containing 500 cc of 10% sodium hydroxide with the addition of 2 g of lead monoxide and 50 g of nitrobenzene and passing a current of 11 amp. Current density employed was 28 amp/dm². The cathode potential remained low until lead deposition was over, and after 2.5 min, it suddenly increased at which stage nitrobenzene was added. The cathode potential vs. time of electrolysis is graphically represented in Fig. 4. Total electricity passed in the whole experiment corresponds to 5% excess over the theoretical quantity required for reduction of nitrobenzene to hydrazobenzene. The first steep fall (A to B) in the cath-

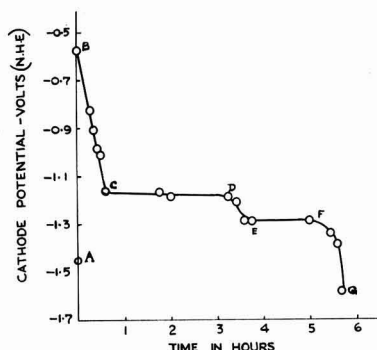


Fig. 4. Cathode potential vs. duration of electrolysis using rotating cathode.

odic polarization is due presumably to depolarizing action of dissolved nitrobenzene. The cathode potential becomes more and more negative (B to C) probably due to the deposition of hydrazobenzene. A stationary state is probably attained in the region C to D. When nitrobenzene concentration drops off, polarization increases (D to E), and again the potential remains steady probably corresponding to reduction of azobenzene (E to F).

Acknowledgment

The authors record their sincere thanks to Dr. K. S. G. Doss, Director of the Institute for his keen interest.

Manuscript received Feb. 24, 1960; revised manuscript received Aug. 8, 1960. This paper was prepared for delivery before the Columbus Meeting, Sept. 18-22, 1959.

Any discussion of this paper will appear in a Discussion Section to be published in the December 1961 JOURNAL.

REFERENCES

1. C. L. Wilson and H. V. K. Udupa, *This Journal*, **99**, 289 (1952).
2. G. S. Krishnamurthy, H. V. K. Udupa, and B. B. Dey, *J. Sci. & Ind. Res. (India)*, **15B**, 47 (1956).
3. G. S. Subramanian, H. V. K. Udupa, and B. B. Dey. "Rotating Cathode Type of Electrolytic Cell for the Reduction of m-Dinitrobenzene to 2:4-Diaminophenol," to be published.
4. B. B. Dey, T. R. Govindachari, and S. C. Rajagopalani, *J. Sci. & Ind. Res. (India)*, **4**, 559 (1946).
5. *Ibid.*, **4**, 569 (1946).
6. K. Sugino and T. Sekine, *This Journal*, **104**, 497 (1957).
7. T. Sekine, *J. Chem. Soc. (Japan) (Pure Chem. Sect.)* **77**, 67 (1956).
8. K. Sugino and T. Sekine, *J. Electrochem. Soc. (Japan)*, **21**, 383 (1953).
9. I. Atanasiu and D. Dumitru, *Rev. chim. (Bucharest)*, **9**, 129 (1958); *C. A.*, **53**, 5916 (1959).
10. W. M. Leslie and J. A. V. Butler, *Trans. Faraday Soc.*, **32**, 989 (1936).

Adsorption of Hydrogen and Oxygen on Electrode Surfaces

R. F. Amlie, J. B. Ockerman, and P. Ruetshchi

The Carl F. Norberg Research Center, The Electric Storage Battery Company, Yardley, Pennsylvania

ABSTRACT

A microvolumetric technique was used to study the desorption of hydrogen and oxygen from electrodes of very large surface area during open-circuit decay of overvoltage. An approximately linear relation was found between the overvoltage at a given current and the total amount of gas desorbed after interruption of current. Double layer capacities, determined from charging curves, increased with increasing number of partially discharged adsorbed species. The average state of charge of the adsorbed species in the double layer at steady-state conditions was found to be smaller than during the transient build-up of overvoltage. Experimental results indicate that unexpectedly long time periods are required to establish steady-state adsorption configurations and charge distributions on solid electrodes, and that the double layer capacities appear to be time-dependent. Within a potential region where the same electrochemical reaction proceeds throughout (in the present case hydrogen or oxygen evolution) and where the Tafel-plot is linear, the capacities, as determined from charging curves, appear to be almost independent of potential.

Recently, a microvolumetric technique has been described to study the desorption of hydrogen and oxygen gas from electrodes of very large surface area in acid solution (1). This technique has been applied in the present work to a series of different electrode materials in alkaline solution. The use of very large surface areas allows the experimental determination of the amount of adsorbed gas and permits a study of the relation between the number of adsorbed species and the electrode potential.

The adsorption and desorption phenomena on electrode surfaces and the attainment of steady-state configurations and charge-distributions on solid-liquid interfaces may require time periods of considerable length. This is particularly well demonstrated with experiments using the "reversed pulse technique" (2). In applying this technique, an electrode is first polarized to a steady

state by application of a constant current or a constant potential. A constant current pulse in the reverse direction is then impressed suddenly to the electrode for a very short period of time to lower the electrode potential by a substantial amount. After this reversed current pulse, the current is interrupted altogether and the electrode left to undergo relaxation on open circuit. By following the electrode potential with an electrometer-input voltmeter of good time-response, one observes that the overvoltage recovers after the reversed pulse quickly on open circuit before it decreases more slowly to the steady-state open-circuit value. This recovery of overvoltage is an indication of the slowness of the rearrangement of charges in the double layer. The slowness of the desorption of reacting species is also demonstrated by the gas desorption rates during open-circuit decay of hy-

drogen or oxygen overvoltage (1). In the present study these slow relaxation effects have been given particular consideration.

Experimental

Adsorption of hydrogen was studied on cadmium and amalgamated zinc electrodes, and adsorption of oxygen on silver oxide and nickel hydroxide electrodes. The electrodes were porous plates of large surface area, as used in nickel-cadmium and silver-zinc storage batteries. All measurements were performed in KOH solutions containing 387 g/liter of KOH (30% per weight or 6.9N). The solutions were titrated before and after the measurements. Electrode potentials were measured against a Hg/HgO reference electrode in the same solution. Most experiments were performed at $30^\circ \pm 0.02^\circ\text{C}$, but some charging and decay curves were also taken at 20° and 40°C . The experimental set-up included a Pyrex glass cell with attached capillary for microvolumetric measurements of evolved gas, and the associated electrical equipment which has been described previously (1). Equipment for automatic recording of evolved gas from electrodes has been developed recently by Conway and Bourgault (3).

The electrodes used here were periodically charged at constant current and left on open circuit, whereby build-up and decay of overvoltage was recorded using an electrometer-input amplifier and a high speed recorder. Triple distilled water was used for preparation of the electrolyte. It must be pointed out that the impurity problem was greatly minimized because of the large ratio between electrode surface and electrolyte volume (in the order of $1000\text{ cm}^2/\text{ml}$ electrolyte).

Amalgamated zinc.—The spongy zinc plates were produced by electrochemical reduction of an intimate mixture of 13 parts of ZnO and 1 part HgO in 7% KOH at $0.3\text{--}3\text{ ma}/\text{cm}^2$ of geometric surface. The plates contained an embedded zinc-plated silver screen. Electrical connection was made by a zinc-plated silver wire, spot-welded to the screen.

The formed zinc plates were inserted in 30% KOH and overcharged at $0.1\text{ ma}/\text{cm}^2$ of geometric surface for 72 hr. Subsequently, the charging and decay curves were taken. On open circuit, the zinc electrode reached no absolutely stable potential in KOH. Traces of oxygen react with zinc to form zinc oxide and zincate. Hydrogen is evolved in minute amounts at all times, due to the reaction between the zinc and the electrolyte. These reactions tend to build up a small zincate concentration in solution. Nevertheless, a fairly stable electrode potential of -1.443 v vs. HgO was reached after a decay period of about 900 sec. In all the experiments reported below for Zn, the electrode was allowed to decay to an open-circuit value of -1.450 v vs. HgO , which is still 7 mv more negative than the "steady" open-circuit potential. This minimizes adsorption effects and possible changes of the true surface area, since practically no zinc was allowed to oxidize or dissolve. Charging curves for build up of hydrogen overvoltage were also started at -1.450 v vs. HgO .

At the end of the experiments, the zinc electrode was overcharged at $0.2\text{ ma}/\text{cm}^2$ of geometric area for 24 hr, rinsed thoroughly but quickly in oxygen-free triple-distilled water and in acetone, and dried in a vacuum. The electrode was then sealed in a Pyrex tube and outgassed at 53°C and 10^{-6} mm Hg prior to BET nitrogen absorption measurements at -195.6°C .

Cadmium.—The cadmium electrode consisted of a highly porous nickel matrix, prepared by sintering Ni-powder under an atmosphere of hydrogen around a Ni-screen, and depositing a thin coating of metallic cadmium of about 100 monolayers, throughout the porous structure.

The formed electrode was overcharged at $10\text{ }\mu\text{a}/\text{cm}^2$ of geometric area for several days in 30% KOH prior to the hydrogen overvoltage build up and decay measurements. The open-circuit potential of a Cd electrode in 30% KOH is -0.910 v vs. HgO in the same solution. In the experiments reported below the Cd electrode was allowed to decay to -0.970 v vs. HgO and was then cathodized again at the next current rate for the recording of the charging curve. At the end of the experiments the electrode was charged over a prolonged period of time, and preparation for BET surface area determination followed the procedure for the amalgamated zinc electrode.

Nickel oxyhydroxide.—The electrode was a sintered nickel plaque of 75% porosity with pore-sizes between 1 and $15\text{ }\mu$. One gram of nickel hydroxide was precipitated per cm^2 throughout the porous structure. Electrical connection was made with a nickel wire which was welded to a nickel screen embedded in the porous electrode. The electrode was anodized in 30% KOH in the cell over prolonged periods of time. The electrolyte was then renewed and the electrode charged for 24 hr at $0.5\text{ ma}/\text{cm}^2$ of geometric area, prior to the start of the build-up and decay experiments. The nickel hydroxide electrode has no stable open-circuit potential. The charged active electrode material loses oxygen irreversibly and changes into a lower oxidation state while the potential keeps changing to less positive values. In the present investigation the potential of 0.440 v vs. HgO was chosen as the endpoint of the oxygen overvoltage decay curves. After the electrode had reached this potential, the current was switched on and the charging curves recorded, starting at the potential of 0.440 v vs. HgO . After completion of the experiments the electrode was charged at $0.5\text{ ma}/\text{cm}^2$ of geometric area over 24 hr and then removed from the cell, washed thoroughly in triple-distilled water, dipped in isopropyl alcohol, and dried in a vacuum. For BET surface area determination the electrode was degassed at 52°C and 10^{-6} mm Hg for 5 hr.

Silver oxide.—The electrode was produced by pressing and sintering fine silver powder ($5\text{--}15\text{ }\mu$) around a silver screen. Connection was made by welding a silver wire to the silver screen. The electrodes were formed in 20% KOH and the silver converted substantially to AgO.

The open-circuit potential of the AgO/Ag₂O electrode in 30% KOH is 0.500 v vs. HgO . Oxygen

Table I. Weight, geometric area, and BET surface area of various electrodes tested

Electrode	Total electrode weight, g	Total geometric area exposed to electrolyte, cm ²	BET surface area, 10 ⁴ cm ²	Ratio of BET to geometric electrode area	BET surface area per unit weight of electrode, m ² /g
Zinc	6.94	84.5	4.0	473	0.58
Cadmium	7.55	64.0	13.0	2030	1.72
Nickel oxyhydroxide	1.63	11.2	14.3	12,780	8.78
Silver oxide	71.76	230.0	6.2	270	0.09
Lead*	70.00	54.4	15.9	2940	0.23
Lead dioxide*	44.02	16.0	35.2	22,000	0.80

* See reference (1).

overtoltage decay curves on open circuit were taken to an endpoint of 0.520 v vs. HgO, which is 20 mv above the stable open-circuit value. This minimized errors due to changes in surface area and self-discharge. Charging curves for oxygen overtoltage build-up were started at 0.520 v vs. HgO. After the experiments the electrode was charged over prolonged periods of time at 0.520 v, and then removed, washed carefully in triple distilled water, and dried in a vacuum over CaCl₂. For BET surface area determination the electrode was subjected to degassing at 50°C and 10⁻⁶ mm Hg for 1 hr.

Results and Discussion

The results of the BET surface area determinations are summarized in Table I. Listed also are the geometric electrode surface and total electrode weight. For comparison, similar data on Pb and PbO₂ electrodes as reported earlier (1) have been included. This table is of interest in comparing the pore-structure of various porous storage battery electrodes.

Charging curves at constant current are shown in Fig. 1 to 4. The currents refer to the total electrode. Because of the very large surface area the true current densities were quite small, in the

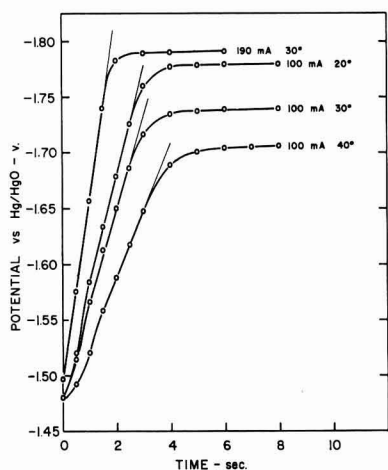


Fig. 1. Build-up of hydrogen overtoltage on zinc at constant current in 6.9N KOH at 30°C.

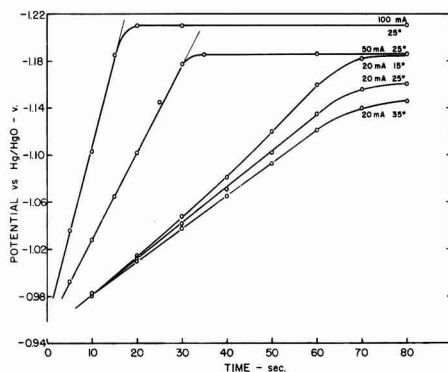


Fig. 2. Build-up of hydrogen overtoltage on cadmium at constant current in 6.9N KOH at 25°C.

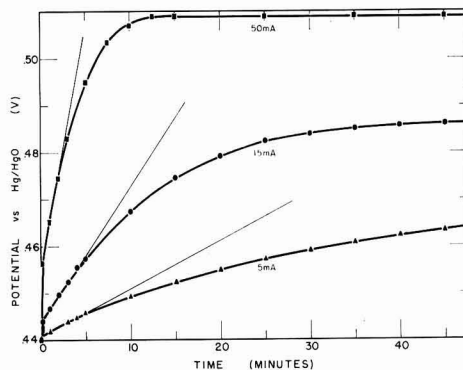


Fig. 3. Build-up of oxygen overtoltage on nickel oxyhydroxide at constant current in 6.9N KOH at 30°C.

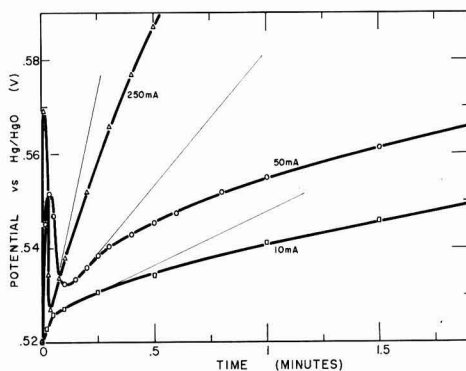


Fig. 4. Build-up of oxygen overtoltage on silver oxide (AgO) at constant current in 6.9N KOH at 30°C.

order of 10⁻⁶ to 10⁻⁸ amp/cm². However, hydrogen overtoltage on Zn, Cd, and Pb and oxygen overtoltage on NiO(OH), AgO, and PbO₂ are large and the listed current density values still fall into the Tafel region.

The double layer capacities, as determined from the charging curves and BET surface areas, are listed in Table II. The results for Pb and PbO₂ (1) are included for comparison. The double layer capacities tend to increase with temperature, but within the variations studied are rather independ-

Table II. Double layer or adsorption capacities from charging curves in the region of hydrogen and oxygen evolution

Electrode reaction and solution	Electrode material	Charging rate, $\mu\text{A}/\text{cm}^2$	Temp, $^{\circ}\text{C}$	Double layer capacity, $\mu\text{fd}/\text{cm}^2$
H_2 evolution 6.9N KOH	Zinc	2.50	20	26
			30	30
			40	41
H_2 evolution 6.9N KOH	Zinc	1.25	30	37
			2.50	30
			4.75	29
H_2 evolution 6.9N KOH	Cadmium	0.154	15	46
			25	50
			35	55
H_2 evolution 6.9N KOH	Cadmium	0.154	25	50
			0.385	51
			0.770	51
O_2 evolution 6.9N KOH	Nickel oxy-hydroxide	0.035	30	2040
			0.105	2120
			0.349	2010
O_2 evolution 6.9N KOH	Silver oxide	0.161	30	440
			0.806	850
			4.03	1100
H_2 evolution 5M H_2SO_4	Lead	0.0629	30	10.8
			0.314	10.5
			1.57	10.7
O_2 evolution 5M H_2SO_4	Lead dioxide	0.0142	30	126
			0.0568	139
			0.284	130

ent of the charging rate except for AgO. The capacities in the region of oxygen evolution are larger than in the region of hydrogen evolution. The charging curves for overvoltage build-up are linear for Zn, Cd, and Pb in the cathodic direction and for PbO_2 in the anodic direction. Nickel oxyhydroxide shows a charging curve with a sharp initial rise and a subsequent gradual, nonlinear rise with steadily increasing apparent capacity. It is evident that a discharge process is involved, probably the build-up of a layer of partially or completely discharged oxygen species or the formation of higher oxides. The charging curve for Ag is even more anomalous, showing an initial spike at the higher currents and a subsequent nonlinear rise, indicating a possible nucleation phenomena for formation of a higher silver oxide (4), involving a Faradaic component.

Overvoltage decay curves and gas desorption during decay are shown in Fig. 5 to 8. Overvoltage

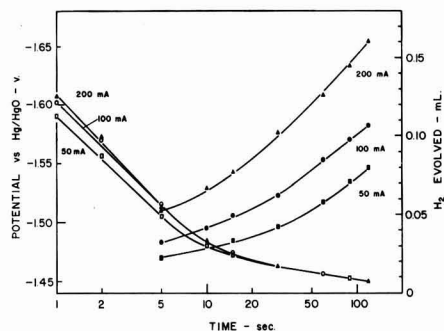


Fig. 5. Decay of hydrogen overvoltage and desorption of hydrogen gas on open circuit for a zinc electrode in 6.9N KOH at 30°C .

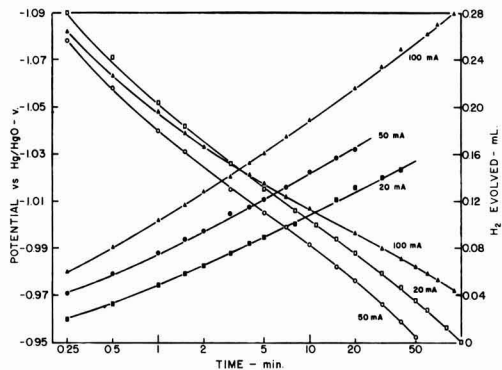


Fig. 6. Decay of hydrogen overvoltage and desorption of hydrogen gas on open circuit for a cadmium electrode in 6.9N KOH at 25°C .

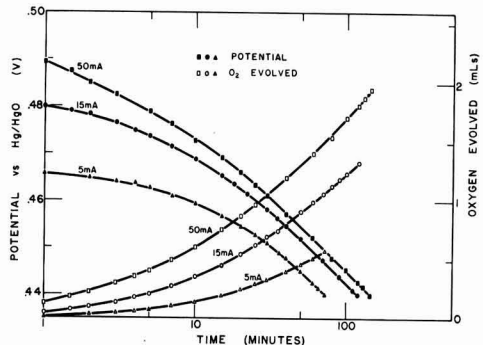


Fig. 7. Decay of oxygen overvoltage and desorption of oxygen gas on open circuit for a nickel oxyhydroxide electrode in 6.9N KOH at 30°C .

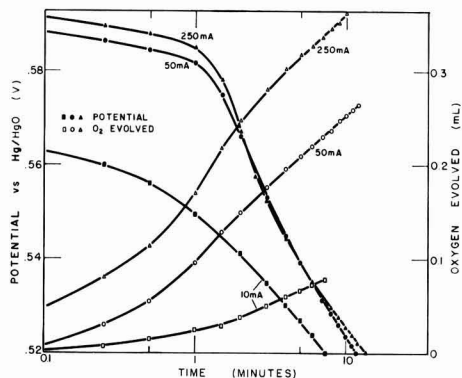


Fig. 8. Decay of oxygen overvoltage and desorption of oxygen gas on open circuit for a silver oxide electrode in 6.9N KOH at 30°C .

decay becomes generally linear with the logarithm of time or with the logarithm of $d\eta/dt$ (5), in the region between initial decay and approach of the stable open-circuit value. The slopes of the decay curves $d\eta/d(\log t)$, where η is the overvoltage and t the time, are listed in Table III and compared with the Tafel slopes obtained from steady-state overvoltage values. Agreement between these val-

Table III. Comparison of Tafel slopes $d\eta/d(\log i)$ with decay slopes $d\eta/d(\log t)$ where η is the overvoltage, i the current density, and t the time

Electrode reaction and electrolyte	Electrode material	Tafel slope $d\eta/d(\log i)$	Ovoltage decay slope $d\eta/d(\log t)$
H ₂ evolution 6.9N KOH	Zinc	0.138	0.120 to 0.135
H ₂ evolution 6.9N KOH	Cadmium	0.06 to 0.07 (slow)*	0.05 to 0.06
H ₂ evolution 6.9N KOH	Cadmium	0.13 to 0.14 (fast)*	0.13 (initial)*
O ₂ evolution 6.9N KOH	Nickel oxy- hydroxide	0.043	0.034
O ₂ evolution 6.9N KOH	Silver oxide	0.046	0.040
H ₂ evolution 5M H ₂ SO ₄	Lead	0.120 (fast)* 0.160 (slow)*	0.145
Oxygen evolu- tion 5M H ₂ SO ₄	Lead dioxide	0.095	0.078

* The terms "slow" and "fast" in Table III indicate the speed of taking the Tafel curve, in going from one current to the next. The term "initial" refers to the initial decay of overvoltage on Cd, not visible in Fig. 6.

ues is close. Deviations from linearity in the overvoltage decay curves may be due in part to other simultaneous reactions such as the spontaneous corrosion of metals (for Zn and Pb, e.g., under evolution of H₂), or the decomposition of oxides (5, 6).

The decay curves for silver oxide are anomalous and show an inflection. The voltage tends to stay at a definite plateau before decaying to the stable AgO/Ag₂O potential. This may be another indication for the presence of an unstable higher oxide (4).

High Tafel slopes for hydrogen overvoltage can be due to adsorption of foreign cations or desorption of foreign anions with increasing potential in the negative direction, such that the positive charge on the solution side of the double layer, and the negative charge on the metal side (and therefore the electrode voltage) are larger than for the same amount of reacting hydrogen ions or water dipoles but in the absence of the foreign species. High Tafel slopes for oxygen evolution (and decay slopes on the other hand) may be due to adsorption of foreign anions or desorption of foreign cations with increasing potential in the positive direction.

The decay of oxygen overvoltage is generally much slower than for hydrogen overvoltage. This may be due to the stronger adsorption forces for oxygen, limiting the desorption rate. Decay of hydrogen evolution on high overvoltage metals (Zn, Cd, Pb) is so fast that the initial portion (nonlinear range with logarithm of time) of the decay curve was not measurable with the electrometer-input amplifier and ¼ second recorder used here. In the decay curves for Zn and Cd the first points recorded were at -1.61 and -1.09 v vs. HgO, respectively, whereas the stable hydrogen overvoltages were about -1.75 and -1.21 v vs. HgO, respectively. The initial decay slope for Cd was quite

steep, about -0.12 as compared to the average of -0.07 in the later stages. With the Cd electrode it seems to be particularly evident that more than one adsorption state is present on the electrode.

The term adsorbed species here means the charged reacting ions in the double layer as well as adsorbed partially discharged species. It must be pointed out that quite generally both reacting ions in the double layer and various adsorbed partially discharged species will be present. The latter contribute to the potential by the polarity of the surface-bond only, like adsorbed atoms on solid-gas interfaces may influence the work function.

In charging up the double layer at constant current, the amount of purely ionic and partially discharged species built into the double layer will depend somewhat on the charging rate. In the experiments reported here, the charging currents were relatively small, and sufficient time was allowed to form adsorbed discharged products. Nevertheless, as shown below, a smaller amount of partially discharged adsorbed species were apparently present during overvoltage build-up than at steady state for a given electrode potential.

During overvoltage decay and corresponding desorption of gas one must consider that removal by discharge of the ionic charges in the outer part of the double layer will have a large influence on the potential because of their small specific capacity. On the other hand, removal of the inner partially discharged species will have a relatively small effect on voltage. The relation between overvoltage decay and amount of gas desorbed must therefore not be expected, a priori, to be a straight line in fast transient experiments.

In Fig. 9 to 12 the amount of gas desorbed has been related to the decay in overvoltage from various prepolarizing currents. It is interesting to note that the number of partially discharged adsorbed hydrogen species seems to increase in the sequence lead < zinc < cadmium. This is also the sequence of the capacities as seen in Table II. Oxygen overvoltage on nickel hydroxide, silver oxide, and lead dioxide is determined mainly by strongly adsorbed, partially discharged oxygen species, which desorb relatively slowly.

Since one must associate each molecule of desorbed hydrogen and oxygen with 2 and 4 elec-

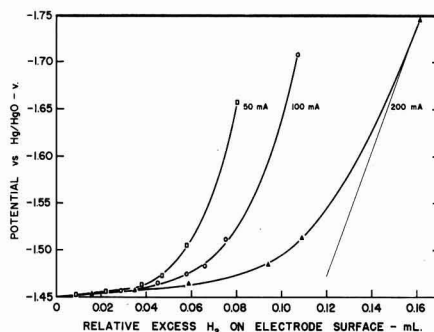


Fig. 9. Relation between electrode potential and desorbed hydrogen during open circuit decay for a Zn electrode in 6.9N KOH at 30°C.

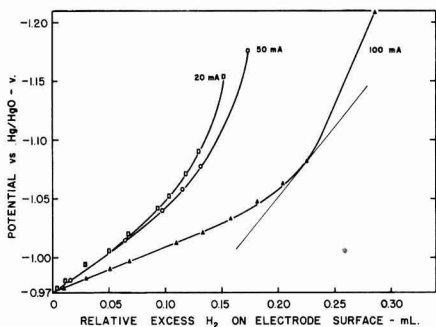


Fig. 10. Relation between electrode potential and desorbed hydrogen during open-circuit decay for a Cd electrode in 6.9N KOH at 25°C.

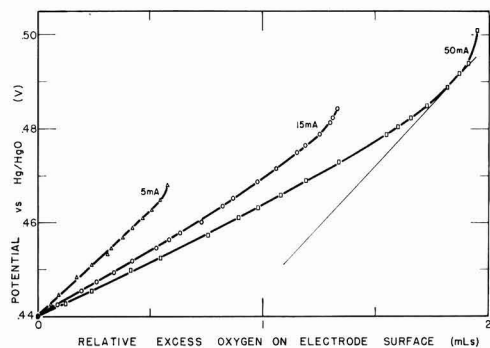


Fig. 11. Relation between electrode potential and desorbed oxygen during open-circuit decay for a NiO(OH) electrode in 6.9N KOH at 30°C.

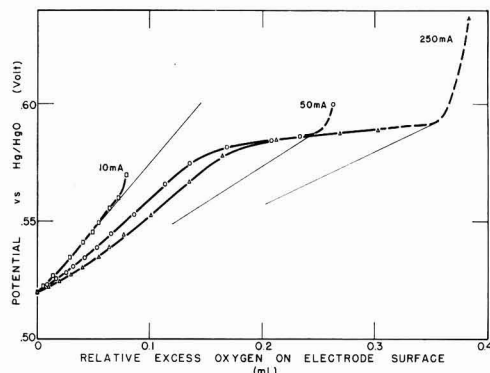


Fig. 12. Relation between electrode potential and desorbed oxygen during open-circuit decay for a AgO electrode in 6.9N KOH at 30°C.

trons, respectively, one can calculate how the voltage of the double layer capacitor should be decreased by the electricity associated with the desorbing gas. If one uses values of the double layer capacitor, as determined from the charging curves, one obtains the straight lines shown in Fig. 9 to 12. The initial decay of overvoltage usually follows these predicted lines rather closely. However, deviations are observed in most cases during the later stages of decay such that more gas is desorbed than

expected from the theoretical lines. While this might in part be due to self-discharge phenomena of the electrodes approaching the "stable" open-circuit state, it must be considered that strongly adsorbed species will desorb last and that the average adsorption state and charge distribution in the double layer are changing during decay. The deviations are to be expected when the slope dV/dt (where V is the voltage and t the time) is widely different between constant current charging and open circuit decay.

Deviations of the curves from the theoretical straight lines also suggest that steady-state adsorption conditions may not have been reached during the initial charging transient, from which the double layer capacities were determined. In general, when a comparison is made for the same electrode potential, a larger number of partially discharged, adsorbed species is present at steady state than after a relatively quick charging transient. In other words, on prolonged polarization additional hydrogen or oxygen is being adsorbed but without an associated large increase in voltage.

Two abnormalities should be noted: (A) In the case of oxygen overvoltage on AgO, oxygen must be adsorbed in a state which justifies the expression of a "higher oxide." In the curves of oxygen overvoltage decay vs. excess gas (Fig. 12), a definite plateau is apparent at 0.585 v, corresponding to the potential of the "higher oxide" (4). (B) In the case of hydrogen overvoltage decay on cadmium the initial slope between potential and excess hydrogen is steeper than the theoretical slope (Fig. 10). This must be connected to the fact that the initial decay rate was faster than the build-up rate. The initial decay corresponds to a smaller specific capacity of the ionic charges discharging first.

While during decay of overvoltage, nonsteady states may produce abnormal hysteresis effects, it is interesting to note that in general a nearly linear relation can be established between the steady-state overvoltage values and the total amount of excess (desorbed) gas. These relations are summarized in Table IV and Fig. 13. Included are values for Pb and PbO₂ from reference (1). The slopes of these lines can be used to compare the average state of charge of adsorbed species during steady

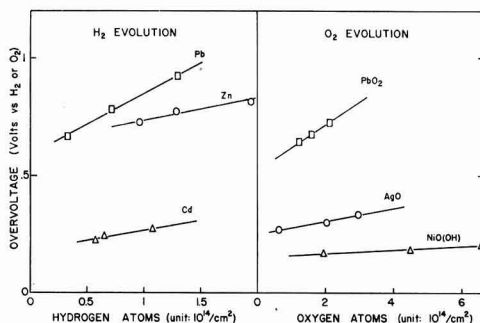


Fig. 13. Steady-state overvoltage values as a function of total amount of desorbed gas atoms per BET cm² after interruption of current.

• Table IV. Steady-state overvoltage values, true current densities, and total amount of gas desorbed during subsequent over-voltage decay (excess gas)

Electrode reaction electrolyte temperature	Electrode material	"Stable" open-circuit potential vs. H ₂ or O ₂ , v	Over-voltage above "stable" O.C. potential, v	True current density, $\mu\text{A}/\text{cm}^2$	Total desorbed hydrogen or oxygen atoms per cm ² of true (BET) area, $\times 10^{14}$
H ₂ evolution 6.9N KOH 30°C	Zinc	-0.511	-0.215	1.25	0.97
		vs. H ₂	-0.265	2.50	1.29
			-0.303	4.75	1.95
H ₂ evolution 6.9N KOH 25°C	Cadmium	+0.023	-0.244	0.154	0.574
		vs. H ₂	-0.265	0.385	0.657
			-0.298	0.770	1.08
O ₂ evolution 6.9N KOH 30°C	Nickel oxyhydroxide	+0.142	+0.028	0.035	1.96
			+0.044	0.105	4.50
		vs. O ₂	+0.061	0.349	6.59
O ₂ evolution 6.9N KOH 30°C	Silver oxide	+0.202	+0.070	0.161	0.623
		vs. O ₂	+0.100	0.806	2.05
			+0.137	4.03	2.98
H ₂ evolution 5M H ₂ SO ₄ , 30°C	Lead	-0.372	-0.293	0.0629	0.33
		vs. H ₂	-0.410	0.314	0.72
			-0.553	1.57	1.3
O ₂ evolution 5M H ₂ SO ₄ , 30°C	Lead dioxide	+0.487	+0.158	0.0142	1.24
		vs. O ₂	+0.190	0.0568	1.61
			+0.242	0.284	2.12

state, as compared with the adsorption state during initial (transient) overvoltage build-up. In general, the average charge of the adsorbed species at steady state is smaller than the average charge during transient overvoltage build-up.

The relation between the total number of atoms desorbed per BET surface area during overvoltage decay and steady-state overvoltage is of interest with regard to the theory of electrostatic interaction in the double layer. An approximately linear relation between "surface coverage" and voltage has been postulated on theoretical grounds (7). If the number, and therefore the charge, of the reacting species on the solution side of the double layer is proportional to the voltage, the electrostatic interaction energy per particle with average charge $Z_i e_0$ is given by

$$(Z_i e_0 / q) \int_0^V q dV = Z_i e_0 V / 2$$

where q is the charge and V the potential difference of the double layer (7). This term must then be added to the chemical energy to obtain the total energy, determining the Boltzmann probability $\exp\{-[(Z_i e_0 V / 2) + \epsilon] / KT\}$ for reacting particles in the double layer. This then corresponds to the exponential term in the Volmer equation.

Table II and Fig. 13 show that electrodes with small double layer capacities have high overvoltage values, and vice versa. Small double layer capacities correspond to small amounts of partially discharged adsorbed species. Also, the rate of decay

of overvoltage and Tafel slope decrease with increasing relative amount of partially discharged adsorbed species. These findings are in agreement with the prediction (8) that overvoltage decreases with increasing adsorption energy.

Acknowledgment

The authors are indebted to W. J. Burgess and M. L. Block of the Physical Chemistry Division for assistance in BET measurements and to C. G. Grimes, Vice President for Research of the Electric Storage Battery Company, for permission to publish this investigation.

Manuscript received July 26, 1960; revised manuscript received Dec. 12, 1960. This paper was prepared for delivery before the Philadelphia Meeting, May 3-7, 1959.

Any discussion of this paper will appear in a Discussion Section to be published in the December 1961 JOURNAL.

REFERENCES

1. P. Rüetschi, J. B. Ockerman, and R. Amlie, *This Journal*, **107**, 325 (1960).
2. P. Rüetschi, R. T. Angstadt, and B. D. Cahan, *ibid.*, **106**, 547 (1959).
3. P. L. Bourgault and B. E. Conway, *J. Electroanal. Chem.*, **1**, 8 (1959/1960).
4. B. D. Cahan, J. B. Ockerman, R. T. Amlie, and P. Rüetschi, *This Journal*, **107**, 725 (1960).
5. V. L. Kheifets and A. B. Sheinin, *Zhur. Fiz. Khim.*, **33**, 1945 (1959).
6. P. C. Milner, *This Journal*, **107**, 343 (1960).
7. P. Rüetschi, Submitted to *This Journal*.
8. P. Rüetschi, *This Journal*, **106**, 819 (1959).

Kinetics of Hydrogen Evolution at Zero Hydrogen Partial Pressure

Sigmund Schuldiner

United States Naval Research Laboratory, Washington, D. C.

ABSTRACT

Polarization curves for the hydrogen evolution reaction on platinum and rhodium were determined in 1M H₂SO₄ solution stirred rapidly with helium. Here the partial pressure of hydrogen gas above the solution was virtually equal to zero. Experimental results indicated that for both metals the rate-determining step in the lowest current density range was primarily the electrochemical desorption of hydrogen atoms. As the current density increased the rate-determining step changed to one that was primarily controlled by atomic combination. Kinetic equations were derived and the calculated relationships compared favorably with the experimental results.

When the partial pressure of hydrogen on an inert hydrogen electrode, e.g., Pt/H₂, is dropped to zero, the reversible $2H^+ + 2e^- = H_2$ reaction no longer occurs on the metal surface. If under these conditions the noble metal electrode is cathodized, hydrogen will be evolved, and if the hydrogen partial pressure above the solution is maintained virtually equal to zero, by sweeping out the evolved hydrogen with an inert gas, as fast as it is formed, the rate of the reverse ionization reaction will effectively be equal to zero. Breiter and Clamroth (1) used this fact to study the hydrogen evolution rate-determining steps on Pt and Au electrodes. In this investigation this technique, with rigorous control of electrode cleanliness and precision of potential measurements, was used to determine the rate-controlling steps on Pt and Rh electrodes.

Experimental Methods and Results

The Teflon cell and experimental method were about the same as previously used (2, 3). One change was in the use of a hydrogen-filled palladium tube anode (4) so that the oxidation reaction taking place at this electrode was the ionization of atomic hydrogen diffusing through the wall of the palladium tube. Also both an α Pd-H/H⁺ electrode (5) and a L&N miniature glass electrode were used as reference electrodes. Both the Pt (99.99%) and Rh (99.5+%) electrodes were small spheres at the end of a short length of wire and each had an apparent area of 0.10 cm². The solution was always 1M H₂SO₄ stirred with helium flowing through the cell at a rate greater than 200 ml/min. Potential measurements were independent of further increases in the helium flow rate.

A particular run was carried out in the following way. After pre-electrolytic cleaning of the solution in a hydrogen atmosphere and activation of the electrodes by alternate anodic and cathodic polarization, purified hydrogen gas flowed through the cell until all the electrodes in the cell came to their equilibrium potentials. The potential of the α Pd-H/H⁺ reference electrode referred to that of a Pt/H₂ electrode was + 0.049 ± 0.001 v. The potential of the miniature glass electrode referred to a Pt/H₂ electrode was + 0.650 ± 0.002 v. The poten-

tial of each of these reference electrodes was checked carefully before and after each run and although the potential could vary, from day to day, within the limits shown, the check for any particular run was within 0.0005 v. After the equilibrium potential of each electrode in the cell was determined, the hydrogen flow through the cell was replaced with a flow of purified helium. A slow flow of hydrogen was maintained only in the interior of the palladium tube anode. The open-circuit potential change on the Pt or Rh electrode was followed on a L&N pH indicator connected to a Sargent Recorder. After about 10 hr, the potential of either a Pt or Rh electrode became fairly steady at a value of about 0.75 v vs. the α Pd-H/H⁺ electrode. This potential was probably influenced by minute amounts of oxygen in the cell. Upon cathodic polarization the potential became increasingly less positive and in the current density ranges shown in Fig. 1 and 2 gave the polarization behavior shown. Potential vs. current density relations were determined for both increasing and decreasing current values. On a given day at least three runs up and down the polarization curve were made and the potential values normally did not deviate from one another by more than a millivolt. The experimental

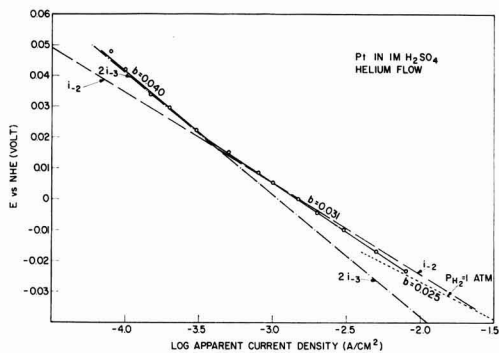


Fig. 1. Log cathodic current density vs. potential, for platinum: o, experimental values; —, calculated values for fast combination step, 1-2; - · - calculated values for fast electrochemical desorption step, 2i-3.

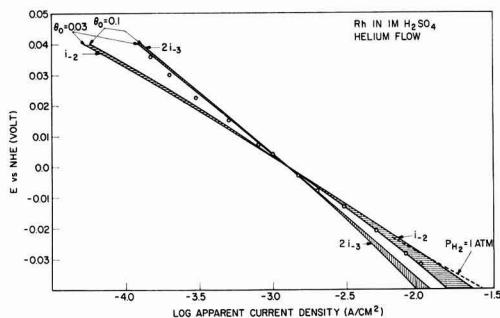


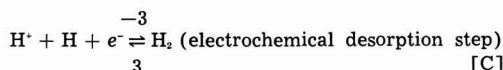
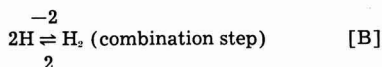
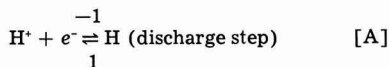
Fig. 2. Log cathodic density vs. potential, for rhodium: \circ , experimental values; horizontal shaded area, calculated region for fast combination step i_{-2} , $0.03 \leq \theta_0 \leq 0.1$; vertical shaded area; calculated region for fast electrochemical desorption step, $2i_{-3}$, $0.03 \leq \theta_0 \leq 0.1$.

results shown as circles in Fig. 1 and 2 represent the average values for at least 10 determinations on several different days. For most runs the α Pd-H/H⁺ reference electrode was used because the small potential difference between this reference and the working cathode allowed an accurate reading of the potential on an expanded calibrated recorder scale to better than 0.5 mv. Polarization curves were also checked with the miniature glass electrode. All potentials given in the figures and in the remainder of this paper are referred to the normal hydrogen electrode (NHE).

Although solution IR values were determined by the interrupter method (6) and the polarization values shown in Fig. 1 and 2 were corrected for this error, polarization of the electrodes was carried out with a constant current supply and current values were determined with a Hewlett-Packard d-c microammeter. The temperature was $26^\circ \pm 1^\circ\text{C}$.

Derivation of Kinetic Equations

Since diffusion effects are minimized, one can visualize that the hydrogen evolution mechanism may consist of the following steps:



where H⁺ represents hydronium ions in the double layer and H hydrogen atoms adsorbed on the electrode surface. Experimental data (2, 3, 6-8) indicate that on Pt and Rh the rate-controlling step is the combination of adsorbed hydrogen atoms to molecules. There is a possibility, however, that when the surface coverage of active adsorbed hydrogen atoms (2, 9) is very low the electrochemical desorption step may predominate, since the rate of the combination step is dependent on the square of the coverage, whereas the parallel electrochemi-

cal desorption step depends on the coverage to the first power. Considering that the discharge step is in virtual equilibrium and that a Langmuir adsorption isotherm applies to the active adsorbed hydrogen atoms,

$$i_{-1} = k_{-1}(\text{H}^+) (1 - \theta) \exp(-\alpha EF/RT) \quad [\text{D}]$$

$$i_1 = k_1 \theta \exp[(1 - \alpha)EF/RT] \quad [\text{E}]$$

and,

$$\theta/(1 - \theta) = K_1(\text{H}^+) \exp(-EF/RT) \quad [\text{F}]$$

where θ is the fraction of available surface covered with active atomic hydrogen and E is the measured potential vs. the normal hydrogen electrode, F is the Faraday, R the gas constant, and T the absolute temperature. The H⁺ concentration in the double layer in pure acid solution can be considered to be constant, as was shown by Frumkin (10, 11). The fraction of available surface covered with active hydrogen at zero potential is defined as θ_0 . Hence,

$$\text{at } E = 0, K_1(\text{H}^+) = \theta_0/(1 - \theta_0) \text{ and}$$

$$\theta/(1 - \theta) = [\theta_0/(1 - \theta_0)] \exp(-EF/RT) \quad [\text{I}]$$

Fast discharge followed by slow combination.—If this mechanism is considered to be the only one operative then the total cathodic current density will be equal to i_{-2} . This is because the hydrogen partial pressure being virtually equal to zero under the experimental conditions used, the molecular atomization step i_2 will be negligible. Then

$$i_{-2} = k_{-2} \theta^2 \quad [\text{G}]$$

When $E = 0$, $\theta = \theta_0$ and i_{-2} is defined as $i_{-2,0}$, then $i_{-2,0} = k_{-2} \theta_0^2$, and

$$i_{-2} = i_{-2,0} \theta^2 / \theta_0^2 \quad [\text{H}]$$

Using Eq. [1]

$$i_{-2} = i_{-2,0} [(1 - \theta)^2 / (1 - \theta_0)^2] \exp(-2EF/RT) \quad [\text{I}]$$

Solving Eq. [1] for θ ,

$$\theta = \frac{\theta_0 \exp(-EF/RT)}{(1 - \theta_0) + \theta_0 \exp(-EF/RT)} \quad [\text{J}]$$

Fast discharge followed by slow electrochemical desorption.—If this mechanism is the only one considered to be operative, then since only one half of the current flow is used in the electrochemical desorption step, the total cathodic current density will be equal to $2i_{-3}$. In this case also the dissociation ionization reaction i_3 is effectively equal to zero. Then

$$2i_{-3} = 2k_{-3}(\text{H}^+) \theta \exp(-\alpha EF/RT) \quad [\text{K}]$$

At $E = 0$, $\theta = \theta_0$,

$$2i_{-3,0} = 2k_{-3}(\text{H}^+) \theta_0 \quad [\text{L}]$$

$$2i_{-3} = 2i_{-3,0} (\theta/\theta_0) \exp(-\alpha EF/RT) \quad [\text{M}]$$

Using the relationship given in Eq. [1]

$$2i_{-3} = 2i_{-3,0} [(1 - \theta)/(1 - \theta_0)] \exp[-(1 + \alpha)EF/RT] \quad [\text{N}]$$

where θ has the value given in Eq. [4].

Calculation of Polarization Curves

Assuming that either of the atomic desorption steps is the only means of desorbing hydrogen, polarization curves for Pt and Rh were calculated using Eq. [3], [4], and [5]. The measured polariza-

zation values for Pt shown in Fig. 1 (circles) indicated that two straight lines could be drawn through them. The higher Tafel slope of 0.040 indicated that the electrochemical desorption step was predominant in this region whereas the lower Tafel slope of 0.031 indicated that the combination step dominated at the higher current density values. By extrapolating the 0.040 slope through zero potential a $2i_{\infty,3}$ value of -1.077×10^{-3} amp/cm² was obtained. The 0.031 slope intersects the zero potential at an $i_{\infty,2}$ value of -1.5×10^{-3} amp/cm². These values are only approximate because neither of these slopes is due purely to one mechanism or the other. It has also been shown by previous work (3) that at these current density values the fraction of available electrode surface covered with active hydrogen is very small (< 0.001). Hence, for both the electrochemical desorption and combination steps, the θ_0 values at $E = 0$ will be negligible compared to unity. Hence the $(1 - \theta_0)$ term in Eq. [3] and [5] will reduce to unity and Eq. [4] reduces to

$$\theta = \frac{\theta_0 \exp(-EF/RT)}{1 + \theta_0 \exp(-EF/RT)} \quad [K]$$

Using the approximate values for $2i_{\infty,3}$ and $i_{\infty,2}$ obtained from Fig. 1 and assuming that $\alpha = 0.5$, $2i_{\infty,3}$ and $i_{\infty,2}$ were calculated for given values of E . The calculated curves are shown as broken lines in Fig. 1.

The measured polarization values for Rh shown in Fig. 2 (circles) cannot be divided accurately into two separate Tafel lines as in the case of Pt. The reason for this can be seen readily when one realizes that for Rh the amount of available surface covered with active hydrogen at $E = 0$ is much greater than for the case of Pt, and there no longer is a linear relationship between E and $\log(-i)$. Results from this laboratory (2) indicate that $0.03 < \theta_0 < 0.1$ at the current density (-1.24×10^{-3} amp/cm²) found by interpolation for $E = 0$. Such an estimate can be made from the published values because in the current density region where the back reaction is negligible, θ values are largely independent of hydrogen partial pressure and are primarily dependent on current density (2, 3). It should also be noted that the definition of θ_0 used in this paper is different from that normally used in conjunction with a hydrogen equilibrium electrode. This is because when the partial pressure of hydrogen is reduced to zero, an equilibrium H_2/H^+ electrode no longer exists. Therefore, θ_0 (also $i_{\infty,2}$ and $i_{\infty,3}$) is defined here in terms of the measured potential being equal to zero and not the current density being equal to zero. In this case, the term overvoltage is no longer applicable since it is normally defined as $\eta = E - E_{eq}$, where E_{eq} is the equilibrium potential.

Using the $E = 0$ approximate current density value of -1.24×10^{-3} amp/cm² and θ_0 values of both 0.03 and 0.1, the curves shown bounding the shaded areas in Fig. 2 are obtained.

Discussion

Owing to the relatively small number of active hydrogen atoms adsorbed on the Pt surface in the

current density range used, the interpretation of the experimental results shown in Fig. 1 and their comparison with the calculated curves are rather simple and straightforward. These results clearly indicate that the desorption of hydrogen atoms from the Pt surface by the combination and electrochemical steps are indeed occurring in parallel. In the lower current density range, electrochemical desorption predominates, and in the higher current density range the combination step predominates.

The dashed line marked $P_{H_2} = 1$ atm, shown in both figures, shows the experimental results obtained for both Pt (3) and Rh (2) at this hydrogen pressure. The closeness of this curve with the Pt and Rh values at the higher current densities confirms that the surface coverage with active hydrogen is largely independent of the hydrogen partial pressure. The difference in slope between the values at 1 atm and at zero hydrogen partial pressure is due to the effects of both the electrochemical desorption in the hydrogen-free solution and the presence of some back reaction in the hydrogen-saturated solution (3).

The polarization of Rh is much more complex because the surface coverage with active atomic hydrogen is significant compared to unity. However, even in this case it is apparent from the data shown in Fig. 2 that the same situation prevails as in the case of Pt. Both atomic desorption steps are evidently operating in parallel, and in the lower current density range the electrochemical desorption predominates, whereas at higher current densities the combination step is more important. Here it should be noted that neither the $i_{\infty,2}$ nor $2i_{\infty,3}$ curves are straight lines, and even though one may be able to draw one or two fairly good straight lines through the experimental points this is undoubtedly owing to the combined influence of the two mechanisms rather than symptomatic of any one particular mechanism.

The fact that the crossover from electrochemical desorption to combination occurs at a significantly lower current density for Pt than for Rh indicates that the rate constant for the combination reaction is higher for Pt. This is most likely owing to a lower heat adsorption of hydrogen atoms on the Pt surface. Thus, even though the number of active hydrogen atoms at any given current density is higher for Rh, their mobility is evidently lower.

Even though the total number of hydrogen atoms associated with the surface may be high, Bockris and Potter (9) and the author (2) pointed out that only a small fraction of these hydrogen atoms may be active. This means that the active hydrogen atoms are those hydrogen atoms on the surface which are in rapid equilibrium with hydrogen ions in solution. Under zero current conditions the active hydrogen atoms are also in rapid equilibrium with the hydrogen gas above the solution. When the partial pressure is reduced to zero, the number of active hydrogen atoms on the surface at zero current density is also equal to zero. On cathodic polarization the number of active hydrogen atoms increases because they are not now in equilibrium with the hydrogen partial pressure. For these elec-

trode systems, one is dealing not simply with a noble metal/hydrogen-atom system, but rather with a (noble metal-associated hydrogen)/active hydrogen-atom system. The heat of adsorption of hydrogen atoms on the noble-metal-associated hydrogen electrode should be much lower than that found for small amounts of hydrogen on these metals in gas phase measurements (12).

A calculation of the activation energy for the reaction and the heat of adsorption of active hydrogen on Rh was made possible by using the value of $K_L = 0.0009$ for the Langmuir constant found in a previous paper (2). Using the relationship of Parsons (13) $K_L = \exp(-\Delta G^\circ/RT) = 0.0009$ where ΔG° is the standard free energy change for the reaction $H_2 + 2M = 2H - M$, the standard states being 1 atm of gaseous H_2 and $\theta = 1/2$ for adsorbed atoms, one obtains $\Delta G^\circ = 4.2$ kcal/mole.

The heat of adsorption q of H_2 was calculated using the methods of Trapnell (14), assuming both a mobile and immobile layer. For either case, q was equal to about 10.5 kcal/mole. This compares with the value of about 28 kcal/mole found by Beeck (12) for a small fraction of surface coverage. This indicates that the hydrogen which is tightly bonded to the Rh surface effectively reduces the heat of adsorption of active hydrogen.

The results for Pt given in Fig. 1 show the effects of both the electrochemical desorption and combination steps and diverge from the results and conclusions of Breiter and Clamroth (1). These investigators interpreted their results for active Pt

as showing that the rate-controlling step was the diffusion of molecular hydrogen away from the electrode surface. The results given in this paper show that this diffusion-controlling mechanism is not likely since a change to the 0.040 slope could not be explained by such a diffusion-controlled step.

Manuscript received Sept. 6, 1960; revised manuscript received Dec. 7, 1960. This paper was prepared for delivery before the Indianapolis Meeting, April 30-May 3, 1961.

Any discussion of this paper will appear in a Discussion Section to be published in the December 1961 JOURNAL.

REFERENCES

1. M. Breiter and R. Clamroth, *Z. Elektrochem.*, **58**, 493 (1954).
2. S. Schuldiner, *This Journal*, **107**, 452 (1960).
3. S. Schuldiner, *ibid.*, **106**, 891 (1959).
4. S. Schuldiner, *ibid.*, **106**, 440 (1959).
5. S. Schuldiner, G. W. Castellan, and J. P. Hoare, *J. Chem. Phys.*, **28**, 16 (1958).
6. S. Schuldiner, *This Journal*, **99**, 488 (1952).
7. S. Schuldiner, *ibid.*, **101**, 426 (1954).
8. J. O'M. Bockris, I. A. Ammar, and A. K. M. S. Huq, *J. Phys. Chem.*, **61**, 879 (1957).
9. J. O'M. Bockris and E. C. Potter, *ibid.*, **20**, 614 (1952).
10. A. N. Frumkin, *J. Phys. Chem. (USSR)*, **9**, 629 (1937).
11. A. N. Frumkin, *Acta Physicochim.*, **6**, 502 (1937).
12. O. Beeck, *Discussion Faraday Soc.*, **8**, 118 (1950).
13. R. Parsons, *Trans. Faraday Soc.*, **54**, 1053 (1958).
14. B. M. W. Trapnell, "Chemisorption," Butterworths Scientific Publications, London (1955).

Effect of the Helmholtz-Gouy Double Layer on the A-C Impedance of the Copper/Copper Oxide Electrode in Aqueous Solution

G. R. Hoey¹

Division of Applied Chemistry, National Research Council, Ottawa, Ontario, Canada

ABSTRACT

The a-c impedance of the copper/copper oxide/metal capacitor is compared with the a-c impedance of the copper/copper oxide electrode in aqueous solution in the frequency range 40 cps to 50 kcps. The copper/copper oxide electrodes were formed by the oxidation of copper at 1068°C. Frequency dispersion of the parallel resistance and capacitance of the oxide capacitor is attributed to relaxation processes involving positive holes. The impedance of the copper/copper oxide electrode in aqueous solution is in quantitative agreement with the impedance of the dry copper oxide capacitor at $f > 5$ kcps. At lower frequencies the former exhibits a frequency dispersion due to Maxwell-Wagner-type two layer dielectric polarization; the two layer dielectric being the oxide and the Helmholtz-Gouy double layer. The equivalent RC circuits of the oxide capacitor and the oxide electrode are discussed.

In studies of the a-c impedance of the filmed electrodes tantalum/tantalum oxide (1), zirconium/zirconium oxide (1), uranium/uranium oxide (2), and passivated nickel (3), the experimentally

found dispersion of capacitance and resistance has been interpreted in terms of oxide film properties; the impedance of the Helmholtz-Gouy double layer was either assumed to have a value independent of film properties or to have a value for thick films negligibly small compared to that of the oxide. The

¹ Present address: Canadian Industries Limited, Central Research Laboratory, McMasterville, Quebec, Canada.

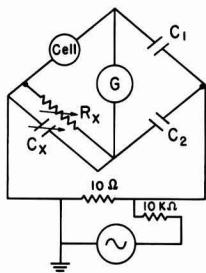


Fig. 1. A-C impedance bridge

present paper on the frequency dispersion of the a-c impedance of the copper/copper oxide electrode in aqueous solution establishes that for a thick compact copper oxide scale on copper these assumptions are invalid at $f < 5$ kcps. This conclusion is drawn from a comparison of the a-c impedance of the copper/copper oxide metal capacitor with that of the copper/copper oxide electrode in aqueous solution. The copper/copper oxide electrode is analogous to a two-layer dielectric of oxide and water and as will be shown exhibits a Maxwell-Wagner-type frequency dispersion of the a-c impedance (4, 5). Maxwell-Wagner dielectric polarization is not peculiar to the copper/copper oxide electrode and would occur at all two-layer dielectrics in a frequency range which is dependent on the particular two-layer structure.

Experimental

The Schering type a-c impedance bridge used in this study is illustrated in Fig. 1. The detector G is a Tektronix type 545 oscilloscope with a 53/54 E differential input preamplifier (input impedance = 10 M Ω) and the oscillator is a Hewlett-Packard Model 202B low-frequency oscillator. C_1 is a General Radio decade capacitor type No. 219-K (1 μ F max) and R_x is an a-c-d-c L&N decade resistance No. 4755 (10 K Ω max). C_1 and C_2 are Astron capacitors the ratio of which was varied by switching in or out a number of capacitors in series and parallel. The bridge was balanced for a particular C_1/C_2 ratio by varying C_x and R_x to give a minimum Y deflection on the oscilloscope. The capacitance ratio C_1/C_2 from 40 cps to 50 kcps was determined by using standard resistances and capacitors in the cell arm of the bridge. All components of the bridge including the cell were shielded. The shields were grounded. The input to the bridge from the oscillator was variable from 5 to 1 mv. The impedance measurements were made on the cell without applied d-c. The parallel capacitance (C_p) and parallel resistance (R_p) of the cell are given by the equations:

$$C_p = (C_1/C_2) \cdot C_x \quad [1]$$

$$R_p = (C_2/C_1) \cdot R_x \quad [2]$$

The accuracy of the impedance bridge is 5% over the ranges: frequency range, 40 cps to 50 kcps; capacitance range, 10^{-8} to 50 μ F; and resistance range, 10 Ω to 50 K Ω .

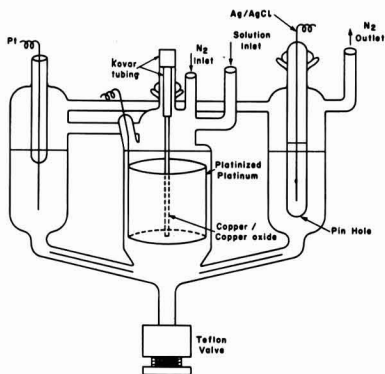
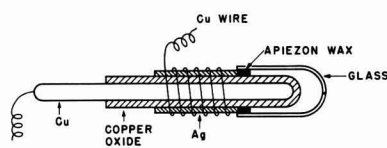


Fig. 2. Electrolytic cell

The cell, Fig. 2, consisted of three compartments between which ion diffusion was minimized by capillary connections. The impedance measurements were made on the main compartment which contains the Cu/Cu₂O wire electrode and the coaxial platinized platinum electrode. A Pt working electrode which was not used for this study and a Ag/AgCl/0.1N KCl reference electrode are contained in the other two compartments. The runs were carried out in a closed system with water bubbler outlets in an atmosphere of nitrogen purified by the method of Meyer and Ronge (6). A buffer solution, 0.1M Na₂HPO₄ and 0.02M NaH₂PO₄ · H₂O (pH = 7.4) was used and when required was purified by preelectrolysis and siphoned from a reservoir into the cell under nitrogen pressure. The potential of the Cu/Cu₂O electrode was recorded on a Speedomax recorder.

The Cu/Cu₂O electrodes were formed by the oxidation of commercially pure copper wire (0.27 cm diameter) at 1068°C for 3 min in dry air. By spectrographic analysis the impurities in the Cu were < 0.01% and the impurities in the copper oxide scale were < 0.05%. It was necessary to place a glass cap on the end of the electrode using Apiezon wax since spalling off of the oxide generally occurred at the end of the Cu wire on cooling after the high temperature oxidation. A W. Edwards and Co. Model 12EA/317 coating unit was used to coat some of the electrodes with films of silver (ca. 2000Å of Ag). Masking of the electrode for this purpose was accomplished by spaghetti tubing. A diagram of a coated electrode is shown in Fig. 3.

Oxide thicknesses were determined by weight measurements before and after removal of oxide by immersion in 1/1 conc HCl with 2% rhodine which inhibits the reaction of acid with Cu; this solution does not react significantly with Cu in the 10 min required to remove the oxide.

Fig. 3. Cu/Cu₂O/ capacitor

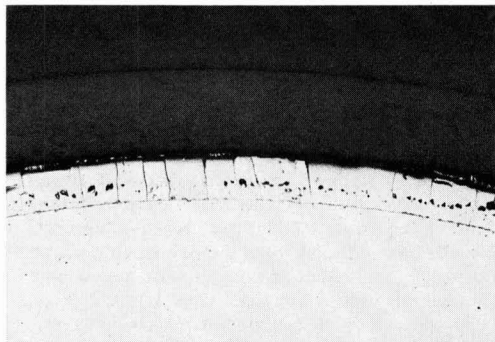


Fig. 4. Metallographic cross section of Cu/Cu₂O electrode; etched. Magnification 250X before reduction for publication.

Results

A metallographic cross section of the oxide scale after etching is shown in Fig. 4. The scale thickness determined from the micrograph, 4×10^{-3} cm, agrees well with the scale thickness of 4.4×10^{-3} cm determined by weight measurements. By x-ray diffraction, the scale is predominantly Cu₂O (ca. 90%) containing outer layers of CuO and an unidentified copper oxide as the remainder in about equal amounts.

The capacitance per unit length of a cylindrical oxide capacitor ($\mu\text{F cm}^{-1}$) is given by the equation:

$$C' = \epsilon \cdot 10^{-9} / 1.798 \ln(1 + d/r) \quad [3]$$

where ϵ is the dielectric constant, d is the oxide scale thickness, and r is the radius of the copper wire. For the case of $d < r$ Eq. [3] approximates to the equation for the parallel plate capacitor, i.e.

$$C = \epsilon \cdot 10^{-9} / 3.595 \pi d \quad [4]$$

where C is the capacitance per unit area ($\mu\text{F cm}^{-2}$). Equation [4] holds to within 3% for the oxide thicknesses studied. The calculated value of the capacitance from Eq. [4] C_a based on a dielectric constant of 10.5 (7), is given for three film thicknesses (d) in Table I. C_b the value of the capacitance obtained by the extrapolation of the C_p vs. $1/f$ curves to infinite frequency and the apparent dielectric constant ϵ_b obtained from C_a are also tabulated.

In Fig. 5, C_p and R_p are plotted vs. $\log_{10} f$ for a Cu/Cu₂O electrode (scale thickness = 6.5×10^{-3} cm) immersed in Hg and for the same electrode coated with Ag, i.e., the Cu/Cu₂O/Ag capacitor. In Fig. 6

Table I. Dielectric constant of the copper oxide scale

$10^8 d$ (cm)	$10^4 C_a$ ($\mu\text{F cm}^{-2}$)	$10^4 C_b$ ($\mu\text{F cm}^{-2}$)	ϵ_b
6.5	1.5	10.0 (a)	70
		9.0 (b)	63
4.1	2.3	11.0 (a)	50
		11.0 (c)	50
4.4	2.5	11.0 (a)	46
		11.5 (c)	48

(a) Electrode coated with Ag; (b) electrode immersed in Hg; (c) electrode immersed in aqueous solution.

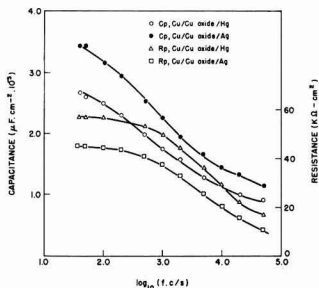


Fig. 5. C_p and R_p for dry copper oxide capacitors vs. logarithm of the frequency in cycles per second.

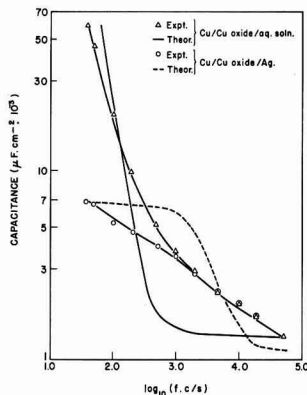


Fig. 6. C_p for the Cu/Cu₂O/Ag capacitor and the Cu/Cu₂O/aqueous solution half cell vs. logarithm of the frequency in cycles per second. Full theoretical curve, Eq. [8]; dashed theoretical curve, Eq. [5].

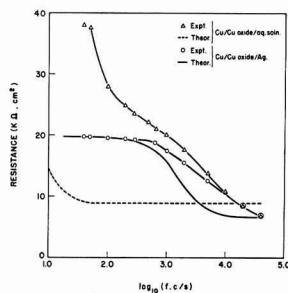


Fig. 7. R_p for the Cu/Cu₂O/Ag capacitor and the Cu/Cu₂O/aqueous solution half cell vs. logarithm of the frequency in cycles per second. Full theoretical curve, Eq. [6]; dashed theoretical curve, Eq. [9].

C_p , in Fig. 7 R_p , and in Fig. 8 $\log_{10}(\tan \delta)$, where $(\tan \delta) = 1/\omega C_p R_p$, are plotted vs. $\log_{10} f$ for a Cu/Cu₂O electrode (scale thickness = 4.1×10^{-3} cm) immersed in aqueous solution and for the same electrode coated with Ag. Calculated values of C_p and R_p are also contained in Fig. 6 and 7 which will be discussed later. The electrolyte resistance, which was determined by using a copper electrode in place of the Cu/Cu₂O electrode, was $10 \Omega \text{ cm}^2$; C_p is $30 \mu\text{F cm}^{-2}$ and R_p is $50 \Omega \text{ cm}^2$ at 1 kcps for the nonoxidized Cu electrode. The impedance measurements on nonilluminated elec-

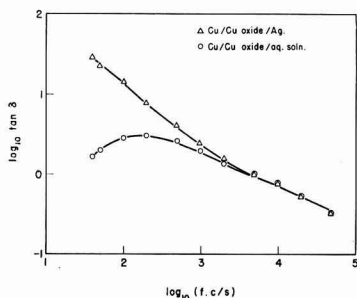


Fig. 8. Log ($\tan \delta$) for the Cu/Cu₂O/Ag capacitor and the Cu/Cu₂O/aqueous solution half cell.

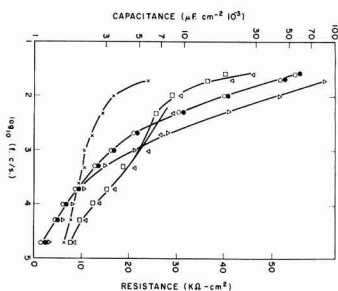


Fig. 9. Effect of light on C_p and R_p for the Cu/Cu₂O/aqueous solution half cell; \circ - C_p and \square - R_p , before illumination; \triangle - C_p and \times - R_p , during illumination; \bullet - C_p and ∇ - R_p , 1 hr after illumination.

trodes were time independent. All impedance measurements were independent of the a-c amplitude from 5 to 1 mv.

It was found that light affected the C_p and R_p measurements due to the photoconductivity of the copper oxide; for this reason and also for proper grounding as mentioned earlier all experiments were done on a cell enclosed in a copper box. In Fig. 9, the effect of light on C_p and R_p caused by a u.v. lamp placed close to the cell is shown. On removal of the lamp C_p and R_p reverted to their original values in 1 hr.

The open-circuit potential of the Cu/Cu₂O electrode in the phosphate buffer solution was -0.14 v vs. the Ag/AgCl/0.1N KCl electrode.

Discussion

Dielectric absorption in the copper oxide capacitor.—The copper oxide scale is fairly uniform in thickness and compact (Fig. 4). Microfissures may be present, but deep penetration into the oxide seems unlikely since C_p and R_p agree to within 30% for the Cu/Cu₂O/Ag and the Cu/Cu₂O/Hg capacitors (Fig. 5); evaporated Ag is assumed to fill up microfissures and Hg does not penetrate pores $< 10^{-3}$ cm diameter at 1 atm pressure (8). The differences observed presumably could be accounted for by surface roughness of the oxide scale, i.e., by variation in oxide thicknesses of approximately 10^{-8} cm. The nature of the frequency dispersion of C_p and R_p is similar for the two dry copper oxide capacitors (Fig. 5) which indicates that the di-

electric absorption in the Cu/Cu₂O/Ag capacitor is due to bulk properties of the oxide rather than microfissures. C_p and R_p at high frequencies are equal within experimental error for the Cu/Cu₂O/Ag capacitor and the Cu/Cu₂O/aqueous solution capacitor (Fig. 6 and 7); the difference in dispersion data for the wet and dry oxide capacitors at low frequencies is probably not an effect of microfissures but, as will be shown in the next section, is most likely due to Maxwell-Wagner absorption. Penetration of water into the oxide scale probably does not occur since the impedance measurements in aqueous solution were not time dependent.

Jepson, *et al.* concluded from comparison of density measurements in various fluids and by surface area measurements (9) that the oxide formed on Cu by oxidation at 960°C is nonporous, in agreement with this work.

C_f , R_f , C_e , and R_e of the first circuit element of Fig. 10(a) make up the RC circuit which may be used to represent the dispersion data of the dry capacitor with copper oxide as dielectric in the frequency range studied. C_f is the high frequency capacitance, R_f is the d-c resistance, and $C_e R_e$ is a relaxation time specifying some polarization process within the oxide film. C_p and R_p are given by the equations

$$C_p = C_f + C_e / (1 + \omega^2 C_e^2 R_e^2) \quad [5]$$

$$R_p = [1/R_f + \omega^2 C_e^2 R_e / (1 + \omega^2 C_e^2 R_e^2)]^{-1} \quad [6]$$

where ω is the angular frequency.

Calculated curves for C_p and R_p are shown in Fig. 6 and 7, respectively, assuming values of $C_f = 1.1 \times 10^{-3}$ μ F, $C_e = 5.1 \times 10^{-3}$ μ F, $R_f = 2.2 \times 10^4$ Ω , and $R_e = 1.14 \times 10^4$ Ω . The experimental curves of C_p and R_p do not fall on the theoretical curves except at high and low frequencies which indicates that a distribution of relaxation times exists for the relaxation process rather than the single relaxation time, $R_e C_e = 5.81 \times 10^{-5}$ sec (10). The relaxation process is probably due to positive holes since the bulk relaxation of electrons and holes is generally in this range of frequencies (11). The

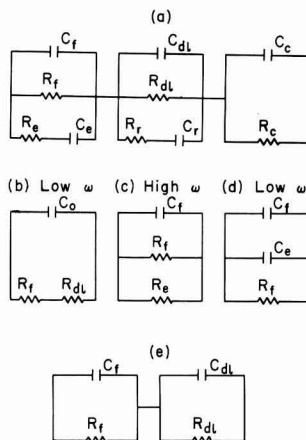


Fig. 10. RC equivalent circuits

relaxation time of photoexcited electrons is $< 10^{-5}$ sec (Fig. 9).

The apparent dielectric constant, ϵ_b , is 5 to 6 times greater than the value, 10.5, obtained for powdered Cu_2O by Hojendahl (7) by the method of mixtures at approximately 1Meps (Table I). This discrepancy may be explained if it is assumed that Maxwell-Wagner polarization occurs at $f > 50$ kcps due to the double layer nature of the copper oxide scale i.e., a thick layer of Cu_2O beneath a layer of higher oxide (Fig. 4). This point will be discussed in the latter part of the next section.

Dielectric absorption in the copper oxide electrode in aqueous solution.—The Helmholtz-Gouy double layer has a pronounced effect on the dielectric dispersion data (Fig. 6, 7, 8, and 9). This type of dispersion is called Maxwell-Wagner polarization (4, 5) which can be demonstrated by the use of the general equivalent RC circuit given in Fig. 10(a). C_{dl} is the electrical double layer capacitance, R_{dl} is the electrical double layer d-c resistance; R_f and C_f is the equivalent circuit for Faradaic impedance of the electrochemical reaction occurring at the oxide-aqueous solution interface; R_e is the cell solution resistance; and C_e is the cell solution capacitance. R_e is $10 \Omega \text{ cm}^2$ and C_e was calculated to be about $4 \times 10^{-6} \mu\text{F cm}^{-2}$ for the cell illustrated in Fig. 2. The impedance of the solution may be neglected in comparison to the total impedance in the frequency range studied since $R_f \gg R_e$ and the time constant $C_e R_e$ is approximately 4×10^{-11} sec.

Consider qualitatively the charging and discharging processes at the left two circuit elements illustrated in Fig. 10(a) as a function of frequency. At high frequencies conduction is mainly through C_f and C_{dl} (displacement current) which does not result in a charge accumulation at the oxide-electrolyte interface. At low frequencies positive hole migration in the oxide film and ion migration in the electrical double layer occurs in phase with the a-c pulse which, since $R_{dl} \neq R_f$, results in a charge accumulation at the oxide-electrolyte interface (5). This type of polarization which causes a real absorption of charge concentrated at the oxide-electrolyte interface and also frequency dispersion of the a-c impedance is called Maxwell-Wagner interfacial polarization. The impedance of the $\text{Cu}/\text{Cu}_2\text{O}$ electrode in aqueous solution was found to be independent of the amplitude of the a-c pulse from 5 to 1 mv. Thus, the a-c amplitude is sufficiently low that the charge absorption from the a-c pulse by the above mechanism does not signifi-

cantly change the charge distribution present normally at the oxide-electrolyte interface.

The entire solution of C_f and R_f and, also, of the series capacitance (C_e) and series resistance (R_e) for a series arrangement of R_e and C_e (Fig. 1), in terms of the components of the equivalent circuit of Fig. 10(a) is too complex to be used. However, the high- and low-frequency approximations of C_p , R_p , C_s , and R_s obtained from the mathematical expression for the equivalent circuit of Fig. 10(a) will be considered.

In Table II high- and low-frequency approximations of C_p , R_p , C_s , and R_s are compared for the $\text{Cu}/\text{Cu}_2\text{O}/\text{Ag}$ capacitor and the $\text{Cu}/\text{Cu}_2\text{O}/\text{aqueous}$ solution half-cell. In the derivation of the limits given in Table II, it was assumed that $C_{dl} \gg C_f \approx C_e \gg C_s$, $R_{dl} \approx R_f \gg R_e$, and $\epsilon_b \approx 50$ (Table I) (these assumptions are valid for the system studied at $f \approx 50$ kcps); ω_1 is a range of angular frequencies at which the inequality, $\omega_1^2 C_f^2 R_e^2 \gg 1$, holds and at values of ω_1 , the impedance of the electrical double layer is negligible compared to the impedance of the oxide scale. The equivalent circuit corresponding to the high- and low-frequency limits for the $\text{Cu}/\text{Cu}_2\text{O}$ electrode in aqueous solution are shown in Fig. 10(c) and in Fig. 10(b), respectively; the high- and low-frequency equivalent circuit approximations for the $\text{Cu}/\text{Cu}_2\text{O}/\text{Ag}$ capacitor are given in Fig. 10(c) and Fig. 10(d), respectively, where,

$$C_o = R_{dl}^2(C_{dl} + C_f)/(R_f + R_{dl})^2 \quad [7]$$

The high- and low-frequency approximations are different for series and parallel bridge arms (Table II). Cole and Hoar's (12) low-frequency approximation for C_s for the $\text{Cu}/\text{Cu}_2\text{O}$ electrode which was $(C_{dl} + C_f)$ is consistent with their particular equivalent circuit, but the disagreement with the value of C_s in Table II arises from the fact that Cole and Hoar did not include R_{dl} in the equivalent circuit for the electrical double layer. Bockris and Conway (13) made a-c impedance measurements on Cu in aqueous solution and interpreted the results in terms of an equivalent circuit which included R_{dl} as well as C_{dl} and Faradaic impedance components. Green (14) has estimated for a semiconductor electrode with surface states that $C(1 \text{ cps}) = C_{dl}$. This is only approximately true since from Fig. 10(b), $C(\omega \rightarrow 0) \rightarrow C_o$ which holds true for semiconductors with and without surface states. Leach (2) measured the impedance of the uranium electrode containing a corrosion film at frequencies, 100, 400, and 1600 cps

Table II. Theoretical high- and low-frequency limits of C_s , R_s , C_p , and R_p .

Circuit element	Cu/Cu ₂ O/Ag	Cu/Cu ₂ O/Ag and Cu/Cu ₂ O/aqueous solution	Cu/Cu ₂ O/aqueous solution
	$\omega = 0$	$\omega = \omega_1$	$\omega = 0$
C_s	∞	C_f	∞
R_s	R_f	$(R_f + R_e)/\omega_1^2 C_f^2 R_f R_e$	$R_f + R_{dl}$
C_p	$C_e + C_f$	C_f	$R_{dl}^2(C_{dl} + C_f)/(R_f + R_{dl})^2$
R_p	R_f	$R_f R_e/(R_f + R_e)$	$R_f + R_{dl}$

in the potential range 0.2-1.4 v and interpreted the results in terms of the film properties, film thickness, and porosity; the effect of the electrical double layer was assumed unimportant which from this work would appear to be a risky assumption unless substantiated by impedance measurements on the dry uranium/corrosion film capacitor. Güntherschulze and Betz (15) observed that at $f = 800$ cps the capacity of a Ta_2O_5 capacitor in Hg and the Ta/ Ta_2O_5 electrode in aqueous solution to be equal which indicates that for the Ta/ Ta_2O_5 electrode Maxwell-Wagner polarization occurs at $f < 800$ cps.

The high-frequency approximations of C_p and R_p for the Cu/ Cu_2O /Ag and the Cu/ Cu_2O /aqueous solution capacitors given in Table II are probably reached to within about 10% at $f = 50$ kcps ($\omega_1 = 3.14 \times 10^5 \text{ sec}^{-1}$). The impedance of the electrical double layer is negligible compared to the impedance of the dry oxide capacitor at $f > 5$ kcps since C_p (Fig. 6) and R_p (Fig. 7) for the two types of capacitors are equal at $f > 5$ kcps. The high-frequency limits of the theoretical dispersion curves of the dry oxide capacitor given in Fig. 6 and Fig. 7 are attained at $f > 10$ kcps. The experimental dispersion curves for the electrolytic capacitor and the dry oxide capacitor have leveled off to some extent at the high frequencies studied since C_b (Table I), obtained by extrapolation of C_p vs. $1/f$ curves to infinite frequency, is 10% lower than the value of C_p at $f = 50$ kcps. At $f < 5$ kcps the dispersion curves for the electrolytic capacitor deviates markedly from the dispersion curves for the dry oxide capacitor due, of course, to the effect of the impedance of the electrical double layer on the total impedance of the electrolytic capacitor at low frequencies. The low-frequency limiting values of C_p and R_p for the electrolytic capacitor given in Table II are not reached in the frequency range studied.

In this work as is generally done in studies of the impedance of the electrical double layer, the impedance data are interpreted in terms of capacitance and resistance rather than capacitance and the loss tangent as done for dielectric studies. As it is to be expected from the C_p and R_p dispersion curves, $\tan \delta$ for the electrolytic Cu_2O capacitor is in agreement with $\tan \delta$ for the dry Cu_2O capacitor at $f > 5$ kcps and in marked disagreement at $f < 5$ kcps (Fig. 8).

The frequency at which Maxwell-Wagner polarization occurs and the values of R_{d1} and C_{d1} may be estimated roughly by solving for C_p and R_p in terms of the components of the simplified 2-layer dielectric in Fig. 10(e) and assuming values for the equivalent circuit components which best fit the experimental dispersion data. Comparison of the electrolytic capacitor with the equivalent circuit of Fig. 10(e) involves the assumptions that (a) the impedance of the electrolyte is small compared to the total impedance; (b) relaxation effects in the oxide dielectric are absent; and (c) the Faradaic impedance may be represented by a resistance the value of which is independent of frequency. Assumption (a) is valid at low frequencies; assumption (b) is definitely invalid from data on the dry capacitor; and assumption (c) is in-

valid (16). The justification for using these assumptions is that they enable an estimate of the minimum impedance of the electrical double layer at the copper oxide surface to be made. The equations for C_p and R_p are (4).

$$C_p = C_b [1 + k/(1 + \omega^2 \tau^2)] \quad [8]$$

$$R_p = \{ \omega C_b [\tau/\tau_f \tau_{d1} + k\omega \tau / (1 + \omega^2 \tau^2)] \}^{-1} \quad [9]$$

where

$$k = [(\tau_f + \tau_{d1} - \tau)\tau - \tau_f \tau_{d1}] / \tau_f \tau_{d1} \quad [10]$$

and

$$\tau = (R_f \tau_{d1} + R_{d1} \tau_f) / (R_f + R_{d1}) \quad [11]$$

$\tau_f = R_f C_f$, $\tau_{d1} = R_{d1} C_{d1}$, and C_b is the capacitance at infinite frequency. The capacitance C_p decreases to the midpoint between the static capacitance ($\omega = 0$) and optical capacitance, ($\omega = \infty$), when $\omega = 1/\tau$ and τ is therefore the time constant of the Maxwell-Wagner polarization.

In Fig. 6 and Fig. 7 theoretical curves for C_p and R_p vs. $\log_{10} f$ are shown for the electrolytic capacitor using values of $R_f = 10^4 \Omega$, $C_f = 10^{-3} \mu F$, $C_{d1} = 2 \mu F$, $R_{d1} = 3 \times 10^4 \Omega$, and $C_b = 10^{-3} \mu F$. There is fair agreement between the calculated and experimental values of C_p and quite poor agreement between R_p values. Qualitatively it can be seen that better agreement would be found if $R_f C_f$ and $R_{d1} C_{d1}$ were taken into account. The time constant τ is 0.15 sec ($f = 1.07$ cps). Therefore, the low-frequency limiting values of C_p and R_p for the electrolytic capacitor (Table II) would be expected to be reached at $f < 1$ cps. The impedance of the electrical double layer at the copper oxide surface in terms of C_{d1} and R_{d1} is considerably higher than the impedance of the electrical double layer at a Cu metal surface; C_p is $30 \mu F \text{ cm}^{-2}$ and R_p is $50 \Omega \text{ cm}^2$ at 1 kcps for nonoxidized Cu wire immersed in the same phosphate buffer solution. Possible explanations for the high impedance are (a) the effective area of the oxide surface is lower than the geometric area, and (b) the electrical double layer at the oxide surface is thicker than that at the copper surface.

In the first section of the discussion it was assumed that the Maxwell-Wagner polarization time constant for the dry two layer copper oxide capacitor was $< 3.18 \mu \text{sec}$, i.e. $f > 50$ kcps. This assumption is consistent with an equation of the form of Eq. [11] if $R_f C_f$ for the thick Cu_2O layer is assumed to be as before 10^{-3} sec and the time constant for the thin layer $R_f C_f'$ is assumed to be $< 3 \mu \text{sec}$, which is reasonable. A detailed study of the dielectric relaxation processes in the oxide dielectric as a function of temperature over a large frequency range would be required before definite conclusions can be made concerning the relaxation processes involved.

Acknowledgments

The author is indebted to Dr. L. D. Calvert for the X-ray analysis and to Dr. M. Cohen for helpful discussions.

Manuscript received May 18, 1960; revised manuscript received Nov. 3, 1960.

Any discussion of this paper will appear in a Discussion Section to be published in the December 1961 JOURNAL.

REFERENCES

1. L. Young, *Trans. Faraday Soc.*, **55**, 842 (1959).
2. J. S. L. Leach, *J. Inst. Metals*, **88**, 24 (1959).
3. G. Okamoto, H. Kobayashi, M. Nagayama, and N. Sato, *Z. Elektrochem.*, **62**, 775 (1958).
4. A. R. von Hippel, "Dielectrics and Waves," pp. 228, 87, John Wiley & Sons, Inc., New York (1954).
5. L. Page and N. I. Adams, Jr., "Principles of Electricity," 2nd ed., p. 64, D. van Nostrand Co., New York (1949).
6. F. R. Meyer and G. Ronge, *Ang. Ch.*, **52**, 637 (1939).
7. K. Hojendahl, *Z. physik Chem.*, **B20**, 54 (1933).
8. J. F. Goodman and S. J. Gregg, *J. Chem. Soc.*, **1956**, 3612.
9. D. W. Aylmore, S. J. Gregg, and W. B. Jepson, *This Journal*, **106**, 1010 (1959).
10. M. Gevers, *Philips Research Repts.*, **1**, 279 (1946).
11. H. C. Montgomery and W. L. Brown, *Phys. Rev.*, **103**, 865 (1956); C. G. B. Garret, *ibid.*, **107**, 478 (1957).
12. M. Cole and T. P. Hoar, *CITCE VIII* (1958), Butterworths, London, 1956, p. 158.
13. J. O'M. Bockris and B. E. Conway, *J. Chem. Phys.*, **28**, 707 (1958).
14. M. Green, "Modern Aspects of Electrochemistry," J. O'M. Bockris, Editor, No. 2, p. 375, Butterworths, London (1959).
15. A. Güntherschulze and H. Betz, *Z. physik.*, **68**, 145 (1931).
16. D. C. Grahame, *This Journal*, **99**, 370C (1952).

Technical Note



The Mechanism of Electrolytic Deposition of Titanium from Fused-Salt Media

Walter E. Reid, Jr.

Metallurgy Division, National Bureau of Standards, Washington, D. C.

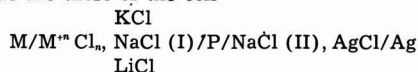
Bockris and co-workers have concluded from polarographic measurements and the appearance of the deposits that the deposition of titanium in fused alkali chlorides occurs by a secondary electrode process (1). However, their polarographic measurements were made at lower concentrations of titanium halide than the usual concentrations used for commercial processes. It has been proposed (1, 2) that the mechanism initially involves the reduction of an alkali-metal ion. The alkali metal then reacts with the titanium halide to give titanium. Under conditions of low concentration of titanium salt and at high current densities, such a mechanism could be operative due to an expected increase in polarization at the cathode, but for deposition at moderate titanium halide concentrations at a current density below the limiting current density for titanium deposition from the melt (the conditions usually employed), this mechanism is improbable.

Static electrode potentials, whether calculated from thermodynamic data or measured experimentally, tell only the order in which the ions will be reduced under equilibrium conditions. Definite conclusions relating to the mechanism of the electro-deposition of a particular metal require, in addition, a consideration of the magnitude of the polarization that occurs during the electrolytic process.

In a recent investigation in this laboratory, measurements were made of the static electrode-potentials of sodium, magnesium, and titanium against the porcelain electrode of Lamb and Labrie (3), which was arbitrarily assigned a value of zero. The electrode potential of magnesium lies between that of sodium and titanium and was included as a gross check of the measurements. All measurements were

made at 600°C in melts having the basic composition: 45 mole % LiCl, 45 mole % KCl, 10 mole % NaCl. The electrode potentials obtained are given in Table I.

In order to compare the emf values measured with the porcelain electrode to the standard E° values calculated from thermal data by Hamer, *et al.* (4), our values are referred to the chlorine electrode. The potentials should also be corrected for concentration, junction potential, and solvent effects. The emf's measured with the porcelain electrode are those of the cell

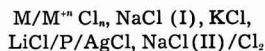


Panish and co-workers (5) have determined the emf's of a silver electrode in varying AgCl-NaCl ratios against a chlorine electrode. For 76 mole % AgCl and 24 mole % NaCl, which is the composition used for the porcelain electrode in this work, they obtained an emf of 0.885 v at 600°C. Assigning this

Table I. Electrode potentials

Electrode	Na, NaCl	Mg, MgCl ₂	Ti, TiCl ₂
Composition of melt	Mole % 10 NaCl	Mole % 9.1 MgCl ₂	Mole % 9.1 TiCl ₂
	45 LiCl	9.1 NaCl	9.1 NaCl
	45 KCl	40.9 LiCl	40.9 LiCl
Observed emf, v	2.54	1.97	1.17
Observed emf relative to Cl ₂ = 0	3.43	2.86	2.06
"Corrected" emf	3.32	2.84	2.04
Standard emf for single component (Hamer and co-workers)	3.42	2.60	1.89

value to the silver silver chloride electrode within the porcelain electrode used here (relative to the chlorine electrode as zero), the observed potentials would be increased by 0.885 v, as shown in Table I. After this correction, the cell now considered is



The over-all cell reaction is



It is assumed that the junction potential of the porcelain electrode is due only to the difference in sodium-ion concentration at the porcelain interfaces. Actually, Lamb and Labrie found that the junction potential was also affected by the potassium ion concentration to some extent (3). Although the potassium ion concentration was varied slightly in the melts used, the magnitude of the effect of potassium ion on the junction potential would be approximately constant. The standard emf of the cell is

$$E^{\circ} = E + \frac{RT}{nF} \ln \frac{a_M^{m+} a_{Na^+}^{(II)} a_{Cl^-}^{-n}}{a_{Na^+}^{(I)}}$$

Evaluation of this expression for the measured electrode potentials, using mole fractions and assuming activity coefficients of one, gives the "corrected" emf values listed in Table I. The activity coefficients of the magnesium and titanium ions will probably be fairly small. Lacking knowledge of these values, the comparison of the "corrected" potentials with the potential values calculated from thermal data will not be exact but are approximate only.

In spite of the uncertainty of the values used in these calculations, these corrected values agree well with the potential measurements made by other workers. Delimarskii (6), in a review, has given the electrolytic decomposition-potentials for various molten salts; the relative reactivities for sodium and magnesium by him are in agreement with the values presented here. Other investigators have obtained standard emf's for Mg (7) and Ti (8) (at low concentrations of the respective metal chlorides in fused salts) that are in good agreement with the values given in Table I. The data of Ingraham (8) indicate a standard emf for Ti, Ti^{++} of 2.010 v at 600°C ($Cl_2 = \text{zero}$) in a KCl-NaCl melt, which provides confirmation for the corrections applied above.

Although not many measurements have been made of overvoltages in fused salts, Piontelli has shown (9) that in fused chloride melts the deposition overvoltages for lead, magnesium, cadmium, tin, and aluminum are essentially ohmic. This indicates that in general the deposition overvoltage for

metals in fused chloride melts would be extremely low. For 8 mole % $TiCl_3$ in LiCl-KCl eutectic at 550°C, Corder and Worner showed that the deposition overvoltage was small even at high current densities (10). Therefore, the large difference in the static electrode potential values for Na^+ and Ti^{++} would indicate that the titanium deposits by a direct mechanism.

The foregoing discussion, in addition to supporting the viewpoint that titanium deposition occurs as a primary electrode reaction, also confirms the reliability of the porcelain electrode as a suitable reference electrode within the limits indicated above.

The magnesium and titanium electrodes that were used were small strips of these metals; however, the design of the sodium electrode used may be of interest. The most satisfactory sodium electrode was prepared as follows.

Sodium was melted in a chamber having an inert atmosphere and was sucked into a Pyrex capillary tube by means of a dropper bulb. The sodium solidified after it had been drawn about 10 cm into the capillary. The upper end of the capillary tube was sealed with a rubber stopper having a hole, drilled half way through the stopper, of diameter slightly less than the outside diameter of the capillary. The remaining length was so pierced that a snugly fitting tungsten lead-wire could be introduced. This tungsten wire was pushed down into the tube as far as it would go. Upon placing the electrode in the melt, some of the sodium escaped, and molten salt entered the capillary and displaced the sodium upward, further around the tungsten wire. This electrode was very stable and varied by only 1 mv over a period of 0.5 hr.

Manuscript received Sept. 12, 1960.

Any discussion of this paper will appear in a Discussion Section to be published in the December 1961 JOURNAL.

REFERENCES

1. J. O'M. Bockris, G. J. Hills, I. A. Menzies, and L. Young, *Nature*, **178**, 654 (1956).
2. R. S. Dean, *Metal Ind. (London)*, **90**, 143 (1957).
3. V. A. Lamb and R. J. Labrie, *This Journal*, **106**, 895 (1959).
4. W. J. Hamer, M. S. Malmberg, and Bernard Rubin, *ibid.*, **103**, 8 (1956).
5. M. B. Panish, R. F. Newton, W. R. Grimes, and F. F. Blankenship, *J. Phys. Chem.*, **62**, 1325 (1958).
6. Yu. K. Delimarskii, *Uspekhi Khim.*, **26**, 494 (1957).
7. H. A. Laitinen and C. H. Liu, *J. Am. Chem. Soc.*, **80**, 1015 (1958).
8. T. R. Ingraham, Private communication; See also S. N. Flengas, *Ann. N. Y. Acad. Sci.*, **79**, 853 (1960).
9. R. Piontelli, *et al.*, *Compt. rend.*, **242**, 1301 (1956); *Rev. Met.*, **53**, 248 (1956).
10. G. D. P. Corder and H. W. Worner, *Aust. J. Applied Sci.*, **2**, 358 (1951).

FUTURE MEETINGS OF The Electrochemical Society



Indianapolis, Ind., April 30, May 1, 2, and 3, 1961

Headquarters at the Claypool Hotel

Sessions will be scheduled on

Electric Insulation, Electronics (including Luminescence and Semiconductors), Electrothermics and Metallurgy,

Industrial Electrolytics (including a Symposium on Fuel Cells), and

Theoretical Electrochemistry

(including a Symposium on Instrumentation)

★ ★ ★

Detroit, Mich., October 1, 2, 3, 4, and 5, 1961

Headquarters at the Statler Hotel

Sessions probably will be scheduled on

Batteries, Corrosion (including a Symposium on Surface Structure vs. Corrosion Behavior), Electrodeposition

(including symposia on Addition Agents and on Electrodeposited Magnetic Films), Electronics (Semiconductors),

Electro-Organics, and Electrothermics and

Metallurgy

★ ★ ★

Los Angeles, Calif., May 6, 7, 8, 9, and 10, 1962

Headquarters at the Statler Hilton Hotel

★ ★ ★

Boston, Mass., September 16, 17, 18, 19, and 20, 1962

Headquarters at the Statler Hilton Hotel

Papers are now being solicited for the meeting to be held in Detroit, Mich., October 1-5, 1961. Triplicate copies of each abstract (*not exceeding 75 words in length*) are due at Society Headquarters, 1860 Broadway, New York 23, N. Y., *not later than May 15, 1961* in order to be included in the program. *Please indicate on abstract for which Division's symposium the paper is to be scheduled, and underline the name of the author who will present the paper.* No paper will be placed on the program unless one of the authors, or a qualified person designated by the authors, has agreed to present it in person. An author who wishes his paper considered for publication in the JOURNAL should send triplicate copies of the manuscript to the Managing Editor of the JOURNAL, 1860 Broadway, New York 23, N.Y.

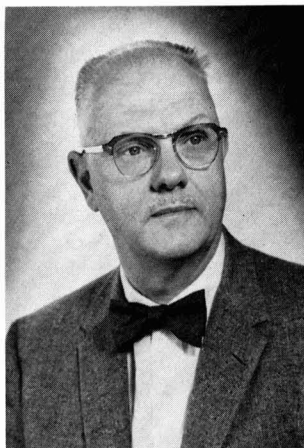
Presentation of a paper at a technical meeting of the Society does not guarantee publication in the JOURNAL. However, all papers so presented become the property of The Electrochemical Society, and may not be published elsewhere, either in whole or in part, unless permission for release is requested of and granted by the Editor. Papers already published elsewhere, or submitted for publication elsewhere, are not acceptable for oral presentation except on invitation by a Divisional program Chairman.



Linford, Gilbertson, and Enck to Take Office in Indianapolis



H. B. Linford



L. I. Gilbertson



E. G. Enck

As a result of the recent annual election, in which the voting is by mail ballot, Henry B. Linford has been elected the new President (1961-1962) of The Electrochemical Society, Lyle I. Gilbertson has been elected third Vice-President (1961-1964), and Ernest G. Enck has been elected Treasurer (1961-1964). They will take office at 8:00 A.M. on Wednesday, May 3, 1961, in Indianapolis, Ind., at the Annual Spring Meeting of the Society.

Dr. Linford, professor of chemical engineering, Columbia University, New York City, replaces Ralph A. Schaefer, director of research, The Electric Storage Battery Co., Carl F. Norberg Research Center, Yardley, Pa. Dr. Schaefer, as Past President, will continue as a member of the Board of Directors.

Lyle I. Gilbertson, administrative director of the Central Research Laboratories, Air Reduction Co., Inc., Murray Hill, N. J., terminates his

second three-year term as Treasurer and begins a three-year term as Vice-President. He will serve with the two previously elected Vice-Presidents, Frank L. LaQue and Walter J. Hamer.

Ernest G. Enck, consultant in long-range planning and general management, with active interest in Boy Scouts, community planning, and conservation programs, Gwynedd Valley, Pa., begins his three-year term as Society Treasurer.

Plans Completed for the Indianapolis Meeting, April 30-May 3, 1961

Arrangements have been completed for the Spring Meeting of The Electrochemical Society to be held in Indianapolis, Ind., from April 30 through May 3, 1961, at the Claypool and Sheraton-Lincoln Hotels. The complete program, including the schedule and abstracts of the papers to be presented, was published in the March JOURNAL, pp. 49C-74C.

Addition to Technical Program

The following paper has been

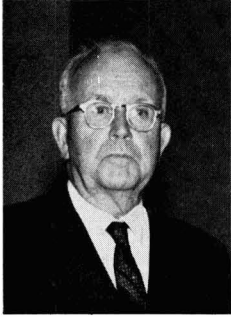
added to the Electrothermics and Metallurgy Symposium on Ultrafine Particles—Particle Size Measurement and Surface Effects on Wednesday afternoon, May 3, in the Florentine Room, Mezzanine:

4:30 P.M.—"Dispersion Strengthening of Copper Using Various Oxides, Carbon, and Tungsten Carbide as the Dispersed Phase" by K. M. Zwilsky, New England Materials Lab., Inc., Medford, Mass., and N. J.

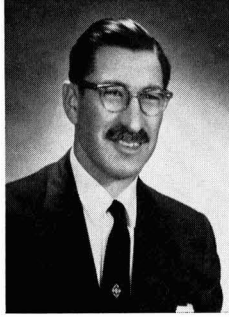
Grant, Dept. of Metallurgy, Massachusetts Institute of Technology, Cambridge, Mass. (Abstract 98A).

Local Committee

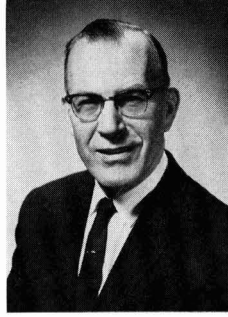
These arrangements have been the result of the labors of the Local Committee headed by the following Chairmen: A. M. Max, General Chairman; J. M. Booe, Co-Chairman; Bernard Agruss, Hotel Arrangements; T. C. O'Nan, Finance; R. R. Haberecht, Registration; M. L.



F. C. Mathers



A. M. Max



J. M. Booe



Bernard Agruss

Whitehurst, Entertainment; R. E. Ralston, Plant Visitation and Transportation; Ambrose Smith, Publicity; Mrs. J. M. Booe, Ladies' Committee Chairman. The Honorary Chairman of the meeting is Professor F. C. Mathers, Honorary Member and a Past President of the Society.

General Functions

The Committee has arranged a program which will not be excessively demanding on those attending. The high light of the affairs will be the Tuesday evening Reception and Banquet in honor of President Ralph Schaefer and Mrs. Schaefer to be held in the Riley Room of the Claypool. In order to make this event available to as many as possible, the price of the cocktails and banquet has been set at \$7.00. In addition to the Presidential Address, a "pops" program will be presented by a 30-piece ensemble from the Indianapolis Symphony Orchestra. This

program will be different and the Committee feels sure all will enjoy it.

Sunday evening, the Ben Franklin Room on the Mezzanine near the registration area will be set up as a hospitality room for an informal get-together for those arriving and registering Sunday afternoon and evening.

For Monday evening, May 1, a "500" mixer has been arranged which will be held in the Riley Room. Refreshments and snacks will be available with the compliments of the Convention Committee.

In addition to the formal events, Indianapolis has a number of night clubs and places noted for excellent food. If any group wishes to form a party, please contact the Local Committee Headquarters in Parlor E on the South Mezzanine. Arrangements will be made, suggestions offered, or any other information and

help the committee can give will be furnished.

For the Ladies

For the ladies, pains have been taken to arrange a delightful program. Coffee and pastry will be served from 9:00 to 10:00 each morning in the Louis XIV Room, which serves also as the Ladies' Headquarters. Those who are late risers are assured that the pastry served with the coffee will make a more than adequate breakfast.

A trip to the Bloomington Campus of Indiana University has been arranged for Monday, May 1, which will be highlighted by a tour of the new Lilly Library, with its collection of rare books, and lunch at the Memorial Union. This will be followed by a trip through scenic Brown County, which at that time of the year is particularly beautiful. The ladies will return in time to join their menfolk for dinner and are cordially invited to attend the "500" mixer Monday evening.

Tuesday has been left free to shop and visit friends after the morning coffee hour. The hotels are within one block of some of the finest stores in the country. There will be time to relax in the afternoon to be ready for the Presidential Reception and Banquet starting at 6:30 P.M.

Wednesday will be a full day, starting with the coffee hour in the morning. Leaving at 10:15 A.M., there will be a sight-seeing tour of Indianapolis followed by lunch at the Columbia Club on the Circle. Following lunch, transportation will be provided to the John Herron Art Institute for a talk and tea. The Circle is only one and one-half blocks from the hotels, so that those who want to prepare to check out can leave the group after lunch.

Plant Visits

Indianapolis has a number of diversified industries of interest to



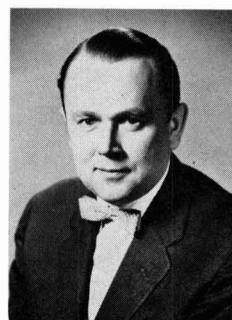
Claypool Hotel, Indianapolis, Ind.



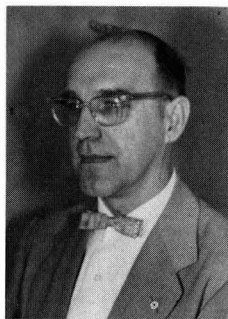
National American Legion Headquarters, Indianapolis, Ind.



T. C. O'Nan



R. R. Haberecht



M. L. Whitehurst



R. E. Ralston



Ambrose Smith

electrochemists. The Committee felt that with three very full days of sessions, few, if any, would want to take time out for plant visits. However, if there is sufficient interest, a tour of several industries can be arranged for Thursday, May 4. These

will include the large telephone set manufacturing plant of Western Electric, the record manufacturing plant of the RCA Victor Record Division of RCA, followed by lunch. This will be followed by a tour of a plant of one of the Lilly pharma-

ceutical plants and the Allison Division of General Motors Powerama exhibit. This can be an educational and enjoyable experience and the Indianapolis Committee would be delighted to have many of you stay over for a day of plant visitation.

Report on First ECS Summer Assistance Award

During the summer of 1960, Mr. V. E. Hauser, Jr., a graduate student at the Dept. of Chemical Engineering, Oregon State College, Corvallis, Ore., received \$800 representing the first Summer Assistance Award of The Electrochemical Society (see page 156C of the July 1960 JOURNAL, Vol. 107, No. 7). The award, funds for which are derived from the income of investments in the Consolidated Fellowship Fund and the Weston Fund, was made "to a fellow or teaching assistant pursuing work between the degrees of B.S. and Ph.D. on a subject in a field of interest to The Electrochemical Society." It was intended to cover a period during which the recipient had no financial support for the continuance of his work.

The following constitutes Mr. Hauser's report on his work:

"In reply to your letter of August 11, 1960 requesting an informal report on the work accomplished by me in connection with the Summer Assistance Award of 1960, I am happy to submit the following statements.

"As you may recall, my research topic is concerned with the problems relating to the design and development of a fuel cell employing the carbon-oxygen reaction. During the summer, this award made it possible for me to make considerable progress toward the construction and study of such a cell.

"In brief, the unit that was constructed this summer contained porous carbon and silver electrodes and employed an electrolyte of lithium and potassium carbonate in a fused state. This cell differed from conventional units of this type inas-

much as it did not employ a porous matrix between the electrodes. The elimination of such a grid allowed for better contact between the electrodes and the electrolyte and significantly reduced the internal resistance of the cell. This design left the electrodes susceptible to flooding; however, operating techniques were perfected that in other ways arrested this phenomenon.

"Cell operation to date has resulted in open circuit potentials up to 47% of the theoretical value. Current densities of 41.0 amp/sq ft have been obtained for limited periods at a potential of 0.25 v. The longest run has been of 35 hr duration. Although these data appear poor compared to most of the current fuel cell research, it is nevertheless believed that these results are not bad for the carbon-oxygen cycle.

"Studies made this summer have pointed out several aspects which require further work or improve-

ment. The main difficulty experienced in the above cell was entrainment of the liquid electrolyte in the vented gas. As a result of this, all runs were made with an electrolyte level of less than half of the desired figure, thereby reducing the performance of the cell.

"Progress also was made on the development of a suitable cathode and a process for producing strong porous silver electrodes. The present method of electrode construction permits the addition of various compounds for investigation of possible catalytic effects. Such effects will be studied in the future.

"In closing, I would, once again, like to take the opportunity to express my gratitude for this award. It allowed me to spend a summer on my research, whereas I otherwise might have been forced to seek employment elsewhere for this period."

On recommendation of the Honors and Awards Committee of the Society, the Board of Directors voted in Houston in October 1960 to approve the issuance of three Summer Assistance Awards for the period June-September 1961 in the amount of \$800 each (see page 270C of the December 1960 JOURNAL, Vol. 107, No. 12). The names of the recipients will be announced in a later issue of the JOURNAL.

Theoretical Division

Enlarged Abstract Booklet, Spring 1961

The Theoretical Division is preparing an "Enlarged Abstracts" booklet for the papers to be presented at the Indianapolis Meeting, April 30-May 3, 1961. This booklet will include the papers of the Symposium on "Modern Instrumentation and Techniques of Electrochemical Measurements," sponsored jointly by the National Science Foundation and The Electrochemical Society, Inc.

The abstracts will be available at \$2.50 during the last two weeks of April from the Secretary-Treasurer of the Theoretical Division:

Dr. Paul Rüetschi
Electric Storage Battery Co.
Research Center
Yardley, Pa.

The booklet also can be purchased during the Indianapolis Meeting.

Division News

Electronics Division

The Nominating Committee (C. T. Lattimer, Chairman; F. J. Biondi, L. Thorington) has selected the following nominees for officers of the Electronics Division during the two-year term 1961-1963:

Chairman—R. J. Ginther, U. S. Naval Research Lab., Washington 25, D. C.

Vice-Chairman (Luminescence)—H. F. Ivey, Westinghouse Electric Corp., Lamp Div., Research Dept., Bloomfield, N. J.

Vice-Chairman (General Electronics)—C. P. Marsden, National Bureau of Standards, Washington 25, D. C.

Vice-Chairman (Semiconductors)—F. H. Horn, General Electric Research Lab., Schenectady, N. Y.

Secretary-Treasurer—A. E. Hardy, Radio Corp. of America, Lancaster, Pa.

Each nominee has given assurance of his willingness to serve if elected.

The Bylaws of the Division provide that additional nominations may be made by petition signed by five members of the Division. Such petitions must be in the hands of the Chairman of the Nominating Committee before the election, and the nominees must have given assurance of their willingness to serve if elected.

The election will be held at the business meeting of the Electronics Division during the Spring Meeting of the Society in Indianapolis, April 30-May 3, 1961.

A. E. Hardy, *Sec.-Treas.*

Electrothermics and Metallurgy Division

The Nominating Committee (A. C. Haskell, Chairman) of the Electrothermics and Metallurgy Division presents the following slate of officers for the 1961-1963 term:

For Chairman—J. H. Westbrook, Ceramic Studies Section, Research Dept., General Electric Co., P. O. Box 1088, Schenectady, N. Y.

For Vice-Chairman—W. E. Kuhn, Carborundum Co., P. O. Box 337, Niagara Falls, N. Y.

For Vice-Chairman—L. H. Juel, Great Lakes Carbon Corp., P. O. Box 637, Niagara Falls, N. Y.

For Secretary-Treasurer—L. M. Litz, Research Labs., National

Carbon Co., P. O. Box 6116, Cleveland 1, Ohio

For Members-at-Large (four required)—T. D. McKinley, Pigment Dept., Experimental Station, E. I. du Pont de Nemours & Co., Wilmington 98, Del.; C. A. Hampel, 8501 Harding Ave., Skokie, Ill.; R. R. Rogers, Mines Branch, Dept. of Mines & Technical Surveys, 551 Booth St., Ottawa, Ont., Canada; M. C. Udy, Strategic-Udy Processes, Inc., 3986 Royal Ave., Niagara Falls, N. Y.

Each nominee has given assurance of his willingness to serve if elected.

The election will be held at the business meeting of the Division to be held during the Spring Meeting of the Society in Indianapolis, April 30-May 3, 1961.

L. H. Juel, *Sec.-Treas.*

Electronics Division Enlarged Abstract Booklet, Spring 1961

The Electronics Division again will print an "Enlarged Abstracts" booklet containing 1000-word abstracts of papers to be presented before the Electronics Division's symposia during the Indianapolis Spring Meeting of the Society, April 30-May 3, 1961.

The booklet will contain about 200 pages and will include approximately 18 papers on Luminescence and 36 papers on Semiconductors.

The booklets are expected to be ready for distribution two weeks prior to the meeting. Copies will be available at the registration desk at Indianapolis.

The price will be \$3.00 per copy with a discount of \$0.50 (\$2.50 net) for orders accompanied by payment and requiring no invoicing. *Orders requiring invoicing will be charged full price even though payment accompanies the order.*

Make checks payable to: Electronics Division, The Electrochemical Society.

Mail to:

Austin E. Hardy
c/o Radio Corp. of America
New Holland Pike
Lancaster, Pa.

Section News

India Section

A business meeting of the Section was held on September 16, 1960 at the Indian Institute of Science, Bangalore-12, with Dr. S. Soundararajan in the chair.

The following nominations for officers of the Section for the year 1960-1961 were approved:

Chairman—M. S. Thacker, Council of Scientific and Industrial Research, Old Mill Rd., New Delhi 2, India

Vice-Chairman—A. Joga Rao, Central Electrochemical Research Institute, Alagappa College P.O., Karaikudi 3, South India

Vice-Chairman—S. Ramaswamy, Mettur Chemical and Industrial Corp., Mettur Dam R.S., India

Secretary-Treasurer—S. Krishnamurthy, Indian Telephone Industries Ltd., Dooravaninager, Bangalore 16, India

The Editor informed the members that Chemical Abstracts Service of U.S.A. intends to publish an Abstracts under the name "Chemical Titles" and participation of the *Bulletin of the India Section*, by mailing its copies by air mail, is solicited. This request was acceded to.

The members expressed grave doubts about the membership of the Section in the event that overseas members are not given a remission in the annual dues of the Society. The Secretary stated that he has taken up the matter with The Electrochemical Society and no reply has been received. The members urged that the Secretary again should take up this matter with the Society and impress on them the possibility of a fall in membership due to stopping of the remission of \$5.00 which has been given for the past five years.

S. Krishnamurthy, *Sec.-Treas.*

Indianapolis Section

The Indianapolis Section held its second technical meeting of the current season on Tuesday, January 24, 1961, at Butler University in Indianapolis. Prior to the technical program, A. Max, General Chairman for the Spring National Meeting in Indianapolis, reported on the current status of convention preparations.

The featured speaker for the evening was E. M. Sherwood, consultant, Division of Chemical Engineering, Battelle Memorial Institute, Colum-

bus, Ohio. His subject was "Chemical Vapor Deposition—A Tool for Research and Industry." After a résumé of the history of the art and a general description of the four basic techniques for accomplishing chemical vapor deposition, Dr. Sherwood discussed the wide variety of materials which have been deposited by these techniques. Following this, he described recent developments and applications in this area, concluding with predictions of future applications and a delineation of certain problem areas where more fundamental information is needed.

T. C. O'Nan, *Sec.-Treas.*

New York Metropolitan Section

A meeting of the Section was held at Victor's restaurant in New York City on January 4, 1961. Speaker was Ralph A. Schaefer, President of the Society.

After a brief review of Society affairs and a prediction of the progress to be expected in the next ten years, Dr. Schaefer discussed electrodeposition technology. Particular emphasis was placed on the factors influencing uniformity of metal deposits and their structures. Dr. Schaefer used slides to illustrate the effects of surface contaminants, such as nickel oxide and graphite, on the surface roughness of the deposit. He pointed out that further study was necessary to determine the effects of addition agents on the properties of the electrodeposits.

J. L. Everhart

Pittsburgh Section

A joint meeting of the Physical and Inorganic Chemistry Group of the Pittsburgh Section of the American Chemical Society and the Pittsburgh Section of The Electrochem-

ical Society was held on January 23, 1961 at the Mellon Institute in Pittsburgh, Pa.

Professor R. H. Cole, head of the Chemistry Dept., Brown University, lectured on the subject "Recent Studies of Dielectric Behavior in Relation to Structures of Liquids and Solids."

It was shown that dielectric constants of polar liquids and solids can give useful information about molecular arrangements and forces, especially when specific forces or cooperative interactions are important. Dielectric behavior appears to vary primarily with the degree of hydrogen bonding.

Dielectric dispersion and loss resulting from molecular orientation give valuable evidence about the kinetics of the processes. Characteristic types of relaxation spectra were presented, and it was noted that few processes follow the expected exponential rate laws.

E. J. Smith, *Sec.-Treas.*

Personals

R. Bakish, in addition to his duties as director of research for The Alloyd Corp., Cambridge, Mass., has been appointed vice-president and member of the Board of Directors of The Alloyd Electronics Corp., which specialized in the application of electron beams to materials.

Daniel Gray, research chemist credited with changing indium from a laboratory curiosity to a commercial metal, has been appointed special consultant on technical problems by Alpha Metals, Inc., Jersey City, N. J. It was Mr. Gray's substitution of common sugar for rare and costly amino acetic acid that made indium plating a commercial practicality. Before joining Alpha Metals, Mr. Gray was a research chemist with Oneida, Ltd., for 42 years.

George Krsek has joined International Rectifier Corp., El Segundo, Calif., as executive vice-president and general manager. In his new position, Dr. Krsek will be responsible for research and development, engineering, purchasing, manufacturing, and sales. He comes to this post from Merck and Co., Inc., Rahway, N. J., where for 13 years he had been active in various technical and management capacities.

J. Donald Moulton has retired as manager of engineering and research

Unpaid Members Off Mailing List April 1

According to the Constitution of the Society, Article III, Section 9, the names of all members whose dues for 1961 are not paid by April 1 must be removed from the mailing list, and will not receive the May issue of the *JOURNAL*. To avoid delay in receipt of *JOURNALS* as published, all members who have not yet sent in 1961 payments are urged to do so immediately.

of the Nickel-Alkaline Battery Division of The Electric Storage Battery Co., and has been appointed consultant to the Chemistry Dept. of the Thomas A. Edison Research Lab., McGraw-Edison Co., West Orange, N. J. He served for over 30 years as chief chemist in charge of research and development for the Storage Battery Division of Thomas A. Edison Inc. and, during his 40 years' experience in the design and development of batteries, has obtained numerous foreign and domestic patents.

Harry Sello now is manager of manufacturing for Fairchild Semiconductor Corp., Mountain View, Calif. Formerly, he was head of pre-production engineering and then process engineering.

William W. Smith has been named manager of engineering and development of The Electric Storage Battery Co.'s Nickel-Alkaline Battery Division, West Orange, N. J. Mr. Smith was manager of alkaline battery development in the engineering department of the company's Exide Industrial Division, Philadelphia, Pa., for the past five years.

Watt W. Webb has been appointed assistant director of research of Union Carbide Metals Co., Niagara Falls, N. Y. He has been with the company since 1947, holding the positions of research metallurgist, senior research metallurgist, and coordinator of the fundamental research group prior to his present promotion.

Clyde A. Crowley

Clyde A. Crowley, of Phoenix, Ariz., died of a heart attack on September 21, 1960 at the age of 58.

Dr. Crowley was born in Ray County, Mo., on June 25, 1902. He studied in Chicago, receiving the degree of B.S. from Chicago Technical College in 1930, M.S. from Loyola University of Chicago in 1934, and Ph.D. in 1940, also from Loyola.

He spent most of his active life in Chicago, teaching in high schools from 1924 to 1932. Concurrently, from 1934 to 1954, he was president and research director of the Technical Service Bureau; from 1937 to 1954, research director for Midcontinent Chemicals Corp.; and from 1944 to 1954, chairman and a research director of Graham, Crowley and Associates. In 1954, he left Chicago to become director of the Engineering and Development Division of the Given Manufacturing Co. in Los Angeles, where he remained un-

til 1956 when he joined the staff of Arizona State University as professor of chemistry, soon becoming chairman of the department.

During the war period 1942-1945, he was a consultant for the U. S. Bureau of Mines and, in 1944, with the U. S. Navy. Immediately after the war in 1945, he was scientific consultant for the Foreign Economic Administration.

For a number of years, he was active in The Electrochemical Society, assisting in the reorganization of the Chicago Section in 1935 and serving as Chairman in 1937-1938. He was on the Membership Committee from 1936-1941, as Chairman during 1938-1941. He was Vice-Chairman of the Electro-Organic Division from 1946 to 1948 and Chairman from 1948 to 1950; he was instrumental in rewriting the Bylaws and framing the current policies of the Division.

Dr. Crowley also was a member of the American Association for the Advancement of Science; American Chemical Society; American Institute of Chemists, of which he was a Fellow; American Society for Testing Materials; Society of Automotive Engineers; and Society of Military Engineers.

News Items

18th International Congress of Pure and Applied Chemistry

Leading scientists from many countries in the world will be heard at the 18th International Congress of Pure and Applied Chemistry to be held in Montreal, Canada, from August 6 to 12, 1961.

Plenary lecturers who will participate are Professor F. S. Dainton, Leeds University, England, who will speak on "New Horizons in Physical Chemistry," and Professor R. Daudel of the National Laboratory for Scientific Research, Paris, France, who will lecture on "Some Recent Results Concerning the Relations between Structure and Chemical Reactivity of Organic Molecules."

Professor G. Schwarzenbach of the Laboratory for Inorganic Chemistry, Zurich, Switzerland, will speak on "Metastable Products of Inorganic Molecules and Ions Formed by Proton Addition and Elimination." The lecture by Professor R. H. Wilhelm of Princeton University, Princeton, N. J., U.S.A., will deal with "Progress Toward the A Priori Design of Chemical Reactors." Academician N. N. Semenov of the Academy of

Sciences, Moscow, U.S.S.R., also has been invited to speak at a plenary session.

Some 70 sectional lectures will be delivered on the various aspects of the four divisions of chemistry with which the conference will deal, Physical Chemistry, Applied Chemistry, Analytical Chemistry, and Organic Chemistry. Among those of special interest to electrochemists are:

"Imperfections and Chemical Reactivity" by Professor F. C. Tompkins, London, England

"Applications of Field Emission to Problems in Adsorption" by Professor R. Gomer, Chicago, Ill., U.S.A.

"Homogeneity or Heterogeneity of the Surface of Metallic Catalysts" by Professor J. Horiuti, Sapporo, Japan

"Electron Optical Studies on the Relations between the Structure of Metal Surfaces and Their Tarnish Films" by Dr. D. W. Pashley, Cambridge, England

"Catalytic Activity of Metals" by Professor G. M. Schwab, Munich, Germany

"The Structure of Molten Salts" by Professor J. O'M. Bockris, Philadelphia, Pa., U.S.A.

"Some Recent Advances in the Study of Electrode Processes" by Professor Paul Delahay, Baton Rouge, La., U.S.A.

"The Electrochemistry of Single Crystals" by Professor R. Piontelli, Milan, Italy.

Symposium on Titrimetric Methods of Analysis, May 8-9, 1961

Dr. D. S. Jackson, chairman of the Symposium Committee, and Dr. R. Bhargava, Program Committee chairman, are pleased to announce that the following distinguished analysts have agreed to deliver keynote addresses at the Symposium on Titrimetric Methods, sponsored by The Chemical Institute of Canada, Analytical Chemistry Division, Cornwall, Ont., Canada, May 8-9, 1961: Professor C. N. Reilley, University of North Carolina, "Chelometric Methods"; Professor J. Fritz, Iowa State University, "Titrations in Nonaqueous Solvents"; Dr. G. Buc, technical assistant to the president, Fisher Scientific Co., "Electrometric Methods."

In addition to contributed papers of about 20 minutes' duration, shorter papers illustrating specific applications will be welcomed. Those who wish to submit papers for this symposium should contact Mr. J. R. McCallum, Secretary-Treasurer, Analytical Chemistry Division, C.I.C.,

c/o Courtaulds (Canada) Ltd., Cornwall, Ont., Canada.

ISA International Conference and Exhibit, Fall 1962

The 17th International Instrument-Automation Conference and Exhibit of the Instrument Society of America will be held in New York City in 1962, in conjunction with the society's annual meeting. The dates have been set for October 15 through 19, 1962, and the Exhibit will be staged in the New York Coliseum. This will be the third time the society has used the Coliseum for exhibits, having first occupied it in 1956 for its 11th International Exhibit, and again in September 1960 for its 15th International Conference and Exhibit.

The annual national show during 1962 will complement the various symposia held under the society's auspices each year. These will be continued, including those on Chemical and Petroleum Instrumentation, Power Instrumentation, Aero-Space Instrumentation, and Instrumental Methods of Analysis, as well as co-sponsorship or cooperation with other national societies in conferences and symposia on Telemetering, Automatic Control, and Nuclear Instrumentation, to name a few.

During the remainder of 1961, ISA will hold two seasonal conferences and exhibits, one in Toronto, Canada, June 6-8, and its third of the year, the Fall Conference and Exhibit, in conjunction with the 16th annual meeting of the society, in Los Angeles, September 11-15.

Newark College of Engineering Receives American Metal Climax Co. Foundation Gift

The Chemical Engineering Dept. of Newark College of Engineering, Newark, N. J., has received \$1,000 from the American Metal Climax Co. Foundation to be used for equipment in its electrochemical laboratories, according to Dr. Charles L. Mantell, department chairman.

The gift, which was presented by the Foundation through Walter L. Brytzcuk, assistant director of research of Amco Research & Development, Inc., an American Metal Climax subsidiary, is the sixth donation by the Foundation to NCE since 1956. The contributions total \$4,240.

In commenting on the Foundation's support, Dr. Mantell stated that the funds have been a strong contributing factor in bringing his department's facilities to a degree of excellence that makes them well

adapted for the original research required by the college's new Doctor of Engineering Science degree, as well as for research for the Master's degree.

As in the past, Dr. Mantell said, the additional \$1,000 will be reserved for the purchase of specialized electrochemical equipment as it is needed by graduate students now involved in advanced research.

Cooperative Program Established for Wider Distribution of Translations of Soviet Technical Data

A new cooperative effort between the United States and a number of European countries to provide broader Western World distribution of translations of Russian and other Eastern European scientific literature that may be useful was announced recently by John C. Green, director of the Office of Technical Services of the U. S. Dept. of Commerce.

A European Translation Center, sponsored by 12 member countries of the European Productivity Agency, has been established at the Technical University at Delft, The Netherlands. It will provide liaison among European countries handling Russian and East European translations, serve as a center for bibliographic information on the availability of translations, and collect noncommercial translations from countries prepared to contribute them.

The Office of Technical Services (OTS), which is the U. S. Government's center for the collection and distribution of translations and related information, is currently assisting the European Translation Center in establishing its procedures for bibliographic and other work. OTS and the European Translation Center will exchange both translations and bibliographic data, and will use uniform methods of classification of the materials. It is contemplated

that the OTS publication, *Technical Translations*, will be used as the announcement medium for material collected by the European Center, which should greatly increase the circulation of the publication in Europe.

"The significance of this cooperative endeavor is that it reduces the language barrier for scientists and engineers of the United States and Western Europe who are trying to keep up with Soviet Bloc developments," Mr. Green commented. "In Western Europe, most scientists can read English translations of Russian work, and, in the United States, many of our scientists can handle translations of Soviet Bloc material in French or German or similar European languages. However, in both the United States and Western Europe, scientists in general do not know the Soviet Bloc languages."

Since 1958, the OTS has been collecting and distributing translations prepared by U. S. Government agencies for their own use. It also gathers and publishes information on translations in progress or completed, which are available from any other source in the U. S., public or private. Among the translations for which OTS provides announcement and reference service are those collected from non-Government sources in the U. S. by the Special Libraries Association (SLA) Translations Collection Center at the John Crerar Library in Chicago.

In cooperation with the SLA Center, the OTS began publishing *Technical Translations* in January 1959 to announce translations available from OTS, SLA, and other sources. It is published twice a month and sold by Superintendent of Documents, U. S. Govt. Printing Office, Washington 25, D. C., at \$12.00 a year (\$4.00 additional for foreign mailing).

The Europeans estimate that their contributions of bibliographic information to *Technical Translations* will add 10-15% to the volume of listings in the first year of the European Center's operation, and that they will eventually double the size of the publication, which now announces about 500 new translations in each issue.

The Netherlands Government is providing financial support for the European Center, which will operate under the legal authority of the Foundation for Scientific Literature Difficult of Access, of which Dr. L. J. Van der Wolk, director of the Library of the Technical University at Delft, is president.

Notice to Members and Subscribers

(Re Changes of Address)

To insure receipt of each issue of the JOURNAL, please be sure to give us your old address, as well as your new one, when you move. Our records are filed by states and cities, not by individual names. The Post Office does not forward magazines.

Formation of the Center was fostered and encouraged by the European Productivity Agency of the Organization for European Economic Cooperation, with the advice and support of the U. S. National Science Foundation.

Soviets Sign Long-Term Contract with N. Y. Scientific Publisher

A new contract establishing terms for exclusive English-language rights to Soviet scientific books for the next six years was signed by Consultants Bureau of New York and Mezhdunarodnaya Kniga, the official Soviet book export agency, in Moscow during October 1960.

Earl and Frances Coleman, publisher and editor-in-chief of Consultants Bureau, spent several weeks in the Soviet Union this past fall. As a result of their meetings with officials of the Soviet book agency and with the directors of 14 Soviet scientific presses, Consultants Bureau will be granted the exclusive world rights in the English language to important Soviet monographs, symposia, conference proceedings, and collections, all on highly specialized scientific and technical subjects.

The new six-year agreement contains automatic renewal provisions at two-year intervals. Mr. Coleman noted that, not only would this contract result in much-improved communications between Soviet and American scientists, but it also is an indication that the official Soviet book agency anticipates a prolonged period of free trade between the U.S.S.R. and the U.S.

This contract covering scientific books follows closely on the heels of

a similar contract signed earlier in 1960 with Mezhdunarodnaya Kniga which granted Consultants Bureau the exclusive rights to translate 23 major Soviet journals in the fields of chemistry, physics, biology, and medicine.

All books published by Consultants Bureau will in the future be made available to English-speaking scientists within six months of their publication in the U.S.S.R. This rapidity of dissemination of significant Soviet research reports will be a direct result of the increased cooperation guaranteed by the new contract.

Where the importance of Soviet conferences warrants even speedier dissemination of their proceedings to the Western scientific community, Consultants Bureau will publish the English translations of these proceedings at the same time as the Russian originals appear in the U.S.S.R. The first instance of such simultaneous publication in Russian and in English occurred on October 20, 1960 with the appearance of "The Structure of Glass" in Leningrad and in New York.

ESB Forms New Marketing Organization for Exide

A new sales and service organization, the Exide Industrial Marketing Division, has been created by The Electric Storage Battery Co., Philadelphia, Pa., to serve as the marketing arm for its Exide Industrial Division and its new Nickel-Alkaline Division.

It combines into one unit the nation-wide Exide industrial sales and service engineering facilities with those of the former Edison Storage

Battery Division of Thomas A. Edison Industries, McGraw-Edison Co., now called the Nickel-Alkaline Division. The Nickel-Alkaline Division, which manufactures nickel-iron and other types of alkaline batteries, was purchased from Edison by ESB in August 1960.

The new marketing organization is headed by Exide's vice-president of marketing, C. J. Moore. It now offers the most complete line of batteries, charging equipment, and related components, as well as the most comprehensive service engineering facilities in the battery industry today.

Exide Industrial Marketing Division offers lead-acid, nickel-cadmium, nickel-iron, and other specialized types of batteries; rectifier and motor-generator types of battery chargers; charge control devices; emergency lighting equipment and other accessories used in electric industrial truck, mining, railway, telephone, and other communications, electric utility, marine, aircraft, and military service.

The division has field sales and service engineering offices in 52 cities.

Yardney Electric Plans New Plant in Stonington, Conn.

Yardney Electric Corp. will take over the 250,000-square-foot plant on ten acres of land of the Raytheon Co. in Stonington, Conn., it was announced recently. Yardney planned to start operations in the plant immediately. The plant will be used to fulfill a substantial contract recently awarded by the U. S. Navy for submarine batteries and other contracts under negotiation.

Manuscripts and Abstracts for Fall 1961 Meeting

Papers are now being solicited for the Fall Meeting of the Society, to be held at the Statler Hotel in Detroit, Mich., October 1, 2, 3, 4, and 5, 1961. Technical sessions probably will be scheduled on Batteries, Corrosion (including a Symposium on Surface Structure vs. Corrosion Behavior), Electrodeposition (including symposia on Addition Agents and on Electrodeposited Magnetic Films), Electronics (Semiconductors), Electro-Organics, and Electrothermics and Metallurgy.

To be considered for this meeting, triplicate copies of abstracts (*not exceeding 75 words in length*) must be received at Society Headquarters, 1860 Broadway, New York 23, N. Y., *not later than May 15, 1961. Please indicate on abstract for which Division's symposium the paper is to be scheduled and underline the name of the author who will present the paper.* No paper will be placed on the program unless one of the authors, or a qualified person designated by the authors, has agreed to present it in person. An author who wishes his paper considered for publication in the JOURNAL should send triplicate copies of the manuscript to the Managing Editor of the JOURNAL, 1860 Broadway, New York 23, N. Y.

Presentation of a paper at a technical meeting of the Society does not guarantee publication in the JOURNAL. However, all papers so presented become the property of The Electrochemical Society, and may not be published elsewhere, either in whole or in part, unless permission for release is requested of and granted by the Editor. Papers already published elsewhere, or submitted for publication elsewhere, are not acceptable for oral presentation except on invitation by a Divisional program Chairman.

The main products of Yardney Electric are Silvercel silver-zinc batteries and Silcad silver-cadmium batteries, which have a broad range of applications, such as submarines, missiles, satellites, torpedoes, and aircraft in the military field and communication systems, photography, and portable electronic equipment in the commercial field.

Consolidated Aluminum's Raffinal Plant Now in Full Operation

The largest superpurity aluminum plant in North America is now in full production. Consolidated Aluminum Corp. completed construction of its expanded Raffinal (superpurity aluminum) plant in June 1960, increasing production more than 200% with capacity for 300,000 pounds per month.

According to a recent announcement by the Business and Defense Services Administration, the demand for superpurity aluminum is expected to more than double by 1965 to over 15,000,000 pounds per year.

Consolidated Aluminum Corp.'s superpurity aluminum has an average purity of 99.996%, with a minimum of 99.992%. CONALCO superpurity aluminum is available in a wide range of sizes, gauges, and forms, including pig, billets, pellets, coiled sheet, and foil.

Consolidated Aluminum Corp. has its plants and general offices at Jackson, Tenn. Sales offices are at New York, Cleveland, Chicago, Dallas, Atlanta, and Los Angeles (La Habra).

International Resistance Co. Enters Semiconductor Field

International Resistance Co., Philadelphia, Pa., has entered the rapidly growing semiconductor field with the purchase of controlling interest in North American Electronics, Inc., of Lynn, Mass.

North American Electronics will continue to operate independent of International Resistance Co., with its present officers remaining unchanged. The NAE Board will be increased from its present 7 members to 11, with IRC holding 6 seats.

NAE's major product lines include more than 600 types of silicon rectifiers and Zener diodes, as well as silicon-controlled rectifiers with unique operating characteristics.

Silicon products are expected to "continue to show the most rapid growth" of any in the semiconductor field, IRC marketing officials said, adding that NAE "has already doubled its sales each year since its inception."

NAE operates in a modern Lynn plant with 25,000 square feet of floor space, ample to meet 1961 anticipated growth in production. Current employment is approximately 130.

Plans already are under way to add "substantially" to facilities to meet 1962 requirements.

Book Review

The Corrosion and Oxidation of Metals, by Ulick R. Evans. Published by Edward Arnold (Pub-

lishers), Ltd., London, 1960. Available from St. Martin's Press, New York City. ix + 1094 pages; \$25.00.

This book is the successor to the author's "Metallic Corrosion, Passivity and Protection," published in 1937 and in "drastic revision" in 1946. In spite of the author's protestations, the present volume may be considered as another "drastic revision" and up-dating of the former book. Written by an outstanding authority in corrosion theory and practice, an expert in teaching and in writing, in fact by the world's "dean

PHYSICAL METALLURGIST PHYSICAL CHEMIST SOLID STATE PHYSICIST

for electronics materials development in

SAN FRANCISCO

as Senior Staff Members of nationally prominent industrial research organization. Ph.D. or equivalent.

Problem solving of a chemical nature in the electronics industry, physicochemical studies, etc.

Solid State device development, problem solving, staff consultant in physics, etc.

Phone collect, or send resume to Mr. Ostrander

Professional & Technical Recruiting Assoc.
Suite C, 825 San Antonio Road
Palo Alto, California
Davenport 6-0744

(fees and relocation costs paid by our client)

of corrosion," the book will be invaluable to the beginner and the expert alike. The price is high but, for once, the book is worth the price; the pages are packed with information that will be useful both for study and for reference for many years to come.

The first section of 760 pages, 18 chapters, is labeled "Qualitative." It is largely descriptive and includes chapters on simple and complex oxidation, electrochemical corrosion, inhibitors, anodic dissolution, and passivation; acid corrosion and hydrogen troubles, waters, boilers, condensers; atmospheric corrosion, protection, nonmetallic and metallic coatings; stress corrosion, corrosion fatigue, cracking. The second section of 150 pages, labeled "Quantitative," describes test methods, deals with mathematical treatment of data, and includes a chapter on statistical considerations. The main treatment of cathodic protection is found in this section. The Appendix of 100 pages is mainly devoted to a short course in chemistry, which will serve as a refresher, and summarizes useful and pertinent principles and theories.

Dr. Evans makes it clear that no author can hope to review the literature of corrosion in a 1000-page book. (In fact, more than 2500 articles dealing with corrosion are now appearing each year in the world's literature.) Still, reference is made to the publications of more than 3000 authors whose work Dr. Evans considers pertinent, appropriate, and representative; the coverage extends through 1958, with a few early 1959 citations. However, as the author says in the preface, he presents his own views on corrosion and substantiates them from the literature; but he tries not to neglect the views of others even though they differ. As an example may be cited the treatment of inhibitors in Chapter V: Dr. Evans is quite convinced that only tangible films can be effective in inhibition, but acknowledges the importance of studying the process which constitutes the initial stage in their formation.

The book is a pleasure to read because the text is simply and clearly written in excellent English. It is illustrated with some 200 figures which help to explain many details. There are practically no annoying typographical errors or other flaws, and mechanically it represents an honest and expert manufacturing job.

C. V. King

Announcement from Publisher

Three-Volume Review of Soviet Progress in Electrochemistry

The proceedings of the "Fourth Soviet Conference on Electrochemistry" was published in March by Consultants Bureau, New York City, in complete English translation. This significant conference heard reports on the latest Soviet progress in the field of electrochemistry and the full texts of the most important papers presented were published in the U.S.S.R. by the Academy of Sciences U.S.S.R. Press in 1959. The Consultants Bureau cover-to-cover English translation appears in three volumes of approximately 300 pages each.

Vol. I contains papers on electrochemical kinetics, the electrical double layer, adsorption at a metal-solution boundary, hydrogen overvoltage, diffusion kinetics, and polarography. Vol. II deals with reduction and oxidation, electrodeposition, electrosolution, oxygen overvoltage, passivity, and corrosion. Vol. III contains reports on applied electrochemistry, electrodeposition, non-ferrous metallurgy, chemical sources of current, and electrolysis in the chemical industry. Papers by such well-known Soviet electrochemists as A. N. Frumkin assure readers of the high quality of the entire collection.

The "Fourth Soviet Conference on Electrochemistry" will be of interest to all scientists concerned with the varied aspects of this important field. Each volume is priced at \$15.00; the three-volume set is priced at \$40.00. Complete tables of contents are available on request from Consultants Bureau Enterprises, Inc., 227 W. 17 St., New York 11, N. Y.

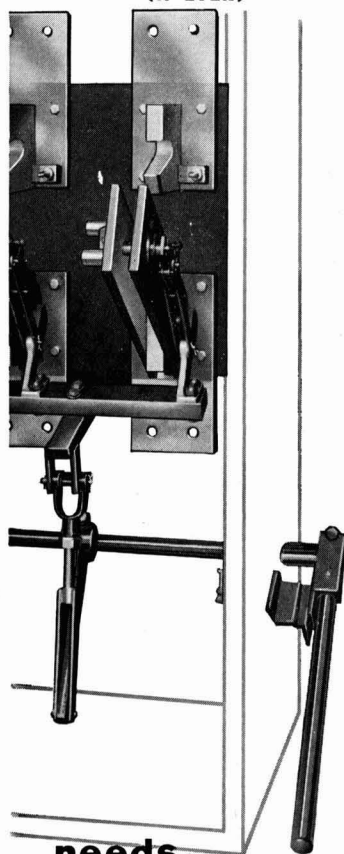
Meetings of Other Organizations

April 10-11—Oklahoma State University Thermodynamics Conference, Oklahoma State University, Stillwater, Okla.

April 17-19—Instrument Society of America, National Symposium on Instrumental Methods of Analysis, Shamrock-Hilton Hotel, Houston, Texas.

April 18-19—Conference on Organic Semiconductors, sponsored by Ar-

RARELY (IF EVER)



needs MAINTENANCE

Pringle disconnect switches for high-current equipment carry as much as 50,000 amperes, continuously, with no more of a heat rise than you would get from copper bus bars bolted together. These switch blades actually are bolted together. Under a constant pressure of 600 lbs./sq. inch. Without springs. Yet, they open easily after months (or years) of closed operation. Heat, fatigue, lack of movement won't affect the operating mechanism. Constant, periodic maintenance is unnecessary.

Less complex than most high-capacity disconnect devices. Less expensive too. Available in single- or multi-pole models, front or rear connected, live front or steel enclosed. With or without high-capacity fuses. For use on crane conductor rails, transformer secondaries, or AC and DC switchboards. Wherever high-current equipment must be isolated for periodic servicing.

Write for Industrial Switch Catalog

PRINGLE
ELECTRICAL MANUFACTURING CO.

1910 NORTH SIXTH STREET
PHILADELPHIA 22, PENNA.

mour Research Foundation and *Electronics* magazine, Morrison Hotel, Chicago, Ill.

April 24-26—National Academy of Sciences, Annual Meeting, Washington, D. C.

April 24-27—American Physical Society Meeting, National Bureau of Standards, Washington, D. C.

May 11-12—American Institute of Chemists, Annual Meeting, Statler Hotel, Washington, D. C.

June 22-24—American Physical Society Meeting, University of Mexico, Mexico City, Mexico.

June 25-30—American Society for Testing Materials, Annual Meeting, Chalfonte-Haddon Hall, Atlantic City, N. J.

daily or project compensation. Work by mail. Indicate background in confidence to *Box A-287, c/o The Electrochemical Society, 1860 Broadway, New York 23, N. Y.*

Chemists and Chemical Engineers—We need physical, organic and inorganic chemists, and chemical engineers to carry out Engineering and development work in the rapidly growing power sources field. Research & Development center located in Minneapolis near University of Minnesota. Battery experience preferred but not required. Send resumes to: J. W. Baxter, Employee & Labor Relations, Gould-National Batteries, Inc., E. 1326 First National Bank Bldg., St. Paul 1, Minn.

Four challenging research positions for experienced surface chemists, in fully-equipped laboratory devoted to research and development on aluminum and copper alloys, involving: A. Electrochemical kinetics, adsorption, and oxide film structure investigations related to finishing processes. B. Studies of interfacial surface reactions between polymeric resins and metal oxide surfaces relating to strength and permanence

of joints in the adhesive bonding of metals. C. Mechanisms relating to surface phenomena, associated with liquid metal-solid metal inter-action as applied to soldering and brazing. D. Surface and electrochemical reactions effecting the kinetics of general, localized, and stress corrosion processes. Pleasant living, with access to major university. Send reply to R. H. Endriss, Personnel Manager, Olin Mathieson Chemical Corp., 125 Munson St., New Haven, Conn.

Employment Situations

Positions Available

Consulting Physicist with thorough knowledge of single crystals, float zoning, semiconductor materials, wanted by established Western European company. Annual retainer,

Advertiser's Index

Great Lakes Carbon Corp., Electrode Division	Cover 2
Lockheed Missiles & Space Division	96C
Olin Mathieson Chemical Corporation	96C
Pringle Electric Manufacturing Company	95C
Professional and Technical Recruiting Associates	94C
E. H. Sargent & Company	84C
Stackpole Carbon Company	83C

PHYSICAL CHEMIST or ELECTROCHEMIST

Ph.D., strong background in fused salts for a basic and applied research program concerned with electrochemical energy conversion devices. This program is unclassified and publications are encouraged. Applicant must be capable of working independently and have a demonstrated experimental ability. Background in electrochemistry is desired but not essential.

Please address confidential inquiries to Mr. R. C. Birdsall, Employment Manager, Lockheed Missiles and Space Division, Dept. M-21B, 962 West El Camino Real, Sunnyvale, Calif. U.S. citizenship or existing Department of Defense industrial security clearance required.

Lockheed

MISSILES AND SPACE DIVISION

SUNNYVALE, PALO ALTO, VAN NUYS, SANTA CRUZ,
SANTA MARIA, CALIFORNIA
CAPE CANAVERAL, FLORIDA • HAWAII

Attractive Openings In FUNDAMENTAL RESEARCH

Challenging, permanent positions for PHYSICISTS, PHYSICAL METALLURGISTS, SOLID STATE PHYSICISTS OR PHYSICAL CHEMISTS at our modern, well-equipped metallurgical research laboratories.

Ph.D. or equivalent for fundamental studies of oxidation of aluminum and copper alloys. Experience in semi-conductor technology or metal physics, together with thorough knowledge of applicable experimental techniques, desirable. Previous experience in aluminum or brass metallurgy preferred.

Ideal community life, with access to major university. Reply to M. F. TIPPLE at

**OLIN MATHIESON
CHEMICAL CORPORATION**

275 Winchester Avenue

New Haven 4, Conn.

The Electrochemical Society

Patron Members

Aluminum Co. of Canada, Ltd.,
Montreal, Que., Canada
International Nickel Co., Inc.,
New York, N. Y.
Olin Mathieson Chemical Corp.,
Chemicals Div., Industrial Chemicals
Development Dept., Niagara Falls, N. Y.
Union Carbide Corp.
Divisions:
Union Carbide Metals Co.,
New York, N. Y.
National Carbon Co., New York, N. Y.
Westinghouse Electric Corp., Pittsburgh, Pa.

Sustaining Members

Air Reduction Co., Inc.,
New York, N. Y.
Ajax Electro Metallurgical Corp.,
Philadelphia, Pa.
Allen-Bradley Co., Milwaukee, Wis.
Allied Chemical Corp.
Solvay Process Div., Syracuse, N. Y.
General Chemical Div., Morristown, N. J.
Alloy Steel Products Co., Inc., Linden, N. J.
Aluminum Co. of America,
New Kensington, Pa.
American Metal Climax, Inc.,
New York, N. Y.
American Potash & Chemical Corp.,
Los Angeles, Calif. (2 memberships)
American Smelting and Refining Co.,
South Plainfield, N. J.
American Zinc Co. of Illinois,
East St. Louis, Ill.
American Zinc, Lead & Smelting Co.,
St. Louis, Mo.
American Zinc Oxide Co., Columbus, Ohio
M. Ames Chemical Works, Inc.,
Glens Falls, N. Y.
Armco Steel Corp., Middletown, Ohio
Basic Inc., Maple Grove, Ohio
Bell Telephone Laboratories, Inc.,
New York, N. Y. (2 memberships)
Bethlehem Steel Co., Bethlehem, Pa.
(2 memberships)
Boeing Airplane Co., Seattle, Wash.
Burgess Battery Co., Freeport, Ill.
(4 memberships)
Canadian Industries Ltd., Montreal, Que.,
Canada
Carborundum Co., Niagara Falls, N. Y.
Catalyst Research Corp., Baltimore, Md.
Columbian Carbon Co., New York, N. Y.
Columbia-Southern Chemical Corp.,
Pittsburgh, Pa.
Consolidated Mining & Smelting Co. of
Canada, Ltd., Trail, B. C., Canada
Continental Can Co., Inc., Chicago, Ill.
Cooper Metallurgical Associates, Cleveland,
Ohio
Corning Glass Works, Corning, N. Y.
Diamond Alkali Co., Painesville, Ohio
Dow Chemical Co., Midland, Mich.
Wilbur B. Driver Co., Newark, N. J.
(2 memberships)
E. I. du Pont de Nemours & Co., Inc.,
Wilmington, Del.
Eagle-Picher Co., Chemical Div., Joplin, Mo.
Eastman Kodak Co., Rochester, N. Y.
Thomas A. Edison Research Laboratory, Div.
of McGraw-Edison Co., West Orange, N. J.
Electric Auto-Lite Co., Toledo, Ohio
C & D Division, Conshohocken, Pa.
Electric Storage Battery Co., Yardley, Pa.
Englehard Industries, Inc., Newark, N. J.
(2 memberships)
The Eppley Laboratory, Inc., Newport, R. I.
(2 memberships)
Exmet Corp., Tuckahoe, N. Y.
Fairchild Semiconductor Corp., Palo Alto,
Calif.
Food Machinery & Chemical Corp.
Becco Chemical Div., Buffalo, N. Y.
Westvaco Chlor-Alkali Div., South
Charleston, W. Va.
Foote Mineral Co., Paoli, Pa.
Ford Motor Co., Dearborn, Mich.
General Electric Co., Schenectady, N. Y.
Chemistry & Chemical Engineering
Component, General Engineering
Laboratory
Chemistry Research Dept.
General Physics Research Dept.
Metallurgy & Ceramics Research Dept.
Aircraft Accessory Turbine Dept.,
West Lynn, Mass.
General Instrument Corp., Newark, N. J.

(Sustaining Members' cont'd)

- General Motors Corp.
Delco-Remy Div., Anderson, Ind.
Guide Lamp Div., Anderson, Ind.
Research Laboratories Div., Detroit, Mich.
- General Telephone & Electronics
Laboratories Inc., Bayside, N. Y.
(2 memberships)
- General Transistor Corp., Jamaica, N. Y.
- Gillette Safety Razor Co., Boston, Mass.
- Globe-Union, Inc., Milwaukee, Wis.
- Gould-National Batteries, Inc.,
Minneapolis, Minn.
- Grace Electronic Chemicals, Inc.,
Baltimore, Md.
- Great Lakes Carbon Corp., New York, N. Y.
- Hanson-Van Winkle-Munning Co.,
Matawan, N. J. (2 memberships)
- Harshaw Chemical Co., Cleveland, Ohio
(2 memberships)
- Hercules Powder Co., Wilmington, Del.
- Hill Cross Co., Inc., West New York, N. J.
- Hoffman Electronics Corp., El Monte, Calif.
- Hooker Chemical Corp., Niagara
Falls, N. Y. (3 memberships)
- Hughes Aircraft Co., Culver City, Calif.
- International Business Machines Corp.,
Poughkeepsie, N. Y.
- International Minerals & Chemical
Corp., Skokie, Ill.
- ITT Federal Laboratories, Div. of
International Telephone & Telegraph
Corp., Nutley, N. J.
- Jones & Laughlin Steel Corp.,
Pittsburgh, Pa.
- K. W. Battery Co., Skokie, Ill.
- Kaiser Aluminum & Chemical Corp.
Div. of Chemical Research,
Permanente, Calif.
Div. of Metallurgical Research,
Spokane, Wash.
- Kawecki Chemical Co., Boyertown, Pa.
- Kennecott Copper Corp., New York, N. Y.
- Keokuk Electro-Metals Co., Keokuk, Iowa
- Libbey-Owens-Ford Glass Co., Toledo, Ohio
- Mallinckrodt Chemical Works, St. Louis, Mo.
- P. R. Mallory & Co., Indianapolis, Ind.
- McGean Chemical Co., Cleveland, Ohio
- Merck & Co., Inc., Rahway, N. J.
- Metal & Thermit Corp., Detroit, Mich.
- Minnesota Mining & Manufacturing Co.,
St. Paul, Minn.
- Monsanto Chemical Co., St. Louis, Mo.
- Motorola, Inc., Chicago, Ill.
- National Cash Register Co., Dayton, Ohio
- National Lead Co., New York, N. Y.
- National Research Corp., Cambridge, Mass.
- National Steel Corp., Weirton, W. Va.
- New York Air Brake Co., Kinney Vacuum
Div., Boston, Mass.
- Northern Electric Co., Montreal, Que.,
Canada
- Norton Co., Worcester, Mass.
- Ovitron Corp., Long Island City, N. Y.
- Peerless Roll Leaf Co., Inc., Union City, N. J.
- Pennsalt Chemicals Corp.,
Philadelphia, Pa.
- Phelps Dodge Refining Corp., Maspeth, N. Y.
- Philco Corp., Philadelphia, Pa.
- Philips Laboratories, Inc., Irvington-on-
Hudson, N. Y.
- Potash Co. of America,
Carlsbad, N. Mex.
- Radio Corp. of America
Tube Div., Harrison, N. J.
RCA Victor Record Div., Indianapolis,
Ind.
- Ray-O-Vac Co., Madison, Wis.
- Raytheon Manufacturing Co.,
Waltham, Mass.
- Reynolds Metals Co., Richmond, Va.
- Rheem Semiconductor Corp.,
Mountain View, Calif.
- Schering Corporation, Bloomfield, N. J.
- Shawinigan Chemicals Ltd., Montreal, Que.,
Canada
- Speer Carbon Co.
International Graphite & Electrode
Div., St. Marys, Pa.
- Sprague Electric Co., North Adams, Mass.
- Stackpole Carbon Co., St. Marys, Pa.
- Stauffer Chemical Co., New York, N. Y.
- Sumner Chemical Co., Div. of
Miles Laboratories, Inc., Elkhart, Ind.
- Tennessee Products & Chemical Corp.,
Nashville, Tenn.
- Texas Instruments, Inc., Dallas, Texas
Metals and Controls Corp.,
Attleboro, Mass.
- Three Point Four Corp., Yonkers, N. Y.
- Titanium Metals Corp. of America,
Henderson, Nev.
- Tung-Sol Electric Inc.,
Newark, N. J.
- Udylite Corp., Detroit, Mich.
(4 memberships)
- Universal-Cyclops Steel Corp.,
Bridgeville, Pa.
- Upjohn Co., Kalamazoo, Mich.
- Victor Chemical Works, Chicago, Ill.
- Western Electric Co., Inc., Chicago, Ill.
- Wyandotte Chemicals Corp.,
Wyandotte, Mich.
- Yardney Electric Corp., New York, N. Y.